SOUND TRANSMISSION THROUGH LINED DUCTS IN PARALLEL

by

William Paul Patrick

B.S., Pennsylvania State University
(1966)

S.M., Massachusetts Institute of Technology
(1968)

SUBMITTED IN PARTIAL FULFILLMENT OF
THE REQUIREMENTS FOR THE DEGREE OF

DOCTOR OF PHILOSOPHY

at the

MASSACHUSETTS INSTITUTE OF TECHNOLOGY

February, 1979

Signature of Author _____
Department of Aeronautics & Astronautics, 30ctober 1978

Certified by _____
Thesis Supervisor

Certified by _____
Thesis Supervisor

Accepted by _____
Chairman, Departmental Graduate Committee

SOUND TRANSMISSION THROUGH LINED DUCTS IN PARALLEL

by

William Paul Patrick

Submitted to the Department of Aeronautics and Astronautics on 3 October 1978 in partial fulfillment of the requirements for the degree of Doctor of Philosophy.

ABSTRACT

A new method to enhance the low frequency sound attenuation characteristics of a lined duct is presented. A rigid, longitudinal splitter plate is used to separate the lined duct section into two parallel branch ducts. The phase speed of the fundamental sound mode in each parallel branch is a function of the liner configuration and can differ substantially from the free space phase speed. By lining the parallel branches dissimilarly, destructive interference of the fundamental mode of the transmitted wave occurs downstream of the parallel absorbers at a selected set of frequencies. Strong reflections also occur at the silencer inlet for a larger set of frequencies due to an acoustical impedance mismatch at the junction of the main duct and the parallel branches. These interference effects, which result from placing the rigid splitter plate into the lined duct, can increase the low frequency transmission loss of the duct by more than two fold over a broad low frequency band and by as much as 5 dB/unit duct width at selected frequencies. The advantages of this new method of sound attenuation over previous methods include (1) the use of thinner acoustic liners to obtain a desired attenuation at low frequencies, and (2) tunability of the muffler by adjusting the length or position of the splitter plate. Potential applications of parallel lined duct mufflers include the reduction of low frequency noise in air delivery systems, stationary gas turbine power plants, inlet and exhaust silencers for aircraft engine test facilities, and piston engine exhaust systems.

Thesis Supervisor: K. Uno Ingard

Title: Professor of Physics and Aeronautics and Astronautics

Thesis Supervisor: Jack L. Kerrebrock

Title: Professor and Head, Department of Aeronautics and Astronautics

ACKNOWLEDGMENTS

In the Middle Ages the guilt or innocence of an accused person was determined by subjecting the accused to an ordeal by fire or water, the outcome of which, it was believed, was predetermined by supernatural forces. The innocent survived the ordeal, the guilty paid their penance. Modern man, while considering such trials barbaric, has invented a barbarism of his own which might be called - the Ordeal by Ph.D. Thesis. The outcome of this modern ordeal is not predetermined although it is decreed by the department faculty who, from the degree candidate's perspective, are not unlike supernatural forces.

As a recent survivor of the Ordeal by Ph.D. Thesis I must be thankful that the pain associated with it comes mainly from the uncertainty that the ordeal will end successfully. Indeed, at this point in time, having passed my thesis defense, the experience seems almost pleasurable. Such pleasure arises when I remember all who helped me throughout my ordeal. I would like to extend my sincerest thanks -

to Prof. Uno Ingard, whose knowledge of acoustics is surely inexhaustible, for his willingness to share that knowledge, his encouragement when progress was slow and his enthusiasm in addition to his financial support;

to Prof. Jack Kerrebrock, who got me into the Ph.D. program, supported me through the early part of the program, and stayed with me until the end;

to Prof. D. Graham Holmes (Clarkson College) for his assistance while serving on my thesis committee while he was at MIT;

to my colleagues, Drs. George Succi and Vijay Singhal, for stimulating discussions on acoustics and for critically listening to my ramblings on sound transmission through lined ducts in parallel, and to Dr. Wai Cheng for his enthusiastic assistance with the analysis and computer programming;

to Dr. Alan Epstein, Thorwald Christensen and Roy Andrew for providing technical assistance during my experimental program;

to my employers, the United Technologies Research Center, for granting me a leave of absence from 1974 to 1976 during which the major part of the thesis research was completed, and for subsequent tuition assistance;

to the Research Computer Center at Bolt, Beranek and Newman Corporation for generously providing the computer time required to develop and run my computer program;

and especially to Gayle Ivey who gave me hope when hope was almost gone, pulled me through to the end and, finally, typed the thesis.

Table of Contents (cont'd)

Table of Contents (cont'd)

Table of Contents (cont'd) Page

Table of Contents (cont'd)

LIST OF FIGURES

CHAPTER I

SUMMARY AND INTRODUCTION

1.1 Summary

A research program has been carried out to investigate the sound transmission characteristics of lined ducts in parallel with particular emphasis on their low-frequency attenuation characteristics. The research program is comprised of three related studies. First, the sound transmission characteristics of a single lined duct section have been investigated. Second, an analytical and experimental study has been conducted to determine the transmission loss of two or more lined ducts joined in parallel. Finally, matrix analysis has been used to develop techniques which will permit the efficient determination of the transmission loss through arrays of lined ducts (parallel, series-parallel, N-ducts in parallel, etc.).

Sound Transmission through Lined Duct Section: Analytical expressions have been derived for the phase speed of the fundamental sound mode in lined rectangular, circular and annular ducts including the effects of mean flow. Measurements were made of the phase speed and the attenuation constant of the fundamental mode in lined rectangular ducts with and without mean flow.

Sound Transmission through Parallel Lined Ducts: The sound transmission characteristics of individual lined duct sections have been combined into an analytical model to predict the transmission loss through a parallel duct array. The accuracy of the analytical model was assessed from

experimental measurements of the sound transmission through several parallel duct configurations. An attempt was made to optimize the lined duct configuration and to identify the controlling parameters in the design of parallel lined ducts. Measurements of sound transmission through the parallel array with and without mean flow have been obtained.

Application of Matrix Techniques to Duct Acoustics: A technique has been developed to facilitate the calculation of transmission loss through arrays of lined and unlined duct sections arranged in series, parallel, and series-parallel combinations. The duct is modeled as a two-port network in which the acoustic variables, pressure and particle velocity, at the inlet and outlet of the duct section are related by forward-transmission, rearward-transmission, admittance, and impedance matrices. A Handbook of Transmission Matrices has been presented which catalogues transmission matrices for most components of a typical duct system. Rules governing the addition of these component matrices for duct systems joined in series and/or parallel have been presented and several example problems have been worked out.

1.2 Introduction

For over forty years researchers in duct acoustics have been attempting to eliminate the unwanted sound which is transported within flow ducts without restricting the flow itself. While they have been fairly successful in developing duct liners to eliminate medium and high frequency noise (i.e. $f > 500$ Hz) without obstructing the flow path, low frequency noise in ducts has proved to be quite persistent and is not easily subdued.

Unfortunately, severe low frequency noise is produced both mechanically and aerodynamically in either discrete or broadband frequencies. Discrete frequencies can be generated by mechanical vibration, periodic excitation of mechanical structures (e.g. noise generated at the piston frequency in a diesel engine) or aerodynamically by vortex shedding. Broadband low frequency noise is generated primarily by turbulent processes such as combustion, aerodynamic throttling, interaction of flow with vibrating panels, flow turning in ducts, etc. These low frequency noise sources are often of such severity that even after favorable dB(A) weighting, they may present serious annoyance problems. Severe low frequency noise may cause mechanical damage also. For example, noise from gas turbine power plants in the 31.5 Hz octave band can excite the natural modes of walls in nearby buildings causing plaster to crack and windows to rattle.[1]

Existing methods of attenuating sound at low frequencies use dissipative duct liners for broadband noise reduction and various resonant chambers to eliminate discrete frequency noise. In either case the thickness of the liner or the length of the resonator varies in direct proportion to the wavelength of the sound to be attenuated. Consequently, for adequate low frequency attenuation dissipative liners must be very bulky and costly and resonant chambers add significantly to the lateral dimensions of the duct.

The purpose of this thesis is to investigate a new method of low frequency sound attenuation in ducts which does not require bulky liners or unwieldy resonant chambers.

1.3 Background

Cho and Ingard[2] have shown that at low frequencies the phase speed of the fundamental mode of a sound wave in a lined duct can be substantially lower than the phase speed in a duct with rigid walls. In fact, they have shown that for a rectangular duct lined on one wall with a porous liner the phase speed of a low frequency sound wave is independent of the liner characteristics and only depends on the liner-duct geometry,

$$\lim_{k\to 0} \frac{\mathrm{Re}(k_z)}{k} = \frac{c_0}{c_z} = \left(1 + \frac{L}{b}\right)^{1/2} \qquad k = \omega/c_0 \qquad (1.1)$$

where k_z and c_z are the wavenumber and phase speed of the fundamental mode in the duct respectively, c_0 is the thermodynamic speed of sound, L is the liner thickness and b is the duct width.

Thus, in effect, a lined duct acts as a delay line for sound waves at low frequencies. This characteristic of lined ducts can be used to advantage by dividing the duct into two parallel ducts using a rigid longitudinal splitter plate as shown in Fig. 1a. By lining each parallel duct section with a different relative liner thickness, destructive interference can be effected between the out-of-phase transmitted waves and reflections from the entrance of the parallel duct assembly can be increased also.

This method of sound filtration is reminiscent of the Herschel-Quincke tube, Fig. 1b, which was invented by Herschel[3] and later developed by Quincke[4] over 100 years ago. In the Herschel-Quincke tube, a rigid duct is divided in two parallel ducts of equal cross-sectional areas but of

different lengths ℓ_1 and ℓ_2 causing a phase difference in the transmitted waves of

$$\Delta\alpha = \alpha_1 - \alpha_2 = k(\ell_1 - \ell_2)$$

At frequencies for which

$$\Delta\alpha = (2n+1)\pi \qquad n = 0,1,2,.....N \qquad (1.2)$$

no sound is transmitted through the Herschel-Quincke tube. This set of frequencies will be referred to as "destructive interference" frequencies in this thesis. Complete destructive interference occurs in the exit duct because the sound waves transmitted through the parallel ducts 1 and 2 are of equal amplitude and opposite phase.

Attenuation peaks also occur at another set of frequencies at which the round trip path length through both branch ducts equals an integral number of wavelengths

$$\Delta\alpha' = \alpha_1 + \alpha_2 = k(\ell_1 + \ell_2) = 2n\pi \qquad (1.3)$$

This phenomenon which will be referred to as the "sing-around" effect in this thesis remained undiscovered for almost 100 years until Stewart[5] analyzed the Herschel-Quincke tube in 1928. The "sing-around" effect is caused by the impedance mismatch resulting from differences in the cross-sectional areas of the branch ducts and the main duct at the entrance and exit of the Herschel-Quincke tube. For the special case of a Herschel-Quincke tube having branch ducts and the main duct of equal cross-sectional area, the "sing-around" effect is absent and attenuation only occurs at the "destructive interference" frequency defined by Eq. (1.2).

Later, Stewart[6] showed that a single general equation defined both the "sing-around" and "destructive interference" frequencies for a Herschel-Quincke tube having branch ducts of unequal cross-sectional areas

$$S_1 \sin\alpha_2 + S_2 \sin\alpha_1 = 0 \tag{1.4}$$

where S_1 and S_2 are the cross-sectional areas of branch ducts 1 and 2 respectively. The attenuation peaks of the Herschel-Quincke tube defined by Eq. (1.4) are quite sharp and it is restricted to use as a narrow band filter.

In contrast to the Herschel-Quincke tube, the attenuation of the parallel lined duct filter is relatively broadband due to the dissipative nature of the lined sections. At selected frequencies the attenuation will be enhanced by destructive interference of the transmitted waves in the exit duct. In general, the transmitted sound waves from the parallel duct sections will not have equal amplitudes because they will have been unequally attenuated in their respective duct sections and the resultant destructive interference will not be complete. However, strong reflections from the filter inlet will occur at the "sing-around" frequency due to acoustical impedance mismatches at the junctions of the main duct and the parallel branches. By suitably choosing the length of the splitter plate and the duct liner configuration these destructive interference effects can be made to occur at very low frequencies for which purely dissipative duct silencers must be extremely bulky to be effective.

Several devices have been patented which attenuate sound by means of parallel ducts. The primary patents are those by Allen and Kurtze[7]

(U.S. Patent 3,113,635) and Bychinsky[8] (3,948,346). Other relevant patents have been awarded to Whitney[9] (3,580,357), Luxton[10] (3,568,791), Giordano[11](3,174,583) and Zorumski[12] (3,830,335). The acoustic filter studied in this thesis, which will be referred to as the Ingard-Patrick device in the following discussion, differs from each of the patented devices in one or more ways. The parallel lined duct filter has the following three key features which, when combined, form an acoustic filter of unique design:

(1) In Fig. 2 the partition forming the boundary between branch ducts is substantially rigid and continuous along its entire length to minimize the vibrational energy flow coupling between the branch ducts along their common boundary. "Substantially rigid" materials include metal plates, metal or PVC pipes, ceramics, etc. An absolutely rigid partition would provide optimal silencer performance.

(2) An acoustic liner in one or both of the adjacent ducts is used to cause the phase speed of the fundamental sound mode in the duct to differ substantially from the free space phase speed. If each duct is lined, differences in liner characteristics are used to affect a phase speed difference between the ducts. Flow velocity and temperature differences in the adjacent ducts may be used in addition to the effects of the liner to accentuate the phase speed differences between adjacent ducts.

(3) The adjacent ducts are of <u>equal</u> physical length (i.e. the flow paths are equal) although of unequal acoustical length. (Note that adjacent ducts of unequal physical length can be used to increase the difference in acoustical length between the lined and unlined ducts.)

One or more of these three key features is lacking in each of the cited patents. A nonrigid partition permitting vibrational energy flow coupling between adjacent ducts along their common boundary is used in the devices of Allen and Kürtze, Giordano, and Zorumski (unlike the rigid partition in the Ingard-Patrick device). Different physical path lengths in the adjacent ducts (unlike the equal physical lengths in the Ingard-Patrick device) are essential features of the devices of Bychinsky, Whitney, Luxton, and some of the embodiments proposed by Allen and Kürtze (i.e. Figs. 2, 4 and 9 in Ref. 7). Bychinsky, Whitney, and Luxton do not use an acoustical liner to alter the phase speed of the sound wave in either of the adjacent ducts of their devices (unlike the Ingard-Patrick device in which the influence of a liner on the phase speed is essential). In Appendix 3 each of the patents cited above is considered individually to emphasize specific differences with the parallel lined duct acoustic filter concept presented in this thesis.

1.4 General Operating Principle of a Parallel Lined Duct Filter

To obtain physical insight into the mechanisms causing sound attenuation in a parallel lined duct filter is not easily done. The sound field within the filter is exceedingly complex. Wave reflections occur at each area and impedance discontinuity within the parallel duct array. Indeed, when Stewart[5] studied the Herschel-Quincke tube fifty years ago he observed, "... the waves travel about the circuit in a very complex manner, impossible to follow without resorting to the use of equations." Such a set of equations will be developed in Chap. 3 and with the aid of a digital computer

the equations will be used to predict the transmission loss of parallel lined duct filters over a wide frequency range.

However, a need exists for a set of approximate equations which define the frequencies at which either "destructive interference" or "sing-around interference" causes local maxima in the attenuation spectrum. The approximate size of a parallel lined duct filter required to attenuate sound at a desired frequency can be determined from these equations. However, final facility design will require the evaluation of the transmission loss from Eqs. (3.19a-n).

In the simplified analysis presented in this section the effect of the generation of higher order modes on wave reflection and transmission at the terminations of the branch ducts is not considered. Also the tuning of the branch ducts due to finite length effects, which is implicit in the analysis of Chap. 3, is ignored. It is assumed in the simplified analysis that waves reflected internally at the exit (or entrance) of the branch ducts have a phase change of 180 degree (Fig. 3). Waves transmitted from one branch which are "reflected" in the adjacent branch (e.g. a transmitted wave from the exit of duct A causes a wave to form in the exit of duct B which travels toward the entrance of duct B) are assumed to experience no phase change. This "reflected" wave is considered a continuation of the transmitted wave.

If in a parallel duct filter one branch is lined and the other unlined (Fig. 2) , the difference in phase between the waves in the two branches after q end reflections will be

$$\Delta\phi_1 = \frac{2(q+1)s}{\lambda}\left(\frac{c_0}{c_z} - 1\right)\pi \qquad (1.5a)$$

where s is the length of the filter and λ the wavelength in the unlined branch. In the low frequency limit the value of c_0/c_z is given by Eq.(1.1). Destructive interference effects are expected to occur when $\Delta\phi_1$ is an odd multiple of π. Alternatively when $q = 1$, $\Delta\phi_1$ can be expressed as

$$\Delta\phi_1 = \left[\frac{\mathrm{Re}(k_z)}{k} - 1\right] ks = (2n+1)\pi \qquad n = 0,1,2,\ldots N \tag{1.5b}$$

At either termination of the parallel duct filter, the wave in each branch will not only be reflected within the branch, but will also induce a "reflected" wave in the adjacent branch, as shown schematically in Fig. 3. After r round trips in the parallel duct filter, the difference in phase between the induced wave and the wave incident upon the entrance of the parallel duct filter will be

$$\Delta\phi_2 = \frac{2rs}{\lambda}\left(\frac{c_0}{c_z} + 1\right)\pi \tag{1.6a}$$

When $\Delta\phi_2$ is an even multiple of π, strong reflections are expected to occur at the entrance to the parallel duct filter. This "sing-around" effect is analogous to the reflections caused at selected frequencies by a half-wave resonator. When $r = 1$, the condition for "sing-around" interference can be expressed as

$$\Delta\phi_2 = \left[\frac{\mathrm{Re}(k_z)}{k} + 1\right] ks = 2n\pi \qquad n = 0,1,2,\ldots.N \tag{1.6b}$$

Another configuration of the parallel lined duct filter is shown in cross-sectional view in Fig. 4. This configuration differs from that of Fig. 2 in providing for the splitter to extend longitudinally along the

duct beyond the lined section. This extension (s' in the analysis) does not produce any relative phase shift in the sound waves traveling in the branch ducts but it does increase the round trip path length which determines the frequency at which a strong reflection occurs at the muffler entrance. If the extension is omitted as in Fig. 2, a strong reflection at the muffler entrance may still be obtained solely from the lined branch and the unlined branch when they provide the necessary phase shift. The extension is a convenient means for tuning the muffler to reject a desired frequency since its length may be more readily changed than the length of the liner. The muffler analysis which follows includes the effect of gas flow direction relative to the direction of sound energy from a source (not shown). The lined duct A is considered to be composed of two sections A1 and A2.

Sound and Flow in Same Direction - as shown in Fig. 4
(Exhaust Muffler)

For destructive interference at the muffler exit the sound waves traveling through duct A must be 180° out of phase with the sound waves traveling through duct B. This condition is satisfied when

$$(k^+_{A1}s + k^+_{A2}s') - (k^+_{B1}s + k^+_{B2}s') = (2n + 1)\pi \qquad (1.7)$$

$$n = 0,1,2,\ldots N$$

In this case $k^+_{A2} = k^+_{B2}$ because the duct sections A2 and B2 are unlined. Thus Eq. (1.7) becomes

$$(k^+_{A1} - k^+_{B1})s = (2n + 1)\pi \qquad n = 0,1,2,\ldots N \qquad (1.8)$$

where

$$k^{+} = 2\pi f/c_z^{+} \tag{1.9}$$

f = frequency of incident sound wave

c_z^{+} = phase speed of the fundamental sound mode in the duct for sound traveling in the direction of the mean flow

Reflections at the entrance to the parallel duct muffler will be enhanced at frequencies determined by the following equations:

For clockwise propagation

$$(k_{A1}^{+}s + k_{A2}^{+}s') + (k_{B1}^{-}s + k_{B2}^{-}s') = 2n\pi \tag{1.10a}$$

and for counter-clockwise propagation

$$(k_{B1}^{+}s + k_{B2}^{+}s') + (k_{A1}^{-}s + k_{A2}^{-}s') = 2n\pi \tag{1.10b}$$

where

$$k^{-} = \frac{2\pi f}{c_z^{-}}$$

c_z^{-} = phase speed of the fundamental sound mode in the duct for sound traveling opposite to the direction of mean flow

Equations (1.10a) and (1.10b) show that the intensity of the "sing-around" effect may be diluted by mean flow because resonance caused by counter-clockwise sound propagation will not occur at the same frequency as clockwise resonance except when M = 0.

Sound and Flow in Opposite Directions
(Intake Muffler)

For destructive interference to occur at the muffler exit (i.e. the end of the muffler away from the incident sound wave) the following equation must be satisfied.

$$(k_{A1}^{-}s + k_{A2}^{-}s') - (k_{B1}^{-}s + k_{B2}^{-}s') = (2n + 1)\pi \qquad (1.11)$$

$$n = 0,1,2,\ldots N$$

In this case, $k_{A2}^{-} = k_{B2}^{-}$ because the duct sections are unlined. Thus Eq. (1.11) becomes

$$(k_{A1}^{-} - k_{B1}^{-})s = (2n + 1)\pi \qquad n = 0,1,2,\ldots N \qquad (1.12)$$

Strong reflections will occur at the entrance to the parallel duct muffler at frequencies determined by the following equations:

$$(k_{A1}^{-}s + k_{A2}^{-}s') + (k_{B1}^{+}s + k_{B2}^{+}s') = 2n\pi \qquad (1.13a)$$

$$(k_{B1}^{-}s + k_{B2}^{-}s') + (k_{A1}^{+}s + k_{A2}^{+}s') = 2n\pi \qquad (1.13b)$$

$$n = 0,1,2,\ldots N$$

For M = 0, Eqs. (1.13a) and (1.13b) are identical. Also note that Eqs. (1.13a) and (1.13b) are equal to (1.10b) and (1.10a), respectively. This shows that the frequencies at which increased reflections occur at the entrance to the parallel duct muffler are independent of the direction of the mean flow in the duct.

To evaluate Eqs. (1.7) - (1.13) requires a knowledge of the phase speed of the sound waves in each of the branch ducts in the presence of mean flow. An analysis performed in Chap. 2 shows that in the low frequency limit the phase speed of the fundamental sound mode in a lined duct with flow can be expressed as follows.

Phase speed in the direction of flow:

$$\frac{c_z^+}{c_0} = (1 + M) \frac{1 - M}{\sqrt{1 + 2\xi + \xi^2 M^2} - M(1 + \xi)} \tag{1.14}$$

Phase speed opposite to the direction of flow:

$$\frac{c_z^-}{c_0} = (1 + M) \frac{1 - M}{\sqrt{1 + 2\xi + \xi^2 M^2} + M(1 + \xi)} \tag{1.15}$$

where M is the Mach number of the flow in the duct and ξ is a geometric parameter defined as follows:

$$\xi = \frac{V_L}{V_a}$$

where V_L is the volume of the void space in the liner and V_a is the volume of the airspace in the duct between the liner and the opposite wall.

At M = 0 Eqs. (1.14) and (1.15) reduce to

$$\frac{c_z^+}{c_0} = \frac{c_z^-}{c_0} = \frac{c_z}{c_0} = \frac{1}{\sqrt{1 + 2\xi}} \tag{1.16}$$

For the rectangular duct geometry of Figs. 2 or 4

$$\xi = \frac{\Omega L}{2b} \tag{1.17}$$

where

b is the duct height between liner and splitter,

L is the thickness of the liner and

Ω is the liner porosity.

For the annular duct configuration shown in the longitudinal cross section in Fig. 5a and transverse cross section in Fig. 5b

$$\xi = \left[\frac{1}{1 - \left(\frac{r_h}{r_t}\right)^2}\right]\left(\frac{\Omega L}{r_t}\right)\left(1 + \frac{\Omega L}{2r_t}\right) \tag{1.18}$$

The splitter in Fig. 5 is hollow to allow the acoustic energy to travel through it as well as between it and the liner. The same design considerations apply as for the rectangular liner for determining the frequency of maximum transmission loss.

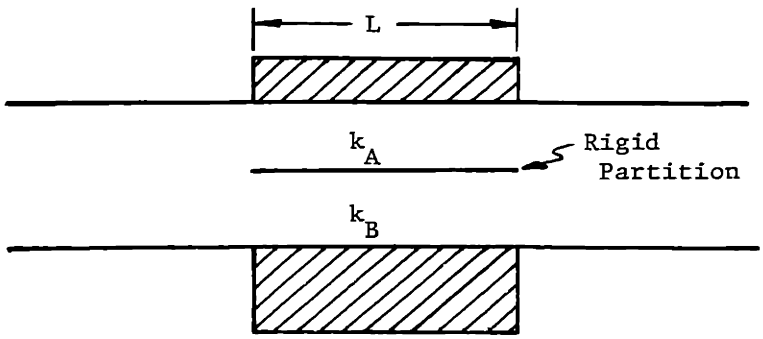

a) Parallel Lined Ducts (reactive-dissipative).

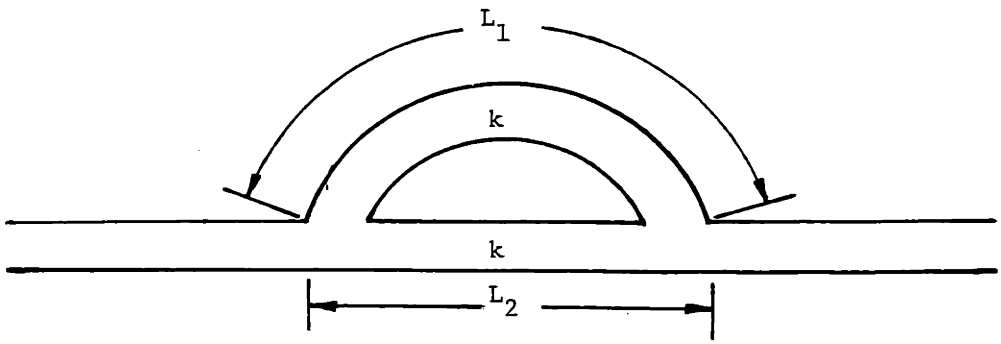

b) Herschel-Quincke Tube (reactive).

FIG. 1: PARALLEL DUCT ACOUSTIC FILTERS

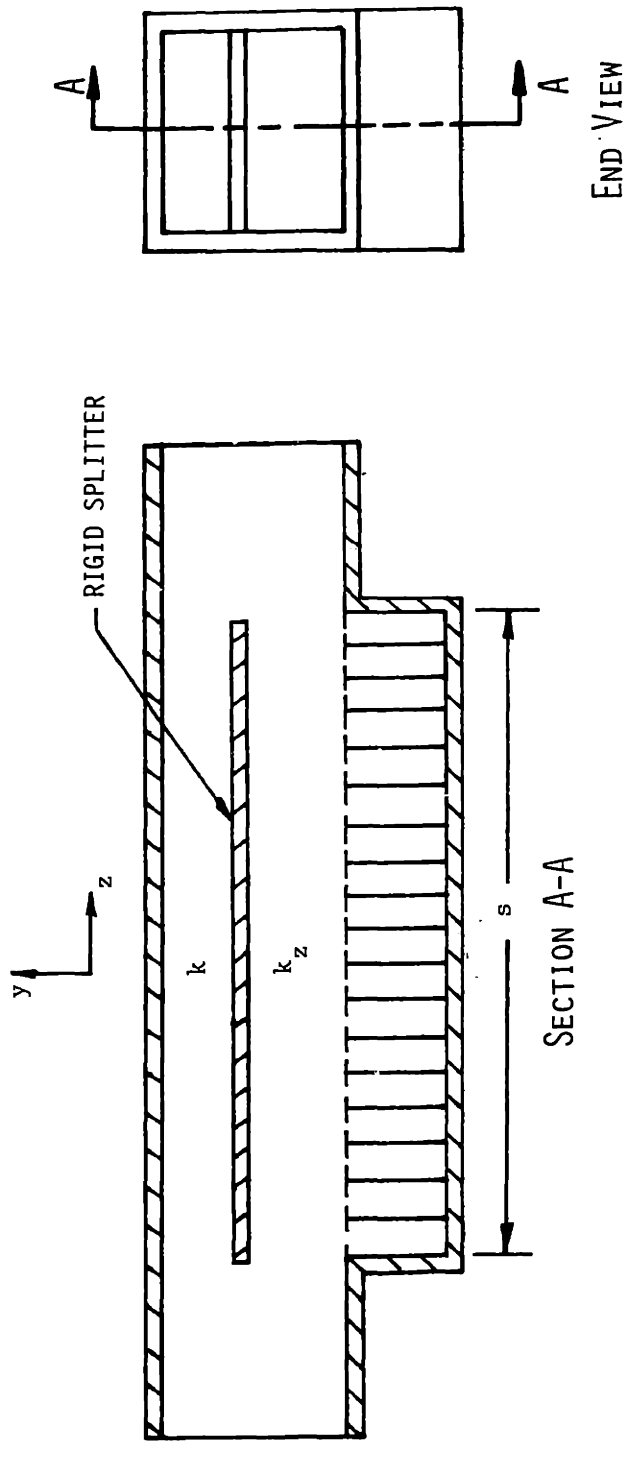

FIG. 2: REACTIVE PARALLEL LINED DUCT FILTER (RECTANGULAR CONFIGURATION)

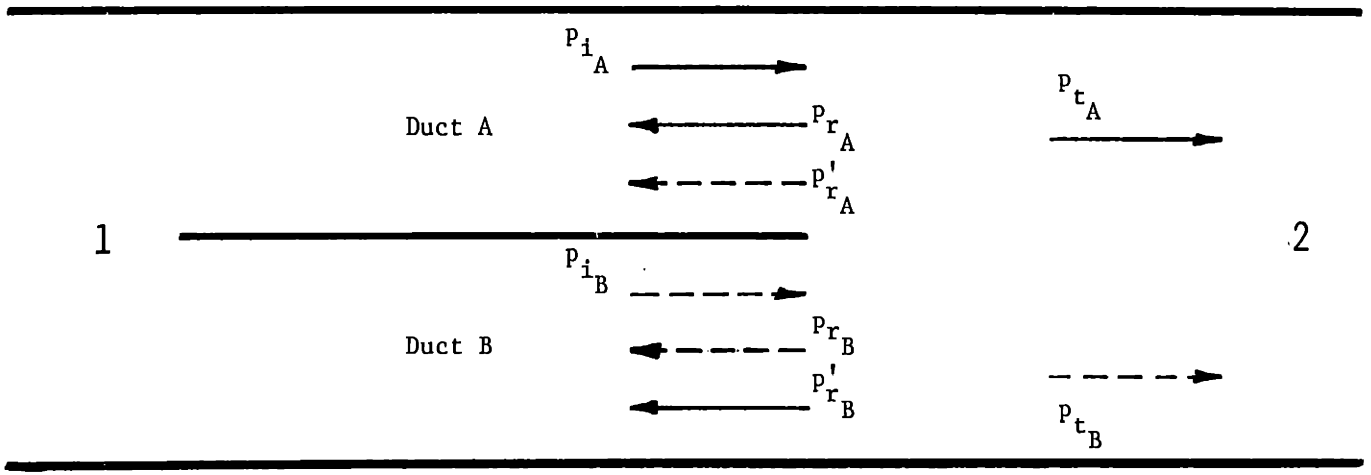

FIG. 3 : REFLECTION CONDITION AT EXIT OF PARALLEL DUCTS

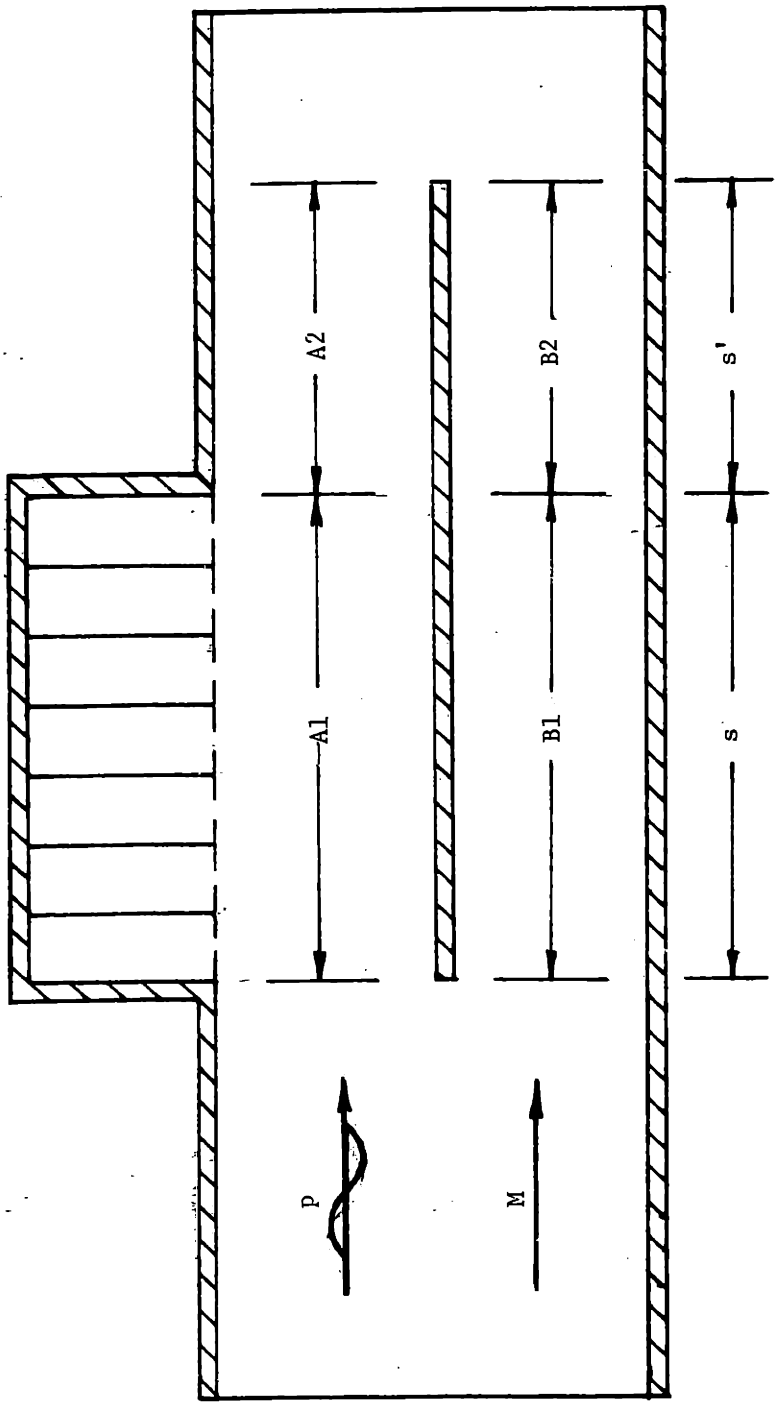

FIG. 4: REACTIVE PARALLEL LINED DUCT FILTER WITH EXTENDED SPLITTER

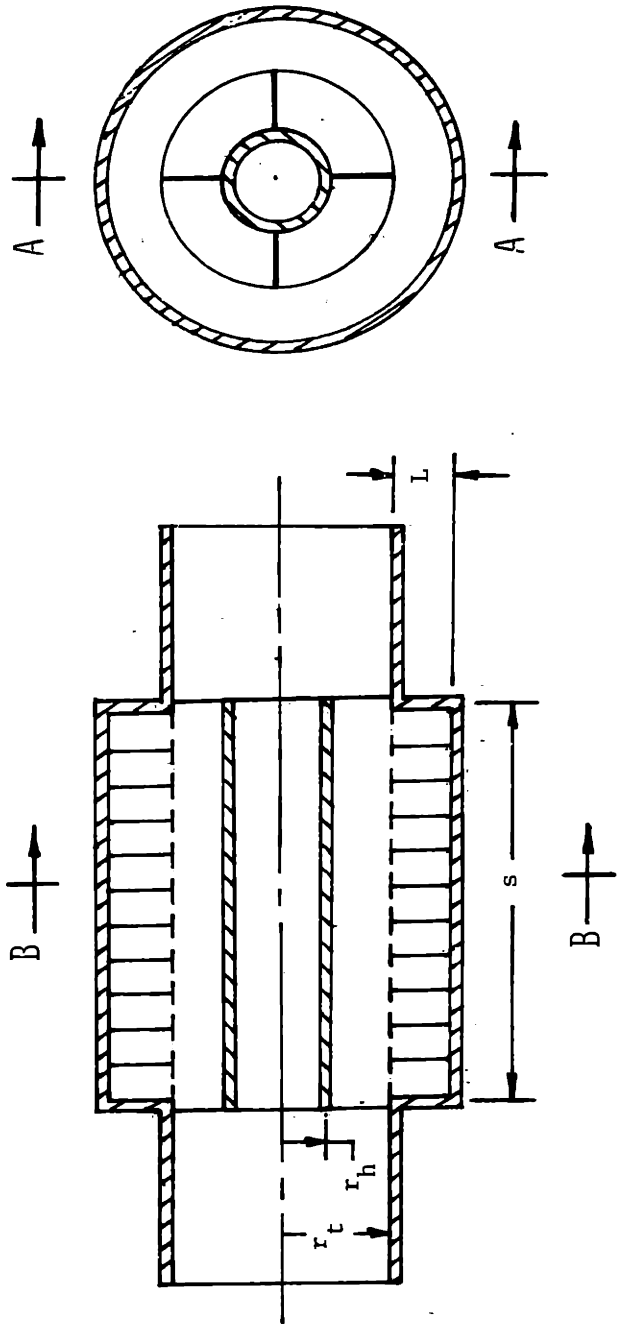

SECTION B-B

SECTION A-A

FIG. 5: REACTIVE PARALLEL LINED DUCT FILTER (CIRCULAR CYLINDRICAL CONFIGURATION)

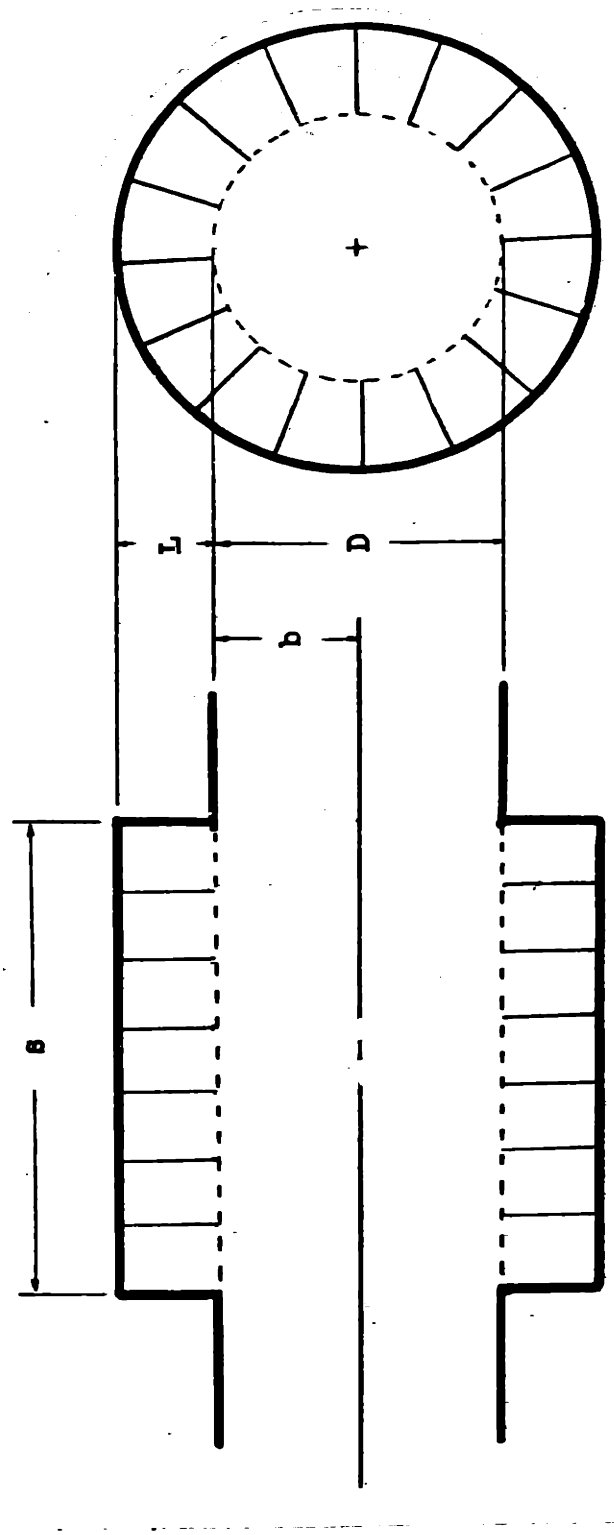

FIG. 6: CIRCULAR DUCT WITH RESONATOR LINER

CHAPTER II

SOUND TRANSMISSION IN CONSTANT AREA DUCTS

In this chapter, the characteristics of sound transmission in constant area ducts are examined. The purpose of this study is to provide a better understanding of the sound transmission within each branch of an acoustic filter consisting of lined ducts in parallel. Therefore, the study will concentrate on the transmission of the fundamental mode at low frequencies only. Lined and unlined ducts will be considered both with and without mean flow.

In Section 2.1 the development of the acoustics of lined ducts is reviewed briefly. The paucity of analysis or data relating the phase speed in the duct to the liner characteristics is noted.

In Section 2.2 an expression for the phase speed at low frequencies is developed for circular, annular and rectangular ducts lined with point-reacting liners with mean flow. Expressions for both porous and resonator liners are obtained.

In Section 2.3 experimental measurements of the phase speed of the fundamental mode in a lined rectangular duct are presented. Soda-straw (point-reacting), partitioned foam, and unpartitioned foam (distributed reaction) liners were tested. The effect of liner reaction on phase speed is noted.

In Section 2.4 measurements of visco-thermal and sound-turbulence interaction losses in rigid rectangular and circular ducts is presented. The purpose of the measurements was to verify existing theories on

parasitic losses in rigid ducts and to assess the effect of visco-thermal losses on model-scale parallel duct muffler performance.

2.1 Duct Acoustics - Historical Perspective

The study of sound transmission in lined ducts began in the late 1930's with the pioneering efforts of Sivian[13] and Morse.[14] Sivian determined the attenuation at low frequencies in rectangular ducts lined with dissipative liners. Morse developed a more general analysis for determining the attenuation and phase speed of sound waves in ducts lined with point-reacting liners. Morse's theory which is applicable to both the fundamental and higher order modes in either rectangular or circular ducts formed the basis for the prediction of sound propagation in lined ducts without flow for almost 20 years. At that time, in the late 1950's, the requirements for silencing the jet engine then going into commercial production stimulated frantic efforts by aircraft manufacturers to develop noise prediction techniques applicable to aircraft engine environments. A recent article by Vaidya and Dean,[15] which reviewed the results of those efforts over the past two decades, shows that highly sophisticated techniques have been developed for predicting the attenuation of sound in aircraft engine ducts.

These sophisticated techniques are not required though for non-flowing ducts having point-reacting liners for which Morse's theory is sufficiently accurate for most applications. However, Morse's theory is cumbersome to use because it requires that the complex wavenumber in a duct with a known wall admittance be determined from a "Morse Chart" which is a mapping of a

conformal transformation between an admittance parameter and a wavenumber parameter used in the dispersion relation. Galaitsis and Ingard[16] eliminated this graphical step by inputing the coordinates of the Morse Chart into a data file and then writing a numerical searching algorithm to determine the roots (i.e., complex wavenumbers) of the dispersion relation from the Morse Chart. Cho and Ingard[2,17] expanded upon the work of Galaitsis and Ingard by presenting a parametric study of the effect of liner configuration and flow resistance on the phase speed (and the attenuation) in rectangular and cylindrical ducts lined with porous or resonator point-reacting liners. Their work appears to be the most comprehensive study of the effect of point-reacting liners on the phase speed of the fundamental mode in a lined duct.

In air conditioning ducts and mufflers with parallel baffles, liners of fiberglass, acoustic foam or other bulk materials are used to provide broadband attenuation of low frequency noise. Ducts lined with such bulk materials have surfaces of distributed reaction unless the liner is segmented with rigid partitions aligned normal to the duct axis to prevent sound waves from propagating in the axial direction within the liner. If the partitions are spaced closer than a quarter wavelength apart the liner will usually act as a point-reacting liner[18] and Morse's theory can be used. For unpartitioned (i.e., non-locally reacting) bulk liners Scott[19,20] developed a theory involving coupled waves propagating axially in the duct and the liner. His results showed that at low frequencies ($kL < 0.5$) non-locally reacting liners attenuated the fundamental sound mode more than point-reacting liners whereas at higher frequencies point-reacting liners

provided better attenuation. The phase speed of the fundamental mode was shown to be lower in a duct lined with a point-reacting rather than a distributed reaction liner at all frequencies considered ($0 < kL < 3.7$). The analysis of ducts having bulk liners has been extended to predict the attenuation in ducts having non-isotropic liners[21] and for ducts with mean flow.[22,23] However, the original studies by Scott remain as the only studies which explicitly considered the effect of bulk liners on the phase speed of the fundamental sound mode in soft-walled ducts.

To date the development of duct acoustics has been primarily directed toward determining the effects of liner configuration on the attenuation in single channel ducts. Liners have been designed which effectively attenuate sound in the medium to high frequency range but low frequency ($f < 100$ Hz) sound attenuation using standard techniques requires massive expensive mufflers. The enforcement of existing regulations governing low frequency noise emissions by the Environmental Protection Agency may stimulate efforts to develop more efficient methods to attenuate low frequency sound. The development of novel techniques involving sound cancellation rather than duct attenuation by acoustic liners may be necessary before cost-effective low-frequency mufflers can be produced. These sound cancellation techniques, whether they use active in-duct sound cancellation[24] with microphones and speaker arrays or use passive lined parallel ducts[25] require a better understanding of the phase speed characteristics of lined ducts. However, no work has been conducted having a primary emphasis on the design of liners to produce specified phase speed characteristics in ducts. Decoupling (if possible) the effects

of a liner on the attenuation and phase speed in a duct has not been studied. In particular, the development of liners producing comparable attenuation spectra but different phase speeds, which would be ideal for parallel ducts, has not been tried.

In the following section a first step is made toward obtaining a better understanding of the effect of liner configurations on the phase speeds in lined ducts. Approximate expressions are derived for phase speeds in lined rectangular, circular or annular ducts with flow. These expressions should be especially useful in determining the length of the splitter plate required for optimal attenuation in a lined parallel duct filter.

2.2 Low Frequency Approximation to the Phase Speed in a Lined Duct

2.2.1 General Expression for Circular and Annular Ducts

The convected wave equation in cylindrical coordinates can be written as

$$\frac{1}{c^2}\frac{\partial^2 p}{\partial t^2} + 2\frac{M}{c}\frac{\partial^2 p}{\partial z \partial t} = (1 - M^2)\frac{\partial^2 p}{\partial z^2} + \frac{\partial^2 p}{\partial r^2} + \frac{1}{r}\frac{\partial p}{\partial r} \tag{2.1}$$

The average acoustic pressure across the annulus can be defined as

$$\overline{p(z)} = \frac{1}{A}\int\int p(r,\theta,z)\, r\, dr\, d\theta \tag{2.2}$$

where $A = \pi(r_t^2 - r_h^2)$.

Since $\frac{\partial p}{\partial z}$ and $\frac{\partial p}{\partial t}$ are independent of r and θ, Eq. (2.1) can be rewritten as

$$\frac{1}{c^2}\frac{\partial^2\bar{p}}{\partial t^2} + 2\frac{M}{c}\frac{\partial^2\bar{p}}{\partial z\partial t} - (1 - M^2)\frac{\partial^2\bar{p}}{\partial z^2} = \frac{1}{A}\int_0^{2\pi}\int_{r_h}^{r_t}\left(\frac{\partial^2 p}{\partial r^2} + \frac{1}{r}\frac{\partial p}{\partial r}\right) r\, dr\, d\theta \tag{2.3}$$

For a harmonic excitation

$$\frac{\partial}{\partial t} = -i\omega \qquad \frac{\partial}{\partial z} = ik_z \tag{2.4a,b}$$

and Eq. (2.3) can be written as

$$\left[-\left(\frac{\omega}{c}\right)^2 + \frac{\omega}{c}k_z M + k_z(1 - M^2)\right]\bar{p} = \frac{1}{A}\int_0^{2\pi}\int_{r_h}^{r_t}\left(\frac{\partial^2 p}{\partial r^2} + \frac{1}{r}\frac{\partial p}{\partial r}\right) r\, dr\, d\theta \tag{2.5}$$

But

$$\int_0^{2\pi}\int_{r_h}^{r_t}\left(\frac{\partial^2 p}{\partial r^2} + \frac{1}{r}\frac{\partial p}{\partial r}\right) r\, dr\, d\theta = 2\pi\left[\left(r\frac{\partial p}{\partial r}\right)_{r=r_t} - \left(r\frac{\partial p}{\partial r}\right)_{r=r_h}\right] \tag{2.6}$$

To evaluate the left hand side of Eq. (2.6) use the momentum equation in the radial direction

$$\rho\left(\frac{\partial v_r}{\partial t} + V_z\frac{\partial v_r}{\partial z}\right) = -\frac{\partial p}{\partial r} \tag{2.7a}$$

which for harmonic excitation can be written as

$$\rho(i\omega - ik_z V_z)v_r = \frac{\partial p}{\partial r} \tag{2.7b}$$

To determine v_r note that the acoustic admittance at the boundary is given by the expression

$$\eta = \rho c\left(\frac{v_r}{p}\right)_{\text{boundary}} \tag{2.8}$$

Using Eq. (2.8) in Eq. (2.7) the radial pressure gradient at the boundaries can be determined

$$\left.\frac{\partial p}{\partial r}\right|_{r=r_t} = i k \eta_t p_t \left(1 - \frac{k_z}{k} M\right) \tag{2.9a}$$

$$\left.\frac{\partial p}{\partial r}\right|_{r=r_h} = -i k \eta_h p_h \left(1 - \frac{k_z}{k} M\right)$$

For a rigid wall, $\eta_h = 0$. Thus $\left.\frac{\partial p}{\partial r}\right|_{r=r_h} = 0$ (2.9b)

Evaluating Eq. (2.6) using Eqs. (2.9a) and (2.9b) and substituting the results into Eq. (2.5) yields

$$k_z^2 + \frac{2Mkk_z}{1-M^2}\left(1 + i\frac{S}{2A}\frac{\eta_t\beta}{k}\right) - \frac{k^2}{1-M^2}\left(1 + i\frac{S}{A}\frac{\eta_t\beta}{k}\right) = 0 \tag{2.10}$$

where S/A is the area of the lined perimeter to the cross-sectional area of the duct and β is a pressure distribution parameter given by the following expression

$$\beta = \frac{p_t}{\bar{p}}$$

Factoring Eq. (2.10) yields

$$\frac{k_z}{k} = -\frac{M}{1-M^2}(1 + i\delta) \pm \frac{1}{1-M^2}\sqrt{1+i2\delta-\delta^2M^2} \tag{2.11a}$$

where

$$\delta = \frac{S}{2A}\frac{\eta_t\beta}{k} \tag{2.11b}$$

2.2.1.1 Circular Duct with a Resonator Liner

To obtain the phase speed of the fundamental mode from Eq. (2.11a) requires an expression for the admittance at the liner surface. In general, the admittance, η , which is the reciprocal of the impedance, ζ, can be written as

$$\eta^{-1} = \zeta = \theta + i\chi \tag{2.12}$$

where θ and χ are the flow resistance and the normalized wall reactance of the liner respectively. For a purely reactive liner the flow resistance is zero and the admittance becomes

$$\eta = - i/\chi$$

For a purely reactive resonator liner in a circular duct (Fig. 6) Cho and Ingard[17] have shown that χ can be expressed as

$$\chi = - \frac{H_0^{(1)}(kb) + \alpha H_0^{(2)}(kb)}{H_1^{(1)}(kb) + \alpha H_1^{(2)}(kb)} \tag{2.13a}$$

where

$$\alpha = - \frac{H_1^{(1)}[k(b+L)]}{H_1^{(2)}[k(b+L)]} \tag{2.13b}$$

At low frequencies χ can be approximated to first order as (see Appendix II)

$$\chi = \frac{2}{kr_i\left[\left(\frac{r_o}{r_i}\right)^2 - 1\right]} \tag{A2.9}$$

where $r_i = b$ and $r_o = b + L$.

Equation (2.11b) can then be written as

$$\delta = -\frac{i}{2}\left[\left(\frac{r_o}{r_i}\right)^2 - 1\right] \tag{2.14}$$

Note that at M = 0, Eq. (2.11a) reduces to a particularly simple expression for the phase speed of the fundamental sound mode in the duct

$$\frac{\mathrm{Re}(k_z)}{k} = \frac{r_o}{r_i} \tag{2.15}$$

which is equal to

$$\frac{\mathrm{Re}(k_z)}{k} = \left[\frac{\text{Void space in duct and liner}}{\text{Void space in duct}}\right]^{1/2}$$

For flow speeds in the range $0 \leq M \leq 1$ the phase speeds of positive- and negative-going waves have been calculated for various liner thicknesses and are presented in Fig. 7a.

2.2.1.2 Annular Duct with a Resonator Liner

For the annular duct configuration shown in Fig. 5 the specific acoustic admittance at the surface of the lined outer wall can be approximated to first order as

$$\eta = -ikL\left(1 + \frac{L}{2r_t}\right) \tag{2.16}$$

Then for $\beta = 1$,

$$\delta = -i\,\frac{r_t}{r_t^2 - r_h^2}\,L\left(1 + \frac{L}{2r_t}\right) \tag{2.17}$$

Substituting Eq. (2.17) into Eq. (2.11a) yields the simple expression

$$\frac{\mathrm{Re}(k_z)}{k} = \left\{ \frac{(r_t+L)^2 - r_h^2}{r_t^2 - r_h^2} \right\}^{1/2} \tag{2.18}$$

which is equal to

$$\frac{\mathrm{Re}(k_z)}{k} = \left[\frac{\text{Void space in duct and liner}}{\text{Void space in duct}} \right]^{1/2}$$

For flow speeds in the range $0 \leq M \leq 1$ the phase speeds of positive- and negative-going waves have been calculated for various liner thicknesses for an annular duct having $r_h/r_t = 0.5$. They are presented in Fig. 7b.

2.2.2 General Expression for Rectangular Ducts

It can be shown that Eqs. (2.11a) and (2.11b) hold for a rectangular duct as well as a cylindrical or annular duct. The convected wave equation in rectangular coordinates can be written as

$$\frac{1}{c^2}\frac{\partial^2 p}{\partial t^2} + 2\,\frac{M}{c}\frac{\partial^2 p}{\partial z \partial t} = (1 - M^2)\frac{\partial^2 p}{\partial z^2} + \frac{\partial^2 p}{\partial x^2} + \frac{\partial^2 p}{\partial y^2} \tag{2.19}$$

Integrating Eq. (2.19) across the duct and using the assumption of harmonic excitation yields

$$\left[-\left(\frac{\omega}{c}\right)^2 + \frac{\omega}{c} k_z M + k_z\left[1-M^2\right] \right]\bar{p} = \frac{1}{A}\left[\ell_y \left(\left.\frac{\partial p}{\partial x}\right|_{x=\ell_x} - \left.\frac{\partial p}{\partial x}\right|_{x=0} \right) \right.$$

$$\left. + \ell_x \left(\left.\frac{\partial p}{\partial y}\right|_{y=\ell_y} - \left.\frac{\partial p}{\partial y}\right|_{y=0} \right) \right] \tag{2.20}$$

Using the momentum equation in the y-direction,

$$\rho\left(\frac{\partial}{\partial t} + V\frac{\partial}{\partial z}\right)u_y = -\frac{\partial p}{\partial y} \tag{2.21}$$

the pressure gradients in the y-direction can be determined

$$\left.\frac{\partial p}{\partial y}\right|_{y=\ell_y} = i\omega\rho\frac{\eta_y}{\rho c}\left.p_b\right|_{y=\ell_y}\left(1-\frac{k_z}{k}M\right) \tag{2.22a}$$

$$\left.\frac{\partial p}{\partial y}\right|_{y=0} = -i\omega\rho\frac{\eta_y}{\rho c}\left.p_b\right|_{y=0}\left(1-\frac{k_z}{k}M\right) \tag{2.22b}$$

Therefore it follows that

$$\ell_x\left(\left.\frac{\partial p}{\partial y}\right|_{y=\ell_y} - \left.\frac{\partial p}{\partial y}\right|_{y=0}\right) = 2i\eta_y(k-k_z M)\bar{p}_{b_y}\ell_x \tag{2.23}$$

where the average boundary pressure amplitude, $\bar{p}_{b_y}$, is

$$\bar{p}_{b_y} = \frac{1}{2}\left[p_{b_y}(0) + p_{b_y}(\ell_y)\right]$$

Similarly

$$\ell_y\left(\left.\frac{\partial p}{\partial x}\right|_{x=\ell_x} - \left.\frac{\partial p}{\partial x}\right|_{x=0}\right) = 2i\eta_x(k-k_z M)\bar{p}_{b_x}\ell_y \tag{2.24}$$

where

$$\bar{p}_{b_x} = \frac{1}{2}\left[p_{b_x}(0) + p_{b_x}(\ell_x)\right]$$

If all walls are lined identically

$$\eta_x = \eta_y = \eta \quad \text{and} \quad \bar{p}_{b_x} \simeq \bar{p}_{b_y} \simeq \bar{p}_b \tag{2.25}$$

Equations (2.20), (2.23), (2.24) and (2.25) can then be combined into a form which is identical to Eq. (2.11) with $\beta = \bar{p}_b/p$.

To determine the wavenumber in the lined duct requires an expression for the frequency-dependent wall admittance, η. In the next section the wall admittance for a purely reactive resonator liner is approximated to first order. In the following two sections, third order approximations to the wall admittance are obtained for a resonator liner with a resistive screen facing and for a point-reacting porous liner.

2.2.2.1 Rectangular Duct Lined on One Wall with a Purely Reactive Resonator Liner

The specific acoustic impedance of a purely reactive resonator liner of depth L is

$$\zeta = i \cot(kL) \tag{2.26}$$

Using a first order approximation to the cotangent

$$\cot(kL) \simeq \frac{1}{kL} \tag{2.27}$$

the specific acoustic admittance can be written as

$$\eta = \zeta^{-1} = - ikL \tag{2.28}$$

For a duct having height b, which is lined on only one wall, S/A in Eq. (2.10) equals 1/b. Also, assuming a uniform pressure distribution across the duct (i.e., $\beta = 1$) Eq. (2.11b) becomes

$$\delta = -i \frac{L}{2b} \tag{2.29}$$

Substituting Eq. (2.29) into Eq. (2.11a) the phase speed of the fundamental sound mode can be approximated as

$$\frac{c_z^{\pm}}{c_0} = (1 + M)\,\frac{1 - M}{\sqrt{1+\frac{L}{b}+\left(M\,\frac{L}{2b}\right)^2} \mp M\left(1+\frac{L}{2b}\right)} \tag{2.30}$$

Note that at $M = 0$ Eq. (2.30) becomes

$$\frac{c_z^{\pm}}{c_0} = \pm\,(1 + \frac{L}{b})^{-1/2} \tag{2.31}$$

which is equivalent to

$$\frac{c_z^{\pm}}{c_0} = \left[\frac{\text{Void space in duct and liner}}{\text{Void space in duct}}\right]^{-1/2}$$

For flow speeds in the range $0 \leq M \leq 1$ the phase speeds of positive- and negative-going waves have been calculated for various liner thicknesses for a rectangular duct of height D lined on one wall with a liner of thickness L. They are presented in Fig. 7c.

2.2.2.2 Rectangular Duct Lined on One Wall with a Resonator Liner with a Resistive Screen Facing

The specific acoustic impedance of a resonator liner of depth L with a resistive screen facing having a flow resistance θ is

$$\zeta = \theta + i\,\cot(kL) \tag{2.32}$$

Using the third order approximation of the cotangent

$$\cot(kL) \simeq \frac{1}{kL} - \frac{kL}{3} \tag{2.33}$$

the specific acoustic admittance can be written as

$$\eta = \frac{1}{\zeta} = \frac{\theta(kL)^2 - ikL\left[1 - \frac{(kL)^2}{3}\right]}{\theta^2(kL)^2 + \left[1 - \frac{(kL)^2}{3}\right]^2} \tag{2.34}$$

For a duct having height b, which is lined on only one wall, S/A in Eq. (2.10) equals 1/b. Also, assuming a uniform pressure distribution across the duct (i.e., $\beta = 1$), Eq. (2.11b) becomes

$$\delta = \frac{L/b}{2kL}\left\{\frac{\theta(kL)^2}{\theta^2(kL)^2 + [1-\frac{(kL)^2}{3}]^2} - \frac{ikL[1-\frac{(kL)^2}{3}]}{\theta^2(kL)^2 + [1-\frac{(kL)^2}{3}]^2}\right\} \tag{2.35}$$

Both the real and imaginary parts of k_z can be determined from Eq. (2.11a) after evaluating δ. Substituting Eq. (2.35) into Eq. (2.11a) and assuming $\theta\, k\, L << 1-(kL)^2/3$, the real part of k_z (i.e., the phase speed) is determined as

$$\frac{Re(k_z)}{k} = -\frac{M}{1-M^2}\left[1+\frac{L}{2b}F(\theta,kL)\right] \pm \frac{1}{1-M^2}\left[1+\frac{L}{b}F(\theta,kL)+M^2\frac{(L/b)^2}{4}F^2(\theta,kL)\right]^{1/2} \tag{2.36a}$$

where

$$F(\theta,kL) = \frac{1-\frac{(kL)^2}{3}}{(\theta kL)^2 + [1-\frac{(kL)^2}{3}]^2} \tag{2.36b}$$

For positive- and negative-going waves in the duct the phase speed is

$$\frac{c_z^+}{c_0} = (1+M)\frac{1-M}{\sqrt{1+\frac{L}{b}F(\theta,kL)+\frac{1}{4}(\frac{L}{b})^2M^2F^2(\theta,kL)} - M[1+\frac{L}{2b}F(\theta,kL)]} \tag{2.37a}$$

$$\frac{c_z^-}{c_0} = (1+M)\frac{1-M}{\sqrt{1+\frac{L}{b}F(\theta,kL)+\frac{1}{4}(\frac{L}{b})^2M^2F^2(\theta,kL)} + M[1+\frac{L}{2b}F(\theta,kL)]} \tag{2.37b}$$

At M = 0, the phase speed for both positive- and negative-going waves reduces to

$$\frac{c_z^+}{c_0} = \frac{c_z^-}{c_0} = \frac{1}{\sqrt{1+\frac{L}{b}F(\theta,kL)}} \qquad M = 0 \tag{2.38}$$

At M = 1, the phase speed for negative-going waves, determined from Eq. (2.37b), reduces to zero.

$$\frac{c_z^-}{c_0} = 0 \qquad M = 1 \tag{2.39}$$

To determine the phase speed for positive-going waves at M = 1 is a bit more complicated because the denominator of Eq. (2.36a) goes to zero as M approaches unity. To avoid the problem expand the denominator in the following manner:

$$[1 + \frac{L}{b}F + \frac{1}{4}(\frac{L}{b})^2 M^2 F^2]^{1/2} = M(1+\frac{L}{2b}F)\left\{1+\frac{(1-M^2)(1+\frac{L}{b}F)}{[M(1+\frac{L}{2b}F)]^2}\right\}^{1/2} \tag{2.40}$$

As M approaches unity the square root on the right hand side of Eq. (2.40) can be expanded

$$\left\{1 + \frac{(1-M^2)(1+\frac{L}{b}F)}{[M(1+\frac{L}{2b}F)]^2}\right\}^{1/2} = 1 + \frac{(1-M^2)(1+\frac{L}{b}F)}{2[M(1+\frac{L}{2b}F)]^2} \tag{2.41}$$

Using the approximation in Eq. (2.41), Eq. (2.37a) reduces to

$$\lim_{M\to 1}\left[\frac{c_z^+}{c_0}\right] = \lim_{M\to 1}\left[\frac{2M(1+\frac{L}{2b}F)}{1+\frac{L}{b}F}\right] = \frac{2+\frac{L}{b}F}{1+\frac{L}{b}F} \tag{2.42}$$

2.2.2.3 Rectangular Duct Lined on One Wall with a Point-Reacting Porous Liner

Consider a rectangular duct lined with a point-reacting porous liner as shown in Fig. 8. The wavenumber of the fundamental mode in the duct is composed of y and z components

$$k^2 = k_y^2 + k_z^2 \tag{2.43}$$

where k_y is the first root of the equation

$$k_y b \tan(k_y b) + i \frac{kb}{\zeta} = 0 \tag{2.44}$$

The specific acoustic impedance of the liner can be written as

$$\zeta = \frac{iqL}{\Omega kL} \cot(qL) \tag{2.45}$$

where Ω is the porosity of the porous liner and q, the wavenumber in the liner, is given by

$$\mathrm{Re}(qL) = kL \sqrt{\frac{\bar{\gamma}}{2}} \left[\sqrt{1 + \left(\frac{\theta}{kL}\right)^2} + 1 \right]^{1/2} \tag{2.46a}$$

$$\mathrm{Im}(qL) = kL \sqrt{\frac{\bar{\gamma}}{2}} \left[\sqrt{1 + \left(\frac{\theta}{kL}\right)^2} - 1 \right]^{1/2} \tag{2.46b}$$

where $\bar{\gamma}$ and θ are the structural factor and the specific flow resistance of the liner respectively.

To obtain a solution to Eq. (2.44) which is valid at low frequencies (i.e., $kL < 1$) replace cot(qL) in Eq. (2.45) with the third order expansion given in Eq. (2.33)

$$\zeta = \frac{i}{\Omega kL} \left[1 - \frac{(qL)^2}{3} \right] \tag{2.47}$$

Substituting Eq. (2.47) into Eq. (2.44), assuming $k_y b << 1$, and using the resulting expression for k_y in Eq. (2.43) yields

$$k_z^2 = k^2 \left\{ 1 + \frac{\Omega L/b}{\left[1 - \frac{(qL)^2}{3} \right]} \right\} \tag{2.48}$$

By using Eqs. (2.46a) and (2.46b) in (2.48) it can be shown after some algebraic manipulation that

$$qL = kL\sqrt{\bar{\gamma}} \left[1 + i \left(\frac{\theta}{kL} \right) \right]^{1/2} \tag{2.49}$$

The specific acoustic admittance can then be written as

$$\eta = \frac{1}{\zeta} = \frac{\frac{\bar{\gamma}\theta}{3}(kL)^2 - ikL\left[1 - \frac{\bar{\gamma}(kL)^2}{3}\right]}{\left(\frac{\bar{\gamma}\theta}{3}\right)^2 (kL)^2 + \left[1 - \frac{\bar{\gamma}(kL)^2}{3}\right]^2} \qquad (\Omega = 1) \tag{2.50}$$

For a duct lined on one wall with a point-reacting porous liner the complex wavenumber in the convected sound field is determined from Eq. (2.11) with the impedance parameter, δ, given by the expression

$$\delta = -i \frac{\Omega L}{2b} G(\bar{\gamma}, \theta, kL) \left[1 - i \frac{\frac{\bar{\gamma}\theta}{3}(kL)}{1 - \frac{\bar{\gamma}(kL)^2}{3}} \right] \tag{2.51a}$$

where

$$G(\bar{\gamma}, \theta, kL) = \frac{1 - \frac{\bar{\gamma}(kL)^2}{3}}{\left(\frac{\bar{\gamma}\theta}{3}\right)^2 (kL)^2 + \left[1 - \frac{\bar{\gamma}(kL)^2}{3}\right]^2} \tag{2.51b}$$

When only the real part of k_z (i.e. the phase speed) is to be determined Eqs. (2.51a,b) and (2.11a) can be combined and simplified for $\bar{\gamma}\theta kL/3 << 1-\bar{\gamma}(kL)^2/3$

$$\frac{k_z}{k} = -\frac{M}{1-M^2}\left[1+\frac{\Omega L}{2b}G(\bar{\gamma},\theta,kL)\right] \pm \frac{1}{1-M^2}\left[1+\frac{\Omega L}{b}G(\bar{\gamma},\theta,kL)+M^2\left(\frac{\Omega L}{2b}\right)^2 G^2(\bar{\gamma},\theta,kL)\right]^{1/2} \tag{2.52}$$

Note that the expression for the phase speed in a rectangular duct with a point-reacting porous liner, Eq. (2.52), is analogous to Eqs. (2.37a,b) in Sec. 2.2.2.2 for the phase speed in a duct lined with a resonator lining with a resistive facing sheet. Following the procedure used in Sec. 2.2.2.2 to take the limits of Eqs. (2.37a,b), the phase speed for positive- and negative-going waves at the M = 0 and M = 1 limits can be shown to be

$$\frac{c_z^+}{c_0} = \frac{c_z^-}{c_0} = \frac{1}{\sqrt{1+\frac{\Omega L}{b}G(\bar{\gamma},\theta,kL)}} \qquad M = 0 \tag{2.53a,b}$$

$$\frac{c_z^-}{c_0} = 0 \qquad \frac{c_z^+}{c_0} = \frac{2+\frac{\Omega L}{b}G(\bar{\gamma},\theta,kL)}{1+\frac{\Omega L}{b}G(\bar{\gamma},\theta,kL)} \qquad M = 1 \tag{2.53c,d}$$

In Fig. 9, the phase speed of the fundamental mode in a non-flowing duct is compared to the exact solution of the dispersion relation for the case $\Omega = 1$, $\bar{\gamma} = 1.5$ and $L/b = 7$ over the frequency range $0.1 \leq kL \leq 1$ for $\theta = 0.5$, 1.0, 2.0 and 4.0. The third order approximation follows the exact solution quite well with a maximum error of less than 5% over the frequency range for which Eq. (2.53a) is valid (i.e., $kL < \frac{2}{\theta}\left[1-\frac{(kL)^2}{2}\right]$).

2.3 Experimental Measurements of Phase Speed in Lined Ducts

Experimental measurements of the phase speed of the fundamental mode in ducts lined with honeycomb and porous liners were made to assess the accuracy of the analytical models developed above.

2.3.1 Description of Experimental Techniques for Measuring Phase Speed

The phase speed of the fundamental mode in a lined rectangular duct was measured in the facility shown schematically in Fig. 10. To test a liner configuration used in the parallel duct assembly, the 12 in long liner section was placed on the lower wall of the facility. The liner section was flanked on either end by additional liner sections of identical configuration to minimize the problem of reflections from the ends of finite length liners. The upper wall of the facility was adjustable and could be set at any desired duct height in the range $0 < b < 0.75$ in.

Two methods were used to measure the phase speed. In the primary method, the phase speed of a traveling wave in a tone burst was determined from the measured time lag between the signals from two microphones located typically one foot apart on the hard wall opposite the lined wall in the duct. To accurately measure the time lag, the microphone outputs were connected to a Tektronix Type 555 Dual Beam Oscilloscope. The output from microphone M1 was connected to Channel A and M2 was connected to Channel B through a delay trigger. By adjusting the vernier on the delay trigger until the signals from Channels A and B were in phase on the oscilloscope screen, the time lag could be measured to an accuracy of 0.005 msec. A second method for measuring the phase speed involved the use of Lissajous figures. The phase angle between microphones for a continuous pure tone

was determined by connecting the outputs from M1 and M2 to the horizontal (x) and vertical (y) deflection plates of the oscilloscope. When the waves were in phase the scope trace formed the line $y = mx$. For out-of-phase waves, $y = -mx$. At least a 180° phase difference was required between microphones to obtain accurate results from Lissajous figures in an attenuating duct. This requirement limited the usefulness of Lissajous figures in the low frequency range.

2.3.2 Measured Phase Speed of Fundamental Mode in Lined Rectangular Duct without Flow

A 1 inch-thick honeycomb type point-reacting non-dissipative liner configuration was constructed from soda straws for the initial testing of the lined parallel duct filtering concept. The measured phase speeds for a duct lined with the soda straw liner are shown in Fig. 11. Configuration A is the lined duct without the rigid partition in place. Configuration B, C and D were obtained by changing the lateral position of the rigid partition in the duct. The calculated low-frequency value of the phase speed for each configuration as given by Eq. (1.1) is also shown in Fig. 11. Note that the phase speed decreases slightly with increasing frequency as the liner approaches its resonance frequency of approximately 3300 Hz. This trend is predicted by the third order approximation [Eq. (2.36)] to the phase speed for a resonator liner having low flow resistance. The curves plotted in Fig. 11 assuming $\theta = 0.1$ would not differ significantly for any θ in the range $(0.1 \leq \theta \leq 0.5)$. This statement will assume more importance in Chap. 3 when we find that the flow resistance of the soda straw liners was apparently much higher

than the value ($\theta = 0.1$) predicted by the Kirchoff theory[27] for visco-thermal losses within the soda straws.

In Fig. 12 the measured phase speed of the fundamental mode in a duct lined with a foam liner is shown. For an unpartitioned liner the phase speed of the fundamental mode is reduced at very low frequencies but quickly approaches the free-space phase speed as the frequency is increased. This trend is predicted by Scott theory[20] for distributed reaction liners.

For a duct with a height of 0.75 in lined on one wall with a one-inch thick Scott Industrial Foam Liner with rigid plates partitioning the liner every 2 in the phase speed of the fundamental mode was 1/1.38 times the free space phase speed over a broad frequency range. At frequencies above 1700 Hz the phase speed decreased as the frequency approached the liner resonance frequency of 2700 Hz. These results follow the trend predicted by Eq. (2.53) for the third order approximation to the phase speed in a duct lined with a point-reacting porous liner. However, the measured phase speed was about 6% higher than the value predicted by Eq. (2.53) at all frequencies measured.

For a much narrower duct ($b = 0.25$ in) the phase speed was reduced to 1/2 the free-space phase speed at 200 Hz but at $f < 800$ Hz the liner displayed the frequency dependent characteristics of a distributed reaction liner rather than a point-reacting liner. For $f > 800$ Hz the phase speed followed the trend predicted by Eq. (2.53) although at a level 30% greater than the phase speed expected for a duct having a point-reacting liner.

The conclusion which can be drawn from these results is that the requirement that ε_1 the ratio of the wavelength to the partition

spacing be greater than 4 is a necessary but not a sufficient condition for the achievement of a point-reacting liner. Trends in the data indicate that one or more of the following parameters may also influence the degree of reaction of the liner.

The ratio of the duct height to the liner thickness, ε_2, influences the frequency range over which the liner has point-reacting characteristics. As ε_2 decreases, the frequency below which the liner has distributed reaction increases. For the small ducts considered in the experimental program, ε_2 may be a measure of the importance of viscothermal losses in the long narrow ducts.

A third parameter, ε_3, the ratio of the liner thickness to the partition spacing in the liner, measures the relative importance of sound propagation parallel to the duct wall within the liner. Liners which are thicker than the partition spacing are expected to have better point-reaction characteristics than the liners considered in this section.

A fourth parameter, ε_4, the ratio of the wavelength to the liner length, may also effect the measured phase speed of the fundamental mode in a lined duct. Rice[28] has shown that an entrance length is required before the fundamental mode reaches an equilibrium wave shape in a lined duct. In the entrance region the shape of the phase front of the sound wave changes from the plane phase front in the rigid duct section to the curved phase front characterizing the equilibrium shape of the fundamental mode in a lined duct. Measurements of the time delay between flush mounted wall microphones within the entrance region therefore do not actually yield the phase speed of the fundamental mode but rather the propagation speed

of the line of constant phase in the lined duct. Thus to accurately determined the phase speed of the fundamental mode within the lined duct measurements must not be made within the entrance region.

The length of the entrance region for the duct configuration tested in Fig. 12 is not known. Rice[28] has shown that for aircraft engine inlets in which the liner is relatively thin compared to the duct diameter the fundamental mode requires approximately one wavelength to attain an equilibrium shape. For the narrow ducts studied in this experimental program, the entrance length is expected to be much shorter. An experimental check was made to determine whether the fundamental mode was in equilibrium between the microphones used for measuring the phase speed. The time delay between several axial microphone locations was used to determine the phase speed in the duct. At each frequency tested, equal phase speeds were measured between each microphone location indicating that the fundamental mode had reached equilibrium within the test section. However, since the optimum attenuation of parallel lined duct filters occurs when the filter length approximates one-half the wavelength of the incident sound wave, the influence of the entrance region should be considered in determining the phase change of sound waves transmitted through each of the branch ducts of the filter.

In addition it should be noted that the effect of liner flexibility may cause the liner performance to be unpredictable by either point- or distributed-reaction theories at low frequencies. Both Morse theory and Scott theory assume the liner to be rigid (i.e. acoustic energy is not dissipated by liner motion). However, this assumption is probably invalid for thick porous liners having narrow air passages.[29]

muffler performance, measurements were made of visco-thermal losses in rigid rectangular and circular ducts. In Fig. 14 the visco-thermal losses in dB per unit duct diameter are plotted vs frequency for the 2 in diameter PVC pipe used in the circular duct facility. Also plotted is the theoretical prediction of Kirchoff.[30] Agreement between theory and experiment is excellent in non-flowing ducts. These data also indicated that the experimental techniques used for measuring transmission loss are dependable.

In Figs. 15a and 15b the losses measured in a rigid 3/4 in x 3/4 in rectangular duct with flow are presented. These losses are caused by both visco-thermal and sound-turbulence interaction effects as discussed by Ingard and Singhal.[31] In Fig. 15a losses are measured for the case of sound propagation in the direction of the mean flow. Note that at almost all frequencies the losses increase monatonically with flow speed. Losses increase faster for low frequencies than high frequencies. In Fig. 15b losses are measured for the case of sound propagation against the direction of the mean flow. For this case the losses increase with increasing flow speed much faster at the higher frequencies. The theory of Ingard and Singhal, however, predicts a frequency independent increase in losses at higher Mach number. It is believed that the assumptions made in the model of Ingard and Singhal are not valid for the conditions tested here wherein the sound wave was in excess of 130 dB. The assumptions in the model of Ingard and Singhal are discussed in Section 4.4.7.

2.3.3 Measured Phase Speed of Fundamental Mode in Lined Rectangular Duct with Flow

A limited amount of experimental data was obtained for the phase speed of the fundamental mode in a 3/4 in x 3/4 in lined duct with mean flow. The liner configuration used to obtain the zero flow phase speed data in Fig. 12 (i.e. 1 in thick Scott Industrial Foam, 100 ppi, rigid partitions every 2 inches) was used for these tests. The phase speed of the sound wave propagating against the mean flow was measured at two mean flow conditions, $M = 0.16$ and $M = 0.23$. The data obtained at frequencies between 200 and 500 Hz are plotted in Fig. 13 vs the phase speed calculated from Eq. (2.30) for point-reacting liners.

At each flow condition the phase speed increased monotonically as the frequency was increased from 200 to 500 Hz. This characteristic is typical for non-locally reacting liners in the low frequency range. When the Mach number was increased at a given frequency the measured phase speed decreased in line with the trend predicted by Eq. (2.30). Whether this trend persists to higher Mach numbers could not be ascertained because of experimental difficulties. For $M > 0.23$ sound waves propagating upstream did not remain sinusoidal but developed steepening wave fronts due to non-linear effects. These non-linear effects resulted from the high sound pressure level (~ 140 dB) which was required to enable the sound waves to be clearly distinguished from the flow noise produced on the flush mounted microphones.

2.4 Measurement of Visco-Thermal and Sound-Turbulence Interaction Losses

To verify existing theories on parasitic losses in rigid ducts and to assess the effect of visco-thermal losses on model-scale parallel duct

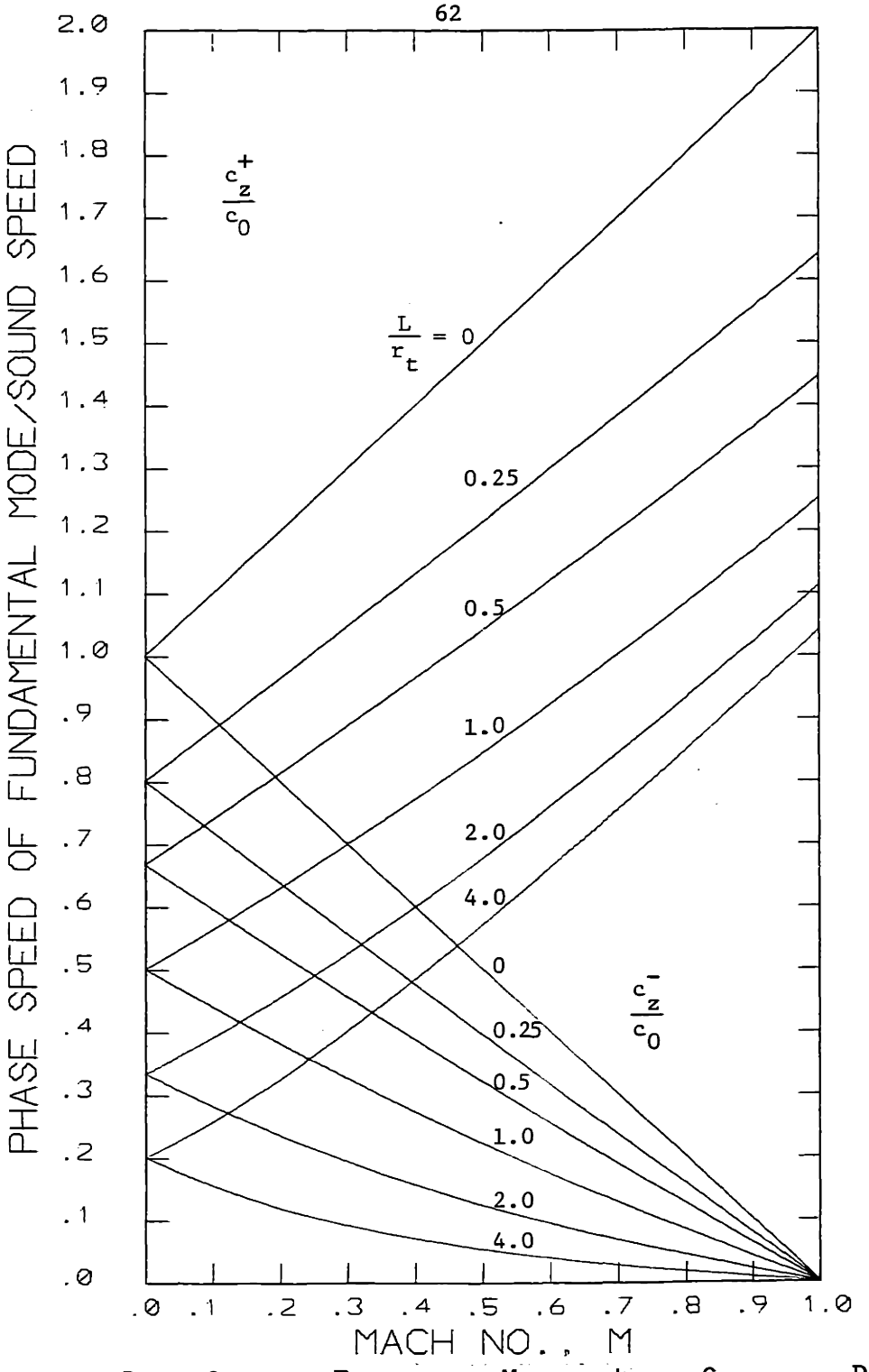

FIG. 7a: PHASE SPEED OF FUNDAMENTAL MODE IN LINED CIRCULAR DUCT

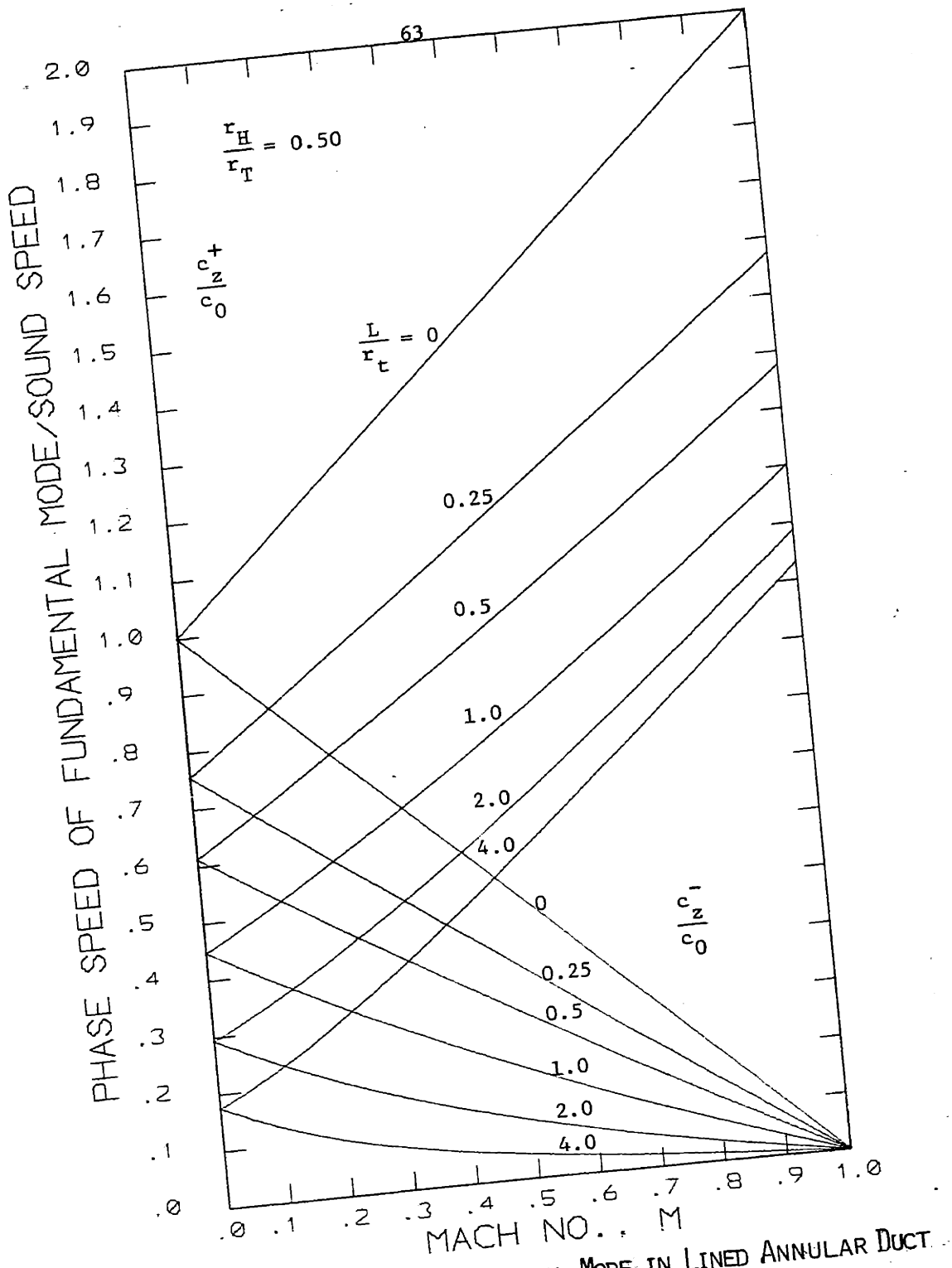

FIG. 7b: PHASE SPEED OF FUNDAMENTAL MODE IN LINED ANNULAR DUCT

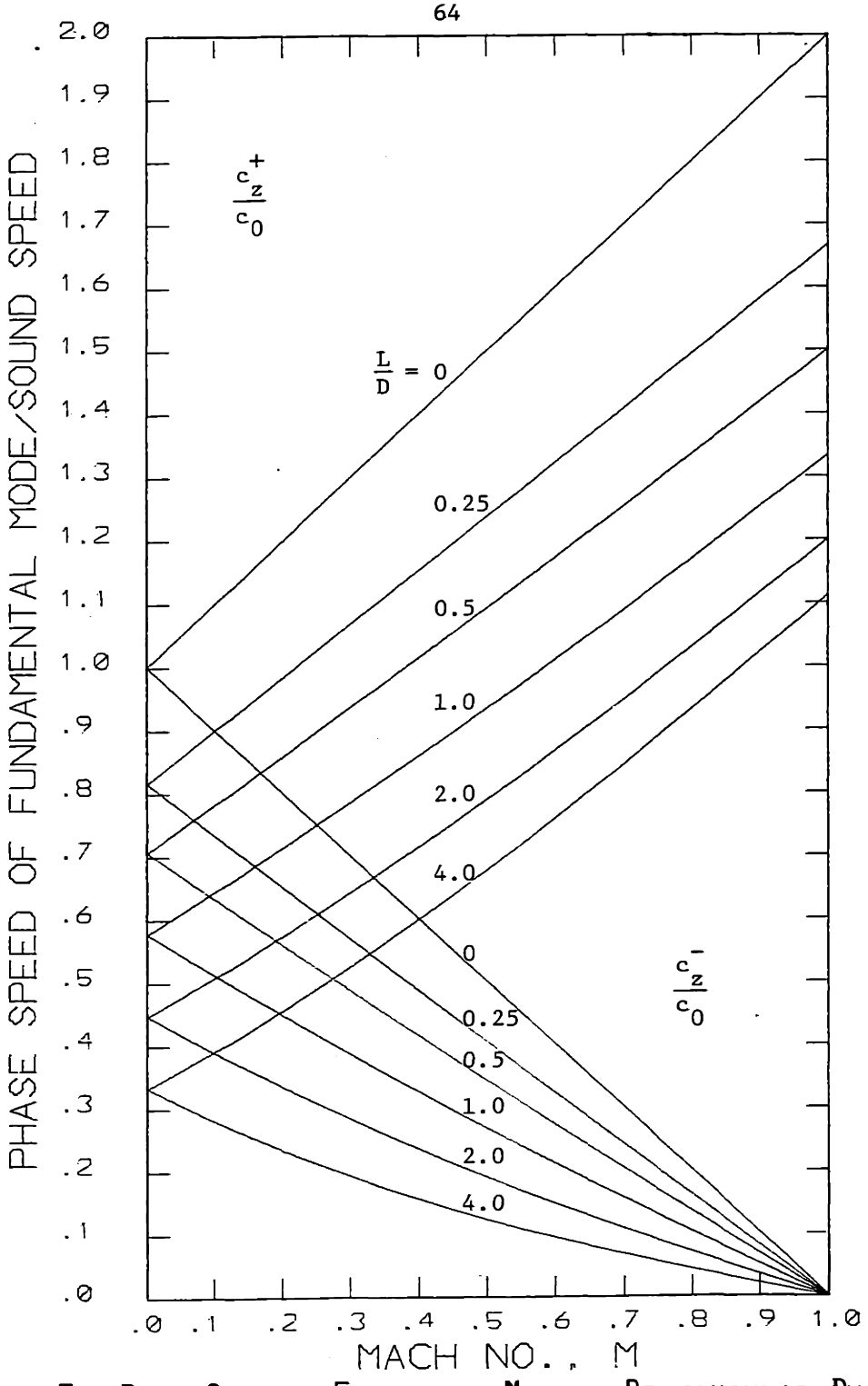

FIG. 7c: PHASE SPEED OF FUNDAMENTAL MODE IN RECTANGULAR DUCT

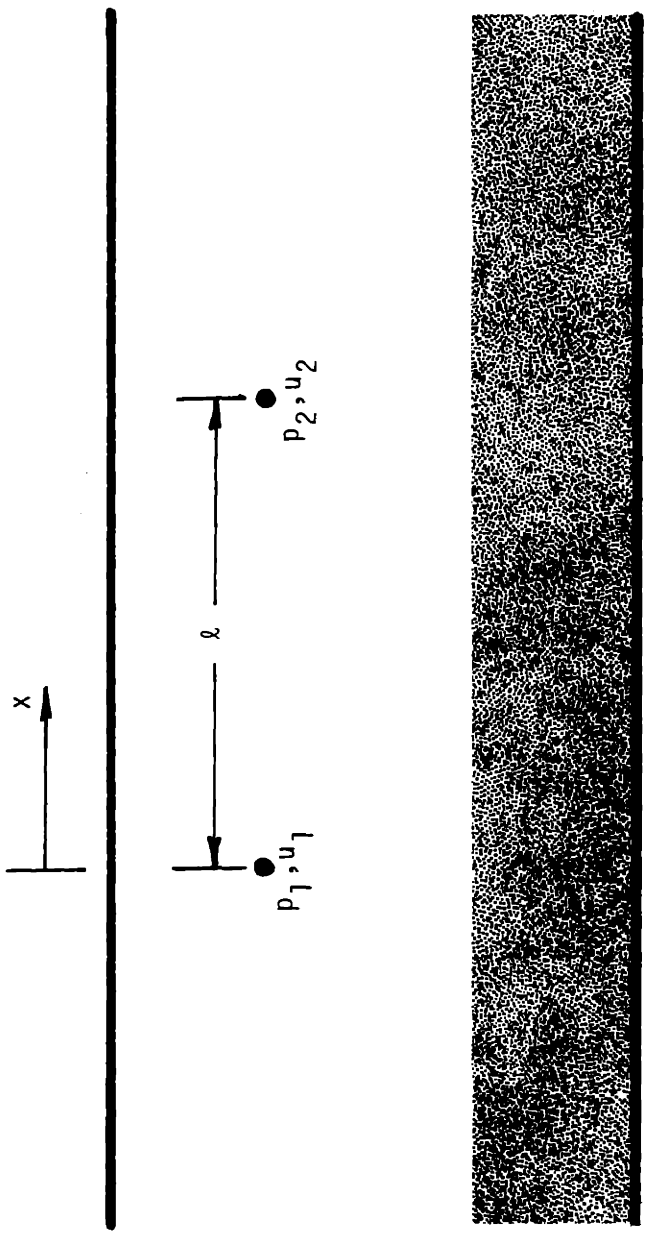

FIG. 8: SOUND TRANSMISSION IN LINED DUCT

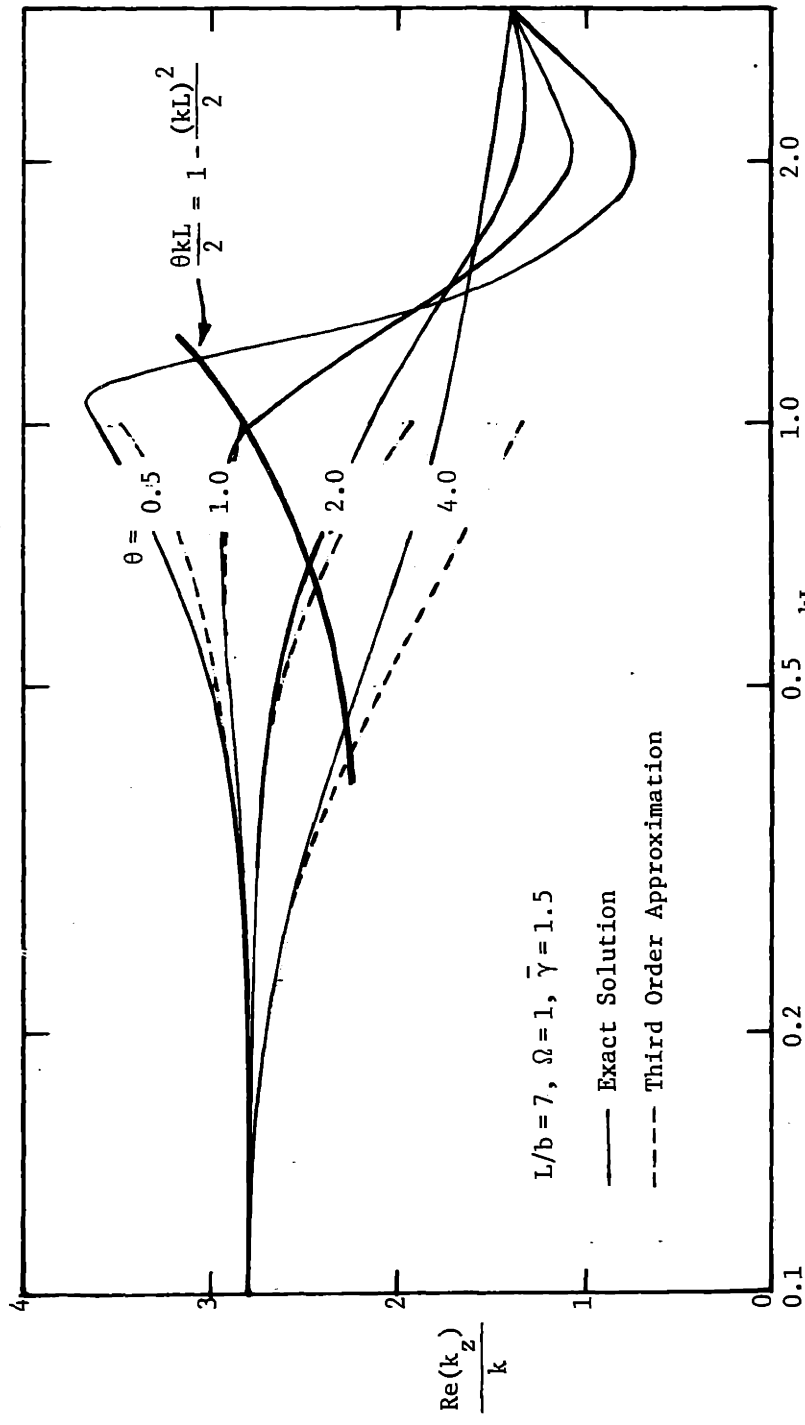

FIG. 9 : PHASE SPEED OF FUNDAMENTAL MODE IN RECTANGULAR DUCT WITH POINT-REACTING POROUS LINER ON ONE WALL

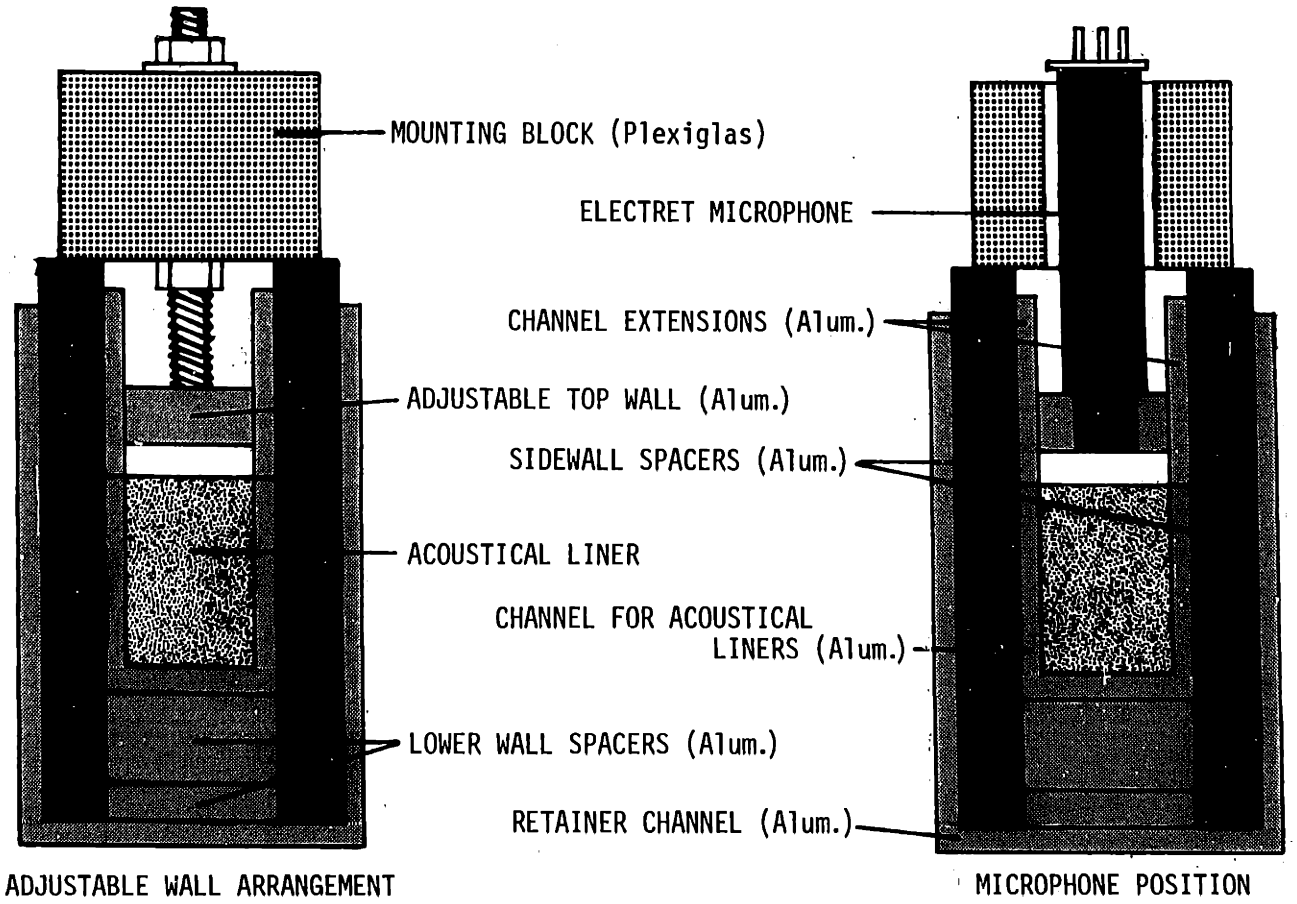

FIG. 10: CROSS-SECTIONAL VIEW OF TEST SECTION USED FOR PHASE SPEED MEASUREMENTS

SYMBOL	b, in.	CONFIG.
□	0.75	A
△	0.47	B
○	0.345	C
▽	0.22	D

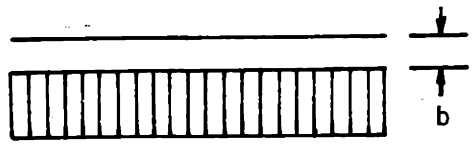

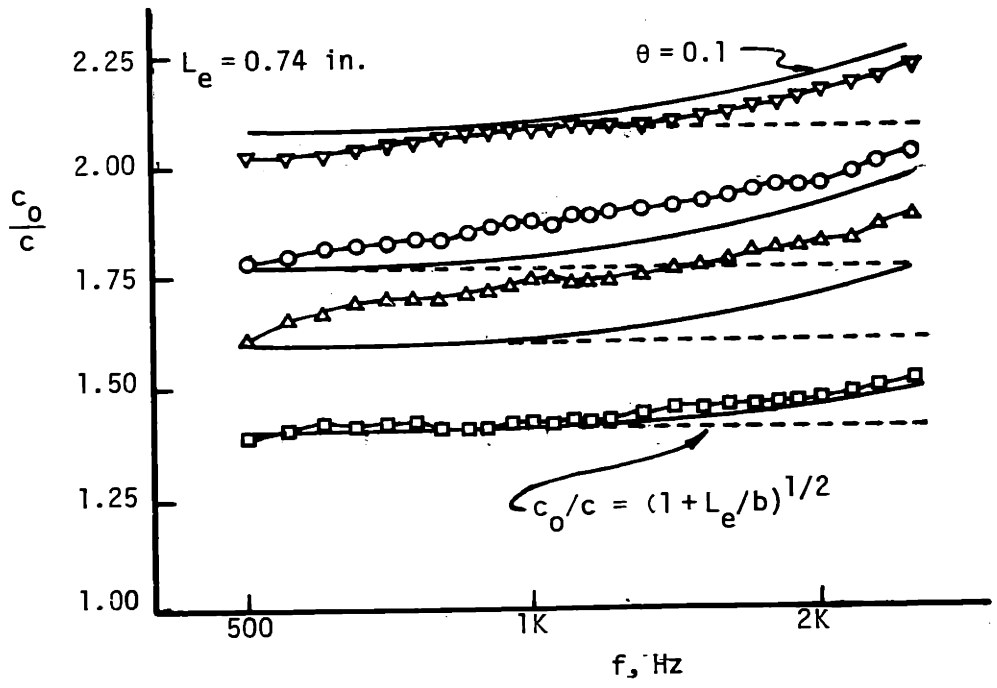

FIG. 11: MEASURED PHASE SPEED OF FUNDAMENTAL MODE IN RECTANGULAR DUCT LINED ON ONE WALL WITH HONEYCOMB-TYPE LINER

Symbol	b (in)	L_{eff} (in)	Partition Spacing	Measurement Technique
○	0.75	0.93	None	Traveling Wave
□	0.75	0.93	2 in	Traveling Wave
▽	0.25	0.93	2 in	Traveling Wave
▼	0.25	0.93	2 in	Lissajous Figs.

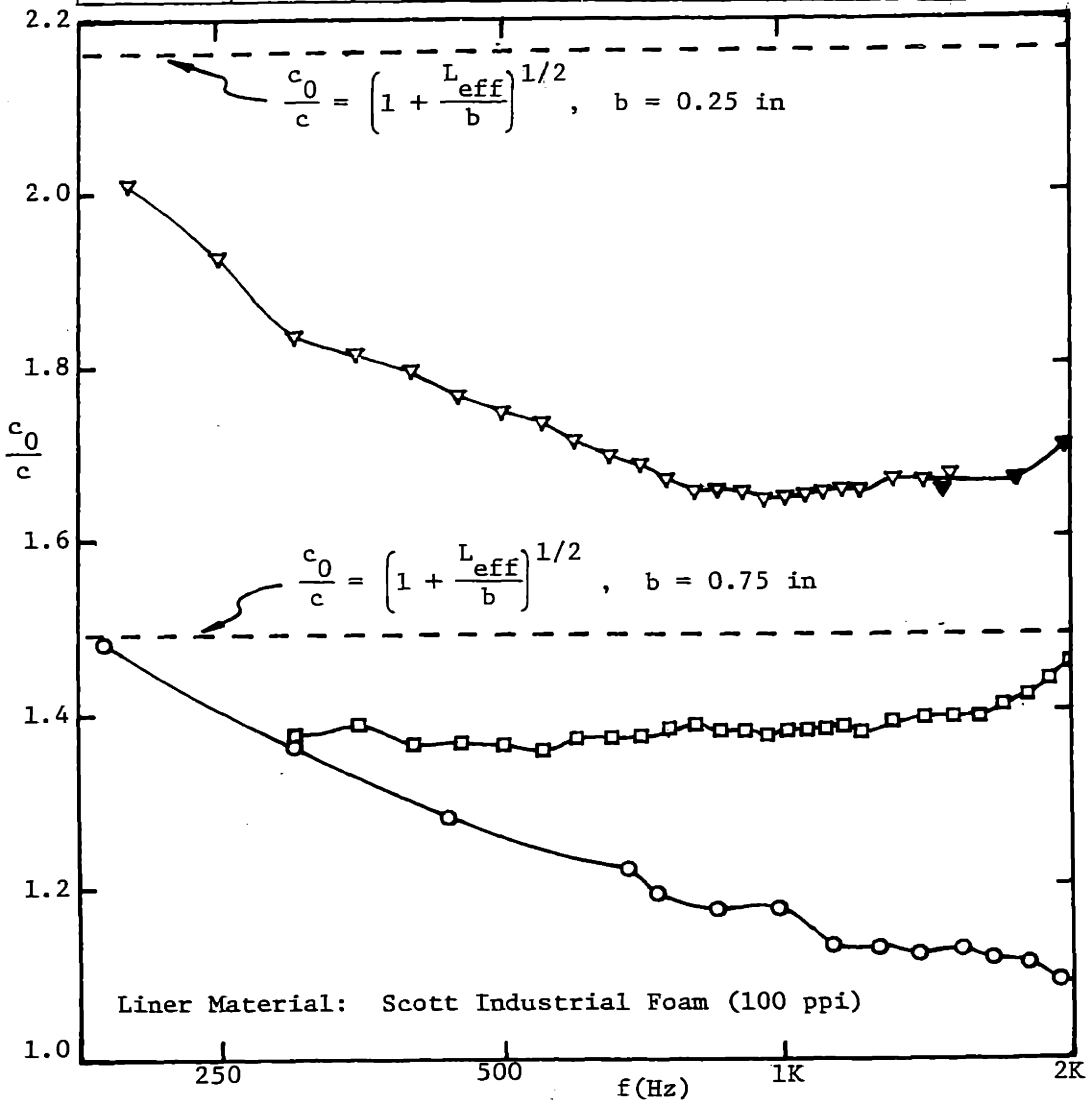

FIG. 12: MEASURED PHASE SPEED IN RECTANGULAR DUCT LINED ON ONE WALL WITH POROUS MATERIAL

Symbol	○	□	△	◇
Freq (Hz)	200	300	400	500

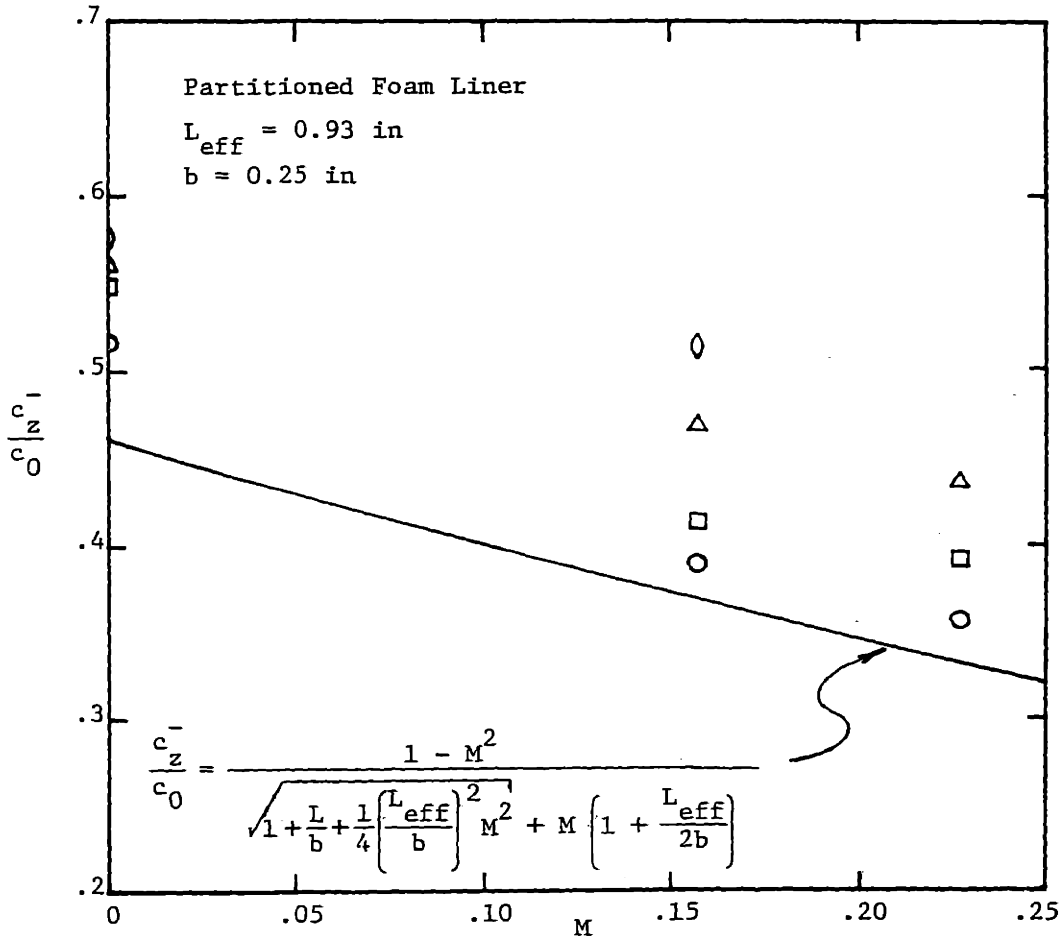

FIG. 13: MEASURED PHASE SPEED FOR UPSTREAM PROPAGATION OF FUNDAMENTAL MODE IN LINED RECTANGULAR DUCT

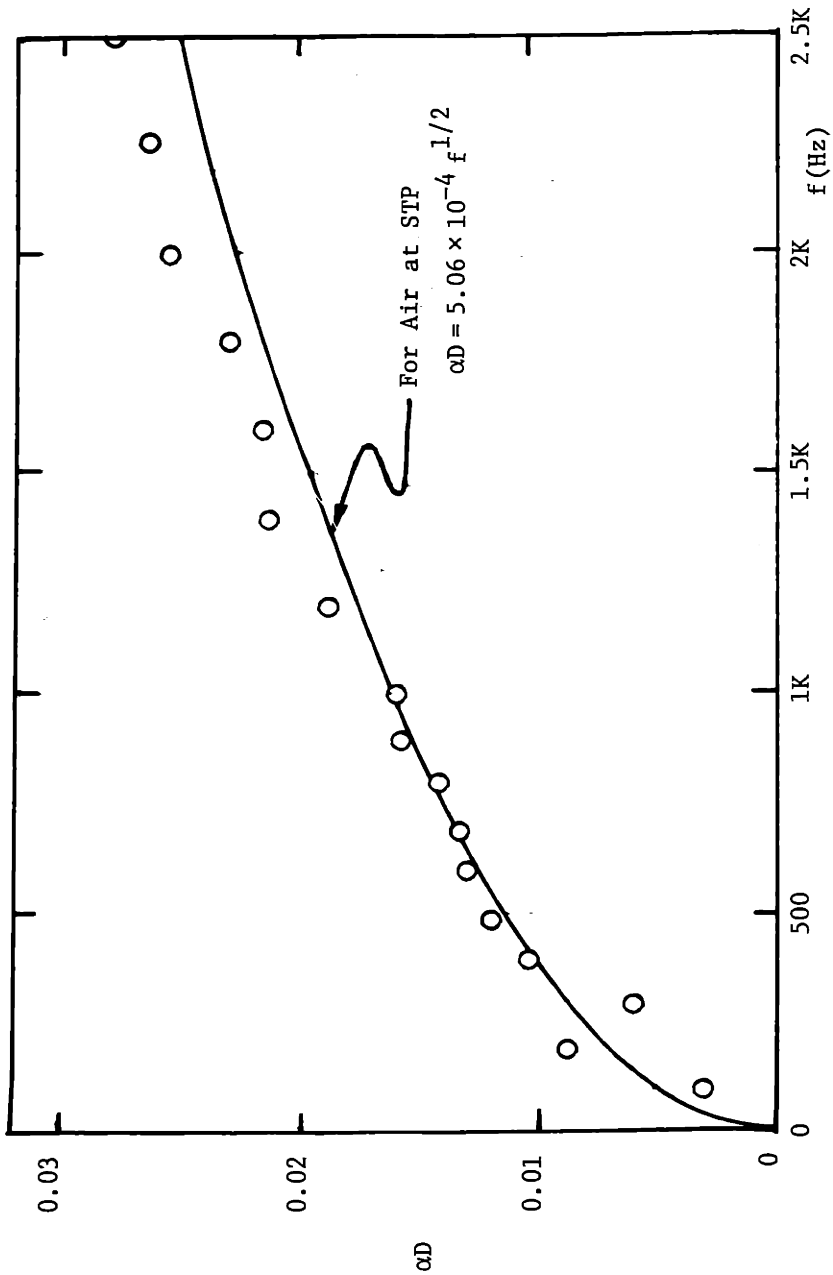

FIG. 14: VISCO-THERMAL LOSSES IN 2-IN DIAMETER PVC PIPE

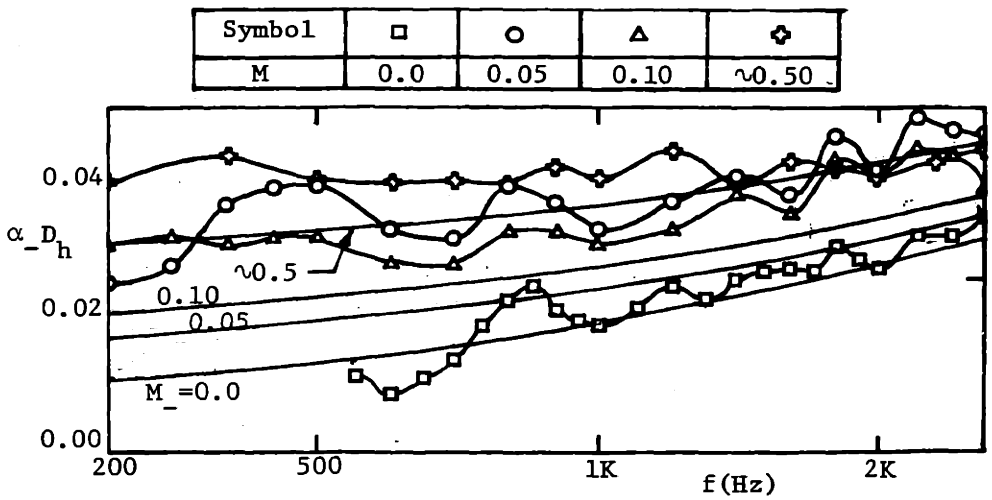

a) Downstream Sound Propagation

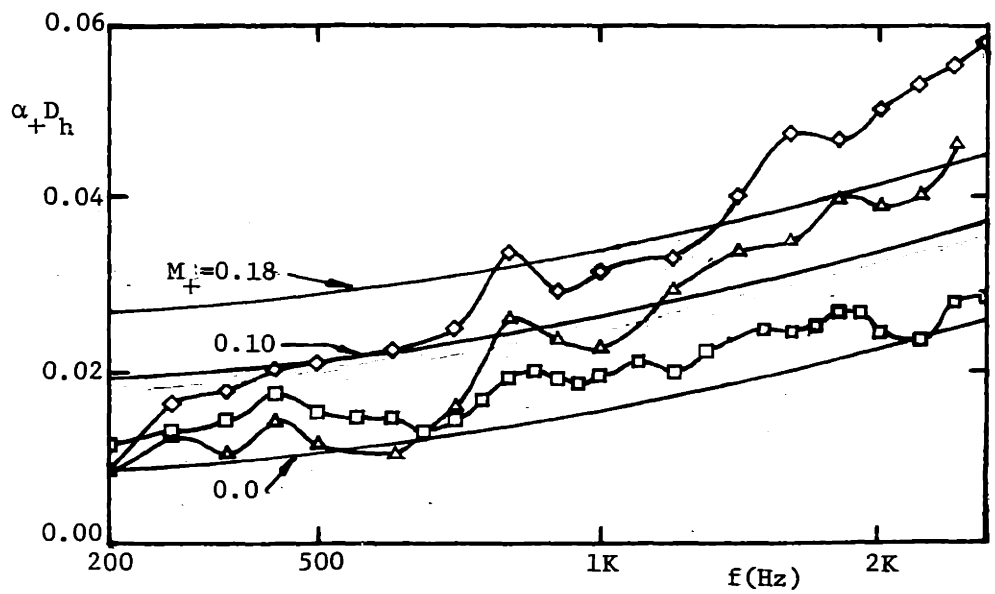

b) Upstream Sound Propagation

FIG. 15 : VISCO-THERMAL LOSSES IN RECTANGULAR DUCT WITH FLOW

CHAPTER III

SOUND TRANSMISSION THROUGH LINED PARALLEL DUCTS

In this chapter the characteristics of sound transmission through lined ducts in parallel are examined. The chapter is divided into four sections: (1) literature review, (2) analytical developments, (3) the experimental program, and (4) a short computer study.

In section 3.1 the published literature concerning sound transmission through parallel ducts is reviewed. Several papers which analyzed and/or tested Herschel-Quincke tubes are discussed but no studies were found of parallel lined duct configurations designed to produce reactive, as well as dissipative attenuation.

In section 3.2 the equations governing sound transmission through lined parallel ducts at low frequencies are derived. The attenuation spectrum is calculated for several rectangular parallel duct configurations lined with point-reacting porous material. The effect of mean flow on the performance of parallel lined duct mufflers is investigated.

In section 3.3 the experimentally determined sound transmission characteristics for several lined parallel duct configurations are reported. Rectangular ducts lined with soda straw, partitioned foam and unpartitioned foam liners were studied. Tuning the muffler by moving or elongating the rigid splitter was investigated for a cylindrical parallel duct lined with a partitioned foam liner. Finally, the attenuation characteristics of a rectangular parallel duct muffler with mean flow were measured.

In section 3.4 a short computer study was undertaken to predict the attenuation characteristics of parallel duct filters in duct systems.

In particular, the sound attenuation spectra of several lined duct configurations (both conventional lined ducts and parallel lined ducts) were compared using the constraint that equal amounts of liner material were used in each configuration. The usefulness of serially cascading lined parallel ducts to obtain broadband attenuation was also investigated.

3.1 Literature Review

Several studies which have been conducted to gain insight into the attenuation characteristics of Herschel-Quincke tubes (i.e. rigid ducts having parallel branches of unequal lengths) could be utilized in the study of lined ducts in parallel. As mentioned in Chap. I, Stewart[5,6] studied the additional attenuation peaks caused by reflections from the front of the filter which are induced by sound waves traveling round trips through both branches of the Herschel-Quincke tube. Trimmer[32] calculated and measured the input impedance of closed and open pipes arranged in various combinations including Herschel-Quincke tubes. Particular attention was paid to the determination of the resonant frequencies of such pipe combinations. Labaw[33] derived expressions for the sound transmission through Herschel-Quincke tubes in series. He also studied the effects of various terminations on the filtering characteristics of such cascaded Herschel-Quincke tubes. In a later paper Labaw[34] verified his theoretical predictions by measuring the sound transmission through five Herschel-Quincke tubes in series terminated by either closed or open ends.

Hahn[35] used a sound wave visualization technique to study the mechanisms of sound attenuation in a glass-walled Herschel-Quincke tube.

At a given frequency Hahn adjusted one branch of the tube which had a trombone-like slide adjustment until maximum attenuation was achieved. At these maximum attenuation conditions dust patterns were used to visualize the resultant standing waves in the transparent tube. The dust patterns indicated that maximum particle velocity (i.e. minimum impedance) occurred at the entrance of the Herschel-Quincke tube. Hahn noted that the incident sound energy accumulated in the Herschel-Quincke tube until the standing waves reached a pressure level at which viscous losses balanced the incident energy flow. Thus, attenuation in a Herschel-Quincke tube is achieved not only by reflection of sound energy back toward the source but also by viscous dissipation in the standing wave pattern within the tube branches.

Recently Fuller and Bies[36,37] presented a detailed analysis and experimental data of sound transmission in an unlined duct bend containing a rigid axial partition. The partition creates parallel branches in the bend having different acoustical path lengths, i.e. a version of the Herschel-Quincke tube patented by Luxton[10] in 1971.

Lined ducts are often divided into parallel branches to increase the lined surface area in the duct, thereby increasing the sound attenuation. Typical configurations include ducts with lined radial baffles,[38] silencers for power plants and engine test cells having lined parallel baffles[29,39] and air delivery systems consisting of multiple lined ducts in parallel.[39] It should be noted, though, that the parallel branches in each of these configurations are lined symmetrically.

Symmetric parallel lined duct designs have evolved naturally from a desire to equalize the dissipative attenuation in each of the parallel branches. It has been assumed that unequal attenuation in the parallel branches would render the silencer ineffective by permitting the sound to "short circuit" the silencer by propagating through the branch having the least attenuation. It will be shown below, however, that the interference effects between dissimilarly lined parallel branches can be used to provide additional reactive attenuation which causes the total attenuation to be greater than the purely dissipative attenuation produced by symmetric parallel lined ducts.

Studies of sound transmission in unsymmetrically lined parallel duct configurations reported in the literature are scarce. Dittmar and Groeneweg[40] reported the performance of full-scale aircraft engine inlet noise suppressors which had nearly symmetric lined ring splitters. Using the analysis of Rice[41] which neglected possible interference effects between parallel passages, Dittmar and Groeneweg could not predict the measured attenuation accurately. The discrepancy between the measured and predicted performance may have been caused in part by the neglected interference effects.

Ko[42,43] derived analytical expressions for the sound transmission through lined circular ducts with flow. He found it necessary to consider elastic[42] and porous[43] splitters which permitted coupling between sound energy in the parallel branches to make the problem tractable. Earlier, Allen[7] had presented a rudimentary analysis which predicted the attenuation

produced by dissimilarly lined ducts in parallel. However, he had considered the wave motion in the parallel branches to be coupled through a nonrigid splitter. The analysis to be presented in the following section will apply to the problem of sound transmission through dissimilarly lined parallel ducts which are separated by rigid splitters to prevent coupling of the sound waves in adjacent branches through their common boundaries. Coupling between the sound waves in the parallel branches can occur only at the entrance and exit of the silencer.

3.2 Transmission Matrix for Parallel Lined Ducts Without Mean Flow

In this section the transmission of the fundamental sound mode through lined ducts in parallel is analyzed. First consider the two lined ducts, A and B, which are parallel branches within a larger duct as shown in Fig. 16. The propagation constants for the fundamental modes in these ducts are known in terms of the acoustic impedance of the liners. The characteristic wave impedances are also known. Therefore, the amplitude of the acoustic pressure and particle velocity at the beginning and end of each duct can be related by means of forward transmission matrices T_A and T_B as described in section 4.4.2.

$$\begin{Bmatrix} p_{1A} \\ \rho c u_{1A} \end{Bmatrix} = T_A \begin{Bmatrix} p_{2A} \\ \rho c u_{2A} \end{Bmatrix} \tag{3.1a}$$

$$\begin{Bmatrix} p_{1B} \\ \rho c u_{1B} \end{Bmatrix} = T_B \begin{Bmatrix} p_{2B} \\ \rho c u_{2B} \end{Bmatrix} \tag{3.1b}$$

where subscripts 1 and 2 refer to the beginning and end of the ducts respectively.

For lined ducts with mean flow the elements of the forward transmission matrices take on the rather complicated forms given in Eqs. (4.58a-d). In the absence of mean flow Eqs. (4.58a-d) reduce to

$$T_A = \begin{bmatrix} \cos k_A L & -i\zeta_A \sin k_A L \\ -\frac{i}{\zeta_A} \sin k_A L & \cos k_A L \end{bmatrix} \tag{3.2}$$

for Duct A where ζ_A is the characteristic wave impedance in the duct. With the x dependence of the wave described by $\exp(-ik_A x)$ the wave impedance is given by

$$\zeta_A = -\frac{k}{k_A} \tag{3.3}$$

The transmission matrix and the wave impedance of Duct B have analogous forms to Eqs. (3.2) and (3.3).

In the following sections the equations governing the acoustic field at the entrance and exit of the parallel ducts are developed. These sections have been adapted from an internal laboratory memorandum written by Ingard.[44]

3.2.1 Exit Conditions

In the exit plane shown in Fig. 17 the field quantities in the individual ducts are (p_{2A}, u_{2A}) and (p_{2B}, u_{2B}). The large duct at the downstream side of the parallel duct is denoted by 2. The plane wave components of the field variables in this duct are (p_2, u_2). The higher order modes generated at the junction between the two ducts will decay exponentially away from the plane of the junction and are assumed not to reach the termination of duct 2. The plane wave, of course, will propagate and be reflected. Thus u_2 and p_2 generally are composed of both outgoing and reflected wave components. The relationships between u_2 and p_2 can be specified only if the length and the acoustic termination (or lining) of duct 2 are given. In the following analysis the general case will be considered and u_2 and p_2 will be treated as independent variables.

A rigorous analysis of the transition of the wave fields from the AB duct to the exit duct 2 is quite complex and could be carried out by means of variational analysis. For the purposes of demonstrating the essential features of the transmission characteristics of the AB duct the fundamental mode in each duct will be replaced with an equivalent plane wave mode with an amplitude equal to the average amplitude of the fundamental mode, but with a propagation constant which is the same as that of the fundamental mode.

Using this simplification, the velocity amplitudes u_{2A} and u_{2B} in the exit planes are considered to be constant across the ducts A and B respectively. Having made this assumption, the pressure amplitude in the exit plane can be computed. This amplitude will not be constant across the ducts. However, the average pressure across each duct will be calculated and used as the first approximation for the average amplitude of the fundamental pressure mode in each duct.

In this way the boundary conditions are satisfied in the exit plane "on the average". To satisfy the boundary conditions exactly requires an analysis in which the velocity and pressure amplitude distributions across the exit plane are not known a priori. These distributions can be obtained, at least formally, from a variational calculation or from the solution of an integral equation.

Having made the above assumptions, the velocity distribution across the exit plane can be considered to be equivalent to two plane pistons with velocity amplitudes u_{2A} and u_{2B} covering the areas S_A and S_B respectively. The pressure field in the exit duct can then be calculated as follows.

Let the amplitude of the plane wave pressure component be $p_2(x)$. In general, this amplitude varies with x depending on how the duct is terminated. For long wavelengths, the variation of p_2 in the distance of about a duct diameter is small. The higher order modes, however,

generated at the junction of the AB duct and the exit duct will decay in about this distance. Therefore, in the region of the decaying higher order modes p_2 can be regarded as constant and equal to the plane wave pressure just outside the decay length of the higher order modes.

Thus the amplitude of the pressure field in the exit duct in the vicinity of the duct junction is given by

$$p_2' = p_2 + \sum_{m=1}^{\infty} A_m \psi_m(k_{my}y) e^{-ik_{mx}x} \tag{3.4}$$

where $\psi_m(k_{my}y)$ are the eigenfunctions describing the variation of the pressure amplitude with the transverse coordinate y and

$$k_{mx} = \sqrt{k^2 - k_{my}^2} \qquad k = \omega/c \tag{3.5}$$

where c = the free space phase speed.

The corresponding velocity field is

$$u_2' = u_2 + \frac{1}{\rho c} \sum_{m=1}^{\infty} A_m \frac{k_{mx}}{k} \psi_m(k_{my}y) e^{-ik_{mx}x} \tag{3.6}$$

where the eigenfunctions $\psi_m(k_{my}y)$ have been normalized such that for the plane wave mode, $\psi_0 = 1/\sqrt{S_2}$, where S_2 is the area of the exit duct.

To obtain the matching conditions at the exit of the AB duct, the velocity field in the exit duct, Eq. (3.6), is set equal to the velocity field in the terminal plane of the AB duct. This velocity field is, at x = 0

$$u_2' = B_0\psi_0 + \sum_{m=1}^{\infty} B_m \psi_m(k_{my}y) = \begin{matrix} u_A \text{ in duct A} \\ u_B \text{ in duct B} \end{matrix} \tag{3.7}$$

where $B_0\psi_0 = u_2$.

It follows from Eqs. (3.6) and (3.7) that

$$A_m\left\{\frac{k_{mx}}{k}\right\} = B_m \qquad (m > 0) \tag{3.8}$$

and from Eq. (3.7) that

$$B_m = \int_A u_A \psi_m(k_{my}y)dS_A + \int_B u_B \psi_m(k_{my}y)dS_B \tag{3.9}$$

Thus

$$B_0 = (u_A S_A + u_B S_B)\psi_0 \tag{3.10}$$

and

$$u_2 = \frac{S_A}{S_2} u_{2A} + \frac{S_B}{S_2} u_{2B} \tag{3.11}$$

Similarly, the pressure field in the exit plane, Eq. (3.4), is at x = 0

$$p_2' = p_2 + \sum_{m=1}^{\infty} \frac{k}{k_{mx}} B_m \psi_m(k_{my}y) \tag{3.12}$$

The average pressure amplitude in the exit plane of duct A is then

$$p_{2A} = p_2 + \frac{1}{S_A} \sum_{m=1}^{\infty} \frac{k}{k_{mx}} B_m \int \psi_m(k_{my}y)dS_A \tag{3.13}$$

Using Eq. (3.9), p_{2A} can be expressed as

$$p_{2A} = p_2 + \zeta_{AA}\rho c u_{2A} + \zeta_{AB}\rho c u_{2B} \tag{3.14a}$$

where

$$\zeta_{AA} = \sum_{m=1}^{\infty}\left[\int\psi_m(k_{my}y)dS_A\right]^2 \frac{k}{k_{mx}}\frac{1}{S_A} \tag{3.15a}$$

$$\zeta_{AB} = \sum_{m=1}^{\infty}\left[\int\psi_m(k_{my}y)dS_A\right]\left[\int\psi_m(k_{my}y)dS_B\right] \frac{k}{k_{mx}}\frac{1}{S_A} \tag{3.15b}$$

Similarly

$$p_{2B} = p_2 + \zeta_{BA}\rho c u_{2A} + \zeta_{BB}\rho c u_{2B} \tag{3.14b}$$

where

$$\zeta_{BA} = \sum_{m=1}^{\infty}\left[\int\psi_m(k_{my}y)dS_B\right]\left[\int\psi_m(k_{my}y)dS_A\right] \frac{k}{k_{mx}}\frac{1}{S_B} \tag{3.15c}$$

$$\zeta_{BB} = \sum_{m=1}^{\infty}\left[\int\psi_m(k_{my}y)dS_B\right]^2 \frac{k}{k_{mx}}\frac{1}{S_B} \tag{3.15d}$$

Note that the coupling impedances ζ_{AA}, ζ_{AB}, ζ_{BA}, and ζ_{BB} fit the general expression

$$\zeta_{ij} = \frac{1}{S_i}\sum_{m=1}^{\infty}\frac{k}{k_{mx}}\left[\int_{S_i}\psi_m(k_{my}y)dS_i\right]\left[\int_{S_j}\psi_m(k_{my}y)dS_j\right] \tag{3.16}$$

3.2.2 Entrance Conditions

The entrance duct, joined to the upstream end of the AB duct, is denoted by 1. The plane wave components of the pressure and velocity amplitudes in 1 are (p_1, u_1) in the vicinity of the entrance to AB. In addition to the plane wave, there will be some higher order modes in the entrance duct in the incident wave and/or the reflected wave.

By analogy with the analysis for the exit plane the matching conditions at the entrance plane can be obtained.

$$p_{1A} = p_1 - \zeta'_{AA}\rho c u_{1A} - \zeta'_{AB}\rho c u_{1B} \tag{3.17a}$$

$$p_{1B} = p_1 - \zeta'_{BA}\rho c u_{1A} - \zeta'_{BB}\rho c u_{1B} \tag{3.17b}$$

$$u_1 = \frac{S_A}{S_1} u_{1A} + \frac{S_B}{S_1} u_{1B} \tag{3.17c}$$

where

$$\zeta'_{ij} = \left(\frac{S_2}{S_1}\right)\zeta_{ij} \tag{3.18}$$

3.2.3 Determination of Transmission Matrix

Using Eqs. (3.1a,b), (3.11), (3.14a,b) and (3.17a-c) a linear relationship between $(p_1,\rho c u_1)$ and $(p_2,\rho c u_2)$ can be obtained. These ten equations are sufficient (after much algebra and perserverance) to express the ten variables p_{1A}, p_{1B}, u_{1A}, u_{1B}, p_{2A}, p_{2B}, u_{2A}, u_{2B}, p_2 and u_2 in terms of p_1 and u_1 in the forward transmission matrix form

$$\begin{Bmatrix} p_1 \\ \rho c u_1 \end{Bmatrix} = T \begin{Bmatrix} p_2 \\ \rho c u_2 \end{Bmatrix} \tag{3.19}$$

where

$$T_{11} = \frac{\alpha_3\beta_1 - \beta_3\alpha_1}{\alpha_3 - \beta_3} \tag{3.19a}$$

$$T_{12} = \frac{\alpha_3\beta_2 - \beta_3\alpha_2}{\alpha_3 - \beta_3} \tag{3.19b}$$

$$T_{21} = a_1 T_{A21} + b_1 T_{B21} - (\alpha_4 - \beta_4)\frac{\alpha_1 - \beta_1}{\alpha_3 - \beta_3} \tag{3.19c}$$

$$T_{22} = \frac{\alpha_2 - \beta_2}{\alpha_3 - \beta_3}(\alpha_4 - \beta_4) + \frac{\beta_4}{\alpha_2} \tag{3.19d}$$

$$\alpha_0 = T_{A11} + \zeta'_{AA} T_{A22} \tag{3.19e}$$

$$\alpha_1 = \alpha_0 + \zeta'_{AB} T_{B21} \tag{3.19f}$$

$$\alpha_2 = \frac{1}{b_2}[\alpha_0 \zeta''_{AB} + \zeta'_{AB}(T_{B22} + \zeta''_{BB} T_{B21})] \tag{3.19g}$$

$$\alpha_3 = \alpha_0 \zeta''_{AA} + T_{A12} + \zeta'_{AA} T_{A22} + \zeta'_{AB}\zeta_{BA} T_{B21} - a_2\alpha_2 \tag{3.19h}$$

$$\alpha_4 = a_1(T_{A22} + \zeta''_{AA} T_{A21}) + b_1 \zeta''_{BA} T_{B21} \tag{3.19i}$$

$$\beta_0 = T_{B11} + \zeta'_{BB} T_{B21} \tag{3.19j}$$

$$\beta_1 = \beta_0 + \zeta'_{BA} T_{A21} \tag{3.19k}$$

$$\beta_2 = \frac{1}{b_2}(\zeta''_{BB}\beta_0 + T_{B12} + \zeta'_{BB} T_{B22} + \zeta'_{BA}\zeta''_{AB} T_{A21}) \tag{3.19l}$$

$$\beta_3 = \beta_0 \zeta''_{BA} + \zeta'_{BA}(T_{A22} + \zeta'_{BB} T_{A21}) - a_2\beta_2 \tag{3.19m}$$

$$\beta_4 = \frac{a_2}{b_2}[a_1 \zeta''_{AB} T_{A21} + b_1(T_{B22} + \zeta'_{BB} T_{B21})] \tag{3.19n}$$

In the following sections the general form of the forward transmission matrix, Eqs. (3.19a-n), is specialized to the rectangular and circular duct configurations tested during the experimental program described in Sect. 3.3.

3.2.3.1 Rectangular Duct

Consider the rectangular duct assembly as shown in Fig. 18 With $d_1 = d_2$, the normalized wave functions in the entrance and exit ducts are identical and equal to

$$\psi_m(k_{my}\, y) = \sqrt{\frac{2}{S_2}} \cos k_{my}\, y \qquad k_{my} = \frac{m\pi}{d_2} \tag{3.20}$$

The coupling impedance at the entrance and exit planes are also identical and are computed in Appendix I to be

$$\zeta_{ij} = \zeta'_{ij} = -i \sum_{m=1}^{\infty} \left[\frac{2kd_j}{m\pi} \left(\frac{d_j}{d_i} \right) \left(\frac{\sin k_{my} d_j}{k_{my} d_j} \right)^2 \right] \tag{3.21}$$

where the assumption has been made that $k \ll k_{my}$. Thus the coupling impedances are related in the following manner:

$$d_A \zeta_{AA} = d_B \zeta_{BB} \tag{3.22a}$$

$$d_A \zeta_{AB} = d_B \zeta_{BA} \tag{3.22b}$$

$$\zeta_{BB} = -\zeta_{BA} \tag{3.22c}$$

$$\zeta_{AA} = -\zeta_{AB} \tag{3.22d}$$

The coupling impedance is reactive and expresses the contributions from the higher order modes in the entrance and exit ducts to the pressures (p_{1A}, p_{1B}) and (p_{2A}, p_{2B}) respectively. For the rectangular

parallel duct filter with the splitter plate aligned on the duct centerline (i.e. $d_A = d_B$) ζ_{AA} can be evaluated from Eq. (3.21) to be

$$\zeta_{AA} = -0.4206\ ikd_1$$

Note that the contribution from the coupling impedance is small and goes to zero as the frequency goes to zero.

3.2.3.2 Cylindrical Duct

Coupling impedances for circular cylindrical ducts have also been derived in Appendix 1. Thus for cylindrical ducts

$$\zeta_{AA} = \frac{4\pi}{S_A}\left(\frac{r_A}{r_B}\right)^2 k \sum_{n=1}^{\infty} \frac{1}{k_{0nr}^2 k_{nx}} \frac{J_1^2(k_{0nr} r_A)}{J_0^2(k_{0nr} r_B) + J_1^2(k_{0nr} r_B)} \qquad \text{(A1.24a)}$$

where k_{0nr} is determined from the expression

$$J_0'(k_{0nr} r_B) = 0$$

For small k the expression being summed in Eq. (A1.24a) is frequency independent and has a value of order one. Thus, for small k, ζ_{AA} is small and can be neglected in Eqs. (3.14a,b) and (3.17a,b).

3.2.3.3 Transmission Matrix Approximation at Low Frequencies

At low frequencies the transmission matrix, Eqs. (3.19a-n), for the rectangular parallel duct configuration shown in Fig. 18 can be reduced to:

$$\begin{Bmatrix} p_1 \\ \rho c u_1 \end{Bmatrix} = \begin{bmatrix} T_{11} & T_{12} \\ T_{21} & T_{22} \end{bmatrix} \begin{Bmatrix} p_2 \\ \rho c u_2 \end{Bmatrix}$$

where

$$T_{11} = \frac{T_{A11}T_{B12}+T_{B11}T_{A12}}{T_{A12}+T_{B12}}$$

$$T_{12} = \frac{2T_{A12}T_{B12}}{T_{A12}+T_{B12}}$$

$$T_{21} = \frac{1}{2}\left[\frac{(T_{A11}-T_{B11})(T_{B22}-T_{A22})}{T_{A12}+T_{B12}} + T_{A21} + T_{B21}\right]$$

$$T_{22} = \frac{T_{A22}T_{B12}+T_{B22}T_{A12}}{T_{A12}+T_{B12}} \qquad (3.23)$$

The transmission loss can be expressed in terms of elements of the transmission matrix in the following form:

$$TL = 20 \log \frac{1}{2} \left| T_{11} + T_{12} + T_{21} + T_{22} \right| \qquad (3.24)$$

The transmission loss for the parallel duct assembly as shown in Fig. 18 has been calculated and is presented in Figs. 19a-d.

3.2.4 Results and Discussion

In Figs. 19a-d the transmission loss per unit duct width has been plotted vs kL, a frequency parameter formed by the product of the free space wavenumber and the liner thickness, for S/W = 2, 4, 6, and 12,

respectively. Transmission loss curves for the duct both with and without the splitter in place are presented for each duct length. The effect of end reflections caused by finite liner length have been included in the calculations for each case.

Two features of these curves should be noted. First, for all cases the broadband attenuation has been enhanced at low frequencies by using the splitter. The upper frequency limit of this enhancement is inversely proportional to the splitter length. Thus, for long splitters, although the low frequency attenuation is quite good, the presence of the splitter degrades the performance of the liner at high frequencies. The reason for this effect is that at higher frequencies the sound wave in the lined section of the duct is attenuated quite strongly by the dissipative liner and its effectiveness in interfering with the sound wave which has traveled through the unlined half of the duct is greatly reduced.

The second notable feature of the transmission loss curves is the occurrence of strong attenuation peaks at selected frequencies. These peaks in the attenuation curves which occur at values of kL for which $\alpha_1 + \alpha_2 = 2n\pi$, are caused by reflections from the entrance of the parallel duct assembly. This phenomenon can be explained in the following manner. The sound wave transmitted through the unlined half of the duct creates a sound field downstream of the parallel duct assembly (Fig. 3). This sound field not only causes a positive-going wave to be transmitted down the exit duct but it also induces a negative-going wave to travel

upstream through the lined half of the duct. For values of kL for which $\alpha_1 + \alpha_2 = 2n\pi$, these negative-going waves arrive at the entrance of the parallel duct exactly out of phase with the incident wave causing strong reflections.

Stewart[6] has shown that in the Herschel-Quincke tube these reflections cause complete cancellation of the incident sound wave. In a parallel attenuating duct, however, the cancellation is incomplete because of the amplitude reduction of the negative-going wave by the liner. Nevertheless, the reflections are quite strong as shown in Fig. 19b where the transmission loss has been increased 3 dB per unit duct width at kL = 0.34 due to reflection.

3.2.5 Effect of Mean Flow on the Performance of Parallel Duct Acoustic Filters

Mean flow through lined parallel duct acoustic filters used as intake or exhaust silencers will effect the filter performance in at least two ways. First, mean flow will change the attenuation of the sound waves within the lined branch ducts. Second, mean flow will alter the phase speed in each of the branches. The effect of phase speed changes on the "destructive interference" and "sing-around interference" frequencies will be analyzed in this section.

The effect of mean flow on the phase speed of low frequency sound waves has been determined in Sect. 1.4 to be

$$\frac{c_z^{\pm}}{c_0} = (1 + M) \frac{(1 - M)}{\sqrt{1 + 2\xi + \xi^2 M^2} \mp M(1 + \xi)} \tag{3.25}$$

where ξ is the ratio of the void space in the liner to the volume of the airspace in the duct.

It will be assumed in this section that the mean flow velocity in the branch ducts equals the flow velocity in the main duct. This assumption is valid only when the branch ducts have approximately equal skin friction coefficients. For small ducts, such as those used in the test program described below, the effects of viscosity are important and unequal frictional characteristics in the branch ducts will cause the mean flow to redistribute itself among the branch ducts to equalize the pressure drop within each parallel branch. The magnitude of the velocity differences in the branch ducts caused by the redistribution can be calculated using the analysis performed in Appendix 5. For configurations in which the flow redistribution is considered important, the flow velocities in each branch duct should be calculated from Eqs. (A5.8) and (A5.9) and used in the analysis which follows.

3.2.5.1 Destructive Interference

For a parallel lined duct muffler of length s having one lined and one unlined branch the lowest frequency at which destructive interference is obtained is given by

$$f_D = \frac{c}{2(\frac{c}{c_z} - 1)s} \tag{3.26}$$

where c and c_z are the phase speeds in the hard- and soft-walled branches respectively. When the filter is used as an exhaust muffler, (i.e. sound and flow in the same direction) f_D becomes

$$f_D = \frac{c_0(c_+/c_0)}{2(\frac{c_+/c_0}{c_{z_+}/c_0} - 1)s} \tag{3.27a}$$

where c_0 is the thermodynamic speed of sound. When used as an intake muffler, (i.e. sound and flow in opposite directions) destructive interference occurs at

$$f_D = \frac{c_0(c_-/c_0)}{2(\frac{c_-/c_0}{c_{z_-}/c_0} - 1)s} \tag{3.27b}$$

Consider the cylindrical parallel lined duct muffler configuration shown in Fig. 20 having a rigid tubular splitter and a lined annulus with a hub-to-tip ratio, r_H/r_T, of 0.707. The destructive interference frequency has been plotted vs flow speed for both intake and exhaust silencer configurations in Fig. 20a for two liner thicknesses. For the exhaust muffler configuration, f_D increases rapidly with increasing mean flow. At M = 0.4, f_D is increased by 100% over its value at M = 0. For the intake configuration the opposite effect occurs. The mean flow lowers the destructive interference frequency substantially. At M = 0.4, f_D is reduced to less than half its value at M = 0. Thus mean flow effects destructive interference primarily by shifting the frequencies at which the attenuation maxima occur.

3.2.5.2 "Sing-Around" Interference

Because of the nonlinear relationship between phase speed and Mach number in a lined duct as given by Eq. (3.25) the time required for a sound wave to make a round trip through both branch ducts

differs for clockwise and counterclockwise circuits. In the configuration shown in Fig. 21a having one lined and one unlined branch the sound wave travels an integral number of clockwise round trips through both branches at frequencies given by

$$f_{SA}^{cw} = \frac{nc_0}{s\left(\frac{c_0}{c_+} + \frac{c_0}{c_{z_-}}\right)} \tag{3.28a}$$

For counterclockwise round trips (Fig. 21b)

$$f_{SA}^{ccw} = \frac{nc_0}{s\left(\frac{c_0}{c_-} + \frac{c_0}{c_{z_+}}\right)} \tag{3.28b}$$

To determine the magnitude of the frequency shifts caused by mean flow again consider the cylindrical parallel lined duct configuration shown in Fig. 20. The "sing-around" frequencies have been plotted vs flow speed in Fig. 20b for clockwise, f_{SA}^{cw}, and counterclockwise, f_{SA}^{ccw}, circuits of the muffler with liner thickness as a parameter. For clockwise circuits, f_{SA}^{cw} decreases monotonically as the flow speed is increased. For counterclockwise circuits, f_{SA}^{ccw} first increases and then decreases with increasing Mach number. However, the difference $f_{SA}^{ccw} - f_{SA}^{cw}$ increases monotonically with Mach number. Since "sing-around" interference is optimized when $f_{SA}^{cw} = f_{SA}^{ccw}$, the above analysis indicates that mean flow will cause "sing-around" interference to occur over a wider frequency band with reduced peak attenuation.

A note of caution should be interjected at this point to assure that the above results are not interpreted too broadly. The "sing-around" frequency determined from the time period required for a sound wave to make a round-trip circuit in the muffler only approximates the frequency at which strong reflections occur at the muffler entrance due to impedance mismatches between the branch ducts and the main duct. When the impedances of the branch ducts differ widely from each other the "sing-around" interference frequency cannot be calculated from the simplified relationships derived in Chap. 1. Stewart,[6] noting this phenomenon, showed that Eq. (1.4) appropriately defined the interference frequencies for Herschel-Quincke tubes having branch ducts of unequal cross-sectional areas. No such analogous expression exists for the lined duct acoustic filter. However, by introducing convective effects into Eqs. (3.19a-n) accurate interference frequencies for lined duct acoustic filters with flow could be determined using a digital computer.

3.3 Experimental Program

In order to demonstrate experimentally the basic idea of the parallel lined duct filter, the interference between waves which have been phase delayed by different amounts, a duct arrangement shown schematically in Fig. 22 was used. Starting with a rectangular duct with one wall lined with a honeycomb type liner (without any resistive cover sheet), a parallel duct filter was obtained merely by inserting a rigid partition in the duct so as to divide it into two parallel branches, one lined and one unlined, as shown.

3.3.1 Transmission Loss Measurements with Reactive Liners

In the experiments described here the main duct consisted of a rectangular 3/4 in. x 3/4 in. tube. As a reference it is interesting to determine first the transmission loss of the duct without a partition. In these measurements an incident pulsed harmonic wave train was used. It was observed by means of two microphones mounted in the wall of the hard-walled duct on the input and output sides of the parallel duct filter. The input microphone was placed sufficiently far from the entrance of the filter so that the incident and reflected waves could be observed separately.

Figure 23a shows the incident (p_i), reflected (p_r), and transmitted (p_t) pulses for the reference duct. The carrier frequency of the pulse is 753 Hz and the pulse length is 5 cycles. In this case the transmission loss (20 log $|p_i/p_t|$) was only about 3 dB.

Figure 23b shows the corresponding data for the parallel duct filter when the partition is present 0.22 in from the lined wall dividing the duct into two branches in parallel, one lined and one unlined. The transmission loss of the filter now exceeds 28 dB. As can be seen by comparing the pulse heights, much of the acoustic energy is now reflected back toward the source. If the measured value of the phase speed in the lined duct portion, as given in Fig. 11, is used, Eq. (1.6b) can be evaluated to show that at 753 Hz $\Delta\phi_2 \simeq 4\pi$, a condition for strong reflection in an ideal nondissipative parallel duct filter.

Similar measurements were carried out at several frequencies in the range from 300 Hz to 2000 Hz for three different values of the separation

of the lined duct wall and the partition. The frequency dependence of the transmission loss thus obtained is shown in Fig. 24, where, for comparison, is shown also the transmission loss for the lined duct with the partition removed. For each of these parallel duct configurations the transmission loss is considerably higher than for the single duct, and the maximum values of the transmission loss occur at frequencies in the vicinity of 400 Hz and 800 Hz, corresponding to $\Delta\phi_2 = 2\pi$ and 4π, respectively.

To assess the accuracy of the analytical solution determined in Sec. 3.2, sound transmission through the parallel duct configuration B, shown in Fig. 22, was measured. The main duct at the inlet and exit of the parallel duct filter was a 3/4 in. x 3/4 in. rectangular tube. The lined branch of the filter was lined with an 1 inch thick soda straw liner having a void volume ratio of 74%. Using the tone burst technique described in the previous section, the transmission loss was determined from the output of two microphones M1 and M2 located 42 inches upstream and 23 inches downstream of the lined section, respectively (Fig. 22). The transmission loss in the duct caused by the soda straw liner (i.e. no splitter) is shown in Fig. 25. At low frequencies (<1 kHz) the measured attenuation was approximately 6 dB. Near the liner resonance frequency the attenuation peaks at approximately 40 dB.

When the splitter was inserted into the duct in a position 0.47 in. from the lined wall, two distinct attenuation peaks were measured at 500 Hz (10.6 dB) and at 1150 Hz (16.2 dB). Using a computer program which evaluated Eqs. (3.19a-n) the transmission loss characteristics were calculated assuming the soda straw liner had an effective flow resistance,

θ, of 0.1. The analysis predicted the frequencies of the attenuation peaks almost exactly. These peak frequencies occurred at $\alpha_1 + \alpha_2 = 2\pi$ and 6π respectively. The level of the attenuation was overpredicted at the peak frequencies and grossly underestimated elsewhere.

The computer program was then modified to include viscothermal losses in the unlined duct sections. Also the effective flow resistance, θ, of the soda straw liner was increased to 0.5. Although this value of θ may seem a bit high for a "non-dissipative" soda straw liner, the large surface area of the liner induces high viscothermal losses. This effect has been discussed by Zwikker et al.[45] The resulting analytical prediction is shown in Fig. 26a. Note that the frequencies at which attenuation maxima occur are almost uneffected by the viscothermal losses. However, the predicted attenuation level between peaks has been much improved.

The splitter was then moved closer to the lined wall (0.345 in.) for a second set of measurements. Attenuation maxima were measured at f = 450, 900 and 2020 Hz (Fig. 26b). The computed transmission loss curve shows good agreement at the first peak (450 Hz) and predicts second and third peaks at 750 Hz and 1950 Hz. The sound transmission level predicted between preaks is quite good.

For the final test, the splitter was moved very close to the lined wall (0.22 in.) to reduce the phase velocity in the lined branch to approximately one-half the free space sound speed. The resulting attenuation spectrum was quite good as shown in Fig. 26c. Attenuation maxima

were recorded at 400 Hz (15.4 dB) and 750 Hz (24.6 dB). The maxima occurred at $\alpha_1 + \alpha_2 = 2\pi$ and 4π, respectively. The attenuation was relatively broadband, being greater than 10 dB in the range $310 < f < 950$ Hz. The calculated transmission loss differed markedly from the experimental results. The reason for this poor prediction is not yet known but could be caused by the extreme closeness of the rigid partition to the lined wall. At the spacing of 0.22 in., the duct width is less than the diameter of the soda straws, and the liner performance may be influenced by the proximity of the hard wall.

3.3.2 Transmission Loss Measurements with Dissipative Liners

Several tests were conducted to determine the performance of parallel duct filters having one branch lined with a dissipative liner. Rectangular and circular duct configurations were tested. The rectangular ducts were tested both with and without mean flow.

3.3.2.1 Rectangular Ducts Without Flow

A set of tests conducted to investigate the effect of lining one branch of a rectangular parallel duct filter with a 1-inch thick partitioned foam liner is shown in Figs. 27a-c. The effect of the rigid partitions alone, which were spaced 2-in. apart in the 1-foot long lined section, is shown in Fig. 27a. The lower curve for the hard-wall parallel duct is a reference condition in which the lined section has been replaced by a hard wall. The measured transmission loss results from viscothermal losses in the duct between the microphone locations and represents the lower bound for transmission loss measurements in this test program.

With the partitioned liner (without foam) in place the duct functions as a low pass filter with a cutoff frequency at approximately 2 kHz. At frequencies above 2300 Hz the attenuation exceeds 40 dB but at low frequencies ($f < 1500$ Hz) the attenuation does not exceed the attenuation "floor" set by viscothermal losses. Inserting a 12-inch long rigid splitter on the centerline of the duct forms a parallel duct filter with a sharp attenuation peak at 1100 Hz with only a minimal transmission loss increase (2-3 dB) over the frequency range $200 < f < 1950$ Hz. For $f > 1950$ Hz the presence of the splitter destroyed the efficient high frequency filtering of the partitioned liner.

In Fig. 27b the tests shown in Fig. 27a were repeated with Scott Industrial Foam (100 ppi) between the partitions. For the duct configuration without the splitter the presence of the foam between the partitions increased the attenuation in the duct over the entire frequency range tested ($200 \text{ Hz} < f < 2300 \text{ Hz}$) as expected. With the rigid splitter inserted on the centerline of the duct three distinct attenuation peaks occurred at 450, 825 and 1200 Hz. At 825 Hz the attenuation of the 1-foot long silencer exceeded 27 dB. Additionally the broadband attenuation was increased substantially to a level exceeding 10 dB over the frequency range $250 < f < 2300$ Hz. These results were anticipated following the analytical predictions shown in Fig. 19a-d for point-reacting porous liners. The arrows indicate attenuation peaks at $\alpha_1 + \alpha_2 = 2n\pi$ which were predicted using phase speeds measured in a lined duct configured identically to duct B.

The importance of using a point-reacting liner in a lined parallel duct filter is evident from the results shown in Fig. 27c. In these tests the duct was lined with an unpartitioned Scott Industrial Foam (100 ppi) liner. This liner had a surface of extended reaction and the phase speed of the fundamental mode, based upon the results shown in Fig. 12, did not differ substantially from the free space phase speed except in the lowest frequency range ($f < 500$ Hz). Insertion of the rigid splitter on the duct centerline did not increase the attenuation substantially at any frequency. At high frequencies the transmission loss was reduced.

Based upon these test results, partitioned foam liners which approximate surfaces of local reaction are good candidate liners for parallel lined duct acoustic filters.

3.3.2.2 Cylindrical Ducts without Flow

For all the parallel lined duct configurations reported above the 1-foot long rigid splitter was aligned conterminously with the 1-foot long liner. Consequently, at high frequencies sound traversing the unlined branch duct was not attenuated at any point by the dissipative liner and propagated unhindered through the parallel lined duct filter. The results reported in this section will show that this problem is not unsolvable.

A parallel lined duct filter was created by inserting a 1-inch diameter rigid tube along the centerline of a 2-inch diameter circular duct lined with acoustical foam as shown in Fig. 28. Fiberglass

fins were used to center the tubular splitter in the duct. The splitter fit tightly in the duct but could be easily repositioned relative to the lined section. The entire filter is comprised of four sections denoted by dimensions s_1 through s_4. The length of the lined duct upstream of the splitter is denoted by s_1; s_2 indicates the length of the lined annulus; s_3 indicates the length of the splitter extending into the exit duct; and s_4 is the length of any extension added to the splitter tube.

In Fig. 29a the transmission loss through the lined duct with and without the splitter installed is shown for $100 \leq f \leq 1000$ Hz. Without the splitter (i.e. s_1 = 14.6 in.) the lined duct provided 50 dB attenuation at 1000 Hz but the attenuation at low frequencies was poor. By inserting a splitter aligned coterminously with the liner (i.e., s_2 = 14.6 in.) the attenuation of the lined duct was improved marginally at frequencies above 350 Hz. The splitter was then withdrawn 4 in. from the lined section into the exit duct. The attenuation at both low and high frequencies increased. After withdrawing the splitter an additional 4 in., 38 dB attenuation was measured at 340 Hz. There was also no significant degradation in the transmission loss at high frequencies. Attenuation over distance s_1 sufficiently reduces the intensity of the high frequency sound waves so that their propagation through the parallel duct array is immaterial.

An effective method of tuning a parallel duct filter is shown in Fig. 29b. By adding an 8.6 in. section to the downstream end of the splitter the frequency of the first attenuation peak was reduced from 340 Hz to 240 Hz in accordance with theory.

3.3.2.3 Rectangular Ducts With Flow

To determine the effects of flow on the performance of parallel lined duct filters, the filter (with partitioned foam liner) tested above (Fig. 27b) was tested in the flow facility shown schematically in Fig. 30. By rotating a portion of the modular duct the filter could be tested as either an intake muffler (sound and flow in opposite directions) or as an exhaust muffler (sound and flow in the same direction). The results of this test program are shown in Figs. 31a,b. In the exhaust muffler configuration (Fig. 31a) the transmission loss of the filter is effected minimally by flows up to M = 0.10. As an intake silencer (Fig. 31b) the filter is relatively unaffected by flow at M = 0.05, although at M = 0.10 the attenuation peak at 880 Hz is shifted to 950 Hz and reduced by 6 dB.

This small measured effect of mean flow on the performance of the parallel lined duct filter is contrary to the significant flow effects predicted by the rudimentary inviscid analysis performed in Section 3.5.2. However, for the small model duct assembly used in these experiments the redistribution of the mean flow between the branch ducts due to viscosity cannot be ignored. Ten static pressure taps along the side walls of the parallel duct assembly confirmed that the flow velocities in the unlined and lined branches were 136 and 104 ft/sec respectively when the velocity in the entrance duct was 120 ft/sec. This mean flow redistribution reduced the travel time difference for clockwise vs counter-clockwise circuits of the muffler as shown in Fig. 32.

Thus, the fact that the performance of the mufflers tested in this experimental program was relatively uninfluenced by mean flow may have been a fortuitous occurrence due to the small muffler size. Tests with much larger models must be conducted before the effects of mean flow on the performance of full-scale lined parallel duct filter installations can be defined.

3.4 Computer Study

3.4.1 Description of Computer Program

A computer program was developed which calculates the transmission loss in a duct system, consisting of unlined sections, conventionally lined sections, and/or duct sections having parallel branches. The program uses a numerical searching algorithm to solve the dispersion relationship in a rectangular duct without flow having a point-reacting porous or resonator liner. The algorithm was written by Galaitsis and Ingard[16] and improved by Cho and Ingard.[2] The solution technique used by Galaitsis is explained in Ref. 46. Using the complex wavenumber determined from the solution of the dispersion relationship, the computer program calculates the forward transmission matrix for each duct section using Eq. (4.63) for a single lined or unlined duct section, Eqs. (3.19a-n) for two ducts in parallel, and Eq. (4.69) for three or more ducts in parallel. The overall transmission matrix for the duct system is then obtained by multiplying together the transmission matrices of all the duct sections. The transmission loss is then determined from a summation of the elements of the overall transmission matrix as indicated in Eq. (4.35). Visco-thermal losses in unlined duct sections can be calculated as an option.

3.4.2 Sound Transmission Through Parallel Ducts in Series

Because of the frequency selective characteristics of lined parallel duct filters it should be possible to join filters, which are tuned to different frequencies, in series to achieve enhanced broadband attenuation. In Fig. 33 the calculated transmission loss is shown for two lined parallel duct filters A and C joined in series by lined duct section B. Filters A and C are configured identically but are of unequal axial length causing them to be tuned to different sets of frequencies. Note that the first four attenuation peaks of the filter system correspond to the first and second "sing-around" frequencies of filters A and C. A third set of attenuation peaks based upon length B, the distance between two impedance discontinuities (i.e. the primary reactive attenuation mechanism in an expansion chamber muffler), which could be expected to influence the attenuation spectrum under certain conditions, was not discernible for this configuration. The attenuation spectrum of the lined duct without the rigid splitters is shown for comparison. Except at the highest frequencies considered the lined parallel ducts in series have superior performance compared to the unpartitioned duct. Moreover, in this high frequency region, although the unpartitioned duct has greater attenuation, the transmission loss of the parallel duct system exceeds 40 dB.

3.4.3 Comparison of Sound Transmission Through Parallel Ducts with Conventional Lined Duct Configurations

It has been shown earlier in Chap 3 that rigid splitters can be used in lined ducts to create parallel branches which enhance the low frequency attenuating characteristics of the duct. The question arises, however, whether other liner configurations can be devised which attenuate

the low frequency noise with equal effectiveness. To determine whether parallel lined ducts are optimal liner configurations for duct systems requiring enhanced low frequency attenuation in addition to effective attenuation at medium and high frequencies the transmission loss through 10 lined duct configurations shown in Fig. 34 was calculated. The 10 configurations consist of uniformly lined ducts (A, B and H), multi-section duct liners (D, E and F), single parallel lined ducts (C and G) and parallel lined ducts in series (I and J). To provide a basis for comparison, each configuration used an equal amount of acoustical liner material.

The calculated attenuation spectra for configurations A, B, D and E (uniform vs multi-section duct liners) are shown in Fig. 35a. These spectra indicate that in the low frequency range multi-section liners provide a marginal increase in attenuation. The attenuation spectra of configurations B, C, F and G (uniform liners vs parallel lined ducts) are compared in Fig. 35b. Configuration B provides the best low frequency attenuation but at high frequencies the filter is ineffective because sound waves in the lined branch are almost completely attenuated and have insufficient amplitude to interfere with the sound waves which propagate through the unlined branch. Configuration G, having a lined section in series with the parallel lined duct section, has more optimal attenuation.

In Fig. 35c attenuation spectra of configurations A, H, I and J are compared to show the effect of placing rigid splitters in series within a lined duct. Both series-parallel duct configurations (H and I) display superior low-frequency attenuation compared to the unpartitioned

ducts. At high frequencies the lined wall between the parallel duct sections in configuration I gives it better performance than configuration H.

Attenuation spectra of the best candidate duct liner configurations are summarized in Fig. 35d. Configuration I (lined parallel ducts in series) appears to be the optimal configuration for applications requiring low, medium and high frequency attenuation. At high frequencies, although the attenuation is less than the attenuation of the unpartitioned duct, it exceeds 20 dB across a wide frequency range.

3.4.4 Sound Transmission Through Three Ducts in Parallel

The effectiveness of acoustic filtering using three ducts in parallel was investigated for the configurations shown in Fig. 36. As in Sect. 3.4.3 each configuration used an equal amount of acoustical liner material. Transmission loss vs frequency for each of these four configurations is shown in Fig. 37. Configuration L, having all three parallel branches lined, has good attenuation at high frequencies but it is not very effective at low frequencies. Better low frequency attenuation is obtained for configuration M due to a large phase speed difference between the unlined branch and the branch with a 2.25 in thick liner. However, neither configuration L nor M is as effective as configuration K (a two-branch parallel lined duct which is equivalent to configuration C) in the low frequency range. Although a complete parametric study may prove otherwise, the pair of three-branch parallel ducts considered here do not present any advantage over two-branch parallel ducts.

3.4.5 Sound Transmission in a Duct Bend Containing a Rigid Splitter

Fuller and Bies[37] have presented data and an analysis for sound transmission in an unlined bend containing a rigid splitter (Fig. 38a). Their complicated analysis used the method of Rostafinski[122] to determine the sound field in the curved branch ducts. Since the phase speed of a sound wave propagating in a rigid duct bend approximates the thermodynamic speed of sound at low frequencies, the partitioned duct bend was modeled as a Herschel-Quincke tube, as shown in Fig. 38b, for this computer study. In this section the results predicted by this Herschel-Quincke tube approximation and the Fuller and Bies analysis will be compared to the experimental data.

The measured and computed results of Fuller and Bies are shown in Fig. 39a. Measured attenuation peaks occurred at k_0h = 0.6, 1.2, 1.8, 2.0, 2.4 and 2.9. The peak at k_0h = 2.0 is caused by destructive interference at the exit of the inner and outer channels of the bend. The remainder of the peaks in the frequency range $0 < k_0 h < 3.0$ are caused by the "sing-around" effect. The analysis of Fuller and Bies predicts the interference frequencies with good accuracy but overestimates the peak amplitudes at all frequencies. At $k_0 h = 1.2$ the predicted attenuation is 20 dB higher than the measured peak.

The results calculated using the Herschel-Quincke tube model are compared to the experimental data of Fuller and Bies in Fig. 39b. The computer program calculated the visco-thermal losses in each rigid branch duct and evaluated Eqs. (3.19 a-n) to determine the transmission matrix for the bend. The analysis predicted interference frequencies at least

as accurately as the Fuller and Bies analysis and the amplitudes were predicted within 3 dB for 5 of the 6 peaks in the frequency range analyzed. Furthermore, the amplitude of the sixth peak was predicted more accurately than the amplitude predicted by the Fuller and Bies analysis. Thus, for low frequencies, at which only the fundamental mode can propagate in the duct, sound transmission through duct bends containing rigid splitters can be predicted quite accurately by modeling the bend as a Herschel-Quincke tube having plane wave propagation within the branches.

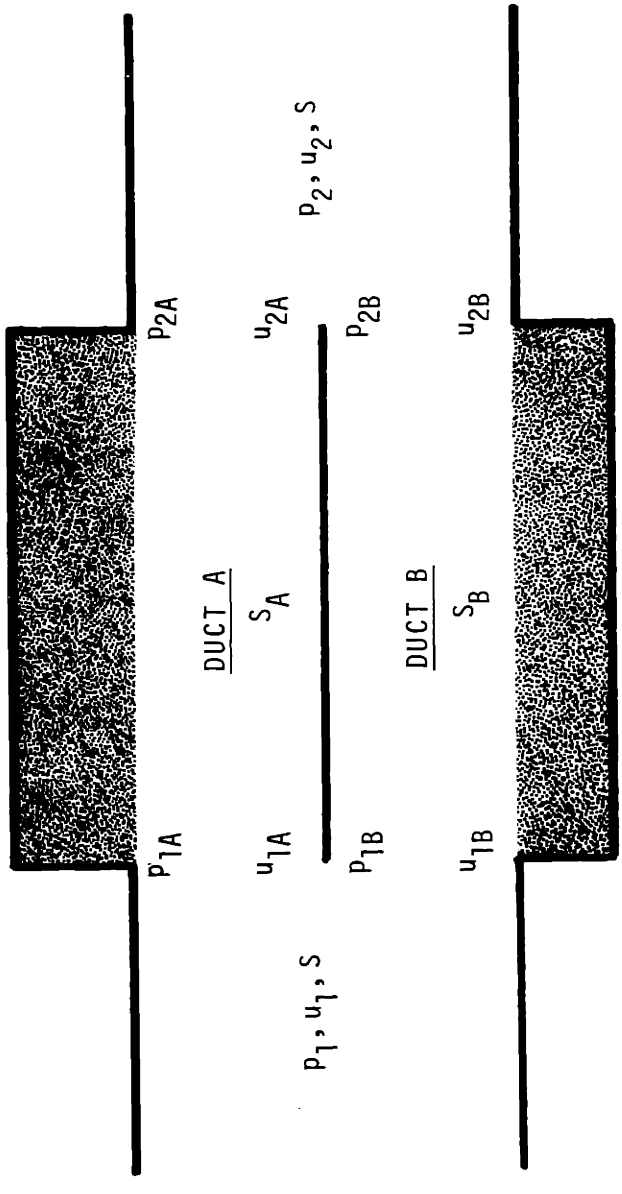

FIG. 16: PARALLEL LINED DUCT

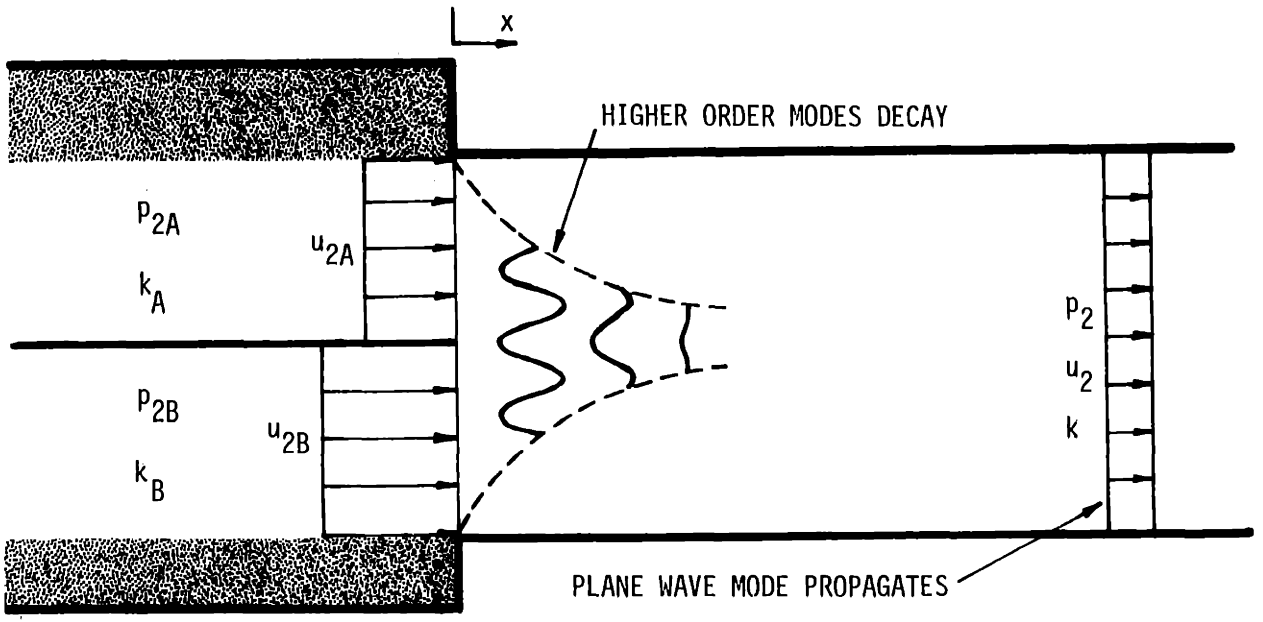

Fundamental mode in each lined duct approximated by equivalent plane wave mode.

- $u_{2A,2B}$ is average velocity amplitude of fundamental mode at exit of Duct A,B
- $k_{A,B}$ is propagation constant of fundamental mode in Duct A,B
- $p_{2A,2B}$ is the spatially averaged acoustic pressure amplitude at the exit plane of Duct A,B

FIG. 17: EXIT CONDITIONS FOR LINED DUCTS IN PARALLEL

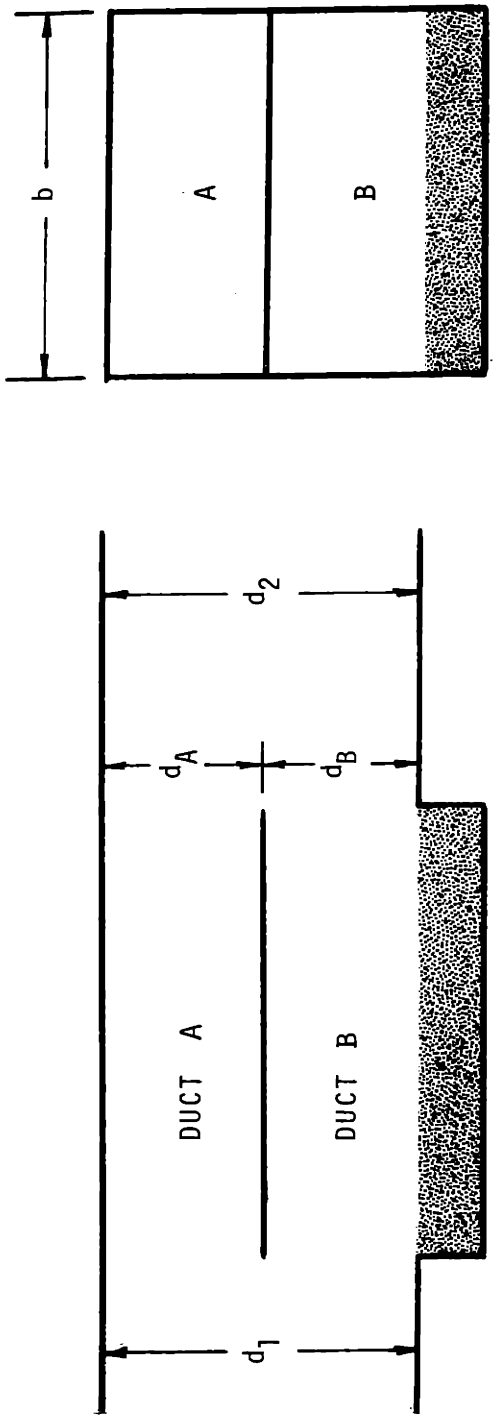

FIG. 18: RECTANGULAR PARALLEL DUCTS WITH ONE WALL LINED

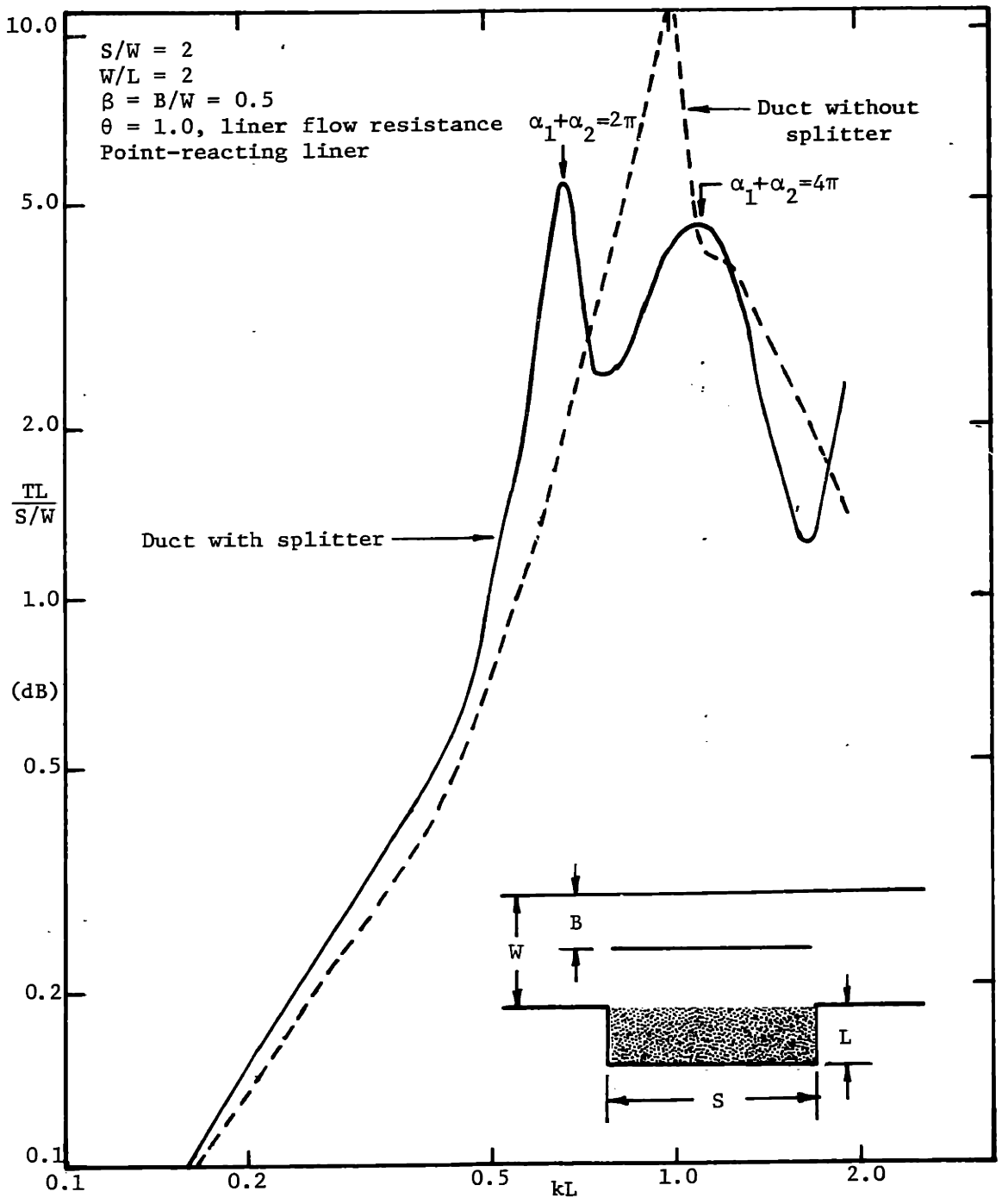

FIG. 19a: CALCULATED TRANSMISSION LOSS OF RECTANGULAR DUCT PER UNIT DUCT HEIGHT (S/W = 2)

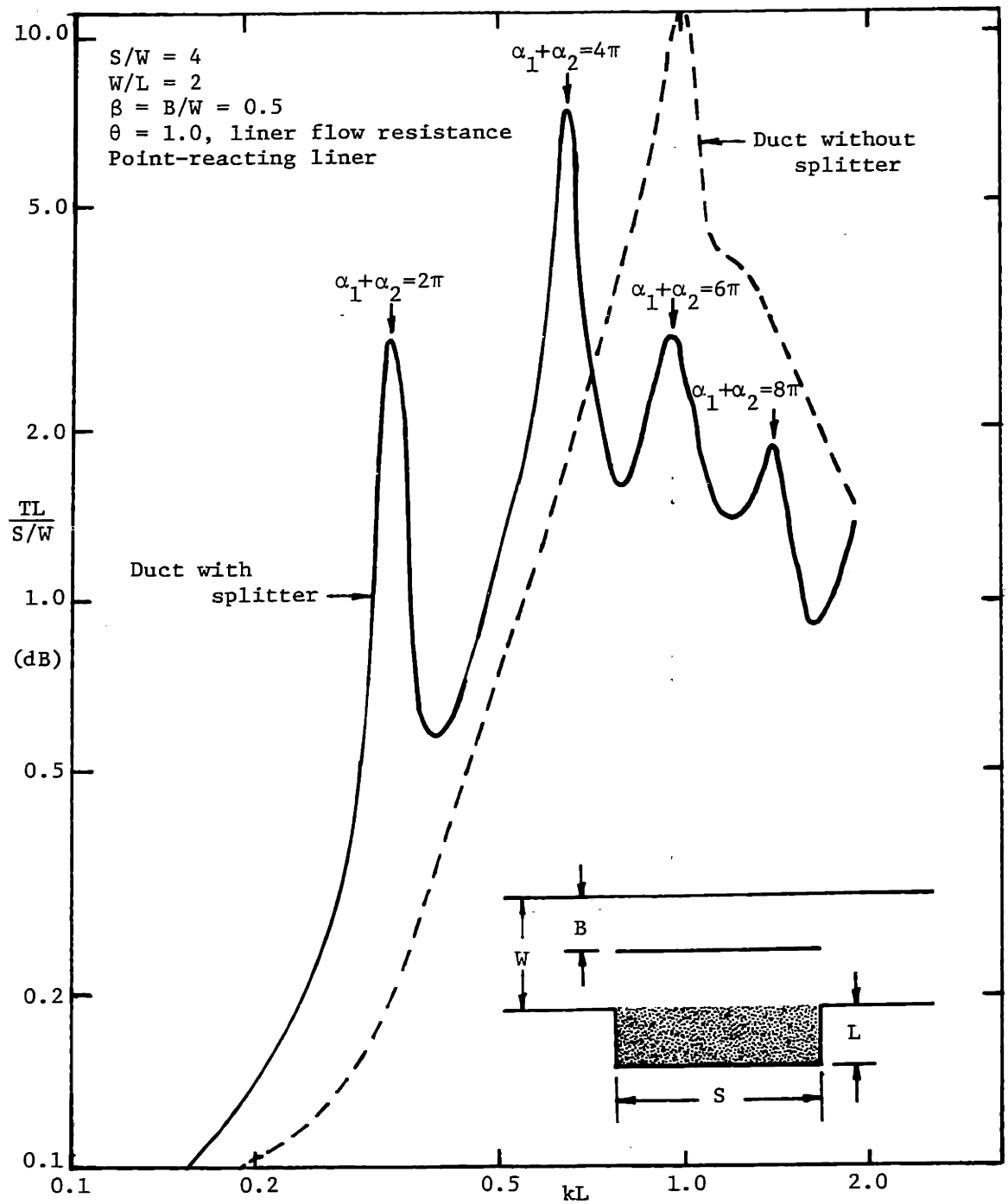

FIG.19b: CALCULATED TRANSMISSION LOSS OF RECTANGULAR DUCT PER UNIT DUCT HEIGHT (S/W = 4)

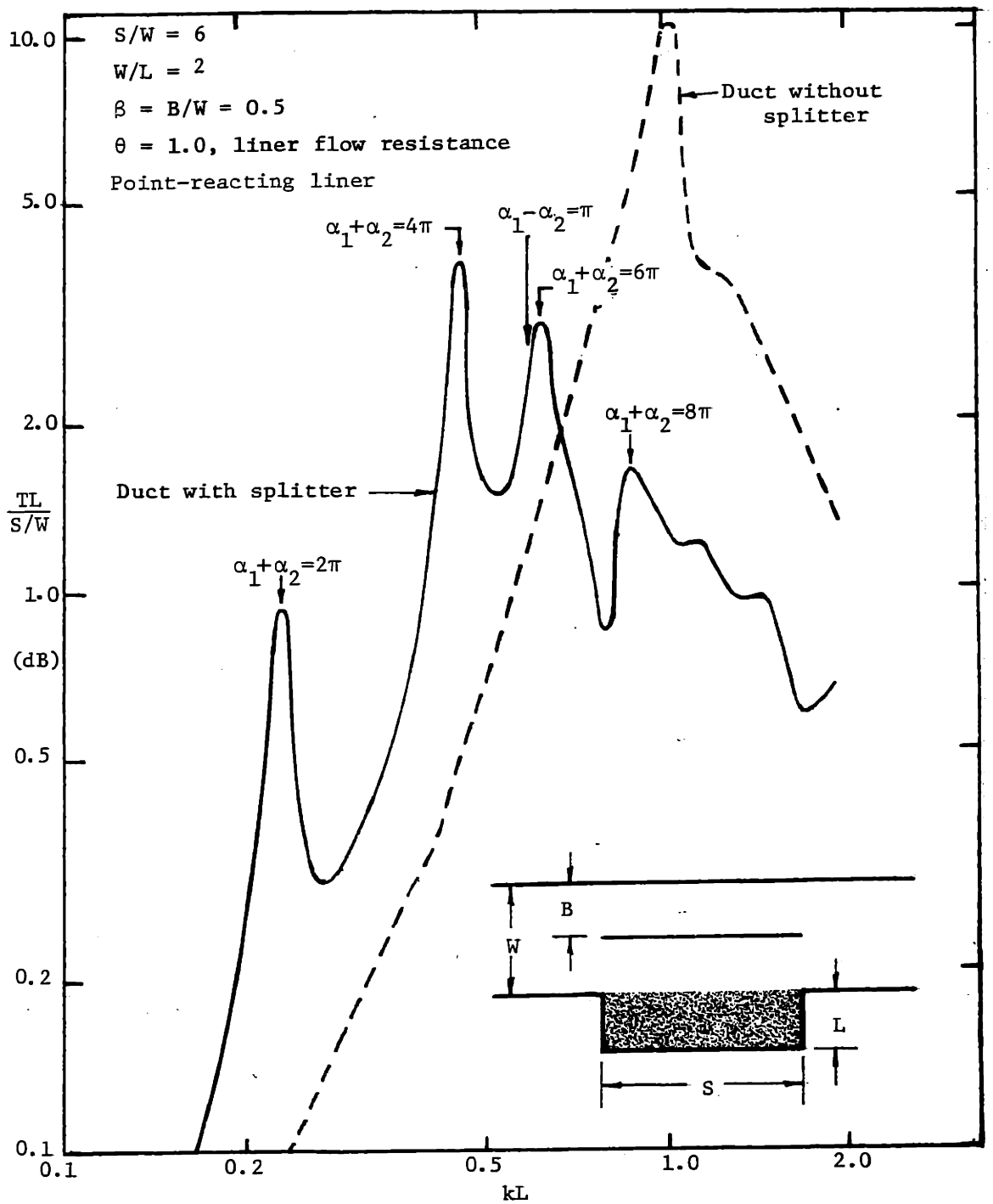

FIG. 19c: CALCULATED TRANSMISSION LOSS OF RECTANGULAR DUCT PER UNIT DUCT HEIGHT (S/W = 6)

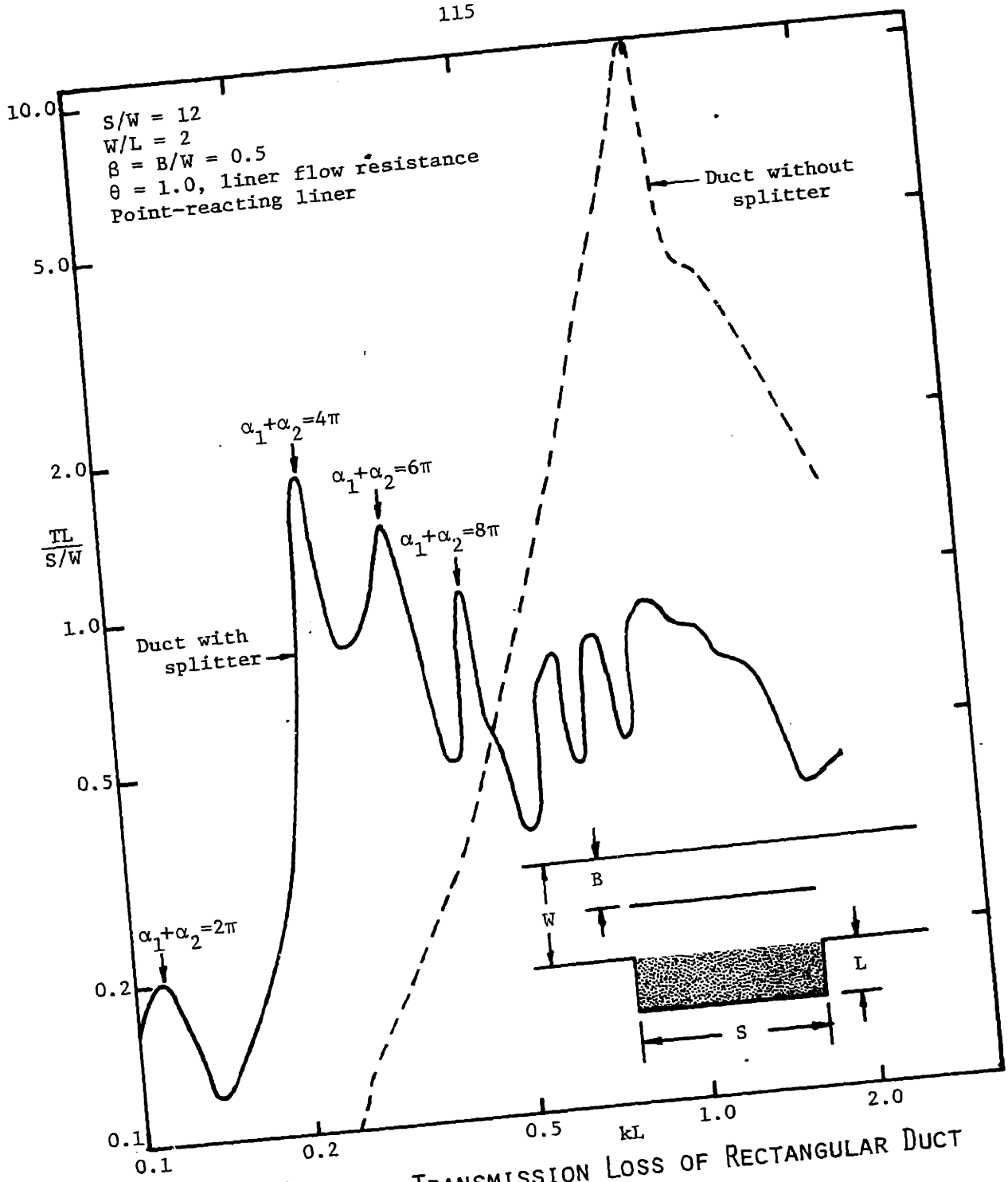

FIG. 19d: CALCULATED TRANSMISSION LOSS OF RECTANGULAR DUCT PER UNIT DUCT HEIGHT (S/W = 12)

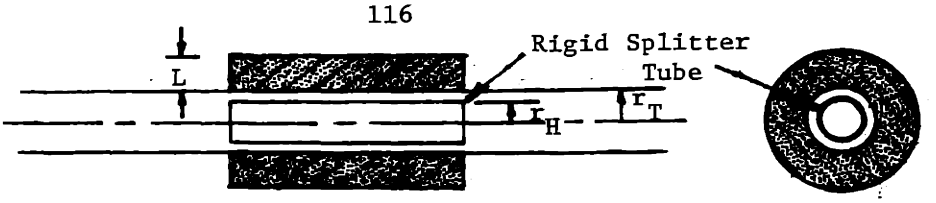

a) Destructive Interference Frequency

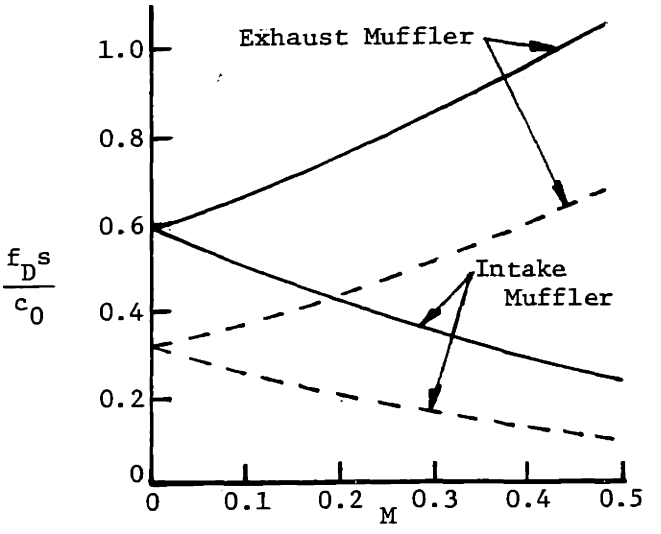

b) Sing-Around Frequency

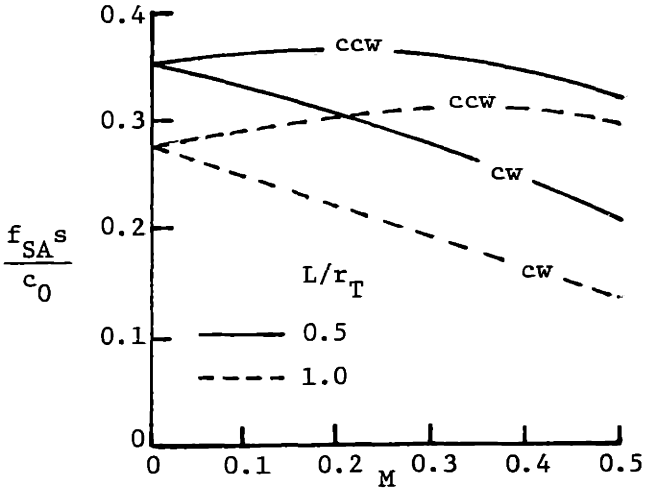

FIG. 20 : EFFECT OF MEAN FLOW ON INTERFERENCE FREQUENCIES

a) Clockwise Circuits

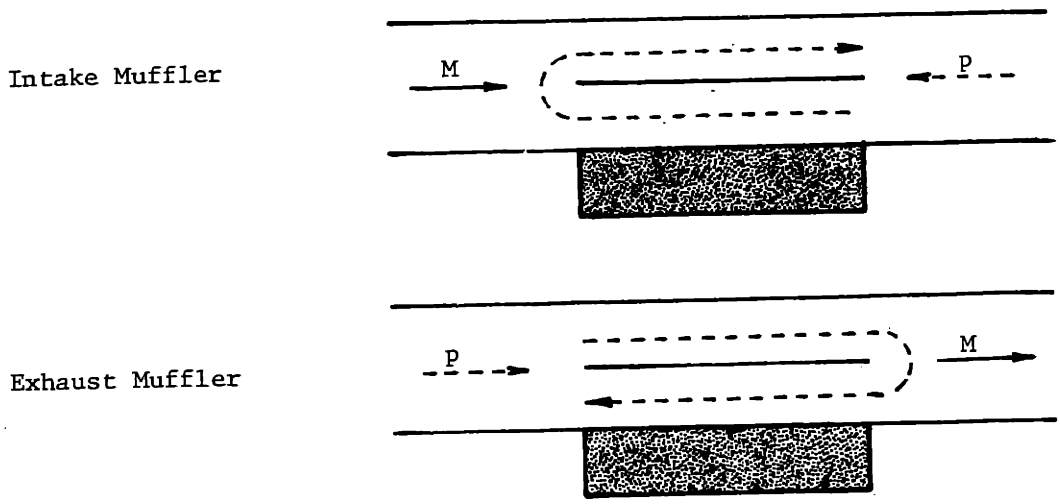

b) Counterclockwise Circuits

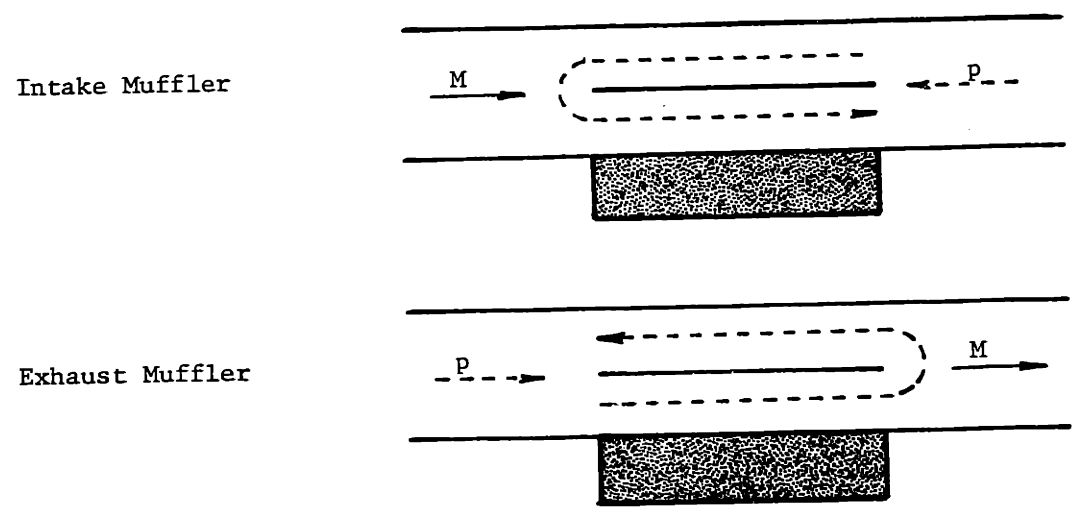

FIG. 21: DIRECTIONS OF SOUND PROPAGATION IN PARALLEL DUCTS WITH MEAN FLOW

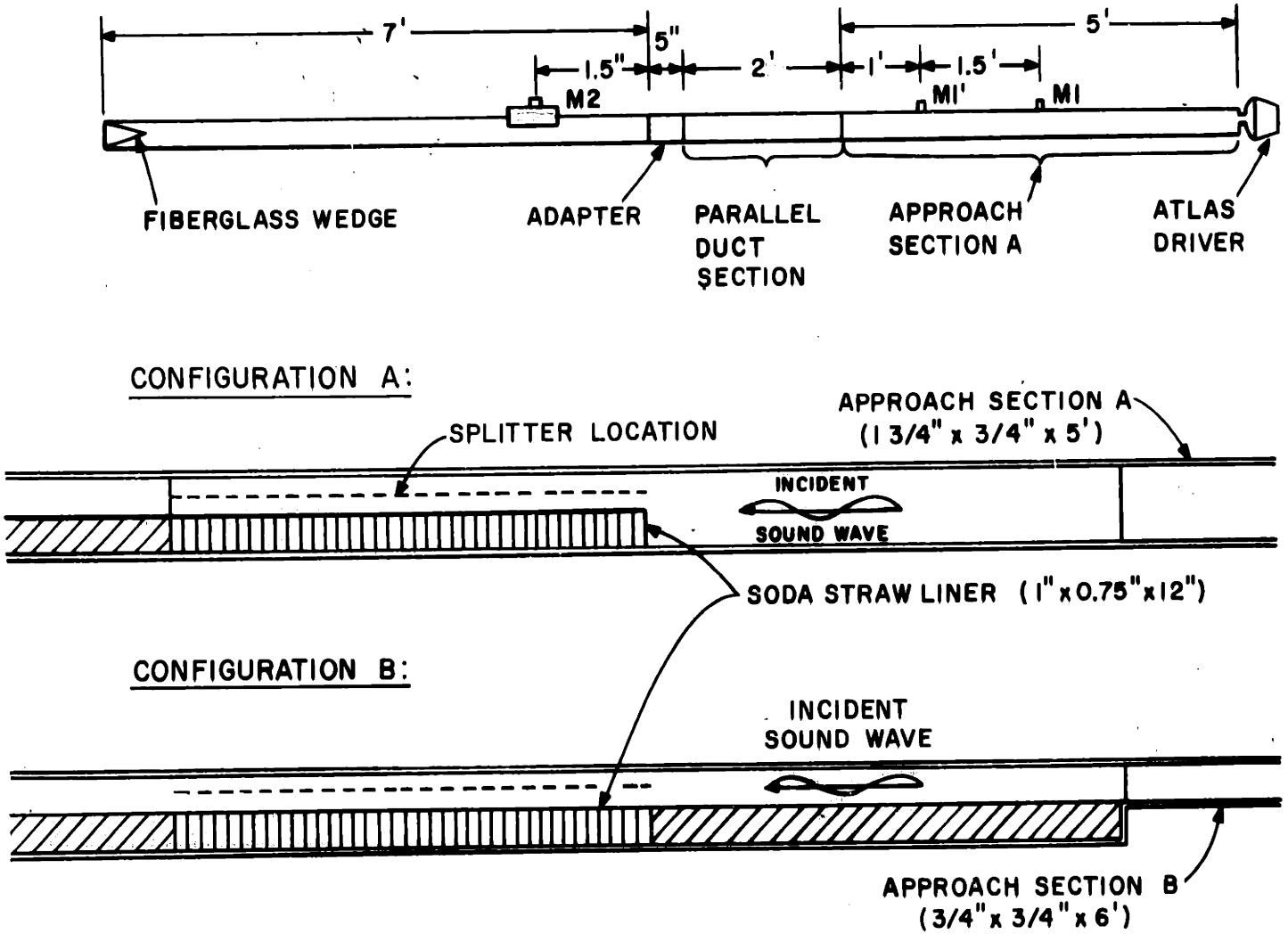

FIG. 22: EXPERIMENTAL CONFIGURATIONS FOR TESTS USING SODA-STRAW LINERS

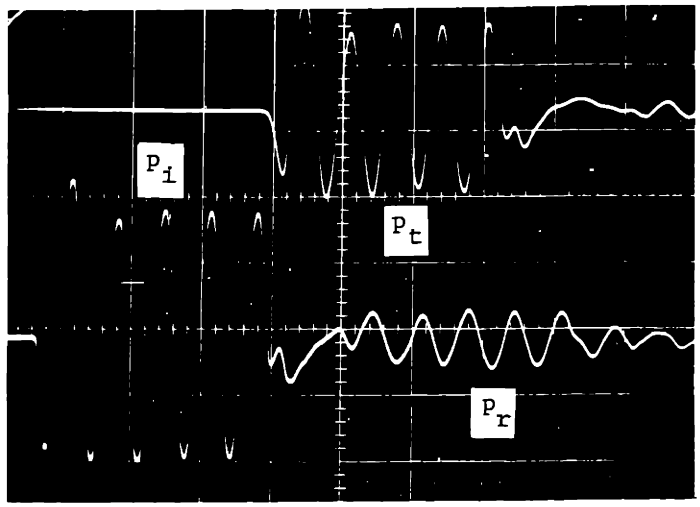

a) 0.75 in × 0.75 in duct lined on one wall with honeycomb liner

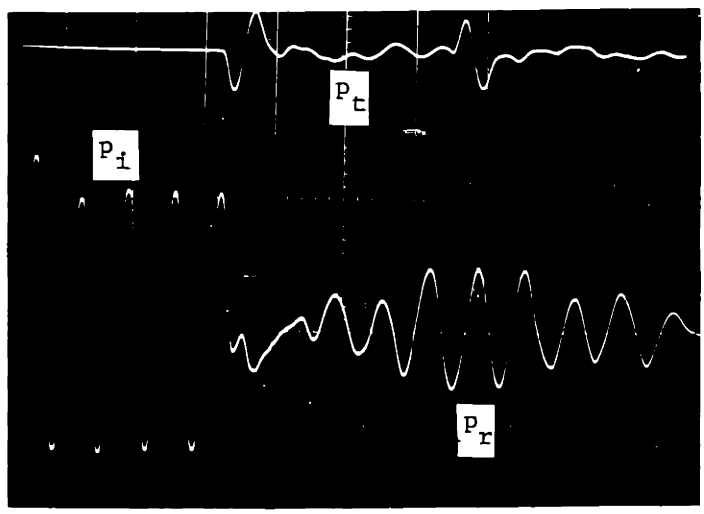

b) Parallel lined duct filter (rigid partition inserted 0.22 in above lined wall)

FIG. 23: TRANSMISSION OF ACOUSTIC PULSE THROUGH 1-FT LONG LINED DUCT SECTION (f = 753 Hz)

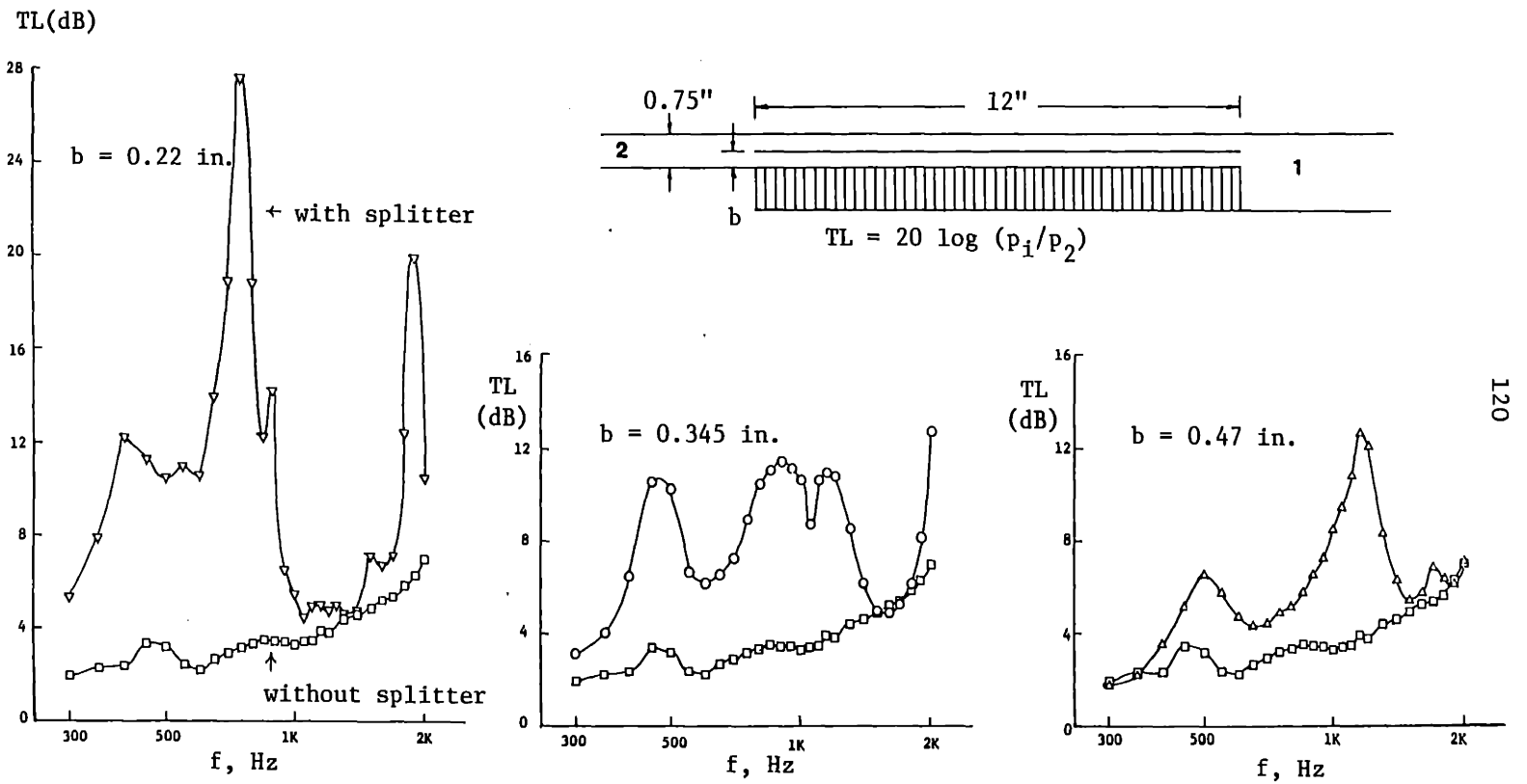

FIG. 24 : MEASURED TRANSMISSION LOSS OF RECTANGULAR PARALLEL DUCT ACOUSTIC FILTER WITH SODA-STRAW LINER. COMPARISON OF PARTITIONED AND UNPARTITIONED DUCTS.

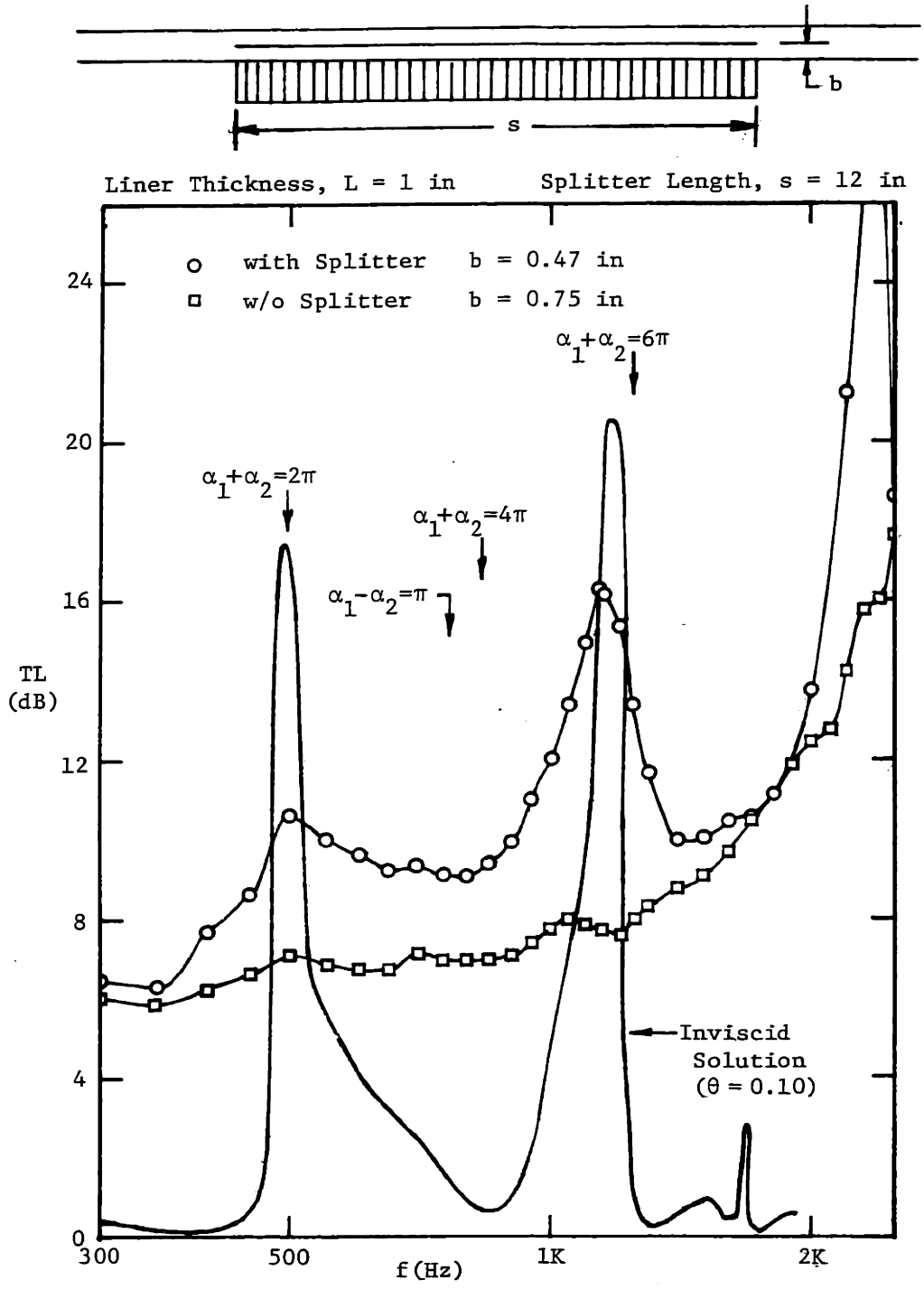

FIG. 25 : MEASURED TRANSMISSION LOSS OF RECTANGULAR PARALLEL DUCT FILTER COMPARED TO INVISCID SOLUTION

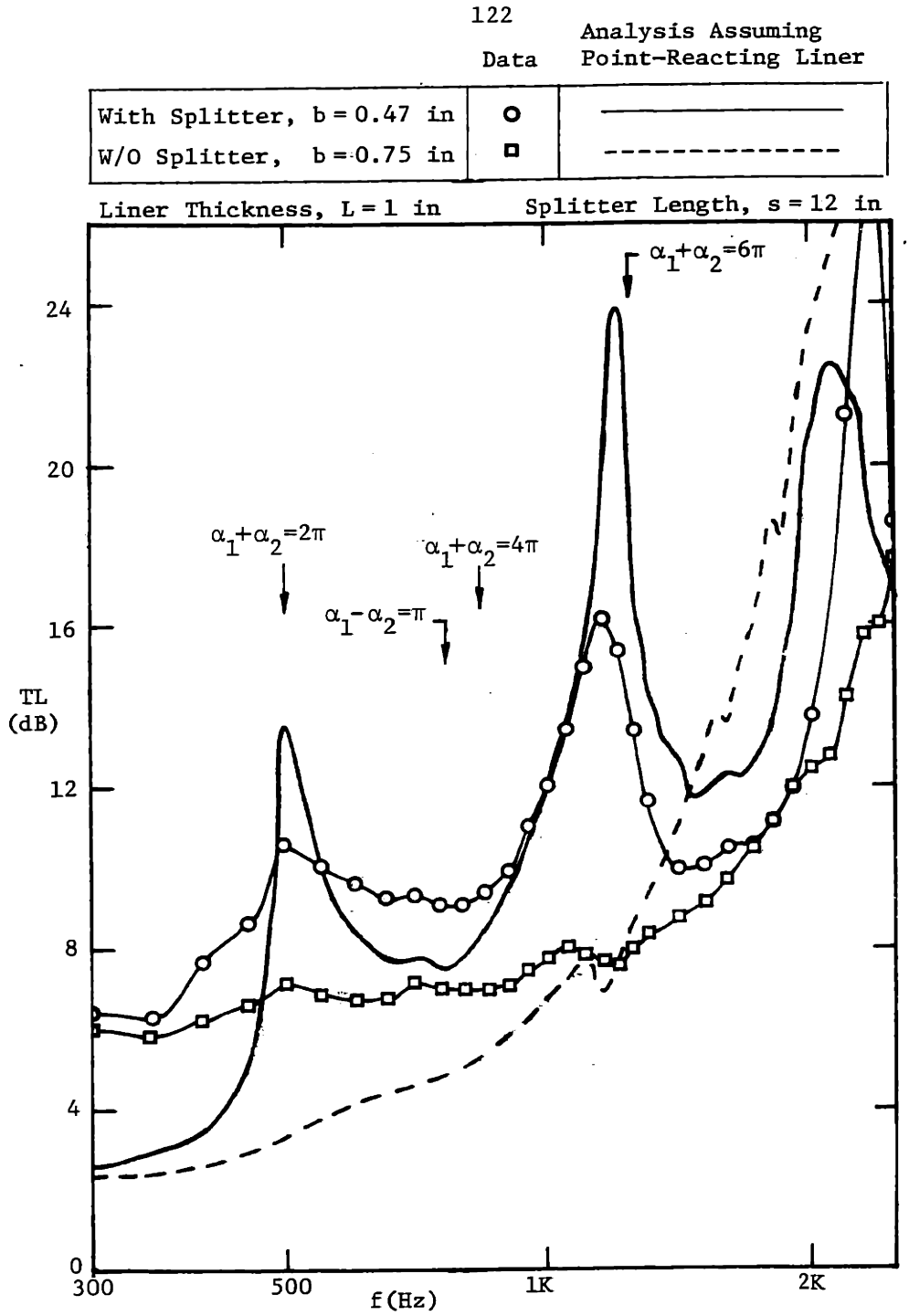

FIG. 26a : TRANSMISSION LOSS OF RECTANGULAR PARALLEL DUCT FILTER HAVING SODA-STRAW LINER IN ONE BRANCH (b = 0.47 in)

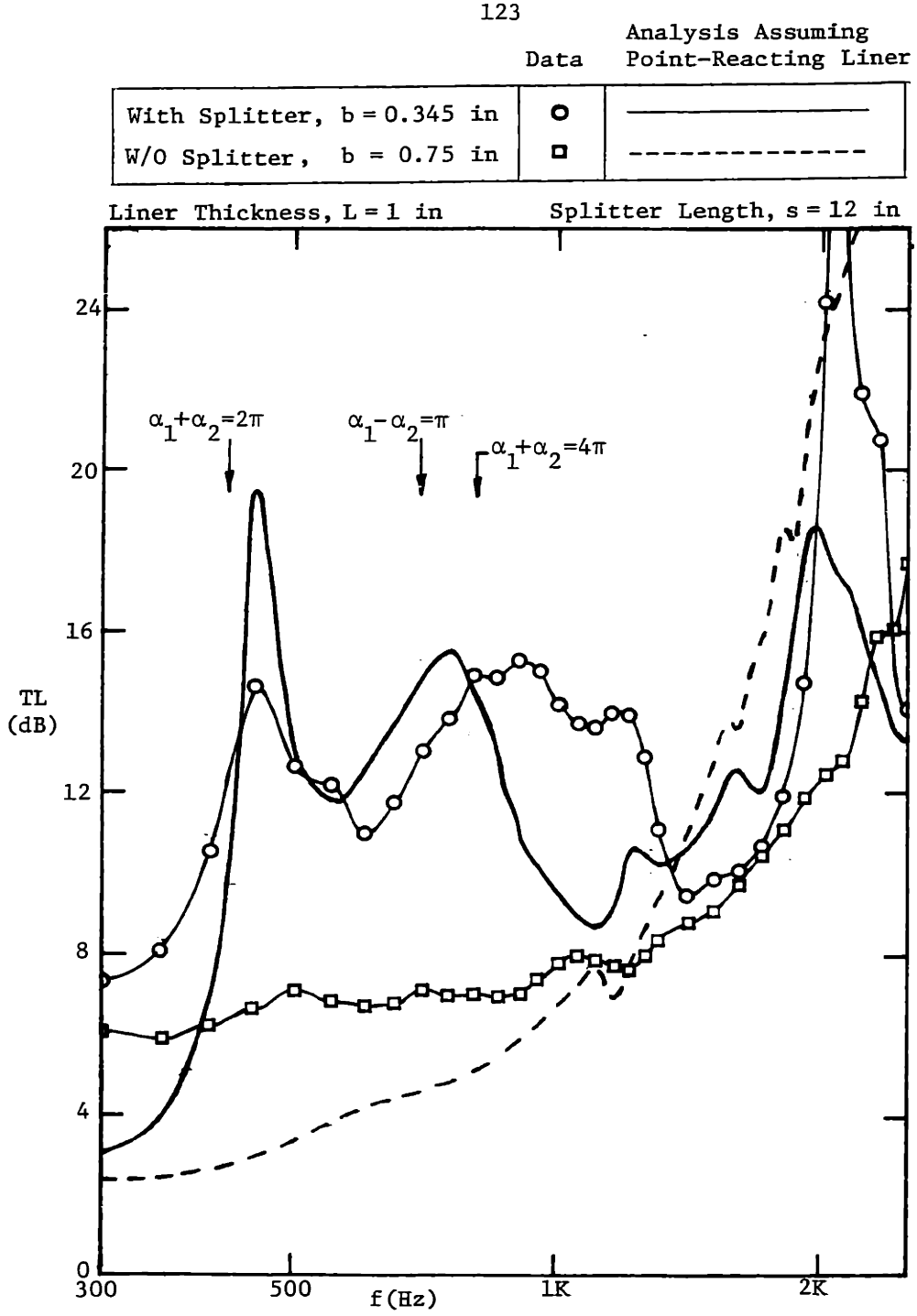

FIG. 26b : TRANSMISSION LOSS OF RECTANGULAR PARALLEL DUCT FILTER HAVING SODA-STRAW LINER IN ONE BRANCH (b = 0.345 in)

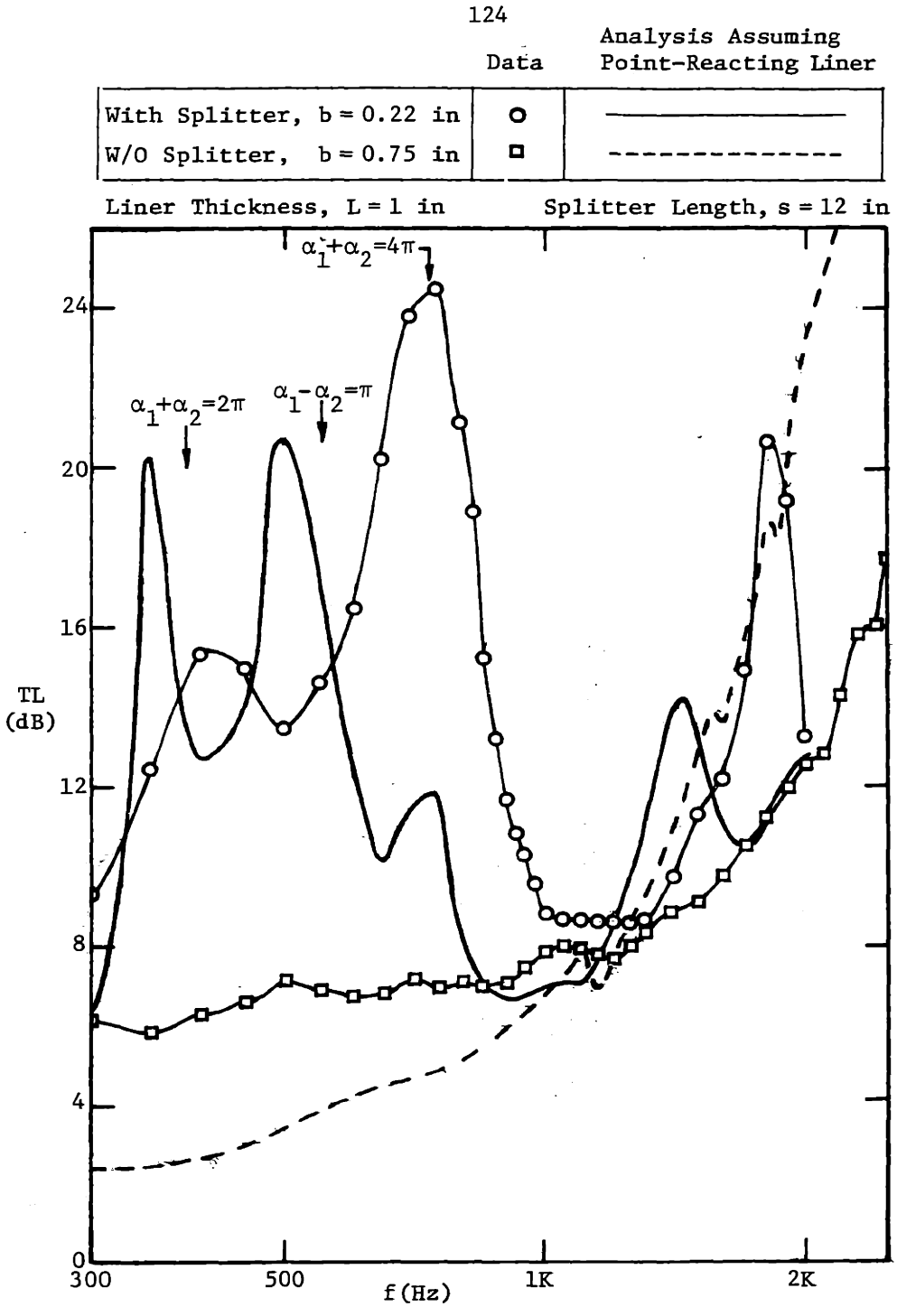

FIG. 26c: TRANSMISSION LOSS OF RECTANGULAR PARALLEL DUCT FILTER HAVING SODA-STRAW LINER IN ONE BRANCH (b = 0.22 in)

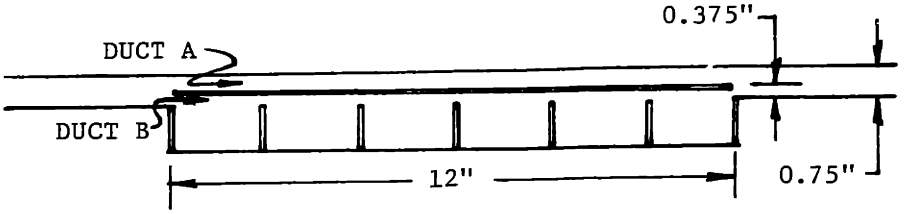

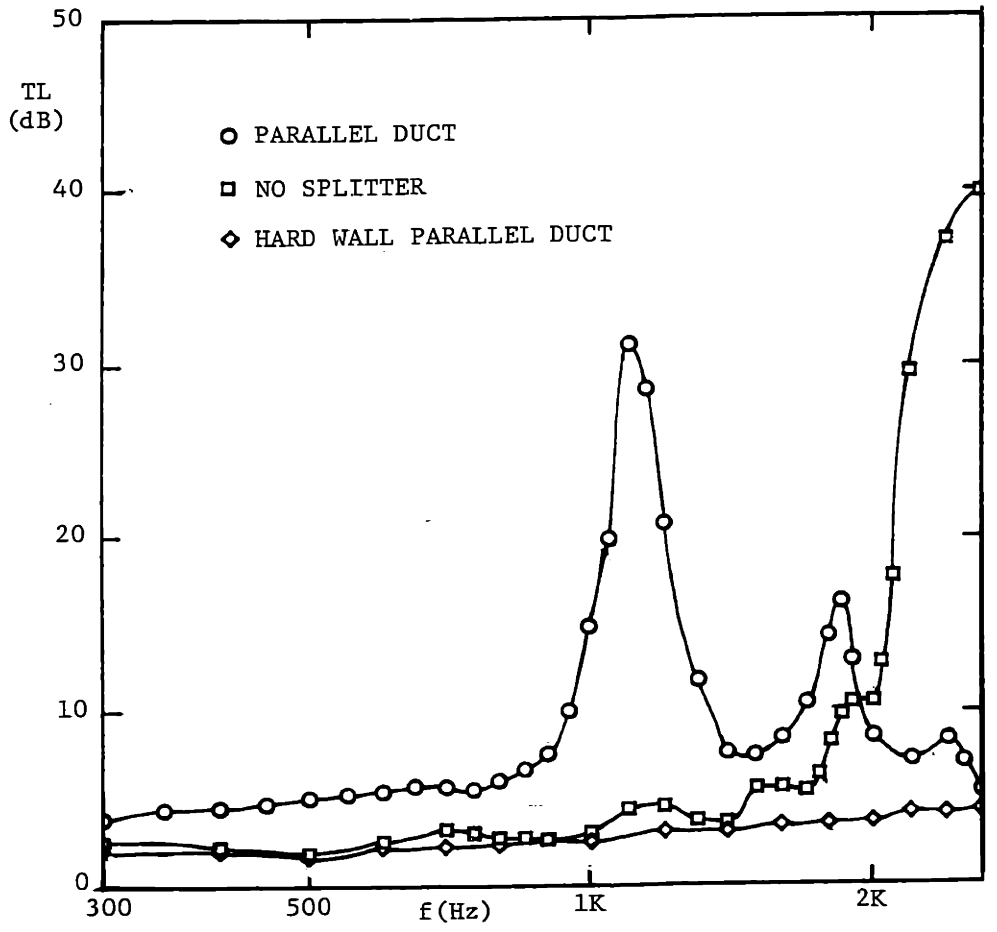

FIG. 27a: RECTANGULAR PARALLEL DUCT WITH NON-DISSIPATIVE PARTITIONED LINER

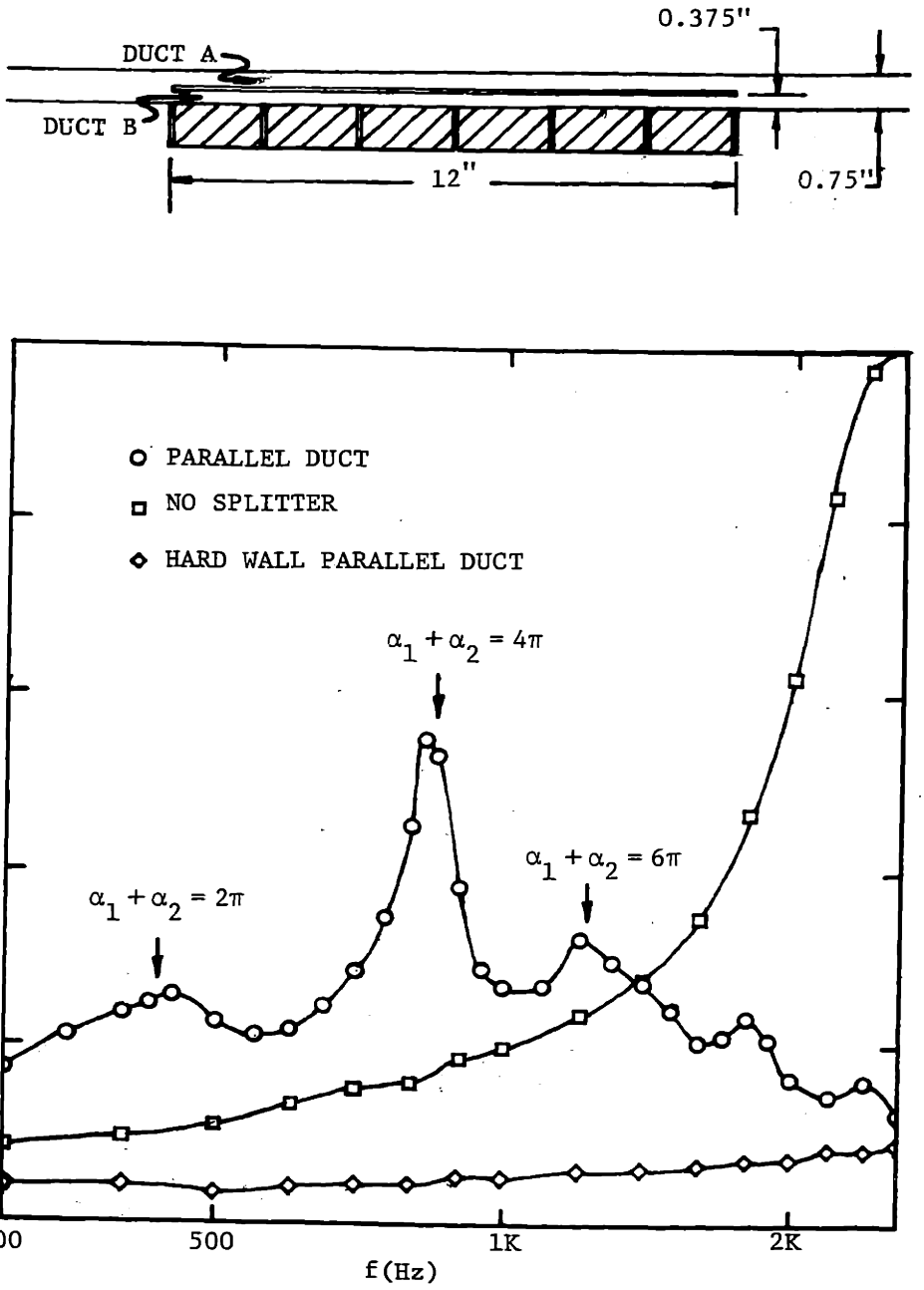

FIG. 27b: RECTANGULAR PARALLEL DUCT WITH FOAM PARTITIONED LINER

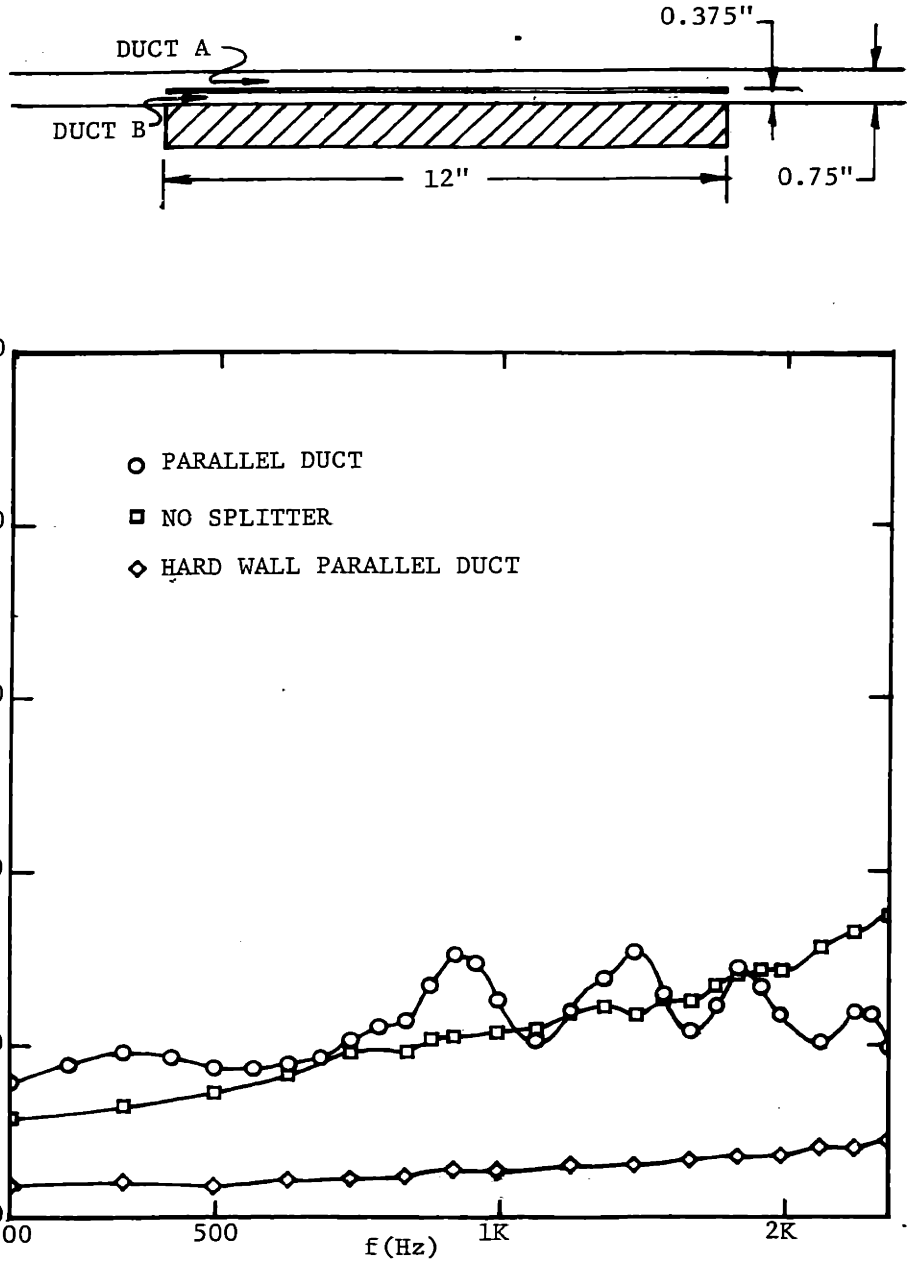

FIG. 27c: RECTANGULAR PARALLEL DUCT WITH UNPARTITIONED FOAM LINER

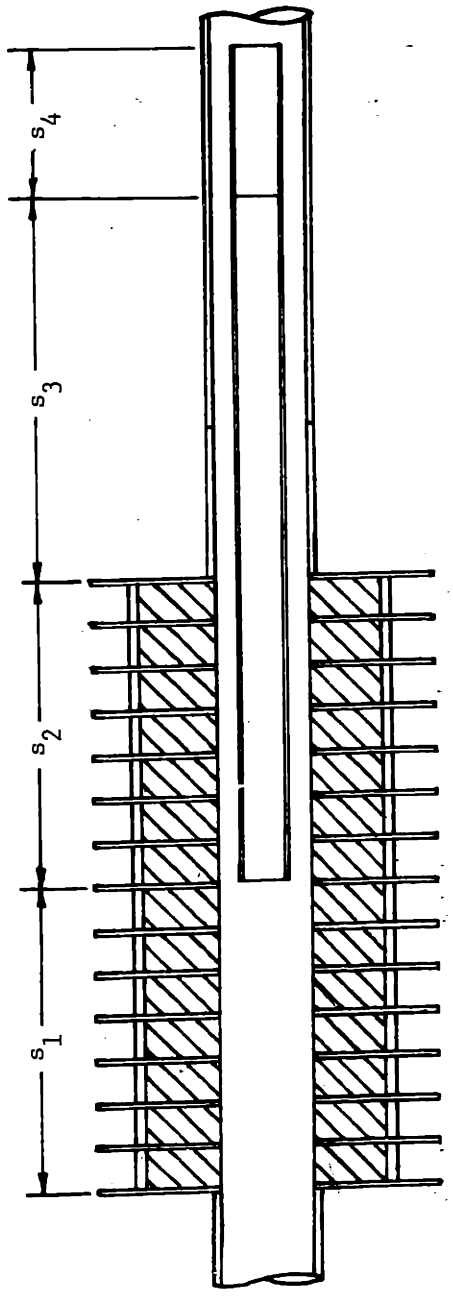

FIG.28 : CYLINDRICAL PARALLEL DUCT WITH FINNED TUBE SPLITTER

Symbol	S_1	S_2	S_3	S_4
□	14.6"	0	0	0
◇	0	14.6"	0	0
✥	4"	10.6"	4"	0

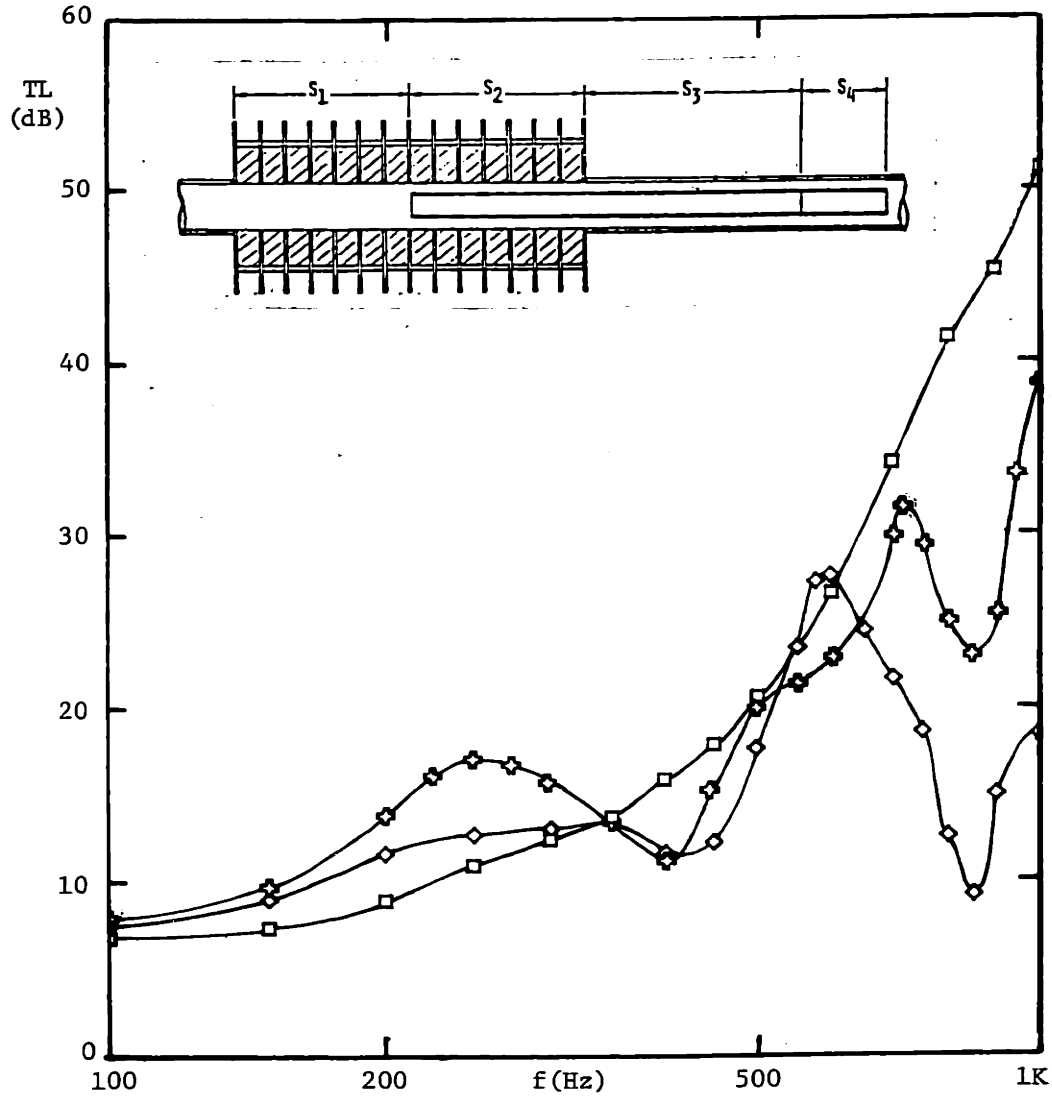

FIG. 29a: CYLINDRICAL PARALLEL LINED DUCT FILTER

Symbol	S_1	S_2	S_3	S_4
□	14.6"	0	0	0
○	8"	6.6"	8"	0
△	8"	6.6"	8"	8.6"

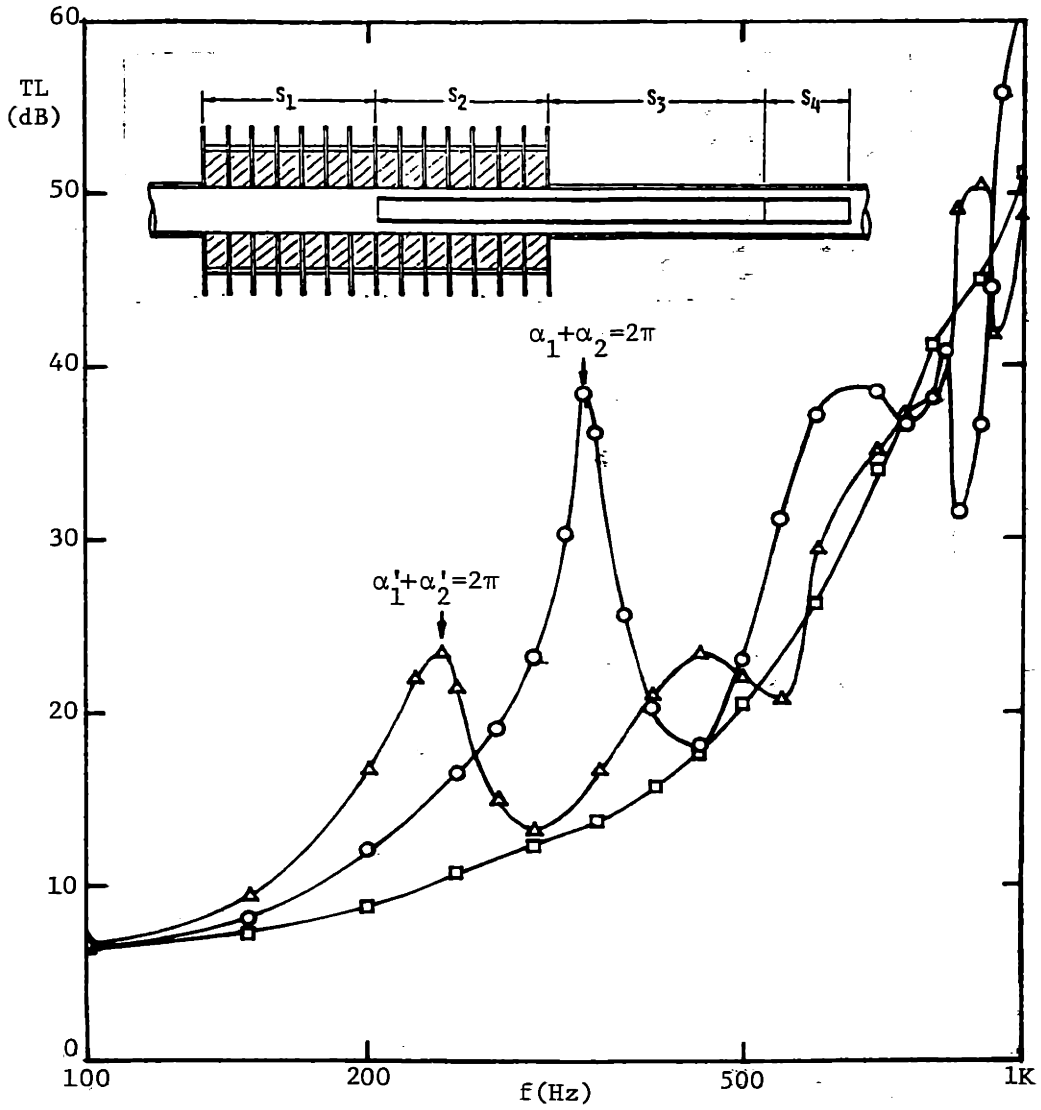

FIG. 29b CYLINDRICAL PARALLEL LINED DUCT FILTER

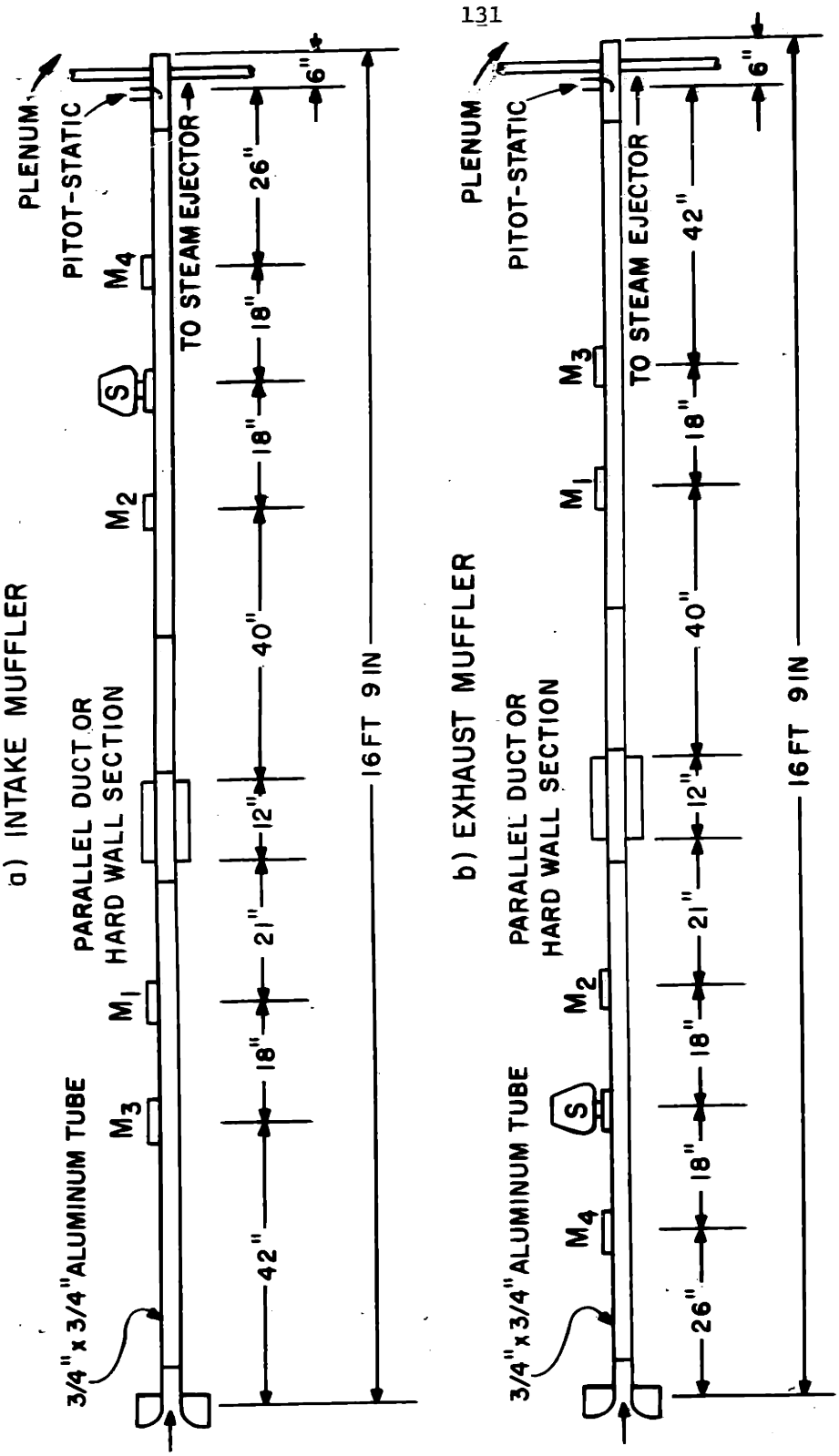

FIG. 30: EXPERIMENTAL CONFIGURATIONS FOR TRANSMISSION LOSS MEASUREMENTS IN RECTANGULAR DUCTS WITH FLOW

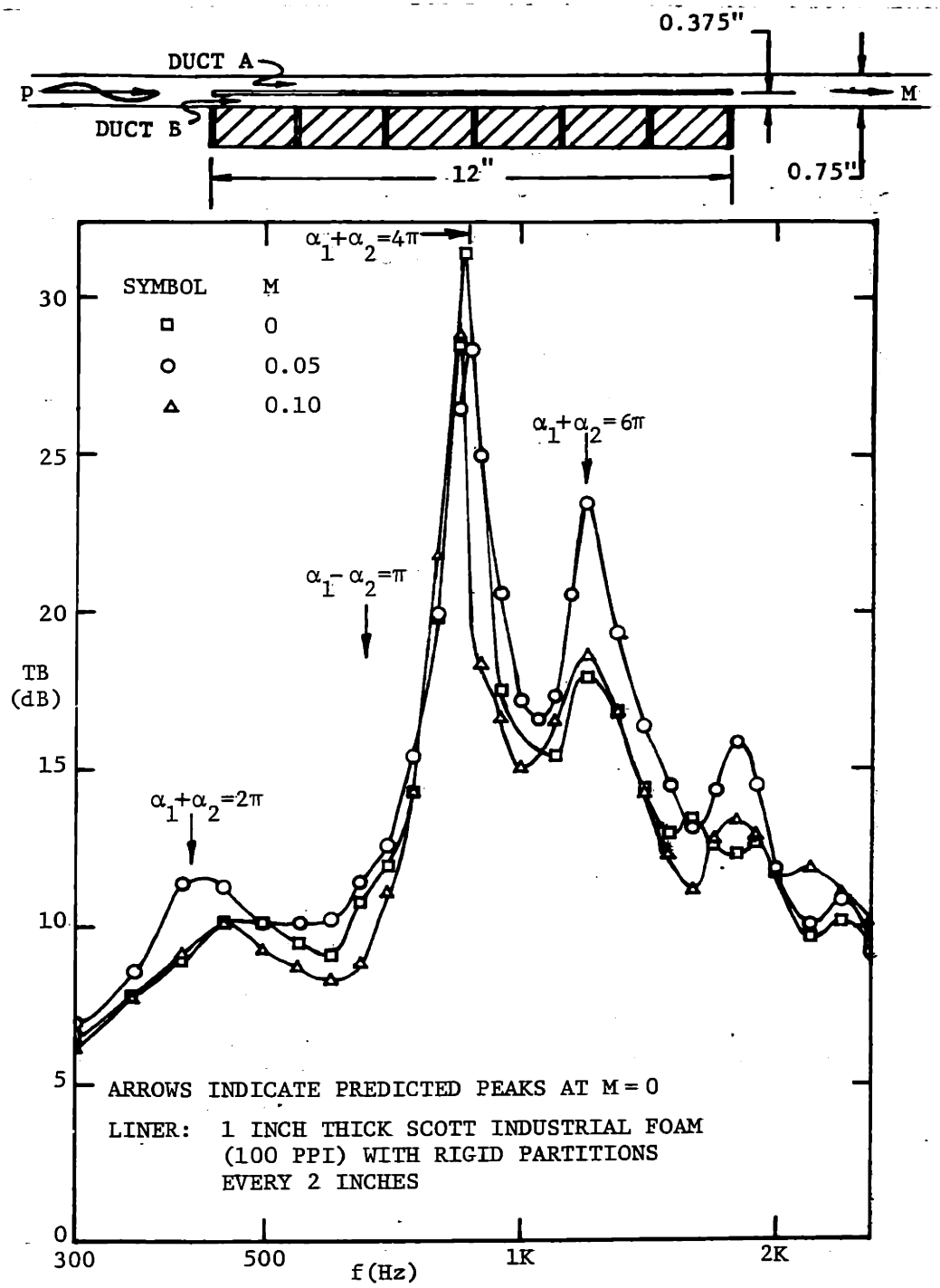

FIG.31a : RECTANGULAR PARALLEL DUCT ACOUSTIC FILTER AS EXHAUST SILENCER

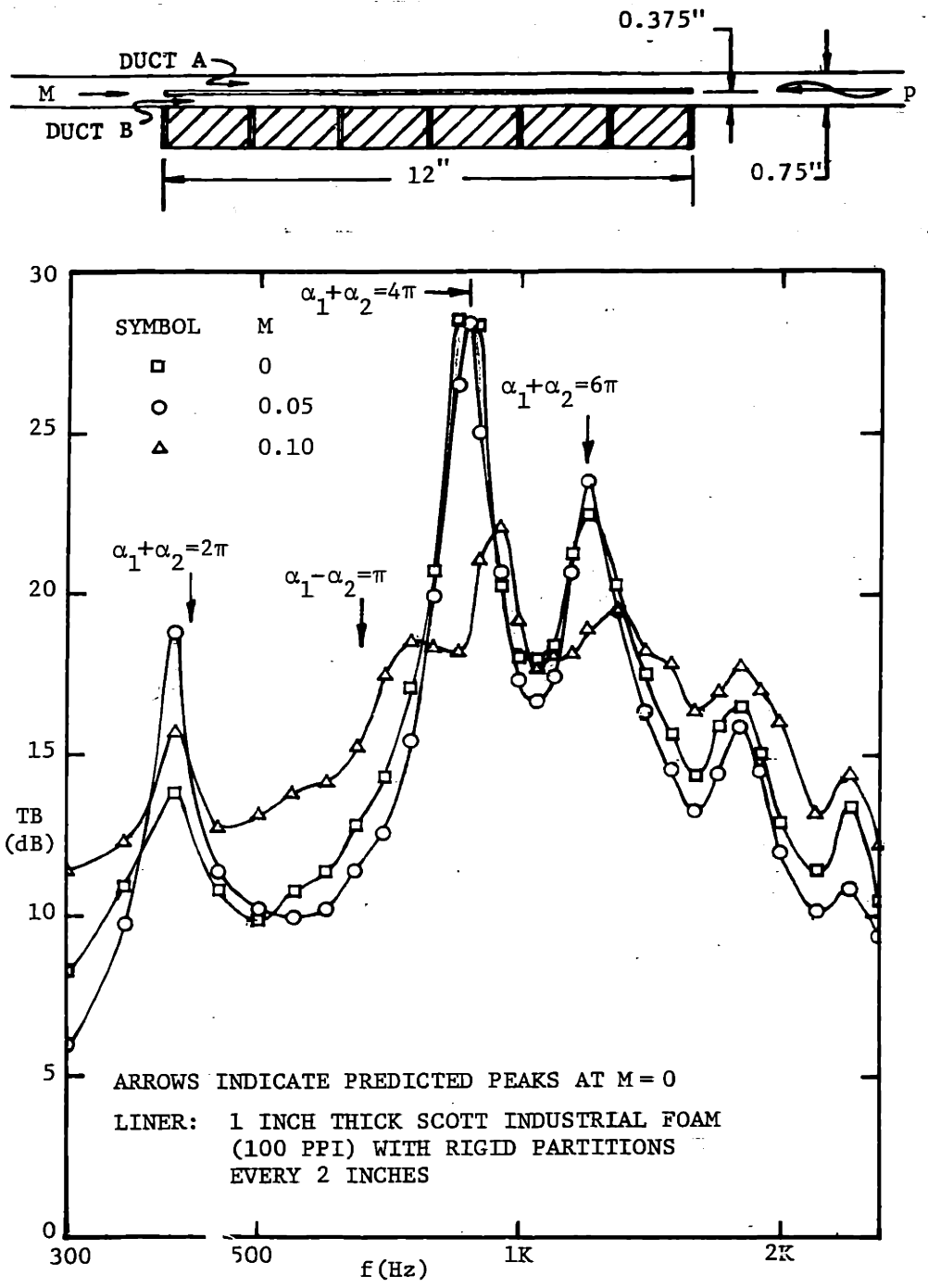

FIG. 31b : RECTANGULAR PARALLEL DUCT ACOUSTIC FILTER AS INTAKE SILENCER

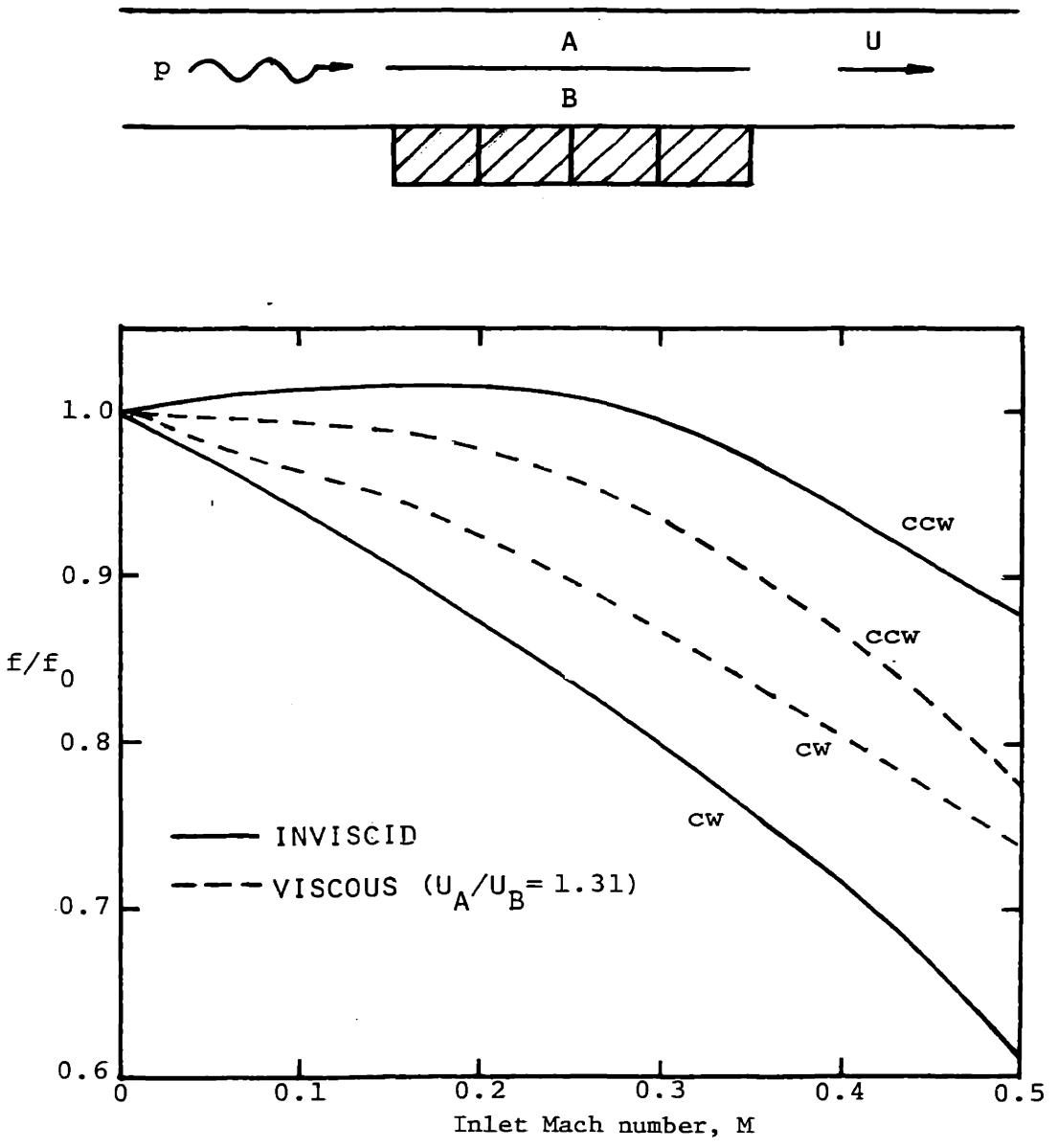

FIG. 32: EFFECT OF FLOW REDISTRIBUTION ON "SING-AROUND" FREQUENCY

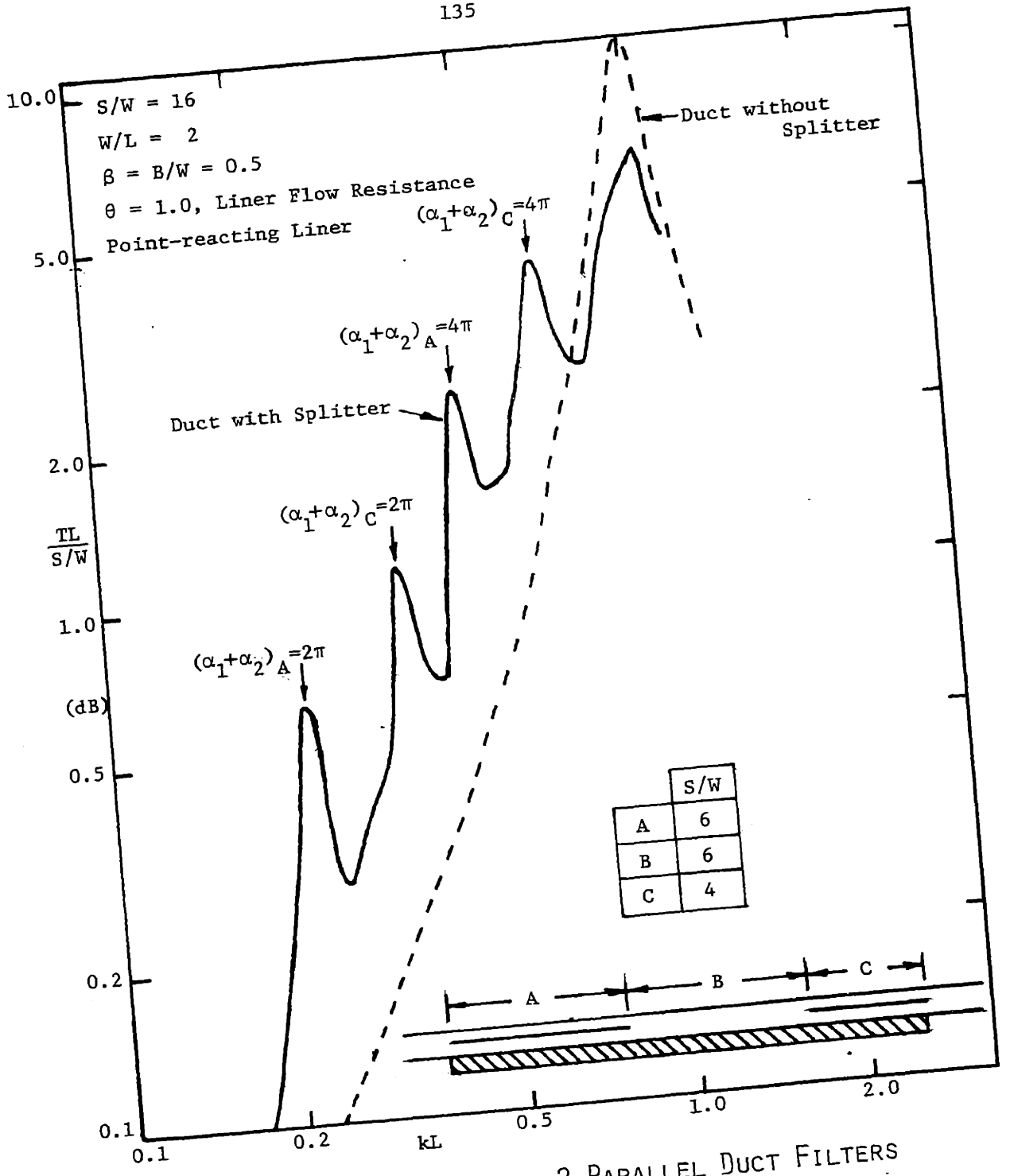

FIG. 33 : TRANSMISSION LOSS OF 2 PARALLEL DUCT FILTERS IN SERIES

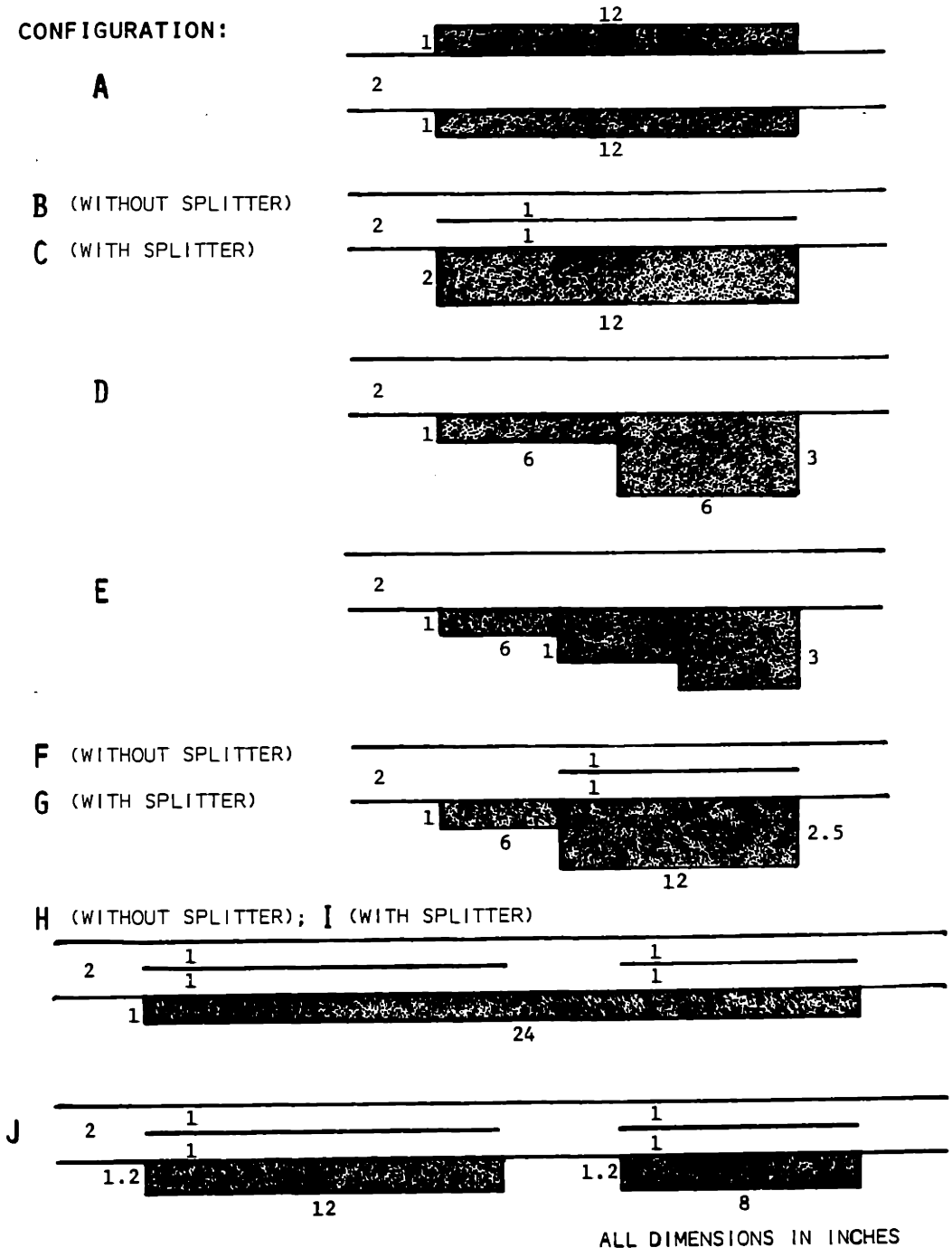

FIG. 34: RECTANGULAR LINED DUCT CONFIGURATIONS

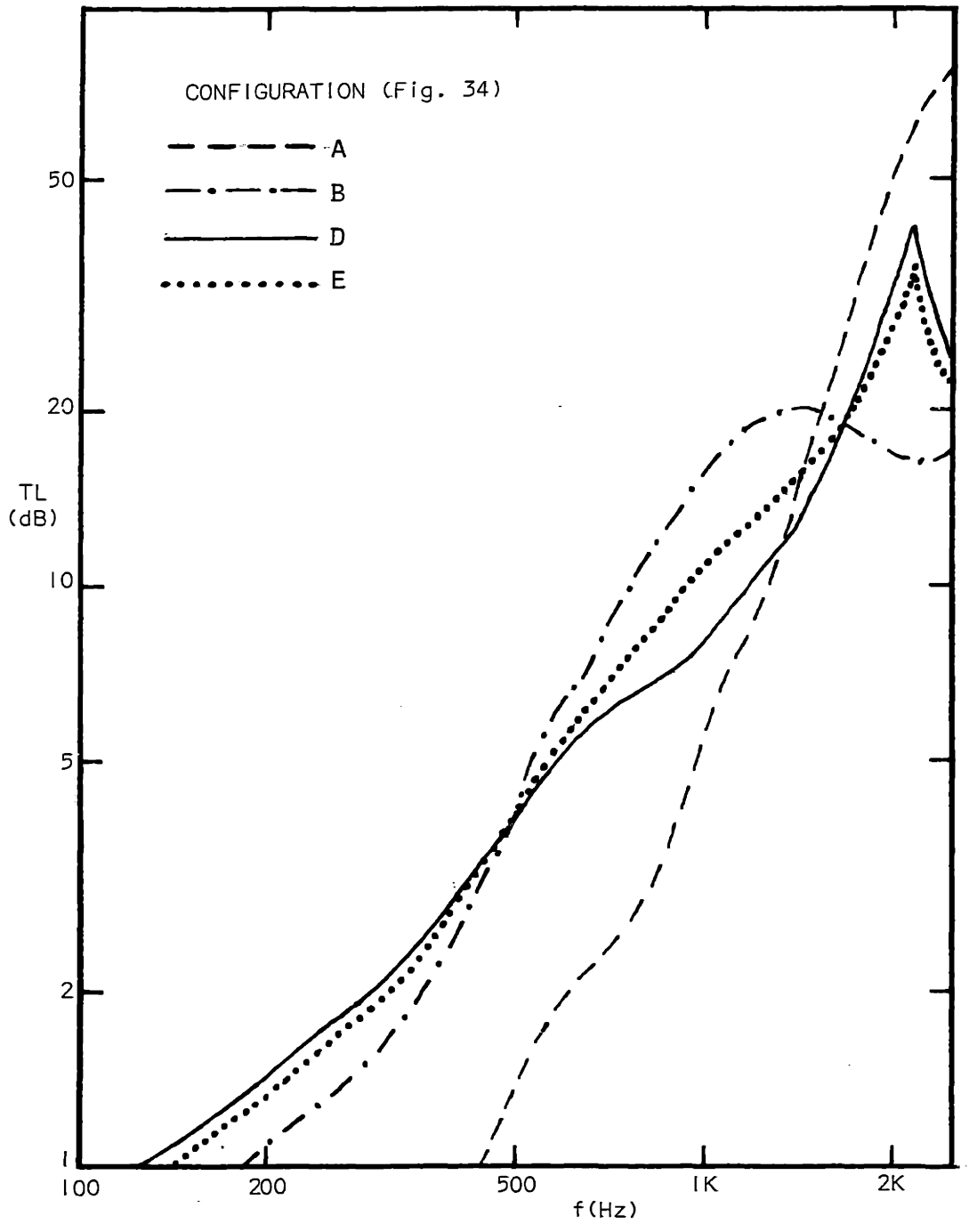

FIG. 35a: TRANSMISSION LOSS OF VARIOUS LINED RECTANGULAR DUCT CONFIGURATIONS HAVING EQUAL AMOUNTS OF ACOUSTICAL MATERIAL

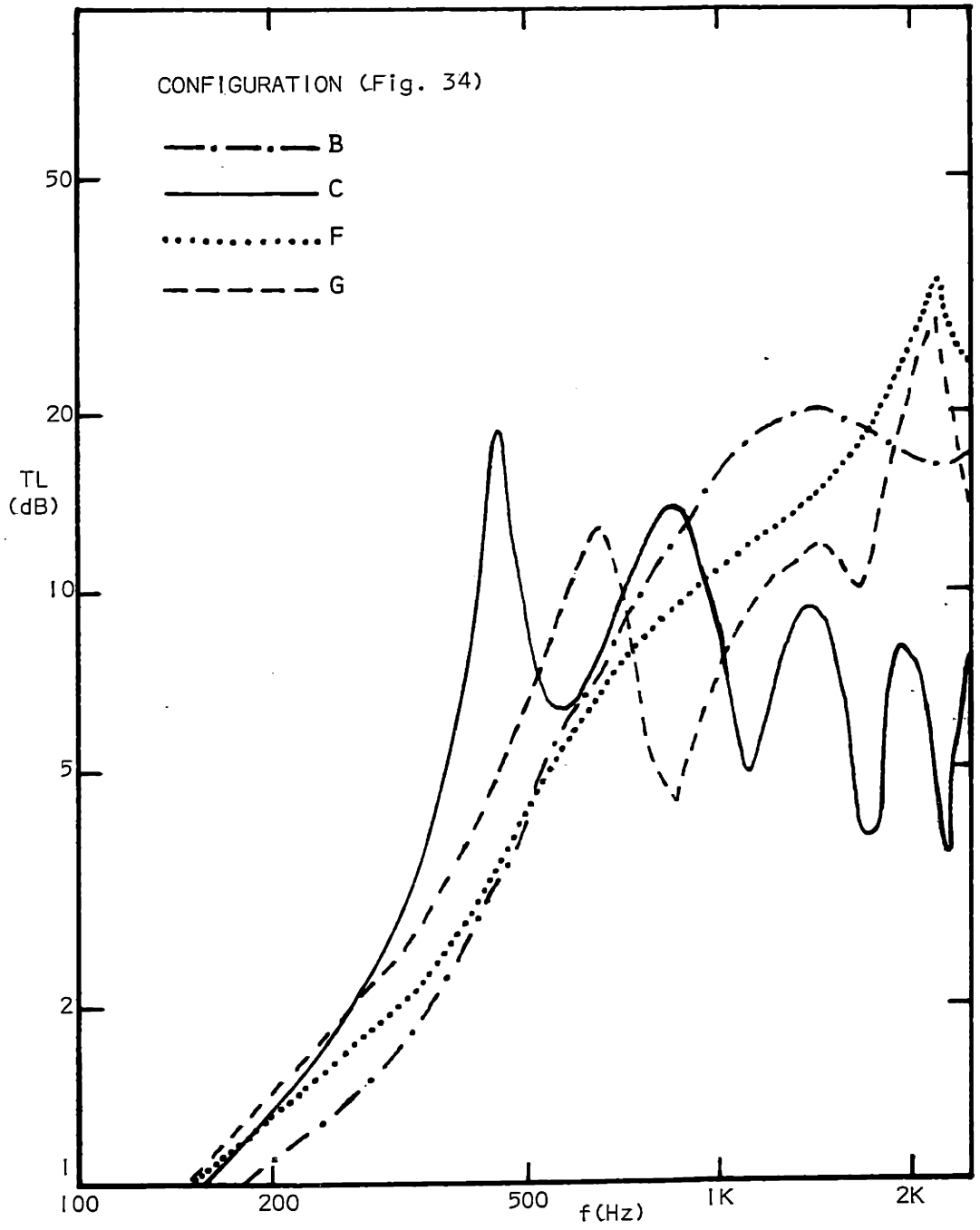

FIG. 35b: TRANSMISSION LOSS OF VARIOUS LINED RECTANGULAR DUCT CONFIGURATIONS HAVING EQUAL AMOUNTS OF ACOUSTICAL MATERIAL

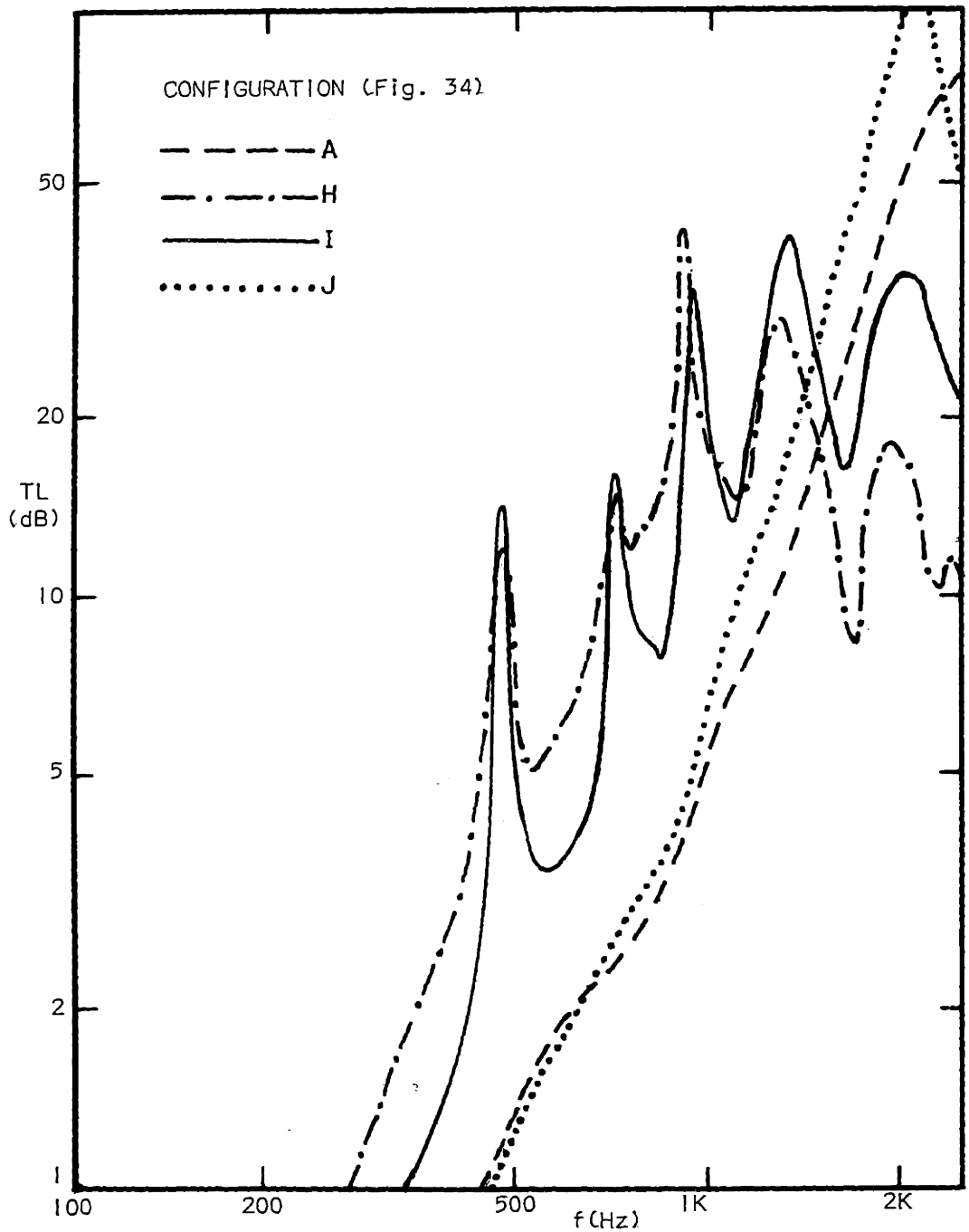

FIG. 35c: TRANSMISSION LOSS OF VARIOUS LINED RECTANGULAR DUCT CONFIGURATIONS HAVING EQUAL AMOUNTS OF ACOUSTICAL MATERIAL.

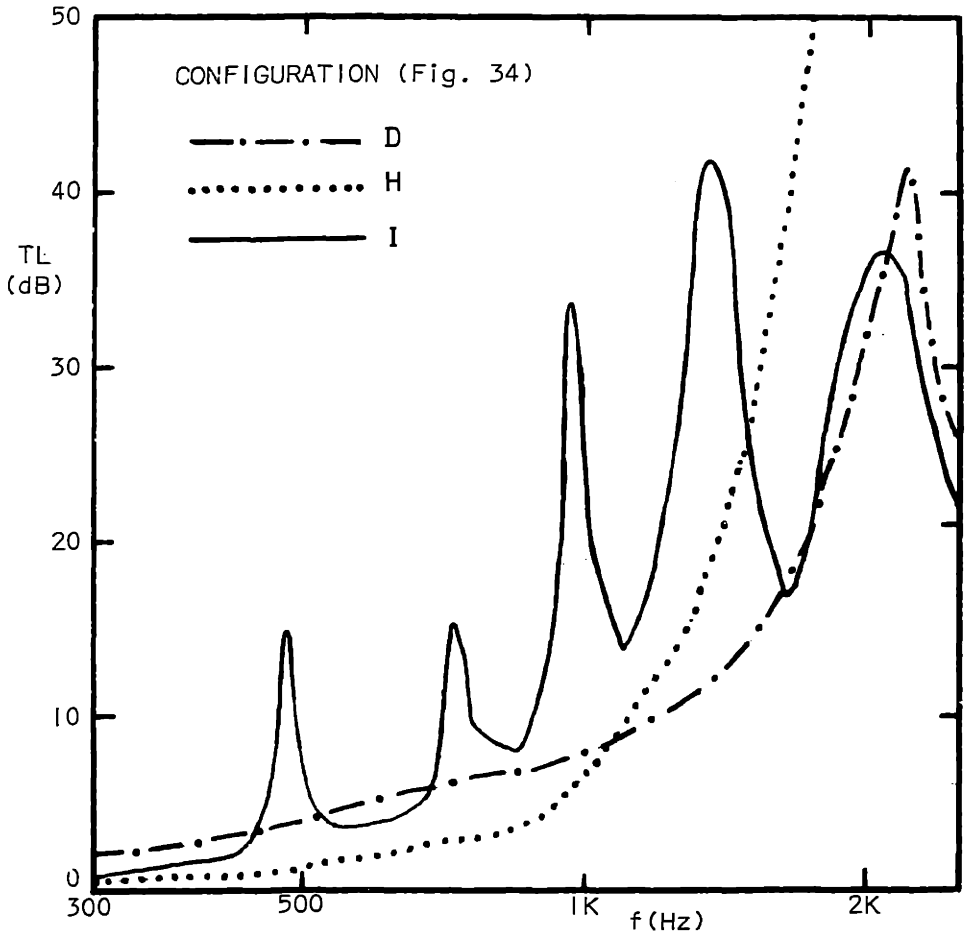

FIG. 35d: TRANSMISSION LOSS OF VARIOUS LINED RECTANGULAR DUCT CONFIGURATIONS HAVING EQUAL AMOUNTS OF ACOUSTICAL MATERIAL - SUMMARY FIGURE

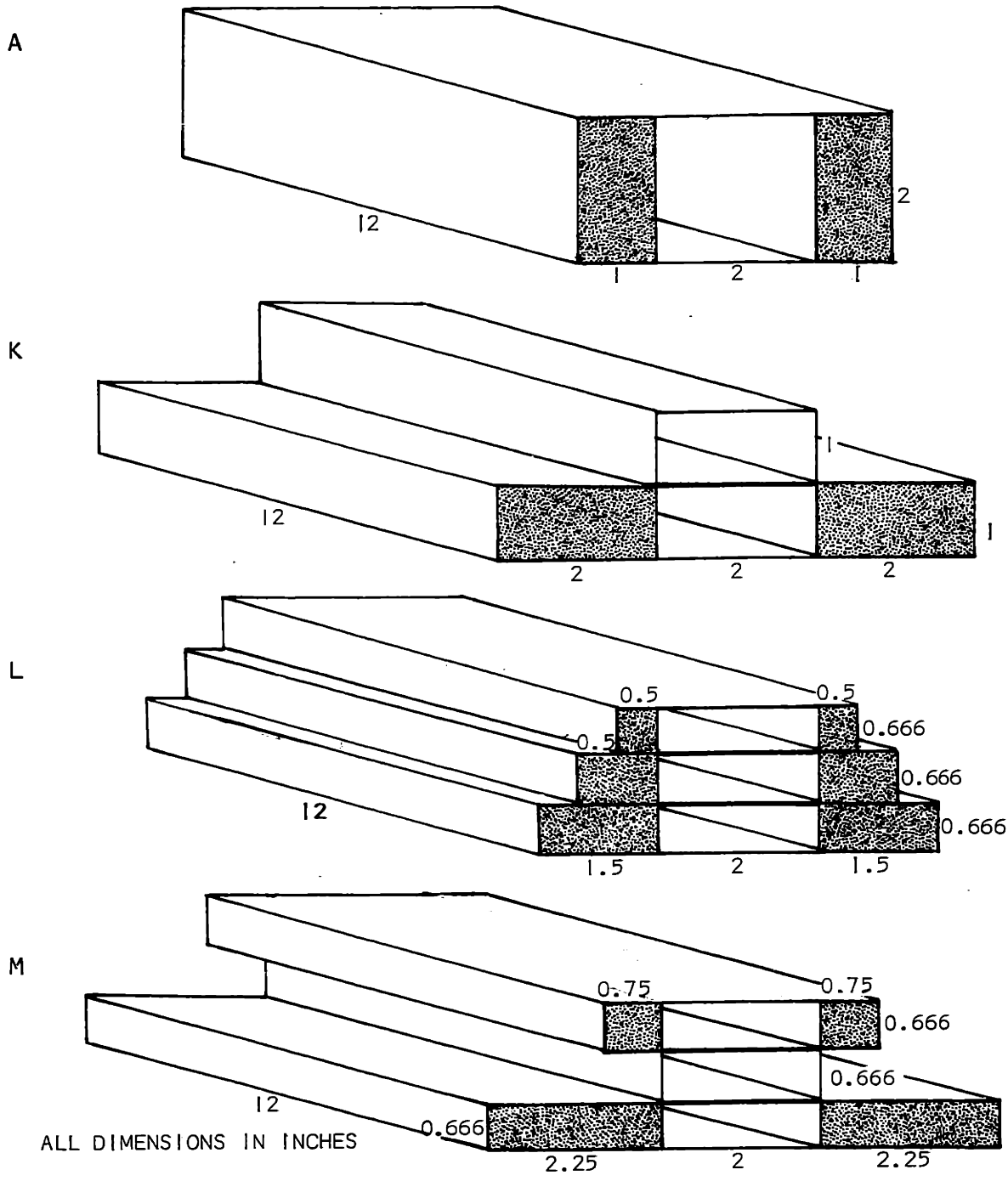

FIG. 36: RECTANGULAR LINED DUCT CONFIGURATIONS

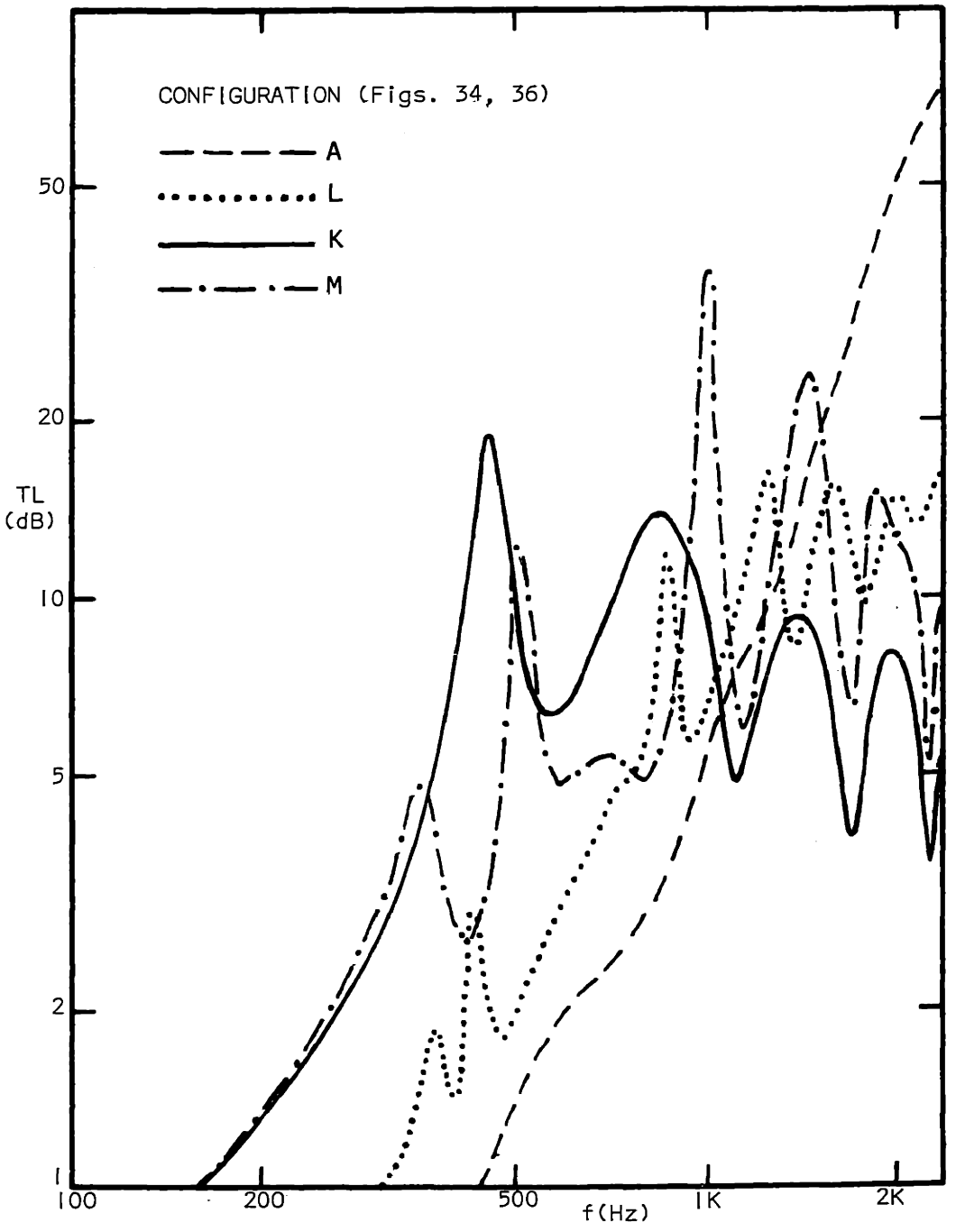

FIG. 37: TRANSMISSION LOSS OF LINED RECTANGULAR DUCTS HAVING 1, 2, AND 3 BRANCHES

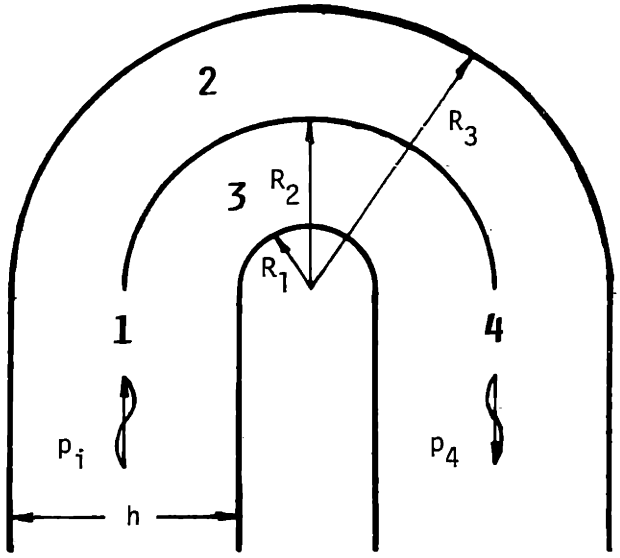

a) Configuration used by Fuller and Bies[37]

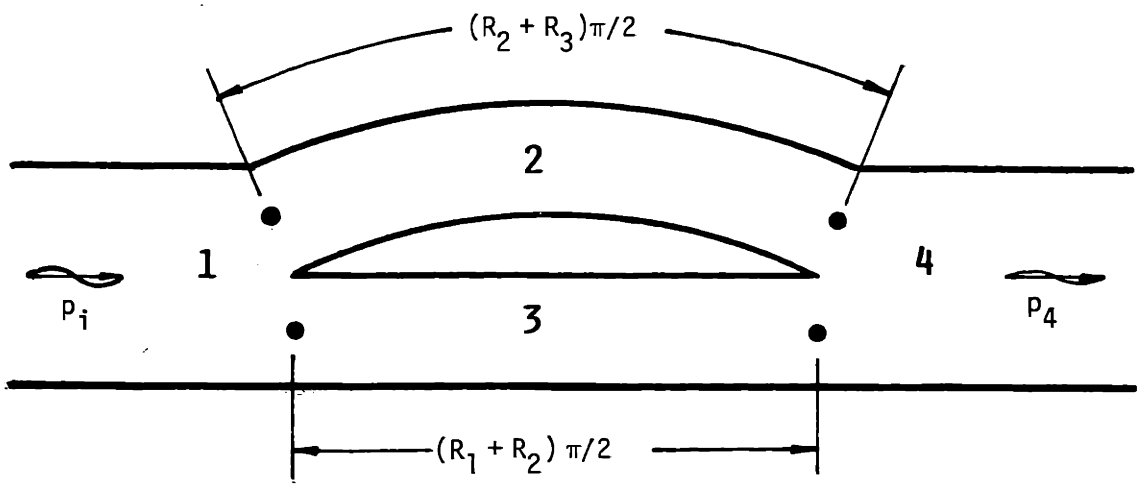

b) Herschel-Quincke tube model

FIG. 38: RIGID SPLITTER IN DUCT BEND

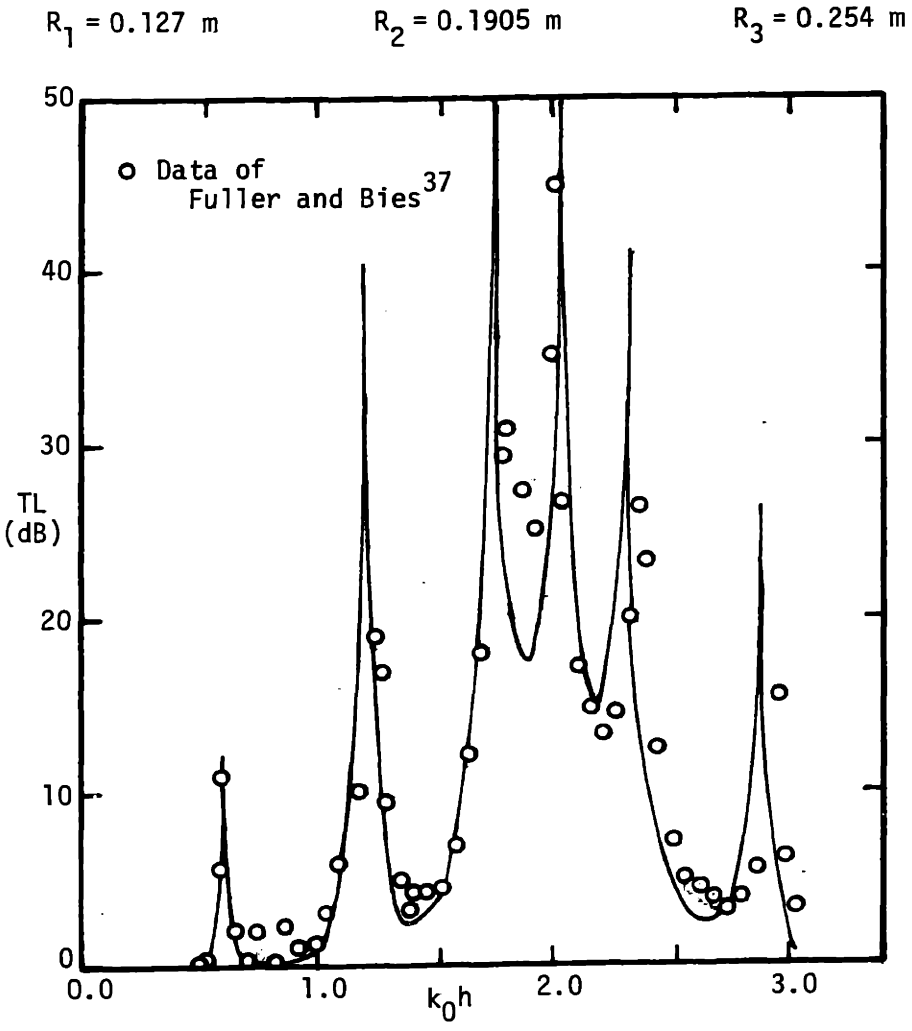

FIG. 39a: TRANSMISSION LOSS IN DUCT BEND WITH RIGID SPLITTER - ANALYSIS OF FULLER AND BIES[37]

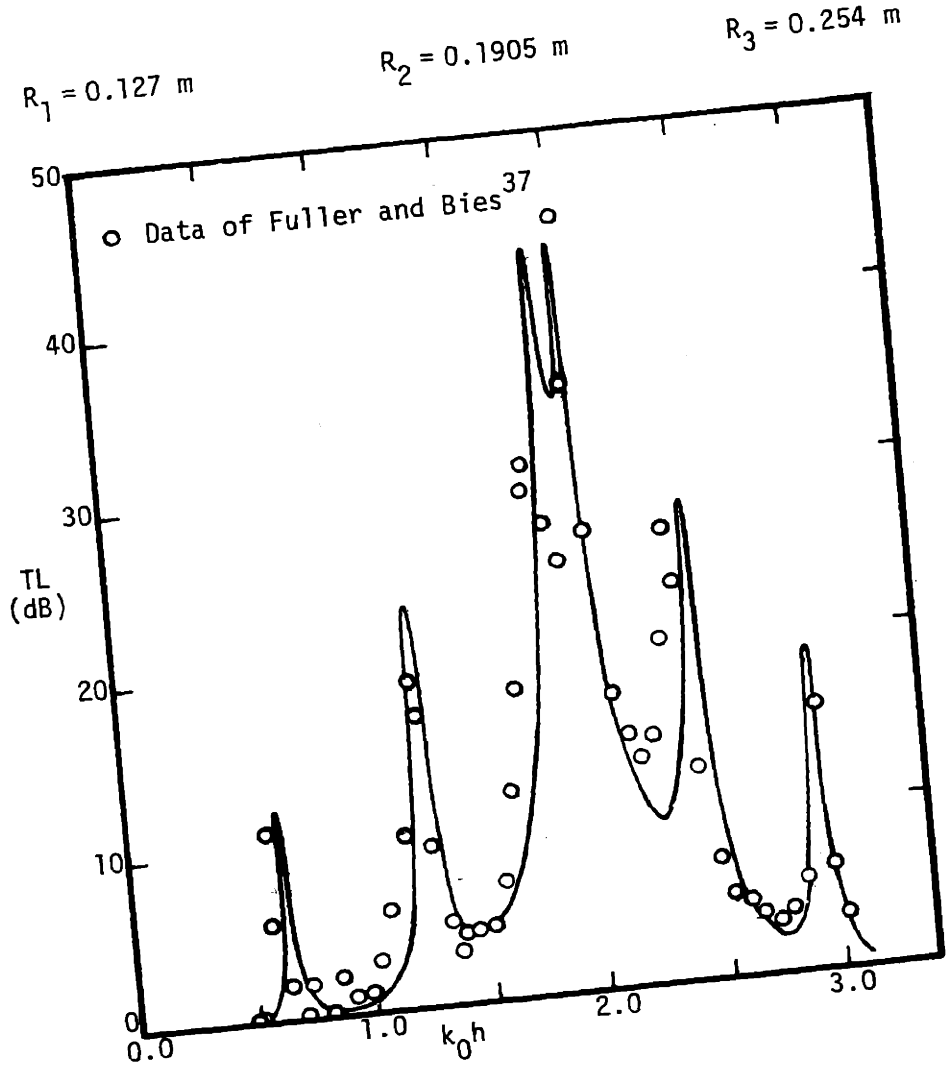

FIG. 39b: TRANSMISSION LOSS IN DUCT BEND WITH RIGID SPLITTER - HERSCHEL-QUINCKE TUBE MODEL

CHAPTER IV

APPLICATION OF MATRIX ANALYSIS TO DUCT ACOUSTICS

4.1 Introduction

The design of duct systems to minimize their transmitted sound requires a calculation procedure which can handle various duct geometries and liner configurations. In theory the transmission characteristics of any duct system can be obtained from the conservation equations (mass, momentum, and energy) applied to the acoustic waves along with a consideration of the system boundary conditions. In practice such calculations can be extremely complicated for non-simple duct geometries. Morever, the solution obtained in this manner is not readily amenable to system optimization.

Similar problems which occur in mechanical and electrical systems have been handled successfully by matrix analysis. By defining impedance, admittance and transmission matrices for each component of the duct system, the sound transmission characteristics for the complete system can be obtained by the appropriate combination of component matrices. System optimization is facilitated because elements of the component matrices appear explicitly in the resultant matrices characterizing the overall duct system.

In this chapter an attempt has been made to unify and simplify the analysis of duct acoustics using matrix techniques by consolidating previous research efforts and adding some new insights and a few example

problems. The chapter has been organized into the following four major sections.

In Section 4.2 a review of the use of transmission matrices in acoustics is presented. The fact that this area of acoustics has not been developed very extensively until recently seems rather surprising, when one considers the common use of electrical analogies in acoustics. Matrix techniques and lumped element analysis are used widely in electronics to simplify complicated electrical circuits. A natural extension of the electrical analogies used in acoustics is to use transmission matrices to simplify the analysis of sound propagation through complicated duct geometries ("acoustic circuits").

In Section 4.3 the matrix techniques necessary for the analysis of sound transmission in lined ducts are developed. Admittance, impedance, forward transmission and rearward transmission matrices applicable to acoustic waves are presented. A table of equivalent matrices is derived to permit the rapid determination of all four fundamental matrices if the elements of only one of the matrices is known. Then the rules governing the addition of the component matrices of lined duct sections joined in series and/or parallel are set forth. The significance of the reciprocity theorem in the analysis of duct systems using transmission matrices is examined. Means for determining the transmission or insertion loss directly from the elements of the transmission matrix are reviewed. And finally, methods for including the effects of mean flow in the matrix elements are described.

In Section 4.4 transmission matrices are obtained from the literature or derived where necessary for the components of a typical duct system. Transmission matrices for an acoustic source, rigid and lined duct sections, ducts in parallel, a discontinuous area change, a transition section, a side branch, muffler connections, hole-cavity resonators and barriers in ducts are collected into a Handbook of Transmission Matrices. For selected duct system components transmission matrices are presented for ducts with and without flow.

Finally, in Section 4.5 four example problems are solved to illustrate the usefulness of the matrix solution techniques developed in this chapter. The solutions include the determination of the transmission loss of an expansion chamber muffler and a series-parallel lined duct combination, the acoustical characteristics of a double-screen acoustical liner and the sound power radiated from the exhaust ducting of a stationary reciprocating engine.

4.2 Review of the Use of Transmission Matrices in Acoustics

Until recently, transmission matrices have been used only sparingly in the analysis of acoustical problems. Acousticians have not yet taken full advantage of the well-developed matrix techniques used in the analysis of electrical and mechanical systems. Therefore, before discussing the uses of transmission matrices in acoustics, a brief digression will be made to survey the matrix techniques used in electronics and mechanics which acousticians may draw upon to improve their analytical techniques.

In the fields of electronics and solid mechanics the analysis of complicated systems has been greatly simplified by the use of matrix techniques and network analysis. Many complicated circuits and structures

can be modeled as two-port networks.[47] These networks can be conveniently characterized as "black boxes," having two input ports and two output ports. Sets of black box parameters may be developed which describe the input-output behavior of the network. Strecker and Feldtkeller[48] presented the first application of matrix algebra to the general treatment of four terminal networks. They showed that interconnection of networks can be handled quite simply by linear addition or multiplication of the black box parameter matrices. Guillemin[49] has written a classical work on the subject including an analysis of parallel, series-parallel and parallel-series network combinations. Matrix analysis of electrical circuits has become an accepted method of network analysis and textbooks on the subject are readily available.[47,50,51]

Drawing upon the experience of electrical engineers in handling complicated circuits, mechanical engineers have adapted matrix techniques to the analysis of mechanical systems. Molloy[52] presented the first systematic development of four-pole theory as a working technique in a field other than electrical. He developed the four-pole parameters for simple mechanical elements (mass, spring and dashpot) and mechanical sources, presented rules for combining mechanical four-poles in series and parallel connections and discussed the measurement of four-pole parameters in mechanical systems. Molloy expanded upon his initial presentation in a later paper[53] which is an excellent comprehensive review of the use of four-pole theory in vibration analysis.

Rubin[54] has presented a unified analysis of vibration problems using transmission matrices. Although the nomenclature in his paper applies

specifically to structural elements, his results apply to linear elements from any field (e.g., structural, electrical, acoustic) which obey reciprocity and also to elements of mixed type (e.g., electromechanical, electroacoustical).

In a later paper,[55] Rubin has examined the properties of immittance (i.e., impedance or admittance) and transmission matrices of multiterminal systems. Although the terminology used for these matrices in the literature is often confusing, as shown in Table IV.1, each of these three fundamental matrices contains the same steady-state frequency-response information for a given mechanical, electrical or acoustical system but in different forms.

TABLE IV.1

ALTERNATE TERMINOLOGY FOR IMPEDANCE, ADMITTANCE AND TRANSMISSION MATRICES

Impedance	Admittance	Transmission
Stiffness	Mobility	Transfer
Modulus	Receptance	Four-Pole
Equivalent Mass	Flexibility	Cascade
	Compliance	
	Influence Coefficients	

Rubin[54,55] has presented a detailed table to assist the reader in quickly determining the admittance, impedance, rearward transmission and forward transmission matrices of mechanical systems, if the elements of only one of

the matrices is known. Lin and Donaldson[56] presented a survey of transfer matrix techniques for analyzing the dynamic behavior of beam structures. They also extended the transfer matrix technique to the analysis of complex structures such as aircraft panels. Leckie[57] has used transfer matrices in the analysis of plate vibrations. Snowdon[58] used matrix techniques to determine the vibration characteristics of a uniform thin rod, a thin circular plate, and various other distributed systems having internal damping.

The techniques of electrical circuit analysis were first applied to duct acoustics by Stewart[59] in 1922. Using analogies between pressure and electromotive force, volume velocity and current, and impedance and the ratio of pressure to volume velocity first pointed out by Webster,[60] Stewart developed a lumped element theory for acoustic filter design. The theory assumed the dimensions of the filter to be vanishingly small compared to a wavelength since the effects of wave motion on the performance of a section or branch was not included in the analysis. Stewart's theory was one-dimensional, non-dissipative and did not include the effects of flow but did work fairly well for small structures or low frequencies although it broke down for large structures and high frequencies because of the distributed nature of the elements at those conditions.

In 1927, Mason[61] extended the work of Stewart by taking into account the wave motion occurring in individual elements, thus permitting the properties of acoustical filters to be determined to higher frequencies. Mason also included the dissipative effects of viscosity and heat conduction in his analysis. Furthermore, he developed the branch transmission theory

of acoustical filtration by studying regular combinations of acoustic elements to determine the equations of recurrent filters, tapered filters and horns.

In 1930 the state-of-the-art of acoustic filter design was formalized in a book by Stewart and Lindsay.[62] Although they presented their equations in the following form

$$p_2 = a\,p_1 + b\,X_1$$

$$X_2 = f\,p_1 + g\,X_1$$

where p is acoustic pressure, X is the volume displacement, and a,b,f and g are linear constant coefficients, which can easily be written in matrix form

$$\begin{Bmatrix} p_2 \\ X_2 \end{Bmatrix} = \begin{bmatrix} a & b \\ f & g \end{bmatrix} \begin{Bmatrix} p_1 \\ X_1 \end{Bmatrix}$$

no specific mention of matrix techniques was made in their text. (This fact is understandable considering that Strecker and Feldtkeller[48] outlined four-pole theory for electrical circuit analysis only three years earlier.)

Indeed, the first paper in which matrix analysis was used to solve an acoustics problem did not appear until 20 years later when Peterson and Bogert[63] used four-pole theory to develop a general circuit analysis for the cochlea of the ear. They used a lumped impedance model for the cochlea which limited their results to the lower audio range. For Peterson the application of matrix techniques to acoustical problems was a natural extension of work he had published earlier[64] in which he enlarged the general theory of Strecker and Feldtkeller for active four-terminal electrical networks.

In the Soviet Union, transmission matrix techniques were used in acoustics primarily in the area of transmission of sound through layered media. Brekhovskikh[65] formulated the transmission matrix for sound transmission through layered media. Ryback and Tartakovskii[66] analyzed the resultant matrix and identified conditions under which total reflection of sound waves in layered media could be achieved.

The transfer matrix approach was extended to engine-exhaust muffler systems without mean flow in 1958 by Igarashi, Toyama, Miwa and Arai in a series of reports[67-69] at the Aeronautical Research Institute in Tokyo.

With the advent of high-speed digital computers in the 60's, matrix analysis became particularly attractive for modeling acoustical problems. Wang[70,71] formulated the problem of sound generation, transmission and radiation from mechanically driven fluid systems (i.e., reciprocating pump, compressor or piston engine) in matrix form specifically to facilitate a computer solution to the problem. Wang dispensed with the usual analysis of a constant current source and modeled the source as an induction system with a general time varying volume. Mutual coupling was permitted between different frequency components of the source although the pressure fluctuations were assumed to remain sufficiently low to sustain the assumption of linearity. Wang took advantage of special properties of matrices and reformulated the problem with transmission matrices one-fourth their original size to reduce computational time substantially. Wang's solution was limited by his formulation of the exhaust system of a multicylinder engine as a lumped parameter air induction system which differs significantly from an exhaust system having near sonic velocity from its exhaust

ports and associated aerodynamic noise generation in the manifold. Additionally, Wang neglected mean flow and viscous effects.

In the 70's, the applications of matrix analysis to duct acoustics has developed along two separate lines. The conventional one-dimensional approach has been improved by Alfredson,[72,73] Ingard,[74,75] Munjal,[76,77] Parrott,[78] Sullivan[79] and others, while a general multi-modal theory has been developed by Zorumski[80] which has attracted a following among his coworkers.[81,82]

The one-dimensional approach has been used in the analysis of reciprocating engine exhaust mufflers, air handling systems, exhaust stack silencers and elsewhere where higher order mode propagation is minimal. Improved correlations between calculated and measured performance have been obtained by addressing the deficiencies in using one-dimensional acoustic filter theory in the analysis of engine exhaust mufflers. These deficiencies include[78,83] to a greater or lesser extent:

a) Mean flow effects (including both generation and convection of noise)

b) Finite pressure effects

c) Yielding of tube walls

d) Uncertainty in modeling the acoustic source

e) Temperature gradients within the exhaust muffler system

f) Viscosity effects at duct and muffler walls

g) Sound-turbulence interactions in the mean flow.

The effect of mean flow on exhaust silencer performance was studied by Alfredson and Davies starting in 1970[72,73] when they developed theoretical

models of exhaust silencer components with mean flow. The behavior of each component was measured individually in a real exhaust system at $M \leq 0.15$ to test and optimize the analytical models. Some of the exhaust silencer components analyzed by Alfredson and Davies - the sudden contraction, sudden expansion, extended outlet and extended inlet - are shown in Figs. 57a-d respectively. Flow through sudden expansions and extended inlets were treated as adiabatic but not isentropic due to jet mixing losses. Experimental data showed the effect of yielding walls to be appreciable for extended inlets and outlets near resonance requiring reflection coefficients less than unity to be used in the indicated regions in Figs. 57c and 57d.

Munjal[76] developed transfer matrices for the side branch resonator and hole-cavity resonator shown schematically in Figs. 57e and 57f respectively. Munjal considered the overall effect of entropy fluctuations caused by turbulence downstream from a row of holes but he did not include the effect of grazing flow on the orifice impedance in his analysis.

Recently Sullivan[79] used a discrete element method to derive transmission matrices for parallel coupled, perforated tube muffler elements. His analysis can be applied to concentric tube resonators, extended inlet and outlet tubes which are perforated, and side branch cavities for which lumped impedance analyses are not valid. Sullivan indicated that mean flow effects and nonlinear characteristics which were not considered in his paper could be handled within the framework of the discrete element method.

Parrott[78] formulated the analytical models of exhaust silencer components developed by Alfredson and Davies into transfer matrices for

application to the design of an expansion chamber muffler for a helicopter. The matrix formulation, which included the effects of yielding walls, mean flow effects on exhaust silencer components and the radiation impedance, facilitated the use of a computer program with an optimization routine for the synthesis of a complete muffler system analytically in contrast to previous trial-and-error techniques. The resulting muffler configuration was tested on a helicopter in hover and found to work satisfactorily in reducing the noise of the first four harmonics of the engine firing frequency, but in the higher frequency range noise amplification of 9 to 14 dB was observed possibly due to self-noise generation in the muffler or an impedance mismatch between the muffler and the source which Parrott modeled as non-reflecting.

Using a quasi one-dimensional assumption for higher order modes, Hogge and Ritzi[84] have extended the conventional matrix theory for application to higher order modes in aircraft engine inlet ducts. They considered only the axial component of the higher order mode in their analysis inasmuch as it is the only component which must be matched across an interface between duct sections. Their analysis permits the determination of the sound power radiated by a single but arbitrary mode from a duct of finite length having an axially varying cross section with throughflow. A limitation of the quasi one-dimensional approach to higher order mode transmission problems is its inability to handle modal distortion at axial changes in wall impedance or duct cross section. These deficiencies in the quasi one-dimensional matrix approach are addressed by Zorumski's theory which is discussed later in this section.

Ingard's contributions to transfer matrix analysis are applicable to air handling systems, exhaust stack silencers, and acoustical barriers in ducts as well as engine exhaust muffler design. Ingard[74] has determined the reflection, transmission and absorption coefficients of an acoustical barrier in terms of elements of the barrier's transmission matrix. Acoustical barriers, which can include screens, perforated plates, flexible membranes, fiberglass, porous foam, and/or rigid honeycomb inserts, can be used as free-standing elements, baffles in duct systems or absorptive wall liners when placed adjacent to the duct wall.

Galaitsis and Ingard[16] used a transmission matrix formulation to study the insertion loss produced by a lined duct section of finite length. They found that for a lined duct section having an $L/D < 10$ the insertion loss per unit length for constant pressure and constant velocity sources differed significantly from the loss calculated assuming an infinitely long duct. Ingard and Patrick[25] determined the transmission matrix for two lined ducts in parallel and utilized the frequency selective characteristics of such an array to design a low-frequency acoustic filter.

Recently, Zorumski[80] has used the acoustic modes as generalized coordinates to develop a set of matrix equations for mode transmission and reflection in the multi-modal acoustic fields of circular and annular ducts with uniform flow. Zorumski's theory assumes that all acoustical problems involving sound generation in, transmission through, and radiation from duct systems can be reduced to the solution of the matrix equation

$$[W]\ \{A\} = \{Q\} \tag{4.1}$$

where [W] is a square matrix of duct wave coefficients, {A} is a column matrix of wave amplitudes and {Q} is a column matrix representing the source mode amplitude. Although Eq. (4.1) is conceptually quite simple, its solution can be quite cumbersome in practice because of the inherent complexity of multi-modal sound fields in ducts.

The transmission loss of a duct system represented by Eq. (4.1) is obtained by inverting [W], whose order is often 50 or larger, or using an iterative procedure to obtain an explicit expression for the amplitude of the transmitted waves. For optimization of liner configurations of ducts having multi-modal sound fields the solution to Eq. (4.1) is reiterated, thus requiring extensive computer time. Arnold[85] has presented sparse matrix algorithms which manipulate the non-zero elements of the matrices into more efficient form for computation. Sparse matrix techniques are especially useful for large matrix systems and offer CPU savings exceeding an order of magnitude over conventional matrix solution routines.

The Zorumski theory has been applied to the problem of optimization of multi-section duct liners by Lansing and Zorumski[81] and Lester and Posey.[82] Lansing and Zorumski analyzed the problems of a rectangular infinite-length duct with airflow having a single change in duct wall acoustic admittance and the sound transmission in and radiation from a finite cylindrical duct with an arbitrary number of duct wall acoustic admittance changes and without airflow. Lester and Posey included the effects of uniform flow in determining the optimum liner configuration for an axisymmetric, multisectioned lined duct. These analytical studies showed multisectioned liners to be superior to uniform liners in

minimizing the sound transmitted from lined ducts. No experimental results were presented, however, to verify the analytical predictions. Furthermore, in most of these studies the acoustic source was modeled as a point source on the centerline of the duct which is not representative of distributed turbomachinery noise sources. Lester and Posey considered one case having three radial modes as the acoustic source for which they determined the optimal liner yielding maximum transmission loss at a single frequency. Hopefully, future research will extend these studies to include more realistic turbomachinery noise sources as well as a comparison with experimental data to permit a better evaluation of the accuracy of the Zorumski theory.

4.3 Development of a Matrix Solution Technique

4.3.1 Characteristics of Matrix Forms

A linear acoustic or mechanical system can be modeled as an n-terminal "blackbox" which responds to imposed forces according to the matrix equation

$$R(\omega) = H(\omega)\, F(\omega) \tag{4.2}$$

where $F(\omega)$ is a column vector of imposed forces, $R(\omega)$ is a column vector of system responses and $H(\omega)$ is the frequency-response matrix.[54] The linear system can be handled as a single entity characterized by its frequency-response matrix which is independent of the preceding or following systems in the network. To determine the response characteristics of a network comprised of linear systems combined in tandem, alternative forms of the frequency response matrix for each system are required. If velocity is

specified as the response parameter, the required matrix forms are the admittance, impedance, forward transmission and rearward transmission matrices.

The admittance matrix $Y(\omega)$ relates the velocities in the system to the corresponding forces. Thus

$$V(\omega) = Y(\omega)F(\omega) \tag{4.3}$$

where $Y(\omega)$ is a square matrix of order n relating the velocities and forces at the n terminals of the system. In linearly elastic and dissipative structures, the admittance matrix is symmetric because of reciprocity. Thus

$$Y(\omega) = Y^{T}(\omega) \tag{4.4}$$

where the superscript T denotes the transpose of the matrix. Reciprocity holds when the product of the forcelike variable and the corresponding displacement gives the total work performed during that displacement. Note that in acoustics the use of pressure as the forcelike quantity requires the use of a corresponding volume velocity to achieve a symmetrical admittance matrix.

The impedance matrix $Z(\omega)$ is the inverse of the admittance matrix. Therefore

$$F(\omega) = Z(\omega)V(\omega) \tag{4.5}$$

where

$$Z(\omega) = Z^{T}(\omega) \tag{4.6}$$

since the inverse of a symmetric matrix is also symmetric.

The transmission matrix $T(\omega)$ relates the input forces and velocities to those at the output terminals. For a two-terminal system

$$\begin{Bmatrix} F_1 \\ V_1 \end{Bmatrix} = [T] \begin{Bmatrix} F_2 \\ V_2 \end{Bmatrix} \tag{4.7}$$

When defined in this manner, T is the forward transmission matrix. The rearward transmission matrix denoted by $\bar{T}$ satisfies the following relationship.

$$\begin{Bmatrix} F_2 \\ V_2 \end{Bmatrix} = [\bar{T}] \begin{Bmatrix} F_1 \\ V_1 \end{Bmatrix} \tag{4.8}$$

The transmission matrix is well suited to problems in acoustics where the performance of an array of acoustical elements connected in series is to be determined. The transmission matrix for the series of elements is obtained by multiplying the transmission matrices of the individual elements.

As noted earlier in Table IV.1 (Sec. 4.2), the terminology used in the literature for these three fundamental matrices has often been confusing. However, the admittance, impedance and transmission matrices contain identical information although in different arrangements. Rubin[54,55] has presented a detailed table to permit the rapid determination of the admittance, impedance, rearward transmission and forward transmission matrices of mechanical systems when the elements of only one of the matrices is known. In Table IV.2, Rubin's results are summarized for the general case in which A, B, C and D are known submatrices of the rearward transmission matrix. Rubin's table has not been reproduced here in its entirety for use in this chapter because the sign convention which he adopted (see Table IV.2), wherein the output force and velocity are positive when directed <u>away</u> from the four-pole for transmission

TABLE IV.2

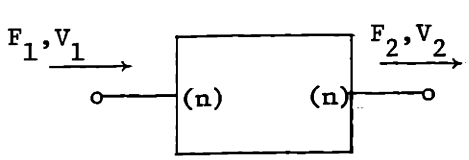

Transmission

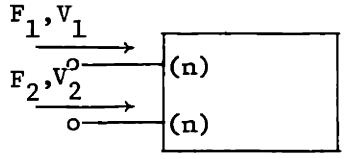

Immittance

Rearward Transmission Matrix ($\bar{T}$):

$$\begin{Bmatrix} F_2 \\ V_2 \end{Bmatrix} = \begin{bmatrix} A & B \\ C & D \end{bmatrix} \begin{Bmatrix} F_1 \\ V_1 \end{Bmatrix}$$

Forward Transmission Matrix (T):

$$\begin{Bmatrix} F_1 \\ V_1 \end{Bmatrix} = \begin{bmatrix} D^T & B^T \\ -C^T & A^T \end{bmatrix} \begin{Bmatrix} F_2 \\ V_2 \end{Bmatrix}$$

Admittance Matrix (Y):

$$\begin{Bmatrix} V_1 \\ V_2 \end{Bmatrix} = \begin{bmatrix} B^{-1}A & -B^{-1} \\ (B^{-1})^T & -DB^{-1} \end{bmatrix} \begin{Bmatrix} F_1 \\ F_2 \end{Bmatrix}$$

Impedance Matrix (Z):

$$\begin{Bmatrix} F_1 \\ F_2 \end{Bmatrix} = \begin{bmatrix} C^{-1}D & -C^{-1} \\ (C^{-1})^T & -AC^{-1} \end{bmatrix} \begin{Bmatrix} V_1 \\ V_2 \end{Bmatrix}$$

Reciprocity Condition:

$$A^T D - C^T B = I$$

matrices but positive when directed toward the four pole for immittance (admittance and impedance) matrices seems inappropriate for acoustical applications.

The acoustic particle velocity is usually considered to be positive in the direction away from the sound source. Thus, in this thesis the transmission and immittance matrices for acoustical circuits will have identical sign conventions. General tables of equivalent matrix forms relevant to acoustical problems will be developed below.

There seems to be no consensus in the literature concerning the most desirable way to formulate the admittance, impedance, and transmission matrices for the analysis of acoustical circuits. For example, the forward transmission matrix has been used in the following four forms:

($p - \rho cu$) formulation:[25,74]

$$\begin{Bmatrix} p_1 \\ \rho c u_1 \end{Bmatrix} = \begin{bmatrix} T_{11} & T_{12} \\ T_{21} & T_{22} \end{bmatrix} \begin{Bmatrix} p_2 \\ \rho c u_2 \end{Bmatrix} \tag{4.9a}$$

($p - uS$) formulation:[79]

$$\begin{Bmatrix} p_1 \\ u_1 S_1 \end{Bmatrix} = \begin{bmatrix} T'_{11} & T'_{12} \\ T'_{21} & T'_{22} \end{bmatrix} \begin{Bmatrix} p_2 \\ u_2 S_2 \end{Bmatrix} \tag{4.9b}$$

($p - \rho uS$) formulation:[76,77]

$$\begin{Bmatrix} p_1 \\ \rho u_1 S_1 \end{Bmatrix} = \begin{bmatrix} T''_{11} & T''_{12} \\ T''_{21} & T''_{22} \end{bmatrix} \begin{Bmatrix} p_2 \\ \rho u_2 S_2 \end{Bmatrix} \tag{4.9c}$$

($p - u$) formulation:[78]

$$\begin{Bmatrix} p_1 \\ u_1 \end{Bmatrix} = \begin{bmatrix} T'''_{11} & T'''_{12} \\ T'''_{21} & T'''_{22} \end{bmatrix} \begin{Bmatrix} p_2 \\ u_2 \end{Bmatrix} \tag{4.9d}$$

where $$T_{11} = T'_{11} = T''_{11} = T'''_{11} \tag{4.9e}$$

$$T_{12} = \frac{S_2}{\rho c} T'_{12} = \frac{S_2}{c} T''_{12} = \frac{1}{\rho c} T'''_{12} \tag{4.9f}$$

$$T_{21} = \frac{\rho c}{S_1} T'_{21} = \frac{c}{S_1} T''_{21} = \rho c \, T'''_{21} \tag{4.9g}$$

$$T_{22} = \frac{S_2}{S_1} T'_{22} = \frac{S_2}{S_1} T''_{22} = T'''_{22} \tag{4.9h}$$

Although each of these four matrix formulations is acceptable for the analysis of duct acoustics, each has certain limitations which should be recognized by the user. In the $(p,\rho cu)$ formulation the particle velocity has been multiplied by ρc to form a product having units of pressure, thus making the matrix elements dimensionless. Having dimensionless matrix elements simplifies the acoustical analysis and, as will be shown below, permits the transmission loss to be determined directly from a summation of the elements of the forward transmission matrix. However, the $(p,\rho cu)$ formulation is not applicable to duct sections with a gradually changing cross-sectional area and an additional transmission matrix must be used across the interface of a discontinuous area change in the duct. For example

$$\begin{Bmatrix} p_1 \\ \rho cu_1 \end{Bmatrix} = \begin{bmatrix} 1 & 0 \\ 0 & \frac{S_2}{S_1} \end{bmatrix} \begin{Bmatrix} p_2 \\ \rho cu_2 \end{Bmatrix} \tag{4.10}$$

across a sudden area change in a duct when viscous and mode conversion losses are ignored.

(p,uS) formulation:
$$\begin{Bmatrix} p_1 \\ u_1 S_1 \end{Bmatrix} = \begin{bmatrix} T'_{11} & T'_{12} \\ T'_{21} & T'_{22} \end{bmatrix} \begin{Bmatrix} p_2 \\ u_2 S_2 \end{Bmatrix} \tag{4.11b}$$

The rearward transmission matrix is obtained by inverting the forward transmission matrix. Thus

(p,ρcu) formulation:
$$\begin{Bmatrix} p_2 \\ \rho c u_2 \end{Bmatrix} \quad \begin{bmatrix} T_{22} & -T_{22} \\ -T_{21} & T_{11} \end{bmatrix} \begin{Bmatrix} p_1 \\ \rho c u_1 \end{Bmatrix} \tag{4.12a}$$

(p,uS) formulation:
$$\begin{Bmatrix} p_2 \\ u_2 S_2 \end{Bmatrix} = \frac{S_2}{S_1} \begin{bmatrix} T'_{22} & -T'_{12} \\ -T'_{21} & T'_{11} \end{bmatrix} \begin{Bmatrix} p_1 \\ u_1 S_1 \end{Bmatrix} \tag{4.12b}$$

The forward and rearward transmission matrices are four-pole matrices whose determinants are unity in accordance with four-pole parameter theory.

The (p,ρcu) formulation of the admittance and impedance matrices can be obtained by writing (4.11a) and (4.12a) in component form and then rearranging terms into the appropriate matrix form. Similarly, the (p,uS) formulation of the impedance and transmission matrices can be determined using Eqs. (4.11b) and (4.12b). The admittance matrix, Y, defined by the expression

(p,ρcu) formulation:
$$\begin{Bmatrix} \rho c u_1 \\ \rho c u_2 \end{Bmatrix} = [Y] \begin{Bmatrix} p_1 \\ p_2 \end{Bmatrix}$$

becomes

$$[Y] = \begin{bmatrix} \frac{T_{22}}{T_{12}} & -\frac{1}{T_{12}} \\ \\ \frac{1}{T_{12}} & -\frac{T_{11}}{T_{12}} \end{bmatrix} \tag{4.13a}$$

(p,uS) formulation:

$$\begin{Bmatrix} u_1 S_1 \\ u_2 S_2 \end{Bmatrix} = [Y'] \begin{Bmatrix} p_1 \\ p_2 \end{Bmatrix}$$

becomes

$$[Y'] = \begin{bmatrix} \frac{T'_{22}}{T'_{12}} & -\frac{S_1}{S_2}\frac{1}{T'_{12}} \\ \\ \frac{1}{T'_{12}} & -\frac{T'_{11}}{T'_{12}} \end{bmatrix} \tag{4.13b}$$

The impedance matrix, Z, defined by the expression

(p,ρcu) formulation:

$$\begin{Bmatrix} p_1 \\ p_2 \end{Bmatrix} = [Z] \begin{Bmatrix} \rho c u_1 \\ \rho c u_2 \end{Bmatrix}$$

becomes

$$[Z] = \begin{bmatrix} \frac{T_{11}}{T_{21}} & -\frac{1}{T_{21}} \\ \\ \frac{1}{T_{21}} & -\frac{T_{22}}{T_{21}} \end{bmatrix} \tag{4.14a}$$

(p,uS) formulation:

$$\begin{Bmatrix} p_1 \\ p_2 \end{Bmatrix} = [Z'] \begin{Bmatrix} u_1 S_1 \\ u_2 S_2 \end{Bmatrix}$$

becomes

$$[Z'] = \begin{bmatrix} \frac{T'_{11}}{T'_{21}} & -\frac{S_1}{S_2}\frac{1}{T'_{21}} \\ \frac{1}{T'_{21}} & -\frac{T'_{22}}{T'_{21}} \end{bmatrix} \qquad (4.14b)$$

In general, by knowing the elements of one of the fundamental matrices it is possible to obtain the other three. These relationships between the forward transmission, rearward transmission, admittance and impedance matrices have been derived for both the (p,ρcu) formulation and the (p,uS) formulation and are given in Tables IV.3a and IV.3b respectively.

The arithmetic rules governing the determination of impedance and immittance matrices of combinations of acoustical elements follow directly from the boundary conditions at the interface of the tandem elements. Consider the lined duct sections joined in series in Fig. 58. Let T_A and T_B be the forward transmission matrices for sections A and B respectively as defined by the following expressions:

$$\begin{Bmatrix} p_{1A} \\ \rho c\ u_{1A} \end{Bmatrix} = [T_A] \begin{Bmatrix} p_{2A} \\ \rho c\ u_{2A} \end{Bmatrix} \qquad \begin{Bmatrix} p_{1B} \\ \rho c\ u_{1B} \end{Bmatrix} = [T_B] \begin{Bmatrix} p_{2B} \\ \rho c\ u_{2B} \end{Bmatrix} \qquad (4.15)$$

At the interface between the two lined sections

$$p_{2A} = p_{1B} \qquad \rho c\, u_{2A} = \rho c\, u_{1B} \tag{4.16}$$

The well known result that the transmission matrix for a series of lined duct sections equals the product of the transmission matrices of the individual sections follows directly from Eqs. (4.15) and (4.16)

$$[T] = [T_A][T_B] \tag{4.17}$$

Equation (4.17) holds for both the forward and rearward transmission matrices.

The admittance and impedance matrices for the series combination can be derived using the overall transmission matrix, (4.17), and the equivalent matrix forms given in Table IV.3. The impedance and admittance matrices for the series combination are

$$[Z] = \frac{1}{Z_{A_{22}} - Z_{B_{11}}} \begin{bmatrix} \text{Det } Z_A - Z_{A_{11}} Z_{B_{11}} & Z_{A_{21}} Z_{B_{21}} \\ -Z_{A_{21}} Z_{B_{21}} & Z_{A_{22}} Z_{B_{22}} - \text{Det } Z_B \end{bmatrix} \tag{4.18}$$

$$[Y] = \frac{1}{Y_{A_{22}} - Y_{B_{11}}} \begin{bmatrix} \text{Det } Y_A - Y_{A_{11}} Y_{B_{11}} & Y_{A_{21}} Y_{B_{21}} \\ -Y_{A_{21}} Y_{B_{21}} & Y_{A_{22}} Y_{B_{22}} - \text{Det } Y_B \end{bmatrix} \tag{4.19}$$

Note, in particular, that the overall impedance matrix is <u>not</u> equal to $Z_A + Z_B$.

To determine the arithmetic rules applicable to duct elements joined in parallel as shown in Fig. 59, the conditions at the interfaces of the duct elements must again be considered. The continuity of particle velocity in the axial direction requires that

$$u_1 S_1 = u_{1A} S_A + u_{1B} S_B \tag{4.20a}$$

$$u_2 S_2 = u_{2A} S_A + u_{2B} S_B \tag{4.20b}$$

and for low frequencies at which only plane waves propagate

$$p_1 = p_{1A} = p_{1B} \tag{4.21a}$$

$$p_2 = p_{2A} = p_{2B} \tag{4.21b}$$

Using the (p,uS) formulation of the admittance matrix, the particle velocity can be related to the acoustic pressure

$$\begin{Bmatrix} u_1 S_1 \\ u_2 S_2 \end{Bmatrix} = [Y'] \begin{Bmatrix} p_1 \\ p_2 \end{Bmatrix} \tag{4.13b}$$

Equations (4.20a) and (4.20b) can be written in matrix form as

$$\begin{Bmatrix} u_1 S_1 \\ u_2 S_2 \end{Bmatrix} = \begin{Bmatrix} u_{1A} & S_A \\ u_{2A} & S_A \end{Bmatrix} + \begin{Bmatrix} u_{1B} & S_B \\ u_{2B} & S_B \end{Bmatrix} \tag{4.22}$$

which can be rewritten as

$$\begin{Bmatrix} u_1 S_1 \\ u_2 S_2 \end{Bmatrix} = \left\{ [Y'_A] + [Y'_B] \right\} \begin{Bmatrix} p_1 \\ p_2 \end{Bmatrix} \tag{4.23}$$

using Eqs. (4.21a,b) and (4.13b).

Thus, the (p,uS) formulation of the admittance matrix for duct sections A and B joined in parallel is

$$[Y'] = [Y'_A] + [Y'_B] \tag{4.24}$$

Note that when using the (p,ρcu) formulation Eqs. (4.20a) and (4.20b) must be written in matrix form as

$$\begin{Bmatrix} \rho cu_1 \\ \rho cu_2 \end{Bmatrix} = \beta_A \begin{Bmatrix} \rho cu_{1A} \\ \rho cu_{2A} \end{Bmatrix} + \beta_B \begin{Bmatrix} \rho cu_{1B} \\ \rho cu_{2B} \end{Bmatrix} \tag{4.25}$$

which requires that

$$[Y] = \beta_A [Y_A] + \beta_B [Y_B] \tag{4.26}$$

where $\beta_A = S_A/S_1$ and $\beta_B = S_B/S_1$.

Having obtained the admittance matrix for the parallel combination, the impedance and forward and rearward transmission matrices can be obtained using either Table IV.3a or Table IV.3b.

In summary, only two arithmetic rules are needed for joining duct elements in tandem:

1) For duct elements in <u>series</u>, the overall <u>transmission matrix</u> is obtained from the product of the transmission matrices of the individual elements.

2) For lined ducts in <u>parallel</u>, the overall <u>admittance matrix</u> is either the sum of the admittance matrices of the individual elements if the (p,uS) formulation is used or the sum of the <u>area weighted</u> admittance matrices for the individual elements if the (p,ρcu) formulation is used.

4.3.2 Reciprocity Considerations

Systems which are linear, passive and vibrate about a stable equilibrium satisfy Lord Rayleigh's General Reciprocity Theorem.[86] Rayleigh determined that for reciprocal systems the impedance matrix is symmetric (i.e., $Z_{12} = Z_{21}$) if the four-pole representation of the acoustical system is defined such that the product of the two conjugate variables at each terminal represents the power fed into the system via that terminal as shown in Fig. 60a. For the four-pole representation shown in Fig. 4b which uses the sign convention to be followed throughout the thesis, the impedance matrix will be antisymmetric (i.e., $Z_{12} = - Z_{21}$). The essential features of reciprocity are uneffected (except for a change of signs) by the sign convention chosen for the four-pole representation of an acoustical system.

For sound waves, a relation which is a corollary of Rayleigh's General Reciprocity Theorem, is commonly used to define the reciprocity condition, i.e.

$$\left(\frac{p_2'}{u_1' S_1'}\right)_{u_2'=0} = \left(\frac{p_1''}{u_2'' S_2''}\right)_{u_1''=0} \tag{4.27}$$

which relates the transmission of sound from position 1 to position 2 (direct experiment) to the transmission of sound from position 2 to position 1 (reciprocal experiment). In the following paragraphs the simplifications to the transmission and immittance matrices resulting from the reciprocity theorem are presented and the conditions under which the reciprocity condition may not be valid for duct acoustics are discussed.

4.3.2.1 Characteristics of Transmission and Immittance Matrices for Systems which Satisfy Reciprocity

Systems which satisfy reciprocity have a certain orderly behavior which produces an interdependence between the four-pole parameters characterizing the system. These known relationships between the four-pole parameters simplify the analysis of reciprocal systems and permit a determination of the system transmission characteristics when two (sometimes only one) independent elements of the transmission matrix are known. For the (p,uS) formulation, reciprocity requires that the determinants of both the forward and rearward transmission matrices equal unity. That is

$$\text{Det } |T'| = T'_{22}\, T'_{11} - T'_{12}\, T'_{21} = 1 \tag{4.28a}$$

$$\text{Det } |\bar{T}'| = \bar{T}'_{22}\, \bar{T}'_{11} - \bar{T}'_{12}\, \bar{T}'_{21} = 1 \tag{4.28b}$$

For the (p,ρcu) formulation the forward and rearward transmission matrices relating acoustic pressure and particle velocity between two duct stations having cross-sectional areas S_1 and S_2 have determinants which are related to the duct area ratio. Thus

$$\text{Det } |T| = T_{22}\, T_{11} - T_{12}\, T_{21} = \frac{S_1}{S_2} \tag{4.29a}$$

$$\text{Det } |\bar{T}| = \bar{T}_{22}\, \bar{T}_{11} - \bar{T}_{12}\, \bar{T}_{21} = \frac{S_2}{S_1} \tag{4.29b}$$

and the determinants equal unity only for constant area ducts. Having a determinant of unity simplifies matrix inversion and reduces the number of independent four-pole parameters to three.

The number of independent four-pole parameters can be reduced to two for symmetrical structures whose attenuation characteristics do not depend upon the direction of sound transmission (e.g., most silencers and mufflers in the linear range of sound pressure level). For these structures

$$T'_{11} = T'_{22} \qquad \bar{T}'_{11} = \bar{T}'_{22} \tag{4.30a,b}$$

A further condition of reciprocity is that the immittance matrices be antisymmetric (when the sign convention shown in Fig.60b is observed). Thus

$$Z'_{12} = -Z'_{21} \qquad Y'_{12} = -Y'_{21} \tag{4.31a,b}$$

For a symmetrical pure reactance four-pole (e.g., some reactive mufflers) only one element of the transmission matrix is necessary to define the transmission characteristics of the system. Shea[87] has shown that the frequency range for which the absolute value of T_{11} is less than unity defines the pass band of the system and, conversely, the frequency range for which $|T_{11}| > 1$ defines the attenuation band.

$$\text{Pass Band: } |T_{11}| < 1$$

$$\text{Attenuation Band: } |T_{11}| > 1$$

4.3.2.2 Conditions under which Reciprocity Assumptions May Be Invalid in Duct Acoustics

The conditions under which reciprocity does not hold in duct acoustics have not been strictly defined in the literature. Duct systems without mean flow generally possess the requisite linear, passive and dynamic characteristics of reciprocal systems. However, for certain duct

systems having discontinuous area expansions at which non-negligible amounts of acoustic energy are dissipated by non-propagating higher order modes, reciprocity may be violated. Also, when a nonlinear liner is not symmetric such that sound traveling in one direction is attenuated differently from sound traveling in the other direction, the reciprocity condition does not hold.

Some disagreement is apparent in the literature regarding the applicability of the reciprocity theorem to ducts lined with porous materials. Rayleigh had held that the presence of dissipative constraints did not violate reciprocity.[86] Janssen,[88] however, contended that reciprocity might not be valid in the presence of sound absorbing porous substances. Ten Wolde[89] later disputed Janssen's contention but Belousov and Rimskii-Korsakov[90] sum up the current situation with their statement: "... the problem of the existence of a reciprocity principle in general form for the case of losses is not altogether clear." It should be noted here that transmission matrices derived below in Section 4.4.2 for duct sections having point-reacting liners and no mean flow do have determinants equal to unity and can be transformed into antisymmetric impedance and admittance matrices, which are sufficient conditions for reciprocity.

The presence of mean flow in a duct causes physical reciprocity to break down because of the phase speed difference for upstream and downstream propagation of sound. Two sources in the duct, one of which is downstream of the other, exist under non-identical conditions, i.e., the phase of the arriving sound waves are unequal, even when the phases of the emergent waves coincide. However, it has been shown that energy reciprocity

is preserved in a moving medium provided the phase speed in the medium is altered by the mean flow only to the first order of the Mach number of the medium.[91] Under certain conditions in flow ducts even the energy reciprocity theorem breaks down. These conditions include the presence of (a) viscous losses which occur at area expansions or contractions, (b) regenerative noise which creates sound sources in the duct in violation of the requirement that the duct element be passive, and (c) duct attenuation characteristics which are biased by the presence of mean flow such that sound traveling in the direction of the mean flow will be attenuated differently from sound traveling against the mean flow.

4.3.3 Determination of Transmission and Insertion Loss from the Transmission Matrix

The convenience of using the transmission matrix to determine the attenuation characteristics of an acoustical circuit has been demonstrated by Ingard[74] who used the forward transmission matrix to demonstrate clearly the difference between the insertion loss and the transmission loss of an acoustical barrier in a duct, as shown in Fig. 61. The insertion loss is defined as

$$IL = 20 \log \left|\frac{p}{p_2}\right| \tag{4.32}$$

where p is the pressure in the duct with the barrier absent and p_2 is the pressure downstream of the barrier after it is inserted into the duct. The transmission loss is defined as

$$TL = 20 \log \left|\frac{p_i}{p_2}\right| \tag{4.33}$$

where p_i is the incident pressure on the upstream side of the barrier in the duct.

Using the (p,ρcu) formulation for the transmission matrix, Ingard has shown that the insertion loss for the barrier in the duct can be expressed as

$$IL = 20 \log \left|\frac{p}{p_2}\right| = 20 \log \left|\frac{T_{11} + T_{12} + \zeta_i (T_{22} + T_{21})}{1 + \zeta_i}\right| \tag{4.34}$$

where T_{ij} are the elements of the barrier forward transmission matrix and ζ_i is the internal impedance of the source. The transmission loss, on the other hand, is simply related to the sum of the elements of the transmission matrix

$$TL = 20 \log \left|\frac{p_i}{p_2}\right| = 20 \log \frac{1}{2} \left|T_{11} + T_{12} + T_{21} + T_{22}\right| \tag{4.35}$$

From Eq. (4.34) it can be noted that the insertion loss depends quite strongly on the source characteristics. For $\zeta_i = 1$ (i.e., the source acts as an anechoic termination) the insertion loss equals the transmission loss. For a constant pressure source, $\zeta_i = 0$, and

$$IL = 20 \log \left|T_{11} + T_{12}\right| \tag{4.36a}$$

whereas for a constant velocity source, $\zeta_i = \infty$, and

$$IL = 20 \log \left|T_{21} + T_{22}\right| \tag{4.36b}$$

Using the (p,uS) formulation for the forward transmission matrix, corresponding expressions for the insertion and transmission loss are

$$IL = 20 \log \left|\frac{p}{p_2}\right| = 20 \log \left| \frac{T'_{11} + \frac{S_2}{\rho c} T'_{12} + \zeta_i (T'_{22} + \frac{\rho c}{S_1} T'_{21})}{1 + \zeta_i} \right| \tag{4.37}$$

$$TL = 20 \log \left|\frac{p_i}{p_2}\right| = 20 \log \frac{1}{2} \left| T'_{11} + \frac{S_2}{\rho c} T'_{12} + \frac{\rho c}{S_1} T'_{21} + T'_{22} \right| \tag{4.38}$$

4.3.4 Effects of Mean Flow on Transmission Matrices

As noted above, sound transmission in ducts with mean flow often does not satisfy the reciprocity theorem. However, this violation of reciprocity does not mean that the analysis of such duct systems using transmission matrices is invalid, only that it is more cumbersome. The rules given in Section 4.3.1.1 for combining transmission and immittance matrices of duct elements in tandem hold for duct systems with and without mean flow. However, the four-pole parameters for each duct section should be defined to include the effects of mean flow. For ducts in parallel an added complication arises because the mean flow field which will distribute itself to equalize the viscous pressure drop through each parallel duct section must be solved before the effects of the mean flow in the branch duct sections can be determined. In general, mean flow effects include the change in phase speed of the convected sound wave, the change in reflection coefficient at the duct exit or inlet, the effect of grazing flow on the impedance of acoustically soft walls particularly resonator liners, and the

increased viscous losses in boundary layers, sound turbulence interactions, sudden area expansions and contractions, etc.

The most prevalent effect of mean flow on the four-pole parameters of a duct section is the change in phase speed of the convected sound wave. For rigid ducts, the wave number is linearly dependent on Mach number. That is,

$$k_- = -\frac{k}{1-M} \qquad k_+ = \frac{k}{1+M} \tag{4.39a,b}$$

where subscripts - and + denote sound waves traveling upstream and downstream respectively. As noted below in the Handbook of Transmission Matrices these convective effects can be incorporated into the forward transmission matrix for a rigid duct section having a constant Mach number, M, as follow

$$\begin{Bmatrix} p_1 \\ \rho c u_1 \end{Bmatrix} = e^{-\frac{ikLM}{1-M^2}} \begin{bmatrix} \cos\left(\frac{kL}{1-M^2}\right) & i\sin\left(\frac{kL}{1-M^2}\right) \\ i\sin\left(\frac{kL}{1-M^2}\right) & \cos\left(\frac{kL}{1-M^2}\right) \end{bmatrix} \begin{Bmatrix} p_2 \\ \rho c u_2 \end{Bmatrix} \tag{4.40}$$

The complex exponential multiplication factor $e^{-\frac{ikLM}{1-M^2}}$ results from phase shifting of the sound waves in the duct. However, since this factor has a pure imaginary exponent it cannot contribute to the transmission loss of the duct which is obtained from the absolute value of the summation of the elements of the transmission matrix.

As shown in Chap. II, the phase speed in lined ducts is a non-linear function of Mach number. The wave number used in the four-pole parameters for acoustically-soft ducts must be obtained from a solution

of the boundary value problem for the duct section. Transmission matrices for several lined duct configurations are given in the Handbook of Transmission Matrices. Additional transmission matrices which include the effects of mean flow are also assembled in the Handbook of Transmission Matrices for visco-thermal losses in rigid ducts, sudden area expansions and contractions, extended inlet and outlet tubes and for sound radiation from the duct inlet or exit.

Of primary concern to noise control engineers is the effect of mean flow on the transmission or insertion loss of mufflers and silencers. Auto and truck mufflers and industrial silencers are usually designed such that the mean flow Mach number does not exceed 0.2. At such low velocities the convective effects are generally negligible producing only slight shifts in the peaks and troughs of the attenuation curve since

$$\frac{k}{1-M^2} > 0.96\ k \qquad @\ M < 0.2$$

Viscous effects at sudden contractions and extended outlets are small. However, tuned elements such as branch resonators, resonant liners and extended inlets could have significant shifts in the attenuation curve near the zero mean flow tuned frequency.

4.4 Determination of Transmission Matrices for Duct System Components

In this section, transmission matrices are determined for most of the components used in typical duct systems. Transmission matrices are obtained from the literature or derived where necessary for an acoustic source, rigid and lined duct sections ducts in parallel, a discontinuous area change in a duct, transition sections, a side branch, muffler connections, hole-cavity resonators and barriers in ducts. The transmission matrices are collected into a Handbook of Transmission Matrices in Section 4.4.9. For selected components, transmission matrices are presented for ducts with and without flow.

4.4.1 Impedance of an Acoustic Source

The acoustic source can be represented schematically as shown in Fig. 40 of the Handbook of Transmission Matrices. The (p,ρcu)formulation of the forward transmission matrix relating the "internal" pressure, p_0, and the source velocity amplitude, u_0, to the pressure, p_1, and the particle velocity, u_1, in the duct near the source can be written as

$$\begin{Bmatrix} p_0 \\ \rho c u_0 \end{Bmatrix} = \begin{bmatrix} 1 & \zeta_i \\ 0 & 1 \end{bmatrix} \begin{Bmatrix} p_1 \\ \rho c u_1 \end{Bmatrix} \tag{4.41a}$$

where ζ_i is the specific internal impedance of the source (i.e., $Z_i/\rho c$). For the (p,uS) formulation of the forward transmission matrix

$$\begin{Bmatrix} p_0 \\ u_0 S_0 \end{Bmatrix} = \begin{vmatrix} 1 & \zeta_i' \\ 0 & 1 \end{vmatrix} \begin{Bmatrix} p_1 \\ u_1 S_1 \end{Bmatrix} \tag{4.41b}$$

where S_0 and S_1 are the source area and cross-sectional area of the duct, respectively, and $\zeta_i' = \rho c \zeta_i / S_1$.

Knowledge of the source impedence is required to design efficient muffler and silencer systems. As shown in Section 4.3.3 the internal impedance of the source is the sole parameter relating the insertion loss of the system to the transmission loss of the muffler. Unfortunately, studies of the acoustic impedance of noisy machinery sources have been sparse. This lack of concern for a detailed knowledge of the complex frequency-dependent source impedance has apparently resulted from questions concerning the value of such information. Attempts to optimize muffler systems by mismatching the source and silencer impedance throughout the frequency spectrum would be time consuming, expensive and perhaps fruitless. Therefore, acousticians have been content to model acoustic sources as either constant pressure sources ($\zeta_i = 0$) or constant velocity sources ($\zeta_i = \infty$). For $\zeta_i = 1$, the source acts as a non-reflecting ρc-termination.

Attempts to model and measure the acoustic impedance of reciprocating engines have been conducted by Wang[70,71] and Galaitsis[92] respectively. Wang modeled the exhaust system of a multicylinder engine as a lumped parameter air induction system with general time varying volume. Wang's lumped parameter assumptions together with his neglect of mean flow and viscous effects limited the usefulness of his impedance model. Galaitsis measured the complex impedance of a diesel engine. Although experimental difficulties limited his measurements to three

engine RPM operating conditions, he was able to conclude that muffler performance predictions could be improved more by improving the understanding of the impedance match between the source and the muffler than by perfecting already accurate prediction techniques for estimating the transmission loss of the muffler alone.

4.4.2 Transmission Matrix for Constant Area Lined Duct Section of Length L

To determine the transmission matrix for a lined duct section of length L with flow, the convected wave equation must be solved using the appropriate boundary conditions. Assuming a uniform mean velocity $\overline{V}$ and no acoustic sources within the duct section under consideration, the convected wave equation for the velocity potential can be written as

$$c^2 \nabla^2 \phi = \left(\frac{\partial}{\partial t} + \overline{V} \cdot \nabla\right)^2 \phi \tag{4.42}$$

The acoustic pressure and particle velocity are determined from the velocity potential using the relations

$$p = \left(\frac{\partial}{\partial t} + \overline{V} \cdot \nabla\right) \phi \tag{4.43a}$$

$$u = -\nabla \phi \tag{4.43b}$$

4.4.2.1 Sound Propagation between Plane Parallel Boundaries

Morse and Ingard[26] have shown that the acoustic pressure of the fundamental mode within a fluid moving in the x direction with uniform velocity V between two plane parallel boundaries can be given by the expression

$$p = P_1 \cos(k_y y)\, e^{-ik_x x}\, e^{i\omega t} \tag{4.44}$$

where

$$k_x^2 + k_y^2 = k^2(1 - \frac{Mk_x}{k})^2 \tag{4.45}$$

at $y = d$ to have finite point-reacting impedance, $z = \rho c/\beta$, continuity of particle displacement at $y = d$ requires that

$$k_y \tan(k_y d) = - i\beta(1 - \frac{Mk_x}{k})^2 k \tag{4.46}$$

For sufficiently large values of the impedance the approximation

$$\tan(k_y d) \simeq k_y d$$

is valid and k_x for the fundamental mode can be written in the form

$$k_{x\pm} = k(\frac{\pm A^{1/2}}{1 \pm MA^{1/2}}) \tag{4.47}$$

where

$$A = 1 + (i\beta/kd) \tag{4.48}$$

4.4.2.2 Sound Propagation in Annular Duct

For an annular duct having a coordinate system defined as shown in Fig. 6 b, Hogge and Ritzi[84] have used the method of separation of variables to obtain the velocity potential for a given mode in the duct

$$\phi_{mn} = e^{i\omega t} e^{-im\theta} R_m(\lambda_{mn} r)\left[F_{mn} e^{-ik_+ x} + G_{mn} e^{-ik_- x}\right] \tag{4.49}$$

when the axial wave numbers k_+ and k_- are given by

$$k_\pm = -\frac{kM}{1-M^2} \pm \left[\frac{k^2}{(1-M^2)^2} - \frac{\lambda_{mn}^2}{1-M^2}\right]^{1/2} \tag{4.50}$$

and the radial mode shape function is given by

$$R_m(\lambda_{mn} r) = J_m(\lambda_{mn} r) + \Gamma_{mn} Y_m(\lambda_{mn} r) \tag{4.51}$$

and F_{mn} and G_{mn} can be considered the Fourier coefficients of the m,n mode for the positive-going and negative-going waves, respectively.

4.4.2.3 Determination of Transmission Matrix

Let $e^{i\omega t} e^{-im\theta} R_m(\lambda_{mn} r) = R_{mn}$. Then Eq. (4.49) can be written as

$$\phi_{mn} = R_{mn}(F_{mn} e^{-ik_+ x} + G_{mn} e^{-ik_- x}) \tag{4.52}$$

Using Eqs. (4.43a,b) u_{mn} and p_{mn} can be obtained from Eq. (4.52)

$$u_{mn} = i R_{mn}(k_+ F_{mn} e^{-ik_+ x} + k_- G_{mn} e^{-ik_- x}) \tag{4.53}$$

$$p_{mn} = i k \rho c R_{mn}\left[(1 - \frac{k_+}{k} M) F_{mn} e^{-ik_+ x} + (1 - \frac{k_-}{k} M) G_{mn} e^{-ik_- x}\right] \tag{4.54}$$

At $x = -L$

$$u_{1mn} = i R_{mn}(k_+ F_{mn} e^{ik_+ L} + k_- G_{mn} e^{ik_- L}) \tag{4.55a}$$

$$p_{1mn} = i k \rho c R_{mn}\left[(1 - \frac{k_+}{k} M) F_{mn} e^{ik_+ L} + (1 - \frac{k_-}{k} M) G_{mn} e^{ik_- L}\right] \tag{4.55b}$$

At $x = 0$

$$u_{2mn} = i R_{mn}(k_+ F_{mn} + k_- G_{mn}) \tag{4.56a}$$

$$p_{2mn} = i k \rho c R_{mn}\left[(1 - \frac{k_+}{k} M) F_{mn} + (1 - \frac{k_-}{k} M) G_{mn}\right] \tag{4.56b}$$

By solving Eqs. (4.56a) and (4.56b) for F_{mn} and G_{mn} and substituting the resulting expression into Eqs. (4.55a) and (4.55b) the forward transmission matrix for an arbitrary mode in a constant area lined duct section with uniform flow at Mach number, M, can be obtained after some algebraic manipulation

$$\begin{Bmatrix} p_{1mn} \\ \rho c u_{1mn} \end{Bmatrix} = \begin{bmatrix} T_{11} & T_{12} \\ T_{21} & T_{22} \end{bmatrix} \begin{Bmatrix} p_{2mn} \\ \rho c u_{2mn} \end{Bmatrix} \tag{4.57}$$

where

$$T_{11} = \frac{k_+ e^{ik_-L} - k_- e^{ik_+L}}{k_+ - k_-} + M \frac{k_+ k_-}{k(k_+ - k_-)} (e^{ik_+L} - e^{ik_-L}) \tag{4.58a}$$

$$T_{12} = \frac{k^2 - Mk(k_+ + k_-) + M^2 k_+ k_-}{k(k_+ - k_-)} (e^{ik_+L} - e^{ik_-L}) \tag{4.58b}$$

$$T_{21} = - \frac{k_+ k_-}{k(k_+ - k_-)} (e^{ik_+L} - e^{ik_-L}) \tag{4.58c}$$

$$T_{22} = \frac{k_+ e^{ik_+L} - k_- e^{ik_-L}}{k_+ - k_-} - M \frac{k_+ k_-}{k(k_+ - k_-)} (e^{ik_+L} - e^{ik_-L}) \tag{4.58d}$$

and $k = \omega/c$ while k_+ and k_- are given by Eq. (4.47) for the fundamental mode propagating between plane parallel boundaries and Eq. (4.50) for an arbitrary mode propagating in an annular duct.

Note that

$$\text{Det } |T| = |T_{11}T_{22} - T_{12}T_{21}| = 1 \tag{4.59}$$

as required for sound fields which satisfy reciprocity.

For the fundamental mode in a rigid duct $\lambda_{00}=0$ and positive- and negative-going waves can be determined from Eq. (4.47) or Eq. (4.50) as

$$k_+ = \frac{k}{1+M} \quad , \quad k_- = -\frac{k}{1-M} \tag{4.60}$$

Substituting Eq. (4.60) into Eq. (4.57) yields the forward transmission matrix for a rigid constant area duct section of length L with uniform flow, M.

$$\begin{Bmatrix} p_1 \\ \rho c u_1 \end{Bmatrix} = e^{-\frac{ikLM}{1-M^2}} \begin{bmatrix} \cos\left(\frac{kL}{1-M^2}\right) & i\sin\left(\frac{kL}{1-M^2}\right) \\ i\sin\left(\frac{kL}{1-M^2}\right) & \cos\left(\frac{kL}{1-M^2}\right) \end{bmatrix} \begin{Bmatrix} p_2 \\ \rho c u_2 \end{Bmatrix} \tag{4.61}$$

The complex exponential multiplication factor $e^{-\frac{ikLM}{1-M^2}}$ will cause phase shifting of the sound waves in the duct but will not contribute to the transmission or insertion loss of a duct section because its exponent is pure imaginary.

To determine the transmission matrix for a lined duct section of length L without flow note that at M = 0, Eq. (4.50) reduces to $k_\pm = \pm k_{mn}$ where $k_{mn} = (k^2 - \lambda_{mn}^2)^{1/2}$. Using these values for k_+ and k_-, Eq. (4.57) reduces to

$$\begin{Bmatrix} p_{1mn} \\ \rho c u_{1mn} \end{Bmatrix} = \begin{bmatrix} \cos k_{mn}L & i\frac{\omega/c}{k_{mn}}\sin k_{mn}L \\ i\frac{k_{mn}}{\omega/c}\sin k_{mn}L & \cos k_{mn}L \end{bmatrix} \begin{Bmatrix} p_{2mn} \\ \rho c u_{2mn} \end{Bmatrix} \tag{4.62}$$

For a plane wave propagating in a rigid duct $k_{mn} = k = \omega/c$ and Eq. (4.62) can be further reduced to its simplest form

$$\begin{Bmatrix} p_1 \\ \rho c u_1 \end{Bmatrix} = \begin{bmatrix} \cos kL & i \sin kL \\ i \sin kL & \cos kL \end{bmatrix} \begin{Bmatrix} p_2 \\ \rho c u_2 \end{Bmatrix} \tag{4.63}$$

4.4.3 Transmission Matrix for N Ducts in Parallel

In Section 3.2 the determination of the transmission matrix for two ducts of equal length aligned in parallel required the simultaneous solution of ten equations relating acoustic pressure and/or particle velocity within each branch duct and across the interfaces at the entrance and exit of the parallel duct section. Using matrix formulations developed in Section 4.3.1 the analysis of the sound transmission through lined duct sections in tandem is greatly simplified. In the following derivation of the transmission matrix of the fundamental mode through N ducts aligned in parallel with no mean flow the efficiency of matrix analysis in duct acoustics is illustrated.

Consider the arrangement shown in Fig. 62, where N ducts of equal length are aligned in parallel within a larger rectangular duct. Each duct section, having cross-sectional area S_i in the parallel array, may be either lined or unlined. Let $T^{(i)}$ be the forward transmission matrix for the i^{th} duct such that

$$\begin{Bmatrix} p_{1,i} \\ \rho c u_{1,i} \end{Bmatrix} = \begin{bmatrix} T_{11}^{(i)} & T_{12}^{(i)} \\ T_{21}^{(i)} & T_{22}^{(i)} \end{bmatrix} \begin{Bmatrix} p_{2,i} \\ \rho c u_{2,i} \end{Bmatrix} \tag{4.64}$$

Using Table IV.3a, the admittance matrix for the i^{th} duct may be determined from the elements of the forward transmission matrix. Therefore,

$$\begin{Bmatrix} \rho c u_{1,i} \\ \rho c u_{2,i} \end{Bmatrix} = \begin{bmatrix} \dfrac{T_{22}^{(i)}}{T_{12}^{(i)}} & -\dfrac{1}{T_{12}^{(i)}} \\ \dfrac{1}{T_{12}^{(i)}} & -\dfrac{T_{11}^{(i)}}{T_{12}^{(i)}} \end{bmatrix} \begin{Bmatrix} p_{1,i} \\ p_{2,i} \end{Bmatrix} \tag{4.65}$$

For low-frequencies when only plane waves propagate

$$p_1 = p_{1,i} \qquad p_2 = p_{2,i} \tag{4.66}$$

and the overall admittance matrix for the N parallel ducts may be obtained by addition of the area-weighted admittance matrices of the individual duct sections in the parallel array. Generalizing Eq. (4.26) for N ducts

$$[Y] = \sum_{i=1}^{N} \beta_i [Y^{(i)}] \tag{4.67}$$

and writing out the matrix elements gives the expression

$$\begin{Bmatrix} \rho c u_1 \\ \rho c u_2 \end{Bmatrix} = \begin{bmatrix} \sum_{i=1}^{N} \dfrac{\beta_i T_{22}^{(i)}}{T_{12}^{(i)}} & -\sum_{i=1}^{N} \dfrac{\beta_i}{T_{12}^{(i)}} \\ \sum_{i=1}^{N} \dfrac{\beta_i}{T_{12}^{(i)}} & -\sum_{i=1}^{N} \dfrac{\beta_i T_{11}^{(i)}}{T_{12}^{(i)}} \end{bmatrix} \begin{Bmatrix} p_1 \\ p_2 \end{Bmatrix} \tag{4.68}$$

The forward transmission matrix, T, for the parallel array can then be determined from Table IV.3a.

$$\begin{Bmatrix} p_1 \\ \rho c u_1 \end{Bmatrix} = [T] \begin{Bmatrix} p_2 \\ \rho c u_2 \end{Bmatrix}$$

where

$$[T] = \begin{bmatrix} \frac{X_1}{Y} & \frac{1}{Y} \\ \frac{X_1 X_2}{Y} - Y & \frac{X_2}{Y} \end{bmatrix} \tag{4.69}$$

$$X_1 = \sum_{i=1}^{N} \frac{\beta_i T_{11}^{(i)}}{T_{12}^{(i)}}$$

$$X_2 = \sum_{i=1}^{N} \frac{\beta_i T_{22}^{(i)}}{T_{12}^{(i)}}$$

$$Y = \sum_{i=1}^{N} \frac{\beta_i}{T_{12}^{(i)}} \qquad \beta_i = \frac{S_i}{S}$$

As shown in Section 4.3.3 the transmission loss for the parallel duct array is determined from the sum of the elements of the transmission matrix

$$TL = 20 \log \frac{1}{2} \left| T_{11} + T_{12} + T_{21} + T_{22} \right| \tag{4.35}$$

Substituting Eq. (4.69) into Eq. (4.35) and noting that for a duct (lined or unlined)

$$T_{11}^{(i)} = T_{22}^{(i)} \qquad X_1 = X_2 = X \tag{4.70}$$

yields the following expression for the transmission loss

$$TL = 20 \log \frac{1}{2} \left| \frac{1}{Y} (X + 1)^2 - Y \right| \tag{4.71}$$

or alternatively

$$TL = 20 \log \frac{1}{2} \left| \frac{(X+Y+1)(X-Y+1)}{Y} \right| \tag{4.72}$$

Equation (4.69) can be used in Eq. (4.72) to express the transmission loss for the parallel array of N ducts in terms of the elements of the transmission matrices, $T^{(i)}$,

$$TL = 20 \log \frac{1}{2} \left| \frac{\left[1 + \sum_{i=1}^{N} \frac{\beta_i}{T_{12}^{(i)}} (T_{11}^{(i)} + 1)\right]\left[1 + \sum_{i=1}^{N} \frac{\beta_i}{T_{12}^{(i)}} (T_{11}^{(i)} - 1)\right]}{\sum_{i=1}^{N} \frac{\beta_i}{T_{12}^{(i)}}} \right| \tag{4.73}$$

4.4.4 Transition Sections

Analysis of the sound transmission characteristics of transition sections is extremely complicated for the general case of multi-modal sound waves with arbitrary mean flow and must be approached numerically. For many practical applications, however, simplifying assumptions can be made to the general problem to permit tractable solutions. For example,

Hogge and Ritzi[84] have modeled aircraft engine inlet ducts, in which the flow is diffused in an expanding duct ahead of the compressor face, as a series of conical connectors having a given uniform flow velocity within each section. They determined the transmission matrix for an arbitrary mode in each conical section. The transmission matrix for the entire inlet can be approximated by multiplication of the matrices of the adjacent conical sections (if mode reflections are ignored at the interfaces between sections having different wall slopes). The transmission matrix for the conical connector determined by Hogge and Ritzi for a multi-modal sound wave with mean flow is given in the Handbook of Transmission Matrices in Fig. 43.

In air handling systems, such as air conditioning ducts, intake and exhaust silencers and mufflers, transition sections are used to join duct sections of different diameters to reduce aerodynamic losses. Most transition sections in these duct systems can be modeled as generalized Bessel connectors or exponential connectors. A generalized Bessel connector is a duct having a cross-sectional area which varies according to the relation

$$S = S_0 \, x^a \tag{4.74}$$

A parabolic connector and a two-dimensional connector with straight walls can be modeled as a Bessel connector having $a = 1$. A Bessel connector having $a = 2$ is a conical connector.

The cross-sectional area of an exponential connector varies according to the relation

$$S = S_0 \, e^{\gamma x} \tag{4.75}$$

where γ is a taper constant.

Typically the dominant part of the spectrum of the sound waves traveling within air conditioning ducts and inlet and exhaust silencers and mufflers is below the cutoff frequency. Thus, most of the sound energy is carried in the fundamental mode. Beckemeyer[93] has presented the following modified version of the Webster horn equation which is applicable to the transmission of the fundamental mode in a variable area duct without mean flow but with a locally reacting liner and axially-variable mean fluid density

$$\frac{\partial^2 p}{\partial x^2} + \frac{1}{(S/\rho)} \frac{\partial (S/\rho)}{\partial x} \frac{\partial p}{\partial x} + k^2 (1 - \frac{i\rho c}{kSZ}) p = 0 \tag{4.76}$$

Using Eq. (4.76) Beckemeyer formulated the transmission matrix for the fundamental mode in a horn having a point-reacting acoustic liner with axially varying impedance, axial gradients in gas temperature and no mean flow. The purpose of his investigation was to determine the effect of the position of a heated slug of gas in the duct system on the reflection coefficient of the horn. Beckemeyer divided the duct system into N axial segments. The rearward transmission matrix for the j^{th} segment having axial length Δ_j is

$$\begin{Bmatrix} p \\ \rho_0 c_0 u \end{Bmatrix}_j = \begin{vmatrix} \bar{T}_{11} & \bar{T}_{12} \\ \bar{T}_{21} & \bar{T}_{22} \end{vmatrix} \begin{Bmatrix} p \\ \rho_0 c_0 u \end{Bmatrix}_{j-1} \tag{4.77}$$

where

$$\bar{T}_{11} = 1 \tag{4.78a}$$

$$\bar{T}_{12} = - i \frac{\Delta j}{S_0} \frac{S_{j-1}}{S_0} k_0 S_0 \int_0^1 \frac{\rho/\rho_0}{S/S_0} d\zeta \tag{4.78b}$$

$$\bar{T}_{21} = - \frac{\Delta j}{S_j} \left[i k_0 S_0 \int_0^1 \frac{(S/S_0)\, d\zeta}{\rho c^2/(\rho_0 c_0^2)} - \int_0^1 \frac{d\zeta}{Z/(\rho_0 c_0)} \right] \tag{4.78c}$$

$$\bar{T}_{22} = \frac{S_{j-1}}{S_j} \tag{4.78d}$$

The matrix coefficients were evaluated by use of trapezoidal integration. The rearward transmission matrix for the entire duct system was then determined by multiplying together the transmission matrices of the N duct segments. Beckemeyer used 200 segments to accurately define his duct system.

In a variable area rigid duct in the absence of mean flow the propagation of the fundamental mode is governed by the following simplified form of the Webster horn equation which is more readily amenable to closed-form solution

$$\frac{\partial^2 p}{\partial x^2} + \frac{\partial(\log S)}{\partial x} \frac{\partial p}{\partial x} + k^2 p = 0 \tag{4.79}$$

4.4.4.1 Bessel Connector

The general solution of Eq. (4.79) for harmonic waves traveling in opposite directions in an acoustical connector is

$$p = \left[A f(x)\, e^{-ikx} + B g(x)\, e^{ikx} \right] e^{i\omega t} \tag{4.80}$$

where for a Bessel connector

$$f(x) = g(x) = (kx)^{-a/2} \tag{4.81}$$

The acoustic particle velocity is determined from the expression

$$u = \frac{i}{\rho_0 \omega} \frac{\partial p}{\partial x} \tag{4.82}$$

Thus $$u = \frac{i}{\rho_0 \omega} \left\{ A\left[f'(x) - ikf(x)\right] e^{-ikx} + B\left[g'(x) + ikg(x)\right] e^{ikx} \right\} e^{i\omega t} \tag{4.83}$$

Evaluating Eqs. (4.80) and (4.83) at $x = x_1$ and x_2 and noting that $f(x) = g(x)$ and $f'(x) = g'(x)$ yields

$$p_1 = f(x_1)\left[Ae^{-ikx_1} + Be^{ikx_1}\right] e^{i\omega t} \tag{4.84a}$$

$$u_1 = \frac{i}{\rho\omega} \left\{ A\left[f'(x_1) - ikf(x_1)\right] e^{-ikx_1} + B\left[f'(x_1) + ikf(x_1)\right] e^{ikx_1} \right\} e^{i\omega t} \tag{4.84b}$$

$$p_2 = f(x_2)\left[Ae^{-ikx_2} + Be^{ikx_2}\right] e^{i\omega t} \tag{4.84c}$$

$$u_2 = \frac{i}{\rho\omega} \left\{ A\left[f'(x_2) - ikf(x_2)\right] e^{-ikx_2} + B\left[f'(x_2) + ikf(x_2)\right] e^{ikx_2} \right\} e^{i\omega t} \tag{4.84d}$$

Solving Eqs. (4.84c) and (4.84d) for A and B in terms of p_2 and u_2 and substituting the expressions obtained into Eqs. (4.84a) and (4.84b) yields

$$p_1 = \frac{f(x_1)}{f(x_2)} \left\{ \left[\frac{f'(x_2)}{kf(x_2)} \sin k\ell + \cos k\ell \right] p_2 + i\rho c u_2 \sin k\ell \right\} \tag{4.85a}$$

$$\rho c u_1 = \frac{i}{[kf(x_2)]^2}\left\{\left[f'(x_2)f'(x_1)+k^2 f(x_1)f(x_2)\right]\sin k\ell\right.$$

$$\left.+k\left[f'(x_1)f(x_2)-f(x_1)f'(x_2)\right]\cos k\ell\right\} p_2$$

$$-\frac{1}{kf(x_2)}\left[f'(x_1)\sin k\ell - kf(x_1)\cos k\ell\right]\rho c u_2 \qquad (4.85b)$$

Using Eq. (4.81), f(x), g(x), f'(x) and g'(x) can be evaluated and inserted into Eqs. (4.85a) and (4.85b) to determine the transmission matrix for a generalized Bessel connector of order a.

$$\begin{Bmatrix} p_1 \\ u_1 S_1 \end{Bmatrix} = \begin{bmatrix} T'_{11} & T'_{12} \\ T'_{21} & T'_{22} \end{bmatrix} \begin{Bmatrix} p_2 \\ u_2 S_2 \end{Bmatrix} \qquad (4.86)$$

where

$$T'_{11} = \left(\frac{S_2}{S_1}\right)^{1/2}\left(\cos k\ell - \frac{a}{2kx_2}\sin k\ell\right) \qquad (4.86a)$$

$$T'_{12} = i\,\frac{\rho c}{(S_1 S_2)^{1/2}}\sin k\ell \qquad (4.86b)$$

$$T'_{21} = i\,\frac{(S_1 S_2)^{1/2}}{\rho c}\left[\left(1+\frac{a^2}{4k^2 x_1 x_2}\right)\sin k\ell + \frac{a}{2}\left(\frac{1}{kx_2}-\frac{1}{kx_1}\right)\cos k\ell\right] \qquad (4.86c)$$

$$T'_{22} = \left(\frac{S_1}{S_2}\right)^{1/2}\left(\cos k\ell + \frac{a}{2kx_1}\sin k\ell\right) \qquad (4.86d)$$

The elements of the forward transmission matrix for a connector having a linear area variation ($S = S_0 x$) and for a conical connector ($S = S_0 x^2$) have been obtained as special cases of the general Bessel connector and are presented in Fig.47 of the Handbook of Transmission Matrices.

4.4.4.2 Exponential Connector

Using the Webster horn equation, Mason[61] has obtained the following expressions for acoustic pressure and particle velocity of the fundamental mode in an exponential horn with no mean flow (Fig. 48):

$$p_2 = e^{-LT}\left[(\cosh k'L + \frac{T}{k'} \sinh k'L)p_1 - i(\frac{\rho c}{S_1} \frac{k}{k'} \sinh k'L)S_1 u_1\right] \qquad (4.87)$$

$$S_2 u_2 = e^{LT}\left[-i(\frac{S_1}{\rho c} \frac{k}{k'} \sinh k'L)p_1 + (\cosh k'L - \frac{T}{k'} \sinh k'L)S_1 u_1\right] \qquad (4.88)$$

where $$\frac{S_2}{S_1} = e^{2LT} \qquad (4.89)$$

and $\sqrt{T^2 - \omega^2/c^2}$ and $\sqrt{P_0 \gamma \rho}$ in Mason's solution have been replaced by k' and ρc respectively. The forward transmission matrix for the exponential connector of length L is obtained by inverting Eqs. (4.87) and (4.88)

$$\begin{Bmatrix} p_1 \\ u_1 S_1 \end{Bmatrix} \quad \begin{bmatrix} T'_{11} & T'_{12} \\ T'_{21} & T'_{22} \end{bmatrix} \quad \begin{Bmatrix} p_2 \\ u_2 S_2 \end{Bmatrix} \qquad (4.90)$$

where

$$T'_{11} = e^{LT}(\cosh k'L - \frac{T}{k'} \sinh k'L) \tag{4.90a}$$

$$T'_{12} = i\, e^{LT} \frac{\rho c}{S_2} \frac{k}{k'} \sinh k'L \tag{4.90b}$$

$$T'_{21} = i\, e^{LT} \frac{S_1}{\rho c} \frac{k}{k'} \sinh k'L \tag{4.90c}$$

$$T'_{22} = e^{LT} \frac{S_1}{S_2} (\cosh k'L + \frac{T}{k'} \sinh k'L) \tag{4.90d}$$

4.4.5 Discontinuous Area Changes in a Duct

Design requirements in certain silencers often make it either infeasible or not desirable to use acoustical connectors having gradual area changes to join duct sections of different cross-sectional areas. The resulting discontinuous area changes designed into auto and truck mufflers, for example, can be classified into the following four distinct types, as shown in Figs. 57a-57d, for purpose of mathematical modeling:

(1) Area contraction (outlet)

(2) Area expansion (inlet)

(3) Area contraction with branch (extended outlet)

(4) Area expansion with branch (extended inlet)

Alfredson and Davies[72,73] modeled each of the four types of discontinuous area changes by using the one-dimensional conservation equations of mass, momentum, and energy across the interface for a duct with mean flow. After experimentally determining the acoustical characteristics of each of the discontinuous area changes in a duct with

mean flow, Alfredson and Davies modified their original mathematical models wherever necessary to improve the correlation between the analysis and the experimental measurements.

In the following paragraphs each of the four discontinuous area changes are considered with a brief mention of the mathematical model required to obtain the transmission matrix for each element.

4.4.5.1 Area Contraction (Outlet)

For an acoustic wave propagating in a gas stream flowing through a discontinuous area contraction (Fig.57a), the flow can be assumed to be isentropic for first order disturbances. Linearized equations relating the fluctuating pressure and velocity on either side of the discontinuity are the energy equation

$$p_1 + \rho c M_1 u_1 = p_2 + \rho c M_2 u_2 \tag{4.91}$$

and the continuity equation

$$S_1 M_1 p_1 + \rho c S_1 u_1 = S_2 M_2 p_2 + \rho c S_2 u_2 \tag{4.92}$$

The forward transmission matrix for a discontinuous area contraction with mean flow obtained by solving Eqs. (4.91) and (4.92) is presented in Fig. 45.

4.4.5.2 Area Expansion (Inlet)

When sound waves propagating in a duct having cross-sectional area S_1 pass through a discontinuous area change into a larger duct having cross-sectional area S_2, higher order modes are created in the larger duct due to the non-uniform excitation of the sound field at the entrance to the larger duct. At frequencies below the cutoff

frequency in the larger duct, the higher order modes formed at the discontinuity decay exponentially with axial distance. The formation of these non-propagating higher-order modes at the discontinuity contributes a mass reactance to the impedance at the interface. The mass reactance is analogous to the additional impedance caused by the end correction, δ, for a piston of area S_1 radiating sound into a duct with area S_2. Ingard[75] has shown that the impedance at the discontinuity can be written as

$$\zeta = \frac{p_1}{\rho c u_1} = \frac{S_1}{S_2} - i k \delta \tag{4.93}$$

From continuity $$u_1 S_1 = u_2 S_2 \tag{4.94}$$

Thus, the forward transmission matrix for a discontinuous area expansion without mean flow can be written as

$$\begin{Bmatrix} p_1 \\ u_1 S_1 \end{Bmatrix} = \begin{bmatrix} 1 & -i \frac{\rho c}{S_1} k\delta \\ 0 & 1 \end{bmatrix} \begin{Bmatrix} p_2 \\ u_2 S_2 \end{Bmatrix} \tag{4.95}$$

Values for the mass end correction, δ, have been calculated by Ingard[94] for various geometries.

Alfredson and Davies[72,73] modeled sound transmission through a discontinuous area expansion with flow both as an adiabatic expansion and as an isentropic (constant pressure) expansion. Comparison of their results with experimental measurements showed the adiabatic expansion model provided a better match with experimental results.

By perturbing the conservation equations of mass, momentum, and energy and retaining only terms to first order in the fluctuating quantities, they obtained the following equations across the interface:

Energy conservation: $$p_1 + \rho c M_1 u_1 = p_2 + \rho c M_2 u_2 - \frac{\varepsilon}{\gamma - 1} \tag{4.96}$$

Mass conservation: $$S_1 M_1 p_1 + \rho c S_1 u_1 = S_2 M_2 p_2 + \rho c S_2 u_2 + S_2 M_2 \varepsilon \tag{4.97}$$

Momentum conservation: $$(S_2 + S_1 M_1^2) p_1 + 2\rho c S_1 M_1 u_1 = (S_2 + S_2 M_2^2) p_2 + 2\rho c S_2 M_2 u_2 + S_2 M_2^2 \varepsilon \tag{4.98}$$

where a momentum source term, $p_1(S_2 - S_1)$, due to the discontinuity has been added to the left hand side of the momentum equation by Alfredson[72] based on experimental evidence. The term ε can be regarded as an irreversible fluctuating pressure loss due to the non-isentropic nature of the expansion. Solving the momentum equation (4.98) for ε and substituting the result into the energy and mass equations (4.96, 4.97) the forward transmission matrix can be determined for an area expansion with flow. The results are presented in Fig.46 of the Handbook of Transmission Matrices.

It should be noted that some disagreement exists in the literature concerning the proper way to model the flow through a discontinuous area expansion. In the Alfredson and Davies model the assumption was made that the flow expands rapidly downstream of the discontinuity and forms a uniform velocity profile across the larger duct after a short adjustment zone. Alfredson and Davies found it necessary to model the expansion as non-isentropic for the analysis to predict their experimental results obtained at $M \leq 0.15$. Cummings,[95]

however, used the Alfredson and Davies model in an attempt to predict the results of Ronneberger[96] who measured reflection and transmission coefficients for a discontinuous area change at speeds up to M = 0.6 and showed that the agreement was poor for M > 0.2. Cummings proposed to model the flow downstream from the expansion as a jet having a constant diameter aligned with the diameter of the smaller duct. The velocity in the jet was assumed to be equal to the velocity in the smaller duct. To account for entropy fluctuations in the flow a vortex layer was assumed to bound the jet. Outside the vortex layer the velocity in the larger duct was assumed to be zero. Using the jet model Cummings accurately predicted the results of Ronneberger up to M = 0.6. Subsequently, Cummings and Haddad[97] showed that neglecting the vortex layer in the jet model changed the reflection coefficient on the order of 1% at M = 0.6. They tentatively concluded that sound transmission through a discontinuous area change with flow could be obtained with sufficient accuracy from a simple isentropic jet model.

4.4.5.3 Area Contraction with a Branch (Extended Outlet)

The flow across an area contraction with a branch has been modeled as isentropic by Alfredson and Davies.[72,73] However, the side branch (Region 2 in Fig.57c) has been assumed to have an impedance, Z_b, given by the expression

$$Z_b = \frac{1 + R_b\, e^{i(\phi - 2kL)}}{1 - R_b\, e^{i(\phi - 2kL)}} \tag{4.99}$$

where R_b is the reflection factor at the branch entrance and ϕ is the phase angle at the end cap. If there is no energy dissipation in the branch, $R_b = R_2$, where R_2 is the reflection factor of the end cap.

In real mufflers, two non-isentropic effects must be incorporated into the model:

(1) The effect of yielding of the silencer walls, and

(2) the production of an entropy wave at the entrance to the smaller duct.

Alfredson and Davies determined that both of these effects could be approximated in the model by retaining the isentropic assumption across the interface and allowing the reflection coefficient, R_2, to have a value less than unity. Values of R_2 between 0.90 and 0.95 have produced the best agreement with experimental data.[73]

Using the model proposed by Alfredson and Davies, Parrott[78] has determined the forward transmission matrix for an area contraction with a branch. His expression is presented in Fig. 45 of the Handbook of Transmission Matrices.

4.4.5.4 Area Expansion with a Branch (Extended Inlet)

The extended inlet is modeled similarly to the extended outlet (Sec. 4.4.5.3) with the exception that the flow across the discontinuity is assumed to be adiabatic for the extended inlet rather than isentropic. The effects of yielding walls cause the reflection factor, R_2, to have a value of 0.98 for typical mufflers.[73] The lower reflection factors of 0.90–0.95, which were required for the extended outlet to force the mathematical models to conform with the measurements, are not required for the extended inlet because the more realistic assumption of adiabatic flow across the expansion permits handling the entropy waves directly in the mathematical model rather than

as an adjustment to the reflection coefficient. The forward transmission matrix for an area expansion with a branch as determined by Parrott[78] is given in Fig. 51 of the Handbook of Transmission Matrices.

4.4.6 Transmission Matrices of Resonators in Ducts

Resonators are frequently used in reactive mufflers, aircraft inlets and other duct systems to reduce discrete frequency noise by matching the natural frequency of the resonator to the noise spectrum. Although various shapes and sizes of resonators are used in typical applications, most resonators can be classified as either (1) side branch resonators or (2) hole-cavity resonators which are essentially side branch resonators with restricted inlet ports.

4.4.6.1 Side Branch Resonator

Side branch resonators, shown schematically in Fig. 49 of the Handbook of Transmission Matrices, are used to reduce low-frequency noise in ducts. At resonance, the side branch appears as a vanishingly small wall impedance to the sound wave thus causing strong reflections at the impedance discontinuity in the duct. For a close-end side branch, resonance occurs when the side branch depth, b, equals one-quarter of the sound wavelength. By making b sufficiently large, resonance can be made to occur at any desired low frequency.

When the cross-dimension, Δx, of the side branch opening is small compared to a quarter wavelength at the highest frequency considered, the side branch can be treated as a lumped parameter system. The forward transmission matrix for the side branch can be obtained by

treating the side branch impedance, Z_b, as a shunt impedance in the equivalent circuit for the duct (see, for example, Parrott[78])

$$\begin{Bmatrix} p_1 \\ \rho c u_1 \end{Bmatrix} = \begin{bmatrix} 1 & 0 \\ \frac{S_b/S_1}{Z_b} & \frac{S_2}{S_1} \end{bmatrix} \begin{Bmatrix} p_2 \\ \rho c u_2 \end{Bmatrix} \tag{4.100}$$

For a close-ended side branch

$$Z_b = -i Y_b \cot k b \tag{4.101a}$$

For an open-ended side branch

$$Z_b = -i Y_b \cot\left(\frac{kb}{2}\right) \tag{4.101b}$$

where Y_b is the acoustic admittance of the side branch walls.

Side branch resonators are effected quite strongly by mean flow in the duct. Lambert[98] noted that mean flow: (1) shifted the side branch resonance frequency, (2) reduced the side branch Q factor, (3) reduced the insertion loss of the side branch to zero at sufficiently high flow velocities and (4) produced (sometimes intense) self-noise due to non-linear excitation of the resonator. This generation of intense self-noise (screech) can be a particularly troublesome problem with side branch resonators in flow ducts. Ingard and Singhal[99] have shown that coupling of cavity-cavity and cavity-duct modes aggravate the noise problem by producing additional screech peaks throughout the frequency spectrum. Because of this self-noise generation and the loss of attenuating effectiveness in addition to the large pressure drop incurred by the mean flow in passing over the open wall cavities, side branch resonators are usually replaced in flow ducts with hole-cavity resonators.

4.4.6.2 Hole-Cavity Resonators

Many types of hole-cavity resonator configurations are used to reduce noise in duct systems. Most of these configurations can be classified as one of the four basic types shown in Fig. 63 :

(a) A single Helmholtz resonator.

(b) A Helmholtz resonator array used as a point-reacting liner.

(c) A concentric tube resonator with a single row of holes.

(d) A concentric tube resonator with multiple rows of holes.

Each of these four configurations must be analyzed in a different manner to determine its acoustical performance.

In configurations (a) and (c) the resonators can be treated as lumped impedance elements. The forward transmission matrix can be written as

$$\begin{Bmatrix} p_1 \\ \rho c u_1 \end{Bmatrix} = \begin{bmatrix} 1 & 0 \\ -\frac{1}{Z_r} & 1 \end{bmatrix} \begin{Bmatrix} p_2 \\ \rho c u_2 \end{Bmatrix} \tag{4.102}$$

when $S_1 = S_2$ which is the usual situation. Expressions for the resonator impedance, Z_r, of configurations (a) and (c) are given in Figs. 52a and 52c, respectively, of the Handbook of Transmission Matrices.

For high sound pressure levels (i.e., > 130 dB) the resistance of the Helmholtz resonator becomes nonlinear due to the viscous dissipation of the kinetic energy in the jets issuing from the resonator orifices. This nonlinearity has been accounted for by Ingard and Ising[100] by adding a second term to the specific acoustic resistance for the resonator which

is dependent on the magnitude of the orifice particle velocity. Thus, θ becomes

$$\theta = k\sqrt{\frac{\delta\nu}{\omega}}\left(1+\frac{t}{d}\right)+\frac{K}{C_D^2}\frac{|v_0|}{c} \tag{4.103}$$

where

$$|v_0| = \frac{|p|}{\rho c(\theta^2+\chi^2)^{1/2}} \tag{4.104}$$

C_D is the discharge coefficient for the orifice and K is a factor valued between 0.37 and 0.43. The other terms are defined in Fig. 52a of the Handbook of Transmission Matrices.

Configuration (d),(Fig. 63), the concentric tube resonator with multiple rows of holes, is a distributed-reaction liner which cannot be analyzed using conventional matrix techniques. However, Sullivan[79] recently presented a discrete element method for modeling parallel coupled, perforated tube muffler elements, shown schematically in Fig. 64 a. His solution can be applied to concentric tube resonators, extended inlet and outlet tubes which are perforated, and side branch cavities for which lumped impedance analyses are not valid.

Sullivan subdivided the muffler into discrete elements by taking slices normal to the flow axis through the tube and its backing volume. Each slice, being a segment of a parallel coupled duct, was described in a 4x4 transmission matrix. An essential component of Sullivan's analysis is the modeling of the specific acoustic admittance boundary a(x). Sullivan assigned acoustic admittance values A_j at finite intervals along the boundary

$$A_j = \int_{x_{j+}}^{x_{j-}} a(x)dS \tag{4.105}$$

where dS is the incremental area of the boundary and

$$x_{j+} = (x_j - x_{j+1})/2 \qquad x_{j-} = (x_{j-1} - x_j)/2 \tag{4.106a,b}$$

for the discrete element representation shown in Fig. 64a . Boundary conditions were then established as

$$p_{1j+1} = p_{1j} \qquad p_{2j+1} = p_{2j} \tag{4.107a,b}$$

$$u_{1j+1} = u_{ij} + v_j \qquad u_{2j+1} = u_{2j} - v_j \tag{4.107c,d}$$

where v_j is the volume velocity normal to the boundary between ducts 1 and 2. Defining the wall acoustic admittance as

$$A_j = \frac{v_j}{p_{1j} - p_{2j}} \tag{4.108}$$

Eqs. (4.107a-d) could be arranged into a 4x4 matrix

$$\begin{Bmatrix} p_{1j+1} \\ u_{1j+1} \\ p_{2j+1} \\ u_{2j+1} \end{Bmatrix} = \begin{bmatrix} 1 & 0 & 0 & 0 \\ A_j & 1 & -A_j & 0 \\ 0 & 0 & 1 & 0 \\ -A_j & 0 & A_j & 1 \end{bmatrix} \begin{Bmatrix} p_{1j} \\ u_{1j} \\ p_{2j} \\ u_{2j} \end{Bmatrix} \tag{4.109}$$

Between stations the admittance was assumed to be zero (i.e., a rigid wall) and the plane wave motion in each duct could be represented as

$$\begin{Bmatrix} p_{1j} \\ u_{1j} \\ p_{2j} \\ u_{2j} \end{Bmatrix} = \begin{bmatrix} \cos k\ell_j & i\frac{\rho c}{S_1}\sin k\ell_j & 0 & 0 \\ i\frac{S_1}{\rho c}\sin k\ell_j & \cos k\ell_j & 0 & 0 \\ 0 & 0 & \cos k\ell_j & i\frac{\rho c}{S_2}\sin k\ell_j \\ 0 & 0 & i\frac{S_2}{\rho c}\sin k\ell_j & \cos k\ell_j \end{bmatrix} \begin{Bmatrix} p_{1j-1} \\ u_{1j-1} \\ p_{2j-1} \\ u_{2j-1} \end{Bmatrix} \tag{4.110}$$

By successively multiplying pairs of transmission matrices given in Eqs. (4.109) and (4.110), a 4x4 transmission matrix characterizing the entire concentric tube resonator is obtained.

$$\begin{Bmatrix} p_{12N} \\ u_{12N} \\ p_{22N} \\ u_{22N} \end{Bmatrix} = [T_{ij}] \begin{Bmatrix} p_{11} \\ u_{11} \\ p_{21} \\ u_{21} \end{Bmatrix} \tag{4.111}$$

Using the definition of the impedance

$$Z_{22N} = \frac{p_{22N}}{u_{22N}} \quad \text{and} \quad Z_{21} = \frac{p_{21}}{u_{21}} \tag{4.112a,b}$$

the 4x4 matrix represented in Eq. (4.111) can be reduced to the 2x2 matrix given in Fig. 53 of the Handbook of Transmission Matrices.

Sullivan applied his approximate method to the analysis of the closed cavity configuration (for which a closed form solution existed) shown in Fig. 64b. He found that by dividing the admittance boundary into only six elements the solution closely approximated the exact solution. Thus, dividing a concentric tube resonator into one element for

each row of holes in the tube would seem more than sufficient to obtain an accurate solution. Although Sullivan's discrete element method does not converge as quickly as finite difference or finite element methods, the speed of a computer solution is vastly superior because it involves only the multiplication of 4x4 matrices and does not require inversion of large order matrices. Finally, it should be noted that although Sullivan's method is limited to one-dimensional analysis it is able to accommodate area change, and mean flow and temperature gradients.

4.4.6.3 Effects of Mean Flow on Resonators in Ducts

The attenuation characteristics of hole-cavity resonators are effected by mean flow in the duct in at least three ways:

(1) Turbulence convected downstream from a row of holes produces entropy fluctuations in the flow.

(2) The mean flow alters the impedance of the orifice and thus the natural frequency of the resonator.

(3) "Self-noise" produced by flow over the resonator liners may cause the resonator to be a net producer rather than an attenuator of sound.

Munjal[76] apparently has made the only attempt to include the effects of mean flow in a transmission matrix formulation for the hole-cavity resonator. Although Munjal included the overall effect of entropy fluctuations in the transmission matrix, he ignored the effect of mean flow on the orifice impedance.

This effect of mean flow on the orifice impedance has been shown to be quite significant. Groeneweg[101] has presented data which

indicates that increasing the mean flow Mach number from zero to 0.5 increases the orifice resistance by a factor of 4. The end correction of the orifice is reduced toward zero as the mean flow eliminates the inertia contribution of the "attached mass" of gas immediately outside the orifice on the duct side. The increased orifice resistance raises the natural frequency of the resonator as shown in Fig. 65 which Chen[102] adapted from the data of Meyer, Michel and Kurtze.[103]

Self-noise produced by resonator liners in flowing ducts has been studied by numerous investigators including Ingard and Dean,[104] Meyer et al.,[103] and Bauer and Chapkis.[105] Hrubes[106] has studied the influence of duct liner geometrical parameters on the characteristics of intense self-noise (screech) produced by resonator liners. Even though the subject of resonator liner screech has been investigated intensively, self-noise produced by resonator liners is not yet well enough understood by acousticians for an attempt to be made to include its effects in the transmission matrix for a hole-cavity resonator with mean flow.

4.4.7 Parasitic Acoustic Attenuation in a Rigid Duct with Flow

An acoustic wave propagating in a rigid duct is attenuated due to the parasitic effects of viscosity and heat conduction at the boundaries and by turbulence throughout the flow field. These effects, which are small compared to the attenuation caused by acoustic liners, nonetheless, can be important in reducing and broadening the resonance peaks in reactive mufflers or in causing significant attenuation in long

narrow ducts. Expressions for the parasitic losses at the duct boundaries in the viscous and thermal boundary layers are well known and were first determined by Kirchoff[30] for the fundamental mode in a circular duct without flow 110 years ago.

Recently, Ingard and Singhal[31] have determined the additional losses due to turbulence in a flowing duct by modeling the oscillatory flow in the sound field as a quasistatic modulation of the steady flow. This assumption is valid at low frequencies for which the wavelength is much larger than the duct diameter. Additionally, Ingard and Singhal assumed that the pressure level in the duct (static plus acoustic) was monotonically decreasing in the mean flow direction. This assumption holds when[29]

$$\frac{|p|}{P} < \left(\frac{\gamma}{4\pi}\right)\left(\frac{\lambda}{D}\right)4C_f M^2 \qquad (4.113)$$

where p is the acoustic pressure, P is the static pressure in the duct, λ is the sound wavelength, D is the duct diameter, C_f is the friction coefficient and M is the Mach number. For $\lambda/D = 4$ and $M = 0.1$ at atmospheric static pressure the assumption of monotonically decreasing pressure level in the duct breaks down for sound pressures above 119 dB. The results of Ingard and Singhal are presented in Fig. 55 of the Handbook of Transmission Matrices together with the forward transmission matrix derived in Section 4.4.2 for sound transmission in an attenuating constant area duct with mean flow.

4.4.8 Radiation of Sound from an Open Ended Duct

The forward transmission matrix representing the radiation of sound from an open-ended duct can be written in the following form[37]

$$\begin{Bmatrix} p_1 \\ u_1 S_1 \end{Bmatrix} = \begin{bmatrix} 1 & Z \\ 0 & 1 \end{bmatrix} \begin{Bmatrix} p_2 \\ u_2 S_2 \end{Bmatrix} \tag{4.114}$$

where Z is the radiation impedance of the open-ended duct. The radiation impedance cannot be uniquely determined unless several parameters are specified including (1) the character of the sound waves in the duct (fundamental mode, spinning modes, etc.), (2) the geometry of the exit (flanged or unflanged), (3) the flow speed in the duct (core flow), (4) the flow speed around the duct (surrounding flow) and (5) pressure, temperature or density mismatches between the core flow and the surrounding flow. Since no theory has been developed which handles the general case of radiation from an open-ended duct, a silencer designer must choose the simplest theory which fits his requirements.

Levine and Schwinger[107] have determined the radiation impedance for a plane acoustic mode radiated from an unflanged pipe without flow. They have shown that radiation impedance is manifested as a radiation resistance and a mass reactance due to an end correction applied to the duct which approaches 0.6133 times the radius of the duct as the frequency goes to zero. Other values of the mass end correction as a function of frequency are shown in Fig. 56 of the Handbook of Transmission Matrices.

Carrier[108] added the effect of flow to the solution of Levine and Schwinger. Mani[109] determined the effect of velocity mismatch at the exit for flat ducts. Recently, Savkar[110] solved the radiation problem for spinning acoustic modes from a cylindrical duct with a plug flow exhaust jet having velocity and temperature mismatches. New models for the radiation impedance for more complex flow situations are in a continuing state of development. However, progress has been slow because of the basic difficulty of obtaining reliable acoustical measurements in turbulent flow against which the mathematical models must be tested.

Parrott[78] has shown, however, that for typical exhaust systems the effects of convection at the open end of the duct are much more important than a precise knowledge of the reflection coefficient at the open end of the duct. He has shown that the increase in radiated acoustic power due to mean flow in the duct can be expressed as

$$\Delta \text{ Radiated Power} = 10 \log \frac{(1+M)^2 - (1-M)^2 R^2(M)}{1 - R^2(0)} \qquad (4.115)$$

where R(M) is a reflection factor which depends upon the Mach number of the mean flow. Measurements have suggested[69] that for typical exhaust muffler systems R(M) is increased over R(0) by only 3 to 5 percent to a value greater than 0.975. Thus, disregarding the effects of Mach number on the reflection coefficient can cause a maximum error of 2 dB in the radiated acoustic power from Eq. (4.115). This effect is small, however, compared to the effects of convection which at M = 0.1 increase the radiated power by 8 dB over the zero mean flow condition.

In Fig. 56 of the Handbook of Transmission Matrices the forward transmission matrix for the radiation from an unflanged duct without flow is presented using a low frequency approximation to the radiation resistance. The reflection coefficient determined using this approximation is compared to the reflection coefficient determined by Levine and Schwinger with good agreement for wavelengths longer than π times the radius of the duct.

4.4.9 Handbook of Transmission Matrices

SOURCE IMPEDANCE

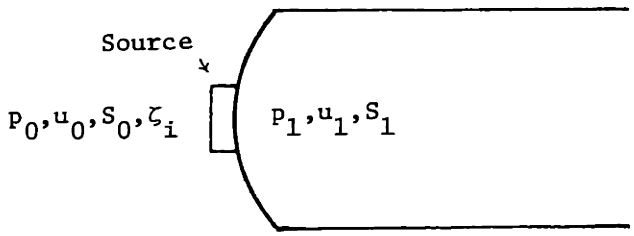

p_0 - "Internal" pressure amplitude of source

u_0 - Source velocity amplitude

ζ_i - Source internal impedance

$$\begin{Bmatrix} p_0 \\ \rho c u_0 \end{Bmatrix} = \begin{bmatrix} 1 & \zeta_i \\ 0 & 1 \end{bmatrix} \begin{Bmatrix} p_1 \\ \rho c u_1 \end{Bmatrix}$$

$$\begin{Bmatrix} p_0 \\ u_0 S_0 \end{Bmatrix} = \begin{bmatrix} 1 & \zeta_i' \\ 0 & 1 \end{bmatrix} \begin{Bmatrix} p_1 \\ u_1 S_1 \end{Bmatrix}$$

$$\zeta_i' = \frac{\rho c}{S_1} \zeta_i$$

Constant pressure source: $\zeta_i = 0$

Non-reflecting source: $\zeta_i = 1$

Constant velocity source: $\zeta_i = \infty$

FIG. 40

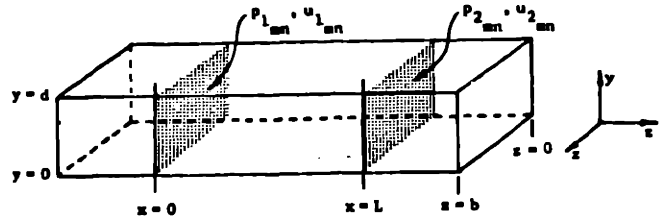

$$\begin{Bmatrix} p_{1_{mn}} \\ \rho c u_{1_{mn}} \end{Bmatrix} = \begin{bmatrix} T_{11} & T_{12} \\ T_{21} & T_{22} \end{bmatrix} \begin{Bmatrix} p_{2_{mn}} \\ \rho c u_{2_{mn}} \end{Bmatrix}$$

where

$$T_{11} = \frac{k_+ e^{ik_-L} - k_- e^{ik_+L}}{k_+ - k_-} + M \frac{k_+ k_-}{k(k_+ - k_-)} (e^{ik_+L} - e^{ik_-L})$$

$$T_{12} = \frac{k^2 - Mk(k_+ + k_-) + M^2 k_+ k_-}{k(k_+ - k_-)} (e^{ik_+L} - e^{ik_-L})$$

$$T_{21} = -\frac{k_+ k_-}{k(k_+ - k_-)} (e^{ik_+L} - e^{ik_-L})$$

$$T_{22} = \frac{k_+ e^{ik_+L} - k_- e^{ik_-L}}{k_+ - k_-} - M \frac{k_1 k^2}{k(k_+ - k_-)} (e^{ik_+L} - e^{ik_-L})$$

$$k_\pm = -\frac{kM}{1-M^2} \pm \left[\frac{k^2}{(1-M^2)^2} - \frac{\lambda_{mn}^2}{(1-M^2)} \right]^{1/2}$$

$$\lambda_{mn}^2 = \left(\frac{m\pi}{b}\right)^2 + \left(\frac{n\pi}{d}\right)^2 - \frac{2ic_m \beta_z k}{b} + \frac{2ic_n \beta_y k}{d} \quad \text{(see Morse and Ingard, p. 506, 29)}$$

where β_z and β_y are the acoustic admittance of the liners in the z and y planes respectively, and $c_i = 1$ for $i = 0$ and 2 for $i > 0$.

For a fundamental mode in a rigid duct with mean flow:

$$\begin{Bmatrix} p_1 \\ \rho c u_1 \end{Bmatrix} = e^{-\frac{ikLM}{1-M^2}} \begin{bmatrix} \cos\left(\frac{kL}{1-M^2}\right) & i \sin\left(\frac{kL}{1-M^2}\right) \\ i \sin\left(\frac{kL}{1-M^2}\right) & \cos\left(\frac{kL}{1-M^2}\right) \end{bmatrix} \begin{Bmatrix} p_2 \\ \rho c u_2 \end{Bmatrix}$$

since $k_+ = \frac{k}{1+M}$ and $k_- = -\frac{k}{1-M}$

For an arbitrary mode in a lined duct at M = 0:

$$\begin{Bmatrix} p_{1_{mn}} \\ \rho c u_{1_{mn}} \end{Bmatrix} = \begin{bmatrix} \cos k_{mn} L & i \frac{\omega/c}{k_{mn}} \sin k_{mn} L \\ i \frac{k_{mn}}{\omega/c} \sin k_{mn} L & \cos k_{mn} L \end{bmatrix} \begin{Bmatrix} p_{2_{mn}} \\ \rho c u_{2_{mn}} \end{Bmatrix}$$

since at M = 0, $k_\pm = \pm k_{mn}$ where $k_{mn} = (k^2 - \lambda_{mn}^2)^{1/2}$

For a plane wave propagating in a rigid duct at M = 0:

$$\begin{Bmatrix} p_1 \\ \rho c u_1 \end{Bmatrix} = \begin{bmatrix} \cos kL & i \sin kL \\ i \sin kL & \cos kL \end{bmatrix} \begin{Bmatrix} p_2 \\ \rho c u_2 \end{Bmatrix}$$

FIG.41: RECTANGULAR DUCT (UNIFORM MEAN FLOW - ARBITRARY MODE)

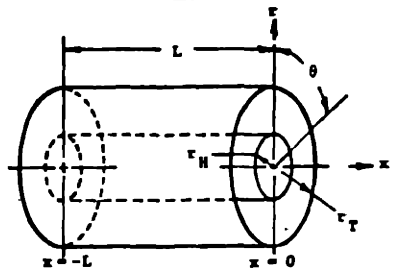

$$\begin{Bmatrix} P_{1_{mn}} \\ u_{1_{mn}} \quad S_1 \end{Bmatrix} = \begin{bmatrix} T'_{11} & T'_{12} \\ T'_{21} & T'_{22} \end{bmatrix} \begin{Bmatrix} P_{2_{mn}} \\ u_{2_{mn}} \quad S_2 \end{Bmatrix}$$

where

$$T'_{11} = \frac{k_+ e^{ik_-L} - k_- e^{ik_+L}}{k_+ - k_-} + M \frac{k_+ k_-}{k(k_+ - k_-)} \left(e^{ik_+L} - e^{ik_-L} \right)$$

$$T'_{12} = \frac{\rho c}{S} \frac{k^2 - Mk(k_+ + k_-) + M^2 k_+ k_-}{k(k_+ - k_-)} \left(e^{ik_+L} - e^{ik_-L} \right)$$

$$T'_{21} = - \frac{S}{\rho c} \frac{k_+ k_-}{k(k_+ - k_-)} \left(e^{ik_+L} - e^{ik_-L} \right)$$

$$T'_{22} = \frac{k_+ e^{ik_+L} - k_- e^{ik_-L}}{k_+ - k_-} - M \frac{k_+ k_-}{k(k_+ - k_-)} \left(e^{ik_+L} - e^{ik_-L} \right)$$

$$k_\pm = - \frac{kM}{1-M^2} \pm \left[\frac{k^2}{(1-M^2)^2} - \frac{\lambda_{mn}^2}{(1-M^2)^2} \right]^{1/2}$$

The eigenvalue λ_{mn} is determined from the wall boundary condition

$$-i\omega\rho \frac{J_m(\lambda_{mn} r_T)}{J'_m(\lambda_{mn} r_T)} = Z_T$$

where Z_T is the wall impedance and J_m is the Bessel function of the first kind of order m.

For an annular duct, boundary conditions at the inner and outer wall are used to determine λ_{mn} and Γ_{mn} using the radial mode shape function given by

$$R_m(\lambda_{mn} r) = J_m(\lambda_{mn} r) + \Gamma_{mn} Y_m(\lambda_{mn} r)$$

where Y_m is a Bessel function of second kind of order m. At the outer wall

$$-i\omega\rho \frac{R_m(\lambda_{mn} r_T)}{R'_m(\lambda_{mn} r_T)} = Z_T$$

and at the inner wall

$$-i\omega\rho \frac{R_m(\lambda_{mn} r_H)}{R'_m(\lambda_{mn} r_H)} = Z_H$$

where Z_T and Z_H are the acoustic impedance of the outer and the inner all, respectively.

FIG. 42: CYLINDRICAL DUCT (UNIFORM MEAN FLOW - ARBITRARY MODE)

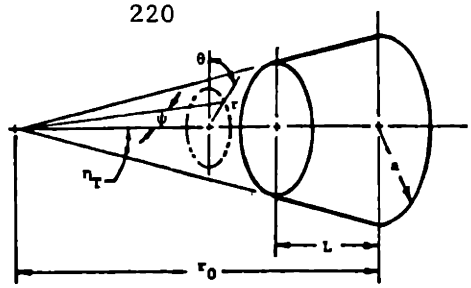

$$\begin{Bmatrix} p_{1_{mn}} \\ u_{1_{mn}} S_1 \end{Bmatrix} = \begin{bmatrix} T'_{11} & T'_{12} \\ T'_{21} & T'_{22} \end{bmatrix} \begin{Bmatrix} p_{2_{mn}} \\ u_{2_{mn}} S_2 \end{Bmatrix}$$

where

$$T'_{11} = \frac{k_+ e^{ik_-L} - k_- e^{ik_+L}}{k_+ - k_-} + M \frac{k_+ k_-}{k(k_+ - k_-)} (e^{ik_+L} - e^{ik_-L})$$

$$T'_{12} = \frac{\rho c}{S_2} \frac{k^2 - Mk(k_+ + k_-) + M^2 k_+ k_-}{k(k_+ - k_-)} (e^{ik_+L} - e^{ik_-L})$$

$$T'_{21} = -\frac{S_1}{\rho c} \frac{k_+ k_-}{k(k_+ - k_-)} (e^{ik_+L} - e^{ik_-L})$$

$$T'_{22} = \frac{S_1}{S_2} \left[\frac{k_+ e^{ik_+L} - k_- e^{ik_-L}}{k_+ - k_-} - M \frac{k_+ k_-}{k(k_+ - k_-)} (e^{ik_+L} - e^{ik_-L}) \right]$$

$$k_\pm = -\frac{kM + 1/r_0}{1-M^2} \pm \left[\frac{k^2 r_0^2 + 2ikr_0 M - 1}{r_0^2 (1-M^2)^2} - \frac{q_{mn}(q_{mn}+1)}{r_0^2 (1-M^2)} \right]$$

The eigenvalue q_{mn} is determined from the wall boundary condition

$$-i\omega\rho \, P^m_{q_{mn}}(\cos\eta_T) / P^{m'}_{q_{mn}}(\cos\eta_T) = Z_T$$

where Z_T is the wall impedance and $P^m_{q_{mn}}$ is the Legendre function of the first kind of order q_{mn} and degree m.

For a conical duct with an inner hub, boundary conditions at the inner and outer wall are used to determine q_{mn} and Γ^m_n using the cross-duct mode shape function, $\Phi(\psi)$, given by

$$\Phi(\psi) = P^m_{q_{mn}}(\cos\psi) + \Gamma^m_n \, Q^m_{q_{mn}}(\cos\psi)$$

where $Q^m_{q_{mn}}$ is the Legendre function of the second kind of order q_{mn} and degree m. At the outer wall

$$-i\omega\rho\Phi(\eta_t)/\Phi'(\eta_t) = Z_T$$

and at the inner wall

$$-i\omega\rho\Phi(\eta_H)/\Phi'(\eta_H) = Z_H$$

where Z_T and Z_H are the acoustic impedance and η_T and η_H are the cone half-angles of the outer wall and the inner wall, respectively.

FIG. 43: CONICAL DUCT (UNIFORM MEAN FLOW - ARBITRARY MODE)

N-DUCTS ALIGNED IN PARALLEL

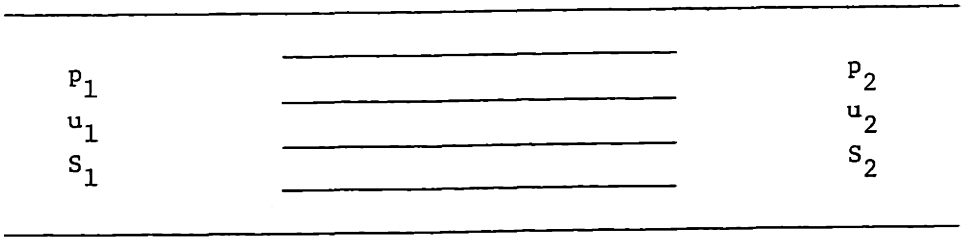

$$\begin{Bmatrix} p_1 \\ \rho c u_1 \end{Bmatrix} = \begin{bmatrix} T_{11} & T_{12} \\ T_{21} & T_{22} \end{bmatrix} \begin{Bmatrix} p_2 \\ \rho c u_2 \end{Bmatrix}$$

where

$$T_{11} = \frac{X_1}{Y} \qquad T_{12} = \frac{1}{Y}$$

$$T_{21} = \frac{X_1 X_2}{Y} - Y \qquad T_{22} = \frac{X_2}{Y}$$

and

$$X_1 = \sum_{i=1}^{N} \frac{\beta_i T_{11}^{(i)}}{T_{12}^{(i)}} \qquad X_2 = \sum_{i=1}^{N} \frac{\beta_i T_{22}^{(i)}}{T_{12}^{(i)}}$$

$$Y = \sum_{i=1}^{N} \frac{\beta_i}{T_{12}^{(i)}} \qquad \beta_i = \frac{S_i}{S}$$

Pressure-Volume Velocity Formulation

$$\begin{Bmatrix} p_1 \\ u_1 S_1 \end{Bmatrix} = \begin{bmatrix} T_{11} & \frac{\rho c}{S_1} T_{12} \\ \frac{S_2}{\rho c} T_{21} & \frac{S_1}{S_2} T_{22} \end{bmatrix} \begin{Bmatrix} p_2 \\ u_2 S_2 \end{Bmatrix}$$

FIG. 44

AREA CONTRACTION

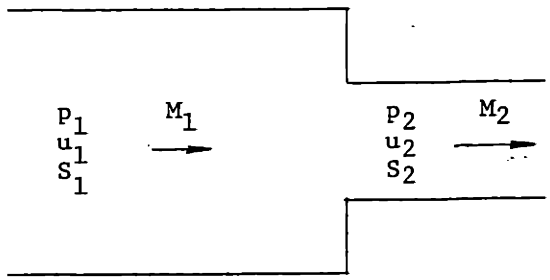

$$\begin{Bmatrix} p_1 \\ u_1 S_1 \end{Bmatrix} = \begin{bmatrix} 1 & \dfrac{\rho c}{S_2} \dfrac{M_2\left[1 - \left(\dfrac{S_2}{S_1}\right)^2\right]}{1 - M_2^2\left(\dfrac{S_2}{S_1}\right)^2} \\ 0 & \dfrac{1 - M_2^2}{1 - M_2^2\left(\dfrac{S_2}{S_1}\right)^2} \end{bmatrix} \begin{Bmatrix} p_2 \\ u_2 S_2 \end{Bmatrix}$$

For $M_2 = 0$:

$$\begin{Bmatrix} p_1 \\ u_1 S_1 \end{Bmatrix} = \begin{bmatrix} 1 & 0 \\ 0 & 1 \end{bmatrix} \begin{Bmatrix} p_2 \\ u_2 S_2 \end{Bmatrix}$$

FIG. 45

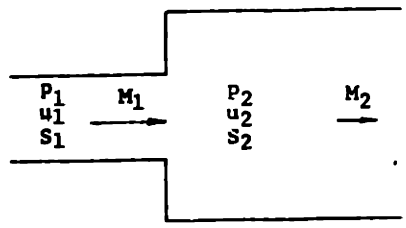

$$\begin{Bmatrix} p_1 \\ u_1 S_1 \end{Bmatrix} = \begin{bmatrix} T'_{11} & T'_{12} \\ T'_{21} & T'_{22} \end{bmatrix} \begin{Bmatrix} p_2 \\ u_2 S_2 \end{Bmatrix}$$

$$T'_{11} = \frac{1 + \left[\left(\frac{S_2}{S_1}\right)^2 (\gamma-1) - 2\gamma \frac{S_2}{S_1} + \gamma\right] M_2^2}{D}$$

$$T'_{12} = \frac{\frac{\rho c}{S_2} \left\{2\left(1 - \frac{S_2}{S_1}\right) M_2 + (\gamma-1)\left[\left(\frac{S_2}{S_1}\right)^2 - 2\left(\frac{S_2}{S_1}\right) + 1\right] M_2^3\right\}}{D}$$

$$T'_{21} = \frac{\frac{S_2}{\rho c}\left[\gamma\left(\frac{S_2}{S_1} - 1\right) M_2^3\right]}{D}$$

$$T'_{22} = \frac{\left[1 + \left(\frac{S_2}{S_1} - 2\right) M_2^2 + (\gamma-1)\left(\frac{S_2}{S_1} - 1\right) M_2^4\right]}{D}$$

where $$D = 1 + \left\{(\gamma-1)\left[1 + \left(\frac{S_2}{S_1}\right)^2\right] + \frac{S_2}{S_1}\left(\frac{S_2}{S_1} - 2\gamma\right)\right\} M_2^2 + \left[(\gamma-1)\left(\frac{S_2}{S_1}\right)^2 \left(\frac{S_2}{S_1} - 1\right)\right] M_2^4$$

For $M_2 = 0$:

$$\begin{Bmatrix} p_1 \\ u_1 S_1 \end{Bmatrix} = \begin{bmatrix} 1 & 0 \\ 0 & 1 \end{bmatrix} \begin{Bmatrix} p_2 \\ u_2 S_2 \end{Bmatrix}$$

FIG. 46: AREA EXPANSION

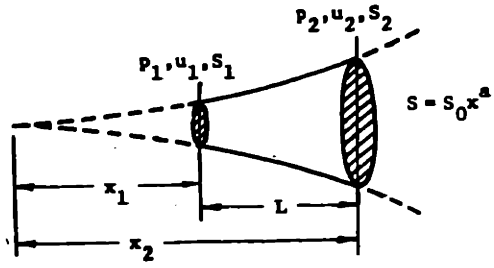

$$\begin{Bmatrix} P_1 \\ u_1 S_1 \end{Bmatrix} = \begin{bmatrix} T'_{11} & T'_{12} \\ T'_{21} & T'_{22} \end{bmatrix} \begin{Bmatrix} P_2 \\ u_2 S_2 \end{Bmatrix}$$

where

$$T'_{11} = \left(\frac{S_2}{S_1}\right)^{1/2} \left(\cos k\ell - \frac{a}{2kx_2} \sin k\ell\right) \qquad T'_{12} = i \frac{\rho c}{(S_1 S_2)^{1/2}} \sin k\ell$$

$$T'_{21} = i \frac{(S_1 S_2)^{1/2}}{\rho c} \left[\left(1 + \frac{a^2}{4k^2 x_1 x_2}\right) \sin k\ell + \frac{a}{2}\left(\frac{1}{kx_2} - \frac{1}{kx_1}\right) \cos k\ell\right]$$

$$T'_{22} = \left(\frac{S_1}{S_2}\right)^{1/2} \left(\cos k\ell + \frac{a}{2kx_1} \sin k\ell\right)$$

For a = 1 (i.e., rectangular connector):

$$T'_{11} = m\left(\cos k\ell - \frac{m^2-1}{2m^2 k} \sin k\ell\right) \qquad T'_{12} = i \frac{\rho c}{S_2} m \sin k\ell$$

$$T'_{21} = i \frac{S_1}{\rho c} m \left\{\left[1 + \frac{(m^2-1)^2}{4m^2 (k\ell)^2}\right] \sin k\ell - \frac{(m^2-1)^2}{2m^2 k\ell} \cos k\ell\right\}$$

$$T'_{22} = \frac{1}{m} \left(\cos k\ell + \frac{m^2-1}{2k\ell} \sin k\ell\right)$$

For a = 2 (i.e., conical connector):

$$T'_{11} = m \cos k\ell - \frac{m-1}{k\ell} \sin k\ell \qquad T'_{12} = \frac{\rho c}{S_2} m \sin k\ell$$

$$T'_{21} = \frac{S_1}{\rho c} \left\{\left[m + \frac{(m-1)^2}{(k\ell)^2}\right] \sin k\ell - \frac{(m-1)^2}{k\ell} \cos k\ell\right\}$$

$$T'_{22} = \frac{1}{m} \left[\frac{m-1}{k\ell} \sin k\ell + \cos k\ell\right]$$

FIG. 47: BESSEL CONNECTOR

EXPONENTIAL CONNECTOR

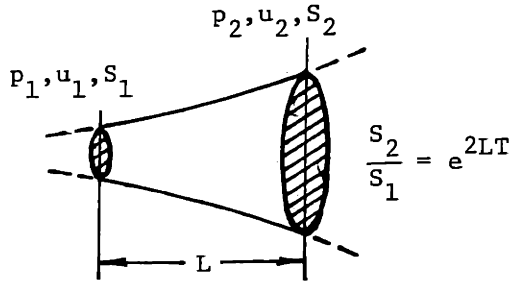

$$\begin{Bmatrix} p_1 \\ u_1 S_1 \end{Bmatrix} = \begin{bmatrix} T_{11} & T_{12} \\ T_{21} & T_{22} \end{bmatrix} \begin{Bmatrix} p_2 \\ u_2 S_2 \end{Bmatrix}$$

where

$$T'_{11} = e^{LT}(\cosh k'L - \frac{T}{k'} \sinh k'L)$$

$$T'_{12} = i\, e^{LT} \frac{\rho c}{S_2} \frac{k}{k'} \sinh k'L$$

$$T'_{21} = i\, e^{LT} \frac{S_1}{\rho c} \frac{k}{k'} \sinh k'L$$

$$T'_{22} = e^{LT} \frac{S_1}{S_2} (\cosh k'L + \frac{T}{k'} \sinh k'L)$$

and $$k' = \sqrt{T^2 - k^2}$$

FIG. 48

SIDE BRANCH RESONATOR

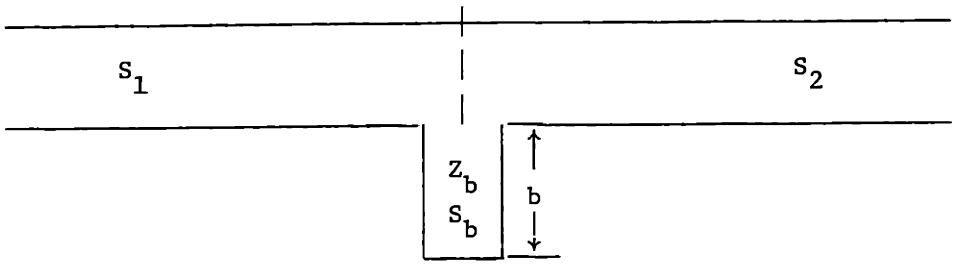

$$\begin{Bmatrix} p_1 \\ \rho c u_1 \end{Bmatrix} = \begin{bmatrix} 1 & 0 \\ \frac{S_b/S_1}{Z_b} & \frac{S_2}{S_1} \end{bmatrix} \begin{Bmatrix} p_2 \\ \rho c u_2 \end{Bmatrix}$$

For a side branch with a closed end

$$Z_b = -i Y_b \cot k b$$

For a side branch with an open end

$$Z_b = -i Y_b \cot\left(\frac{kb}{2}\right)$$

where Y_b is the acoustic admittance of the side branch walls.

FIG. 49

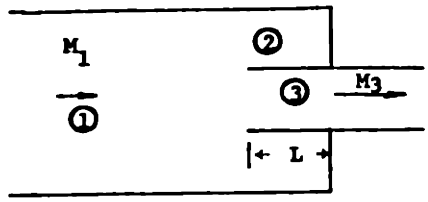

$$\begin{Bmatrix} p_1 \\ u_1 S_1 \end{Bmatrix} = \begin{bmatrix} T'_{11} & T'_{12} \\ T'_{21} & T'_{22} \end{bmatrix} \begin{Bmatrix} p_3 \\ u_3 S_3 \end{Bmatrix}$$

$$T'_{11} = \frac{1 - \frac{1}{Z_b}\frac{S_3}{S_1}\frac{S_2}{S_1} M_3 - \left(\frac{S_3}{S_1}\right)^2 M_3^2}{1 - \left(\frac{S_3}{S_1}\right)^2 M_3^2}$$

$$T'_{12} = \frac{\frac{\rho c}{S_3}\left\{\left[1 - \left(\frac{S_3}{S_1}\right)^2\right] M_3 + \frac{1}{Z_b}\frac{S_3}{S_1}\frac{S_2}{S_1} M_3^2\right\}}{1 - \left(\frac{S_3}{S_1}\right)^2 M_3^2}$$

$$T'_{21} = \frac{\frac{S_2}{\rho c Z_b}}{1 - \left(\frac{S_3}{S_1}\right)^2 M_3^2} \qquad T'_{22} = \frac{1 + \left(\frac{1}{Z_b}\frac{S_2}{S_3}\right) M_3 + M_3^2}{1 - \left(\frac{S_3}{S_1}\right)^2 M_3^2}$$

where

$$Z_b = \frac{1 + R_b\, e^{i(\phi - 2kL)}}{1 - R_b\, e^{i(\phi - 2kL)}}$$

and R_b is the reflection factor at the branch entrance and ϕ is the phase angle at the end cap. If there is no energy dissipation in the branch, $R_b = R$, the reflection factor of the end cap.

For $M_3 = 0$:

$$\begin{Bmatrix} p_1 \\ u_1 S_1 \end{Bmatrix} = \begin{bmatrix} 1 & 0 \\ \frac{S_2}{\rho c}\frac{1}{Z_b} & 1 \end{bmatrix} \begin{Bmatrix} p_3 \\ u_3 S_3 \end{Bmatrix}$$

FIG. 50: EXTENDED OUTLET (AREA CONTRACTION WITH BRANCH)

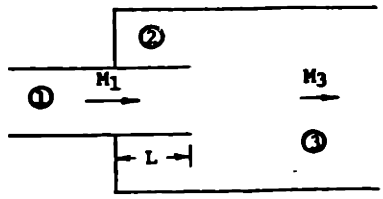

$$\begin{Bmatrix} p_1 \\ u_1 S_1 \end{Bmatrix} = \begin{bmatrix} T'_{11} & T'_{12} \\ T'_{21} & T'_{22} \end{bmatrix} \begin{Bmatrix} p_3 \\ U_3 S_3 \end{Bmatrix}$$

$$T'_{11} = \frac{1+\left[\left(\frac{S_3}{S_1}\right)^2 (\gamma-1) - 2\gamma\frac{S_3}{S_1} + \gamma\right] M_3^2 + \frac{1}{Z_b}\frac{S_3}{S_1}\frac{S_2}{S_1}\left[M_3^2 + (\gamma-1)M_3^3 + \frac{S_3}{S_1}M_3^4\right]}{D}$$

$$T'_{12} = \frac{\frac{\rho c}{S_3}\left\{2\left(1-\frac{S_3}{S_1}\right)M_3 + (\gamma-1)\left[\left(\frac{S_3}{S_1}\right)^2 - 2\left(\frac{S_3}{S_1}\right)+1\right]M_3^3 - \frac{1}{Z_b}\frac{S_3}{S_1}\frac{S_2}{S_1}\left[2M_3^2 - (\gamma-1)M_3^4\right]\right\}}{D}$$

$$T'_{21} = \frac{\frac{S_1}{\rho c}\left\{\gamma\left[\frac{S_3}{S_2}\left(\frac{S_3}{S_2}-1\right)\right]M_3^3 - \frac{1}{Z_b}\frac{S_2}{S_1}\left(1+\gamma M_3^2\right)\right\}}{D}$$

$$T'_{22} = \frac{\left\{1+\left(\frac{S_3}{S_1}-2\right)M_3^2 + \left[\left(\frac{S_3}{S_1}-1\right)(\gamma-1)\right]M_3^4\right\} - \frac{1}{Z_b}\frac{S_2}{S_3}\left[2M_3 + (\gamma-1)M_3^3\right]}{D}$$

where

$$D = 1+\left\{(\gamma-1)\left[1+\left(\frac{S_3}{S_1}\right)^2\right] + \frac{S_3}{S_1}\left(\frac{S_3}{S_1}-2\gamma\right)\right\}M_3^2 + \left[(\gamma-1)\left(\frac{S_3}{S_1}\right)^2\left(\frac{S_3}{S_1}-1\right)\right]M_3^4$$

$$+\frac{1}{Z_b}\frac{S_2}{S_1}\left[\left(\frac{S_3}{S_1}-2\right)M_3 + \left(\frac{S_3}{S_1}\right)^2 M_3^3\right]$$

$$Z_b = \frac{1+R_b\, e^{i(\phi-2kL)}}{1-R_b\, e^{i(\phi-2kL)}}$$

and R_b is the reflection factor at the branch entrance and ϕ is the phase angle at the end cap. If there is no energy dissipation in the branch, $R_b = R$, the reflection factor of the end cap.

For $M_3 = 0$:

$$\begin{Bmatrix} p_1 \\ u_1 S_1 \end{Bmatrix} = \begin{bmatrix} 1 & 0 \\ -\frac{S_2}{\rho c Z_b} & 1 \end{bmatrix} \begin{Bmatrix} p_3 \\ u_3 S_3 \end{Bmatrix}$$

FIG. 51: EXTENDED INLET (AREA EXPANSION WITH BRANCH)

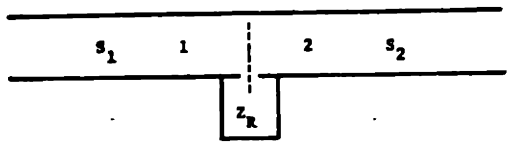

$$\begin{Bmatrix} p_1 \\ \rho c u_1 \end{Bmatrix} = \begin{bmatrix} 1 & 0 \\ -\frac{1}{Z_r} & \frac{S_2}{S_1} \end{bmatrix} \begin{Bmatrix} p_2 \\ \rho c u_2 \end{Bmatrix}$$

a) Single Helmholtz resonator or resonator array treated as a lumped impedance.

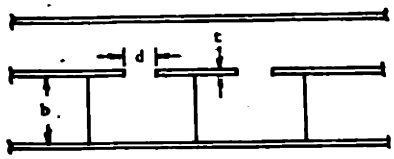

$Z_r = \rho c(\theta + i\chi)$ where $\theta = k\sqrt{\frac{\delta\nu}{\omega}}\left(1+\frac{t}{d}\right)$

$\chi = k(t+\delta) - \sigma\cot(kb)$, $k = \omega/c$

and ν is the kinematic viscosity of the gas, σ is the open area ratio of the resonator array and δ is the orifice end correction (see Ingard [29]).

b) Concentric tube resonator with single row of holes.

$$Z_r = \frac{1}{\frac{1}{Z_{r_1}} + \frac{1}{Z_{r_2}}} + i\omega\frac{t'}{S} + \frac{ck_r^2}{2\pi}$$ where $Z_{r_1} = -iY_{r_1}\cot(k_r\ell_{r_1})$

$Z_{r_2} = -iY_{r_2}\cot(k_r\ell_{r_2})$

$k_r = \omega/c_r$

and c_r is the wave propagation velocity in the resonator, Y_r is the admittance of the resonator walls, S is the total area of all the holes in the row and t' is the "effective" thickness of the holed tube (see Munjal et al.[31]).

FIG. 52: HOLE-CAVITY RESONATOR (LUMPED IMPEDANCE ASSUMPTION)

HOLE-CAVITY RESONATOR
(Parallel Coupled Ducts)

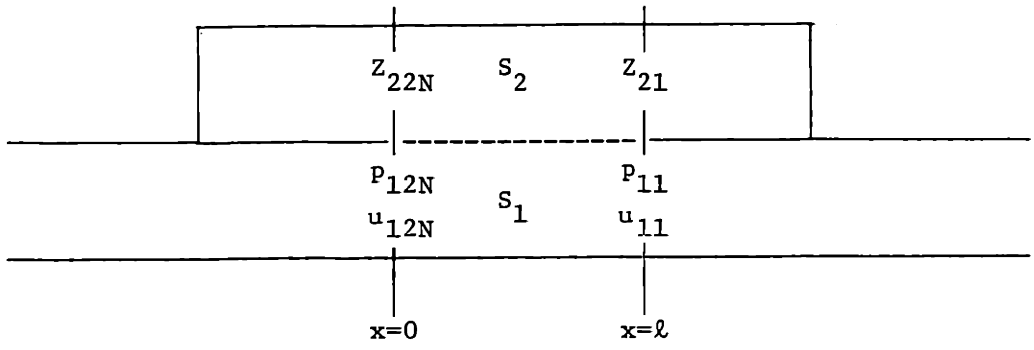

$$\begin{Bmatrix} p_{12N} \\ u_{12N} \end{Bmatrix} = \begin{bmatrix} T'_{11} & T'_{12} \\ T'_{21} & T'_{22} \end{bmatrix} \begin{Bmatrix} p_{11} \\ u_{11} \end{Bmatrix}$$

where $T'_{11} = T_{11} + \frac{AB}{E}$ and $A = T_{14} + Z_{21}T_{13}$

$T'_{12} = T_{12} + \frac{AC}{E}$ $B = T_{31} - Z_{22N}T_{41}$

$T'_{21} = T_{21} + \frac{DB}{E}$ $C = T_{32} - Z_{22N}T_{42}$

$T'_{22} = T_{22} + \frac{DC}{E}$ $D = T_{24} + Z_{21}T_{23}$

$E = (T_{44} + T_{43}Z_{21})Z_{22N} - (T_{34} + T_{33}Z_{21})$

The elements of the 4×4 matrix $[T_{ij}]$ are determined by

$$[T_{ij}] = \prod_{K=1}^{2N-1} [E]_K$$

where

$$[E]_K = \begin{bmatrix} 1 & 0 & 0 & 0 \\ A_K & 1 & -A_K & 0 \\ 0 & 0 & 1 & 0 \\ -A_K & 0 & A_K & 1 \end{bmatrix} \begin{bmatrix} \cos k_1\ell_K & i\frac{\rho c}{S_1}\sin k_1\ell_K & 0 & 0 \\ i\frac{S_1}{\rho c}\sin k_1\ell_K & \cos k_1\ell_K & 0 & 0 \\ 0 & 0 & \cos k_2\ell_K & i\frac{\rho c}{S_2}\sin k_2\ell_K \\ 0 & 0 & i\frac{S_2}{\rho c}\sin k_2\ell_K & \cos k_2\ell_K \end{bmatrix}$$

where ℓ_K is the axial distance between stations and A_K is the wall acoustic admittance at station K.

FIG. 53

ONE-DIMENSIONAL BARRIER

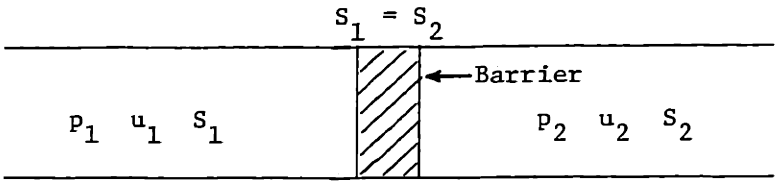

$$\begin{Bmatrix} p_1 \\ \rho c u_1 \end{Bmatrix} = \begin{bmatrix} 1 & \zeta_B \\ 0 & 1 \end{bmatrix} \begin{Bmatrix} p_2 \\ \rho c u_2 \end{Bmatrix}$$

where ζ_B is the specific acoustic impedance of the barrier

Flexible Membrane: $\zeta_B = - i\omega m$ m = Mass per unit area

Flexible Screen: $\zeta_B = \dfrac{\theta \zeta_s}{1+\zeta_s}$

where $\zeta_s = - i\omega m \left[1 - \left(\dfrac{\omega_0}{\omega}\right)^2\right]$, $\omega_0^2 = \dfrac{K}{m}$

Rigid Screen: $\zeta_B = \theta$

Rigid Screen with Inductance: $\zeta_B = \dfrac{1}{\sigma} \left[\theta - i \dfrac{\omega}{c} d(1-\sigma)\right]$
(Perforated Liner)

m = mass per unit area

θ = flow resistance

K = equivalent spring constant per unit area of screen

σ = fractional open area of screen

d = diameter of perforations

FIG. 54

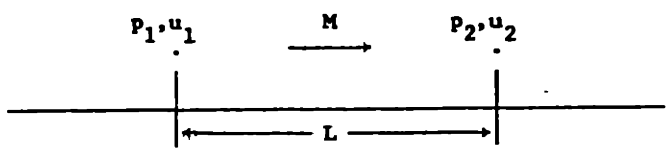

$$\begin{Bmatrix} p_1 \\ \rho c u_1 \end{Bmatrix} = \begin{bmatrix} T_{11} & T_{12} \\ T_{21} & T_{22} \end{bmatrix} \begin{Bmatrix} p_2 \\ \rho c u_2 \end{Bmatrix}$$

where

$$T_{11} = \frac{k_+ e^{ik_-L} - k e^{ik_+L}}{k_+ - k_-} + M \frac{k_+ k_-}{k(k_+ - k_-)} \left(e^{ik_+L} - e^{ik_-L}\right)$$

$$T_{12} = \rho c \frac{k^2 - Mk(k_+ + k_-) + M^2 k_+ k_-}{k(k_+ - k_-)} \left(e^{ik_+L} - e^{ik_-L}\right)$$

$$T_{21} = -\frac{1}{\rho c} \frac{k_+ k_-}{k(k_+ - k_-)} \left(e^{ik_+L} - e^{ik_-L}\right)$$

$$T_{22} = \frac{k_+ e^{ik_+L} - k_- e^{ik_-L}}{k_+ - k_-} - M \frac{k_+ k_-}{k(k_+ - k_-)} \left(e^{ik_+L} - e^{ik_-L}\right)$$

$$k_+ = \frac{1}{1+M} \left[k + i(\beta_v + \beta_t)\right] \qquad k_- = -\frac{1}{1-M} \left[k + i(\beta_v + \beta_t)\right]$$

$\beta_t = 0.0244 \dfrac{M}{a \mathrm{Re}_a^{1/4}}$, Turbulence Attenuation Coefficient

$\beta_v = \dfrac{k}{4a} \left[\delta_V + (\gamma - 1)\delta_K\right]$, Visco-Thermal Loss Coefficient

$\delta_V = \left(\dfrac{\nu}{\pi f}\right)^{1/2}$, Viscous Acoustic Boundary Layer Thickness

$\delta_K = \left(\dfrac{\kappa}{\pi c_p f}\right)^{1/2}$, Thermal Acoustic Boundary Layer Thickness

a = Hydraulic Radius = Duct Perimeter/Duct Cross-Sectional Area

FIG. 55: VISCO-THERMAL AND SOUND-TURBULENCE INTERACTION LOSSES IN A CONSTANT AREA DUCT WITH FLOW

RADIATION IMPEDANCE

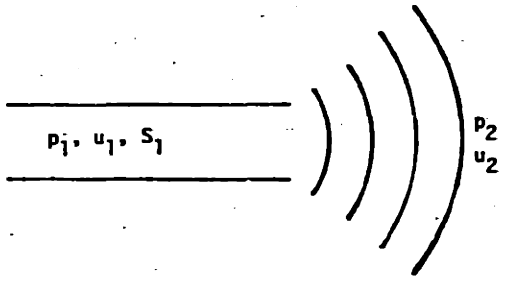

$$\begin{Bmatrix} p_1 \\ \rho c u_1 \end{Bmatrix} = \begin{bmatrix} 1 & \zeta_R \\ 0 & 1 \end{bmatrix} \begin{Bmatrix} p_2 \\ \rho c u_2 \end{Bmatrix}$$

For an unflanged circular duct with radius a

$$\zeta_R = \theta_r - i\chi_r$$

where

$$\chi_r = k\delta$$

and at low frequencies

$$\theta_r = \frac{1}{4}(ka)^2$$

where δ, a frequency dependent end correction determined by Levine and Schwinger, is plotted below. The pressure reflection coefficient determined using the low frequency approximation for θ_r compares quite favorably with Levine and Schwinger's results for ka < 2.

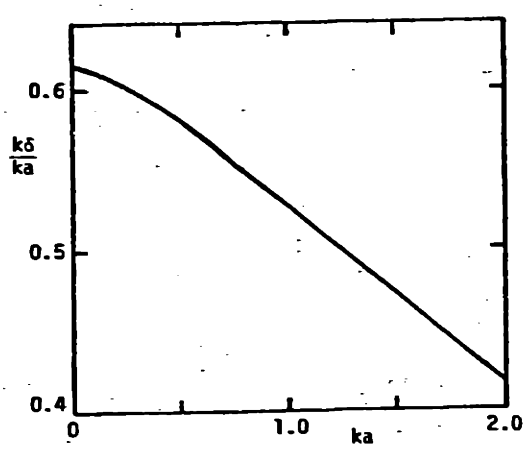

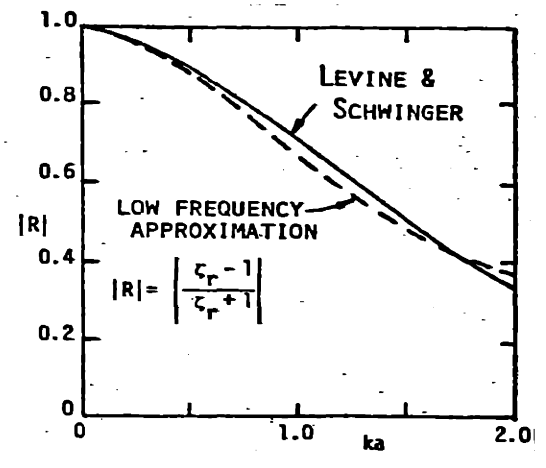

FIG. 56

4.5 Example Problems

In this section four example problems are presented to illustrate the ease with which transmission matrices can be used to solve typical problems which may be encountered in the field of duct acoustics. The transmission matrix solution technique is used to determine the transmission loss of a simple expansion chamber and a series-parallel lined duct combination. The acoustical characteristics (impedance, reflection, and absorption) of a multi-screen acoustic liner are determined using both the point- and distributed-reaction assumptions. In the final example, a matrix solution for the sound power radiated from the exhaust ducting of a stationary reciprocating engine is formulated to indicate how a complete acoustic system including source, transmission and radiation can be modeled using transmission matrices.

4.5.1 Example Problem No. 1: Transmission Loss of a Simple Expansion Chamber Muffler

Consider a simple expansion chamber of length L and cross-sectional area S_2 having inlet and outlet ducts with cross-sectional areas S_1 and S_3 respectively, as shown in Fig. 66. The acoustic pressure and volume velocity at stations 2A and 2B at either end of the expansion chamber can be related by the forward transmission matrix:

$$\begin{Bmatrix} p_{2A} \\ u_{2A}S_{2A} \end{Bmatrix} = [T'] \begin{Bmatrix} p_{2B} \\ u_{2B}S_{2B} \end{Bmatrix} \tag{4.116}$$

where

$$T'_{11} = T'_{22} = \cos kL \tag{4.116a,b}$$

$$T'_{12} = i \frac{\rho c}{S_2} \sin kL \tag{4.116c}$$

$$T'_{21} = i \frac{S_2}{\rho c} \sin kL \tag{4.116d}$$

Across the interfaces of the area discontinuities the acoustic pressure and volume velocity are unchanged. Thus Eq. (4.116) can be written as

$$\begin{Bmatrix} p_1 \\ u_1 S_1 \end{Bmatrix} = [T'] \begin{Bmatrix} p_3 \\ u_3 S_3 \end{Bmatrix} \tag{4.117}$$

With reference to Eq. (4.38) the transmission loss in dB can then be obtained directly from the elements of the transmission matrix

$$TL = 20 \log \left| \frac{p_i}{p_3} \right| = 20 \log \frac{1}{2} \left| T'_{11} + \frac{S_3}{\rho c} T'_{12} + \frac{\rho c}{S_1} T'_{21} + \frac{S_3}{S_1} T'_{22} \right| \text{ dB} \tag{4.118}$$

Evaluating Eq. (4.118) using Eqs. (4.116a-d) yields

$$TL = 10 \log \left| \left(\frac{m_2 + m_1}{2m_2} \right)^2 + \left(\frac{1}{2m_2} \right)^2 (m_2^2 - 1)(m_1^2 - 1) \sin^2 kL \right| \text{ dB} \tag{4.119}$$

where $m_1 = S_2/S_1$ and $m_2 = S_2/S_3$. When $S_1 = S_3$, Eq. (4.119) reduces to

the well-known result [Eq. (12.4) in Ref.111)

$$TL = 10 \log \left| 1 + \frac{1}{4} \left(m - \frac{1}{m}\right)^2 \sin^2 kL \right| \text{ dB} \qquad (4.120)$$

where $m = m_1 = m_2$.

4.5.2 Example Problem No. 2: Transmission Loss of a Series-Parallel Lined Duct Combination

The transmission loss of the series-parallel lined duct configuration shown in Fig. 67 can be determined directly using results obtained in Sections 4.3 and 4.4. First, the forward transmission matrix, T_{BC}, for parallel ducts B and C is obtained from Eq. (4.69) with i = 2,

$$T_{BC} = \begin{bmatrix} \frac{X_1}{Y} & \frac{1}{Y} \\ \frac{X_1 X_2}{Y} - Y & \frac{X_2}{Y} \end{bmatrix} \qquad (4.69)$$

where

$$X_1 = \frac{\beta_B T_{B11}}{T_{B12}} + \frac{\beta_C T_{C11}}{T_{C12}} \qquad (4.121a)$$

$$X_2 = \frac{\beta_B T_{B22}}{T_{B12}} + \frac{\beta_C T_{C22}}{T_{C12}} \qquad (4.121b)$$

$$Y = \frac{\beta_B}{T_{B12}} + \frac{\beta_C}{T_{C12}} \qquad \beta_i = \frac{S_i}{S} \qquad (4.121c,d)$$

Then the overall forward transmission matrix, T, is obtained by premultiplying the forward transmission matrix of the parallel array, T_{BC}, by T_A, its counterpart for duct section A.

$$T = T_A T_{BC}$$

$$= \begin{bmatrix} \frac{T_{11}X_1}{Y} + T_{12}\left(\frac{X_1X_2}{Y} - Y\right) & \frac{T_{11}}{Y} + \frac{T_{12}X_2}{Y} \\ \frac{T_{21}X_1}{Y} + T_{22}\left(\frac{X_1X_2}{Y} - Y\right) & \frac{T_{21}}{Y} + \frac{T_{22}X_2}{Y} \end{bmatrix} \qquad (4.122)$$

where $[T_A] = [T_{ij}]$. For the parallel lined ducts A and B, $T_{A11} = T_{A22}$ and $T_{B11} = T_{B22}$ permitting the simplification $X_1 = X_2 = X$. The transmission loss for the series-parallel duct combination is then determined from a summation of the elements of the overall forward transmission matrix, T, using Eq. (4.35).

$$TL = 20 \log \frac{1}{2}\left|\frac{X}{Y}(T_{11} + T_{12} + T_{21} + T_{22}) + \frac{1}{Y}(T_{11} + T_{21}) + \left(\frac{X^2}{Y} - Y\right)(T_{22} + T_{12})\right| \qquad (4.123)$$

4.5.3 Example Problem No. 3: Determination of Attenuation Characteristics of Multi-Screen Acoustic Liners

Broadband attenuation in duct systems is obtained in most applications with the use of porous sheet or bulk lining materials such as acoustical foam, fiberglass or mineral wool. However, such porous sheet materials have the following undesirable characteristics:

1. Urethane foam crumbles with age.
2. Fiberglass liners change impedance with age due to matting.
3. Gas flows erode bulk and non-metallic porous sheet liners.

4. Urethane foams are flammable and are sometimes banned by fire codes.
5. Liners made of porous materials are difficult to clean of accumulated oil and dirt.

Additionally, most porous sheet and bulk lining materials cannot withstand high temperature environments. Therefore it is desirable to develop liner configurations using more durable materials for broadband attenuation. Liners consisting of multiple layers of screens, perforated plates or sintered metal sheets separated by appropriately sized air spaces can be configured to produce broadband attenuation. Such liners also have the extra advantage that their acoustic impedance can be varied as desired by inducing airflow through the liner.

In the following sections, the specific acoustic impedance and the absorption and reflection coefficients are determined for a double-screen acoustic liner using both point-reaction and distributed-reaction assumptions. Then a computer program is used to evaluate the acoustical characteristics of several multi-screen liner configurations.

4.5.3.1 Double-Screen Liner with Local (Point) Reaction

A cross-sectional view of a double-screen point-reacting acoustic liner is shown in Fig. 68. Screen 1, having specific acoustic resistance r_1 is located a distance ℓ_1 from the hard wall. Screen 2, having specific acoustic resistance r_2, is located a distance ℓ_2 away from screen 1. Rigid partitions normal to the wall make the liner locally reacting by preventing sound waves from propagating parallel to the rigid wall within the liner.

For a sound wave normally incident upon the liner the acoustic pressure and particle velocity at the face of the liner (p_1,u_1) can be related to the acoustic pressure and particle velocity at the wall (p_5,u_5) by using the transmission matrix, T, as follows:

$$\begin{Bmatrix} p_1 \\ \rho c u_1 \end{Bmatrix} = T \begin{Bmatrix} p_5 \\ \rho c u_5 \end{Bmatrix} \tag{4.124}$$

where $T = T_{1-2}\ T_{2-3}\ T_{3-4}\ T_{4-5}$ (4.125)

and

$$T_{1-2} = \begin{bmatrix} 1 & \zeta_{s2} \\ 0 & 1 \end{bmatrix} \tag{4.126a}$$

$$T_{2-3} = \begin{bmatrix} \cos k\ell_2 & -i \sin k\ell_2 \\ -i \sin k\ell_2 & \cos k\ell_2 \end{bmatrix} \tag{4.126b}$$

$$T_{3-4} = \begin{bmatrix} 1 & \zeta_{s1} \\ 0 & 1 \end{bmatrix} \tag{4.126c}$$

$$T_{4-5} = \begin{bmatrix} \cos k\ell_1 & -i \sin k\ell_1 \\ -i \sin k\ell_1 & \cos k\ell_1 \end{bmatrix} \tag{4.126d}$$

where $\zeta_{s1} = r_1/\rho c$ and $\zeta_{s2} = r_2/\rho c$ for screens 1 and 2 respectively. To increase the effective flow resistance of the liner, perforated plate facing sheets can be added to the screens, Fig. 69, thereby increasing

the acoustic particle velocity past the screen. The specific acoustic impedance for such a composite plate-screen layer has been modeled by Ingard[75] as

$$\zeta_s = \frac{1}{\sigma}\left[\frac{r}{\rho c} - 0.85\, i\, kd_h(1-\sigma)\right] \tag{4.127}$$

where σ and d_h are the open area ratio and the hole diameter of the perforated plate respectively.

The specific acoustic impedance at the face of the liner is given by

$$\zeta_1 = \frac{p_1}{\rho c u_1} \tag{4.128}$$

or, using the elements of the transmission matrix in Eq. (4.124)

$$\zeta_1 = \frac{T_{11}p_5 + T_{12}\rho c u_5}{T_{21}p_5 + T_{22}\rho c u_5} \tag{4.129}$$

But, at the wall, $u_5 = 0$. Therefore

$$\zeta_1 = \frac{T_{11}}{T_{21}} \tag{4.130}$$

After carrying out the indicated matrix multiplication in Eq. (4.125) and performing some algebraic manipulation the specific acoustic impedance can be written as

$$\zeta_1 = \theta_1 - i\chi_1 \tag{4.131}$$

where $\theta_1 = A/C$ and $\chi_1 = B/C$

$$A = \left\{1 + [1+\zeta_{s1}\zeta_{s2}]\tan^2 k\ell_2\right\}\zeta_{s1}\tan^2 k\ell_1 + \zeta_{s2}(\tan k\ell_1 + \tan k\ell_2)^2 \tag{4.132a}$$

$$B = \left\{[1-\zeta_{s1}^2]\tan^2 k\ell_1 - 1\right\}\tan k\ell_2 - (1-\tan^2 k\ell_2)\tan k\ell_1 \tag{4.132b}$$

$$C = \zeta_{s1}^2 \tan^2 k\ell_1 \tan^2 k\ell_2 + (\tan k\ell_1 + \tan k\ell_2)^2 \tag{4.132c}$$

The absorption coefficient, $\alpha_1(\phi)$, the fraction of the acoustic power incident at angle ϕ which is absorbed by the liner can be written as

$$\alpha_1(\phi) = 1 - |R_1(\phi)|^2 \tag{4.133}$$

where $R_1(\phi)$ is the pressure reflection coefficient which can be written as

$$R_1(\phi) = \frac{\zeta_1 \cos\phi - 1}{\zeta_1 \cos\phi + 1} \tag{4.134}$$

After substituting Eq. (4.128) into Eq. (4.134), $\alpha_1(\phi)$ becomes

$$\alpha_1(\phi) = \frac{4\theta\cos\phi}{(\theta\cos\phi+1)^2+(\chi\cos\phi)^2} \tag{4.135}$$

Note that Eq. (4.135) holds for point-reacting liners alone since the assumption was made in obtaining Eq. (4.131) that the specific acoustic impedance at the face of the liner was independent of the incidence angle, ϕ.

In a diffuse field the average absorption coefficient, $\bar{\alpha}_1$, is obtained by integrating $\alpha_1(\phi)$ over a hemisphere in the following manner:

$$\bar{\alpha}_1 = 2\int_0^{\frac{\pi}{2}} \alpha_1(\phi)\sin\phi\cos\phi\, d\phi \tag{4.136}$$

Using the expression for $\alpha_1(\phi)$ from Eq. (4.135), Eq. (4.136) can be integrated to yield

$$\bar{\alpha}_1 = \frac{8\theta}{(\theta^2+\chi^2)}\left\{1-\frac{\theta}{\theta^2+\chi^2}\ln[(\theta+1)^2+\chi^2]+\frac{\theta^2-\chi^2}{(\theta^2+\chi^2)\chi}\tan^{-1}\left(\frac{\chi}{\theta+1}\right)\right\} \tag{4.137}$$

Equation (4.137) is equivalent to Eq. (9.5.8) in Morse and Ingard's text (Ref. 26, p. 580) in which the average absorption coefficient is expressed in terms of the specific acoustic conductance and susceptance.

4.5.3.2 Double-Screen Liner with Extended (Distributed) Reaction

An unpartitioned double-screen acoustic liner, as shown in Fig. 68b, is a surface of extended reaction. The specific acoustic impedance at the surface of the liner is dependent upon the incidence angle of the sound wave. However, the effect of incidence angle can be accounted for by dividing the incident sound wave into components parallel and normal to the liner and by assuming that only the normal wave component is attenuated by the liner. The specific acoustic impedance at the face of the liner is then obtained directly from the expression for the specific acoustic impedance of a point-reacting liner by replacing k with $k\cos\phi$ in Eqs. (4.132a-c). Thus, for a surface of extended reaction

$$\zeta_1(\phi) = \theta_1(\phi) - i\chi_1(\phi) \tag{4.138}$$

where

$$\theta_1(\phi) = \frac{A(\phi)}{C(\phi)} \quad \text{and} \quad \chi_1(\phi) = \frac{B(\phi)}{C(\phi)}$$

and

$$A(\phi) = \left\{1 + [1+\zeta_{s1}\zeta_{s2}]\tan^2(k\ell_2 \cos\phi)\right\} \zeta_{s1}\tan^2(k\ell_1 \cos\phi) + \zeta_{s2}[\tan(k\ell_1\cos\phi) + \tan(k\ell_2\cos\phi)]^2 \tag{4.139a}$$

$$B(\phi) = \left\{[1 - \zeta_{s1}^2]\tan^2(k\ell_1\cos\phi) - 1\right\}\tan(k\ell_2\cos\phi) - [1 - \tan^2(k\ell_2\cos\phi)]\tan(k\ell_1\cos\phi) \tag{4.139b}$$

$$C(\phi) = \zeta_{s1}^2\tan^2(k\ell_1\cos\phi)\tan^2(k\ell_2\cos\phi) + [\tan(k\ell_1\cos\phi)+\tan(k\ell_2\cos\phi)]^2 \tag{4.139c}$$

4.5.3.3 Computed Absorption Coefficients for Multi-Screen Acoustic Liners

A computer program was written to calculate the acoustical characteristics of multi-screen liners by successively multiplying pairs of forward transmission matrices (for the screen and adjacent interspace) until the overall transmission matrix for the multi-screen liner was obtained. The complex acoustical impedance and the absorption and reflection coefficients were then calculated using the equations developed above for either point-reaction or distributed-reaction liners.

The computed absorption coefficients for double-screen acoustic liners of standard 4-inch thickness are shown in Fig. 70. The liners were assumed to have a composite perforated plate-resistive screen structure shown in Fig. 69. The open area ratio of the plates was assumed to be 10%. In Figs.70a and 70b the absorption spectra of single screen liners having specific acoustic resistance, r, of 0.1 and 0.2 are shown for reference. Note that at the anti-resonance points (1700 Hz and 3400 Hz) the single screen liners are poor absorbers of acoustic energy. In Figs.70c-f the effect of the position of the inner screen of a double-screen liner is shown. As the inner screen (r_1= 0.2) nears the outer screen (r_2= 0.1) the liner becomes an efficient absorber over a wide frequency range. For L1 = 3.33 in the absorption coefficient averages 85% in the range $500 \leq f \leq 4000$ Hz. The results are shown for two assumed hole sizes on the perforated plates, 1/8 in and 1/4 in dia. For the larger holes the liner is a more efficient absorber at the lower frequencies whereas the 1/8 in holes extend the flat absorption spectrum to higher frequencies.

In Fig. 71 the absorption spectrum for a triple screen composite liner is shown. The inner screen has a resistance of 0.2 whereas the two outer screens each have resistances of 0.1. Each plate has an open area ratio of 10%. The resulting absorption spectrum is extremely flat and exceeds 80 % over the frequency range $500 < f < 3440$ Hz. For the screen alone, without the attached perforated plate, the absorption coefficient averaged only 50% over the same frequency range. These

results show that multi-screen liners can be used to produce broadband attenuation without the drawbacks of porous liners mentioned above.

4.5.4 Sound Radiation from Exhaust Ducting of Reciprocating Engine

Large stationary reciprocating engines often radiate intense low frequency sound from their exhaust ducts. The sound which occurs at the piston frequency of 10-30 Hz is difficult to attenuate with conventional muffler systems but can be minimized by proper choice of the exhaust duct length. By chosing the duct length which causes an impedance mismatch between the source and the exhaust ducting at the piston frequency, the sound power radiated from the piston into the duct can be minimized. The time-averaged intensity of the sound wave produced by the piston, having constant velocity amplitude, is determined from the expression

$$p = Z \mid U_p \mid^2 A/2 \tag{4.140}$$

where Z is the impedance of the exhaust ducting (including radiation from the end of the duct), A is the cross-sectional area of the duct, and U_p is the velocity amplitude of the piston.

For an open-ended duct of length L the duct impedance can be shown to be

$$Z = i\rho c \cot(kL + \frac{\pi}{2} + \zeta_r) \tag{4.141}$$

where ζ_r is the radiation impedance at the open end of the duct. At low frequencies $\zeta_r \simeq 0$ and Z has a maximum value of $L = \lambda/4$ and a minimum value at $L = \lambda/2$. Thus the radiated sound power can be minimized by having an exhaust duct one-half wavelength long. However, at 20 Hz such

an exhaust duct would be 28 feet long and might not be an economical solution. To justify the additional cost incurred, the sound power reduction effected by the additional ducting must be estimated beforehand.

To obtain an accurate assessment of the dB reduction in sound power level effected by the additional ducting the real effects of visco-thermal losses and frequency dependent radiation impedance should be included in the analysis. By using transmission matrices to formulate the problem these real effects can be easily considered. The forward transmission matrix for the overall duct system can be obtained by multiplying together the forward transmission matrices for the source, the duct and the outlet.

$$T_S = T_S \; T_D \; T_R \tag{4.142}$$

$$T_S = \begin{bmatrix} 1 & \zeta_S \\ 0 & 1 \end{bmatrix} \tag{4.142a}$$

$$T_D = \begin{bmatrix} \cos kL & i\frac{k_o}{k} \sin kL \\ -i\frac{k}{k_o} \sin kL & \cos kL \end{bmatrix} \tag{4.142b}$$

$$T_R = \begin{bmatrix} 1 & \zeta_R \\ 0 & 1 \end{bmatrix} \tag{4.142c}$$

where ζ_S is the internal impedance of the source, ζ_R is the radiation impedance at the open end of the duct and k includes the effect of visco-thermal losses in the exhaust ducting. The overall transmission loss of the exhaust duct is obtained from Eq. (4.35)

$$TL = 20 \log \frac{1}{2} |T_{11} + T_{12} + T_{21} + T_{22}| dB$$

The effects of mean flow in the exhaust duct can be included in the analysis by replacing T_D with the transmission matrix given in Fig.41 of the Handbook of Transmission Matrices and by including the effects of mean flow in the radiation impedance, ζ_r.

a. Sudden Contraction

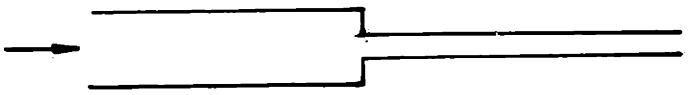

b. Sudden Expansion

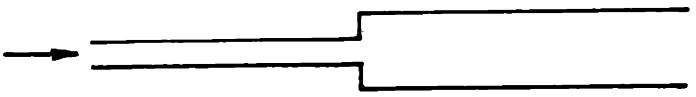

c. Extended Outlet

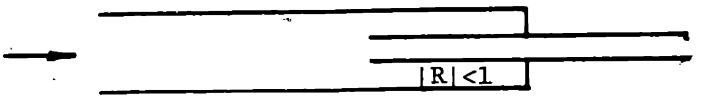

d. Extended Inlet

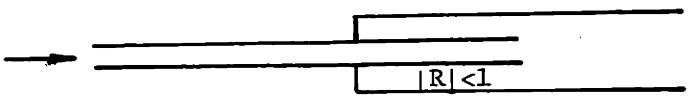

e. Side Branch Resonator

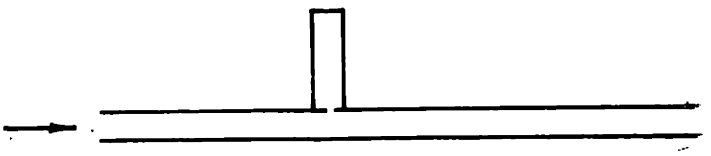

f. Hole-Cavity Resonator

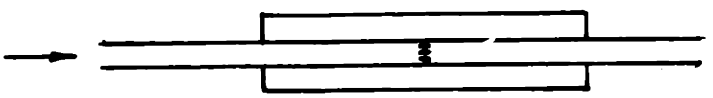

FIG. 57: EXHAUST SILENCER COMPONENTS

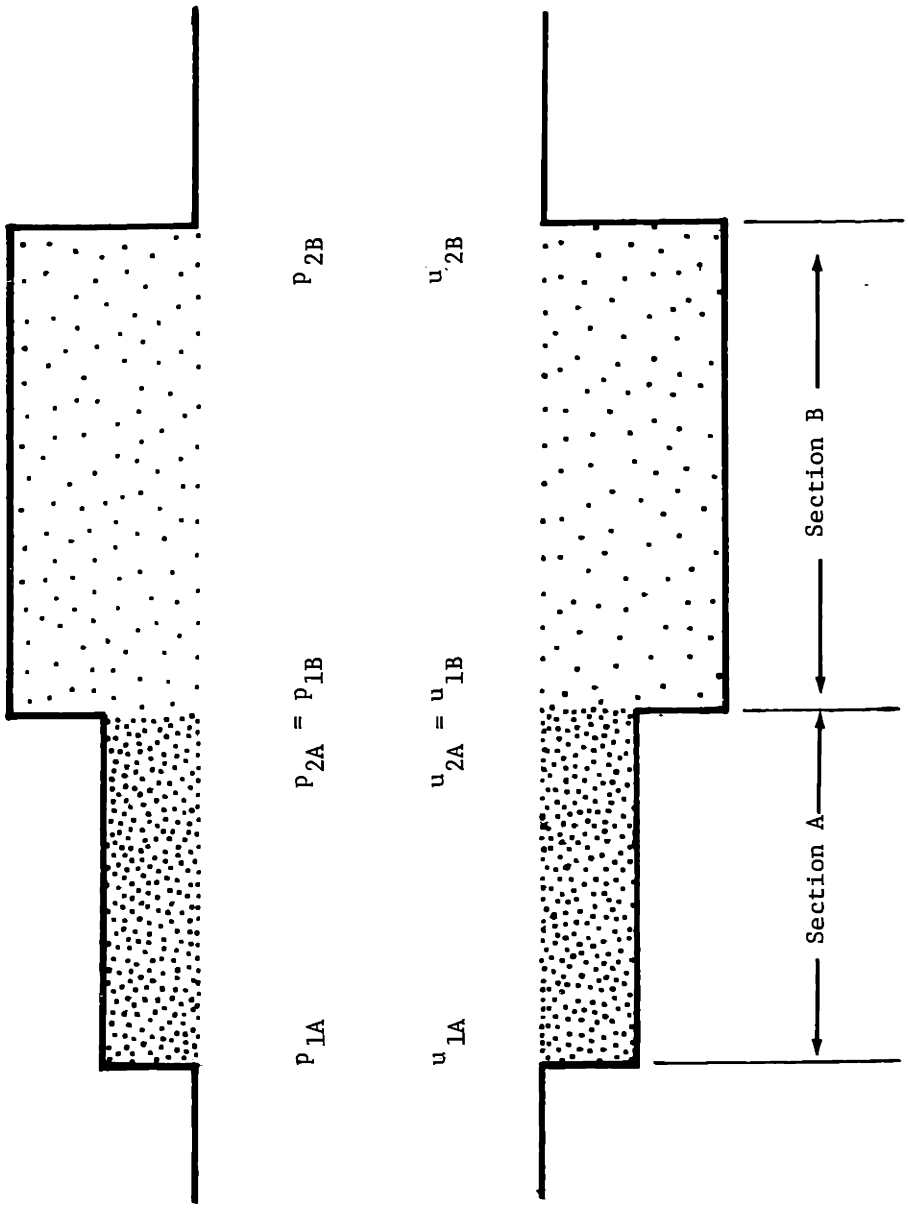

FIG. 58: LINED DUCT SECTIONS JOINED IN SERIES

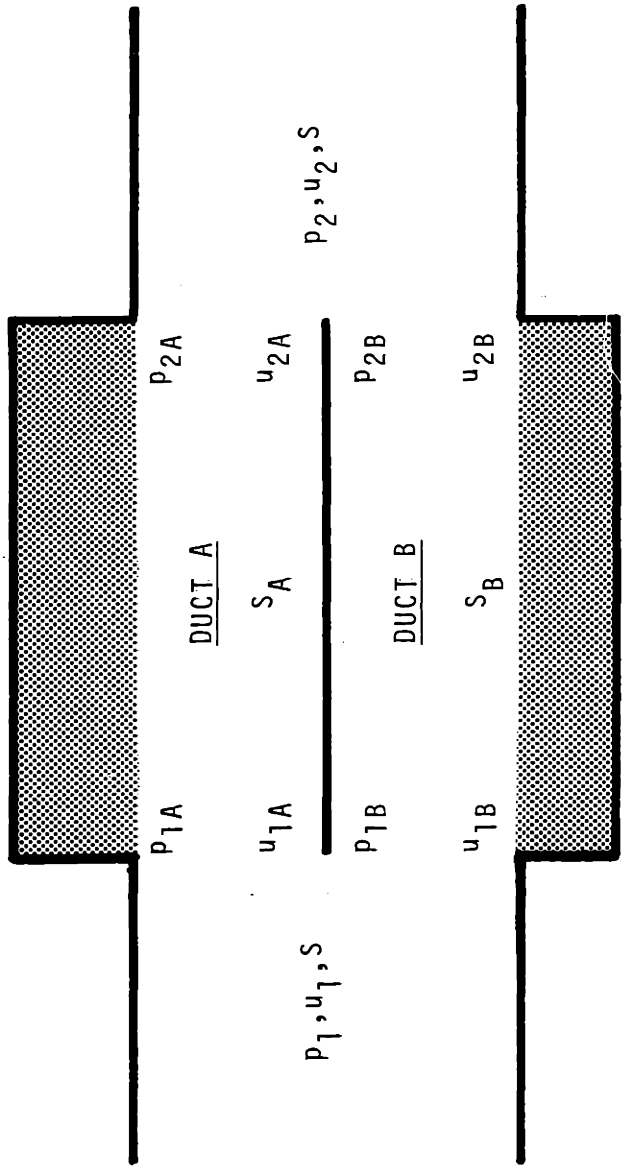

FIG. 59: PARALLEL LINED DUCTS

Arrows define positive directions.

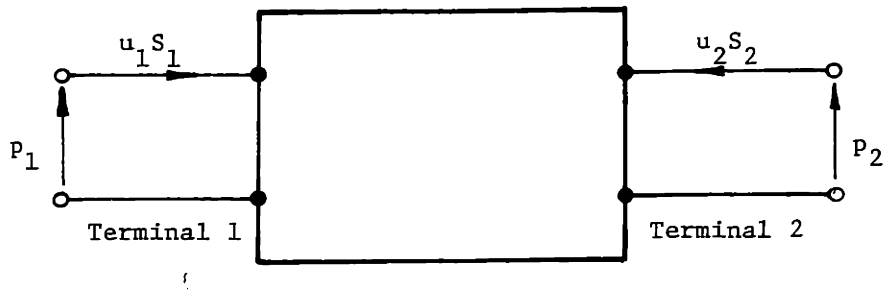

a) Sign convention which satisfies reciprocity.

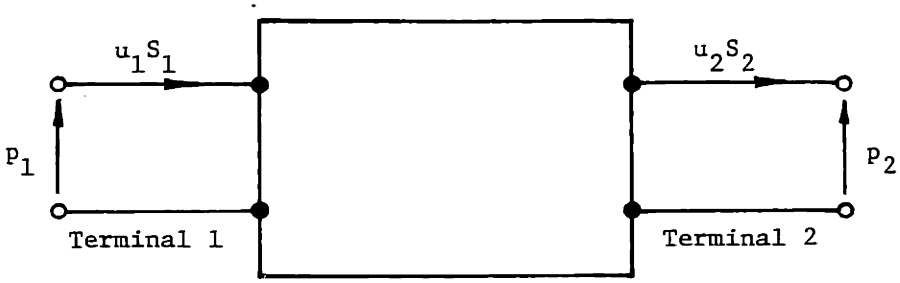

b) Sign convention used in this thesis.

FIG. 60: FOUR-POLE REPRESENTATIONS OF AN ACOUSTICAL SYSTEM

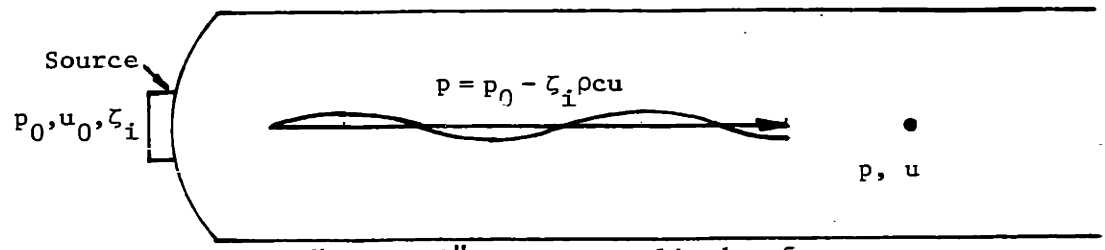

p_0 - "internal" pressure amplitude of source

u_0 - source velocity amplitude

ζ_0 - source internal impedance

a) Sound field produced by source in semi-infinite duct.

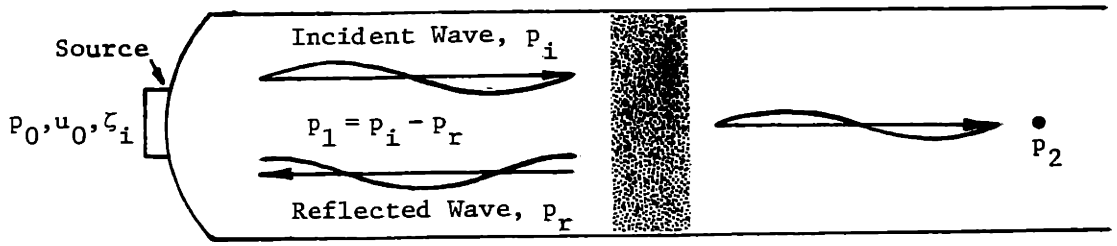

b) Sound field produced by source in semi-infinite duct containing a barrier.

Insertion Loss: $IL = 20 \log \left| \frac{p}{p_2} \right|$

Transmission Loss: $TL = 20 \log \left| \frac{p_i}{p_2} \right|$

FIG. 61 : INSERTION AND TRANSMISSION LOSS IN DUCT WITH BARRIER

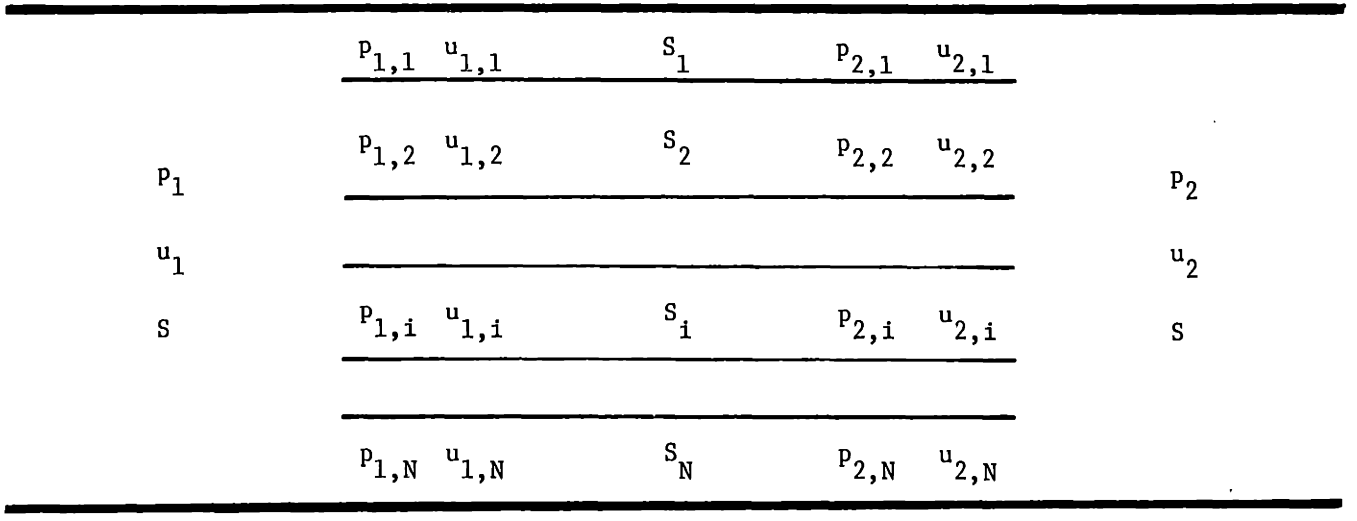

FIG. 62 : SOUND TRANSMISSION THROUGH N LINED DUCTS IN PARALLEL

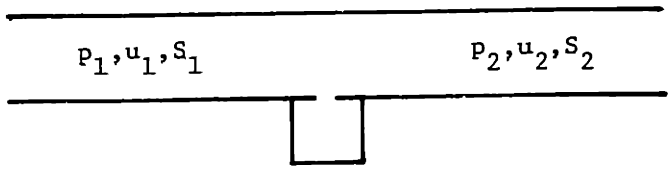

a) Single Helmholtz Resonator

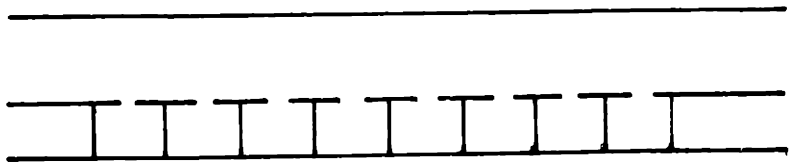

b) Helmholtz Resonator Array

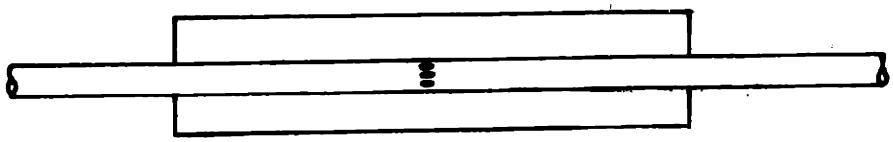

c) Concentric Tube Resonator with Single Row of Holes

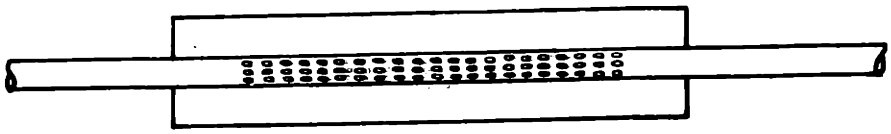

d) Concentric Tube Resonator with Multiple Rows of Holes

FIG. 63 : HOLE-CAVITY RESONATORS

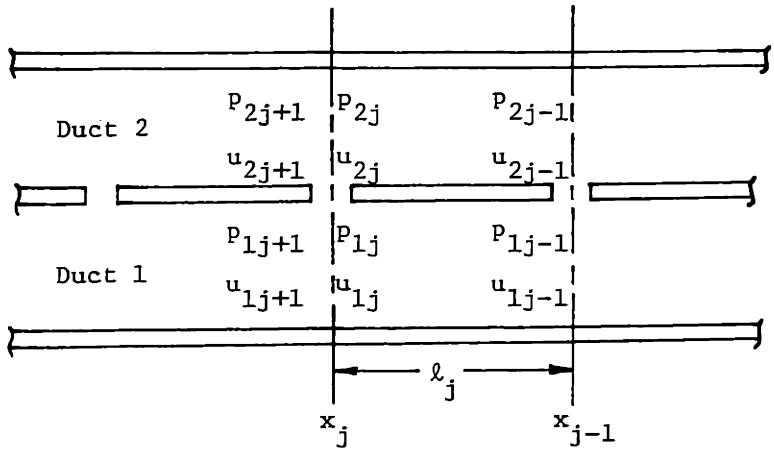

a) Discrete Element Approximation

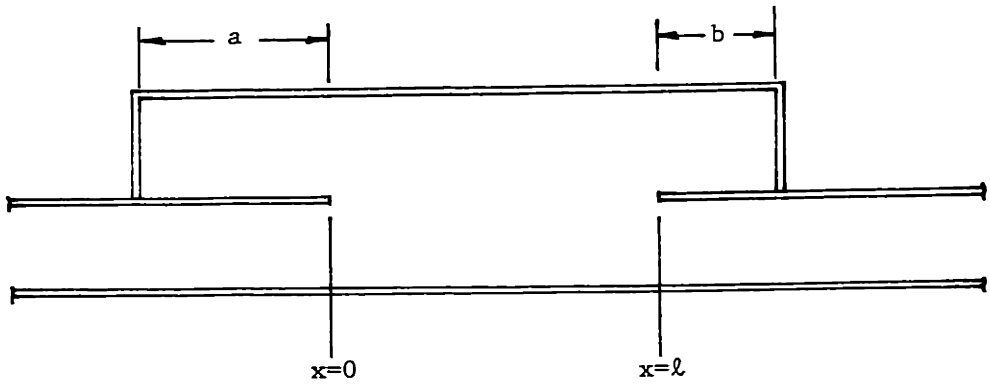

b) Closed Cavity Flow Duct

FIG. 64: CONFIGURATIONS USED BY SULLIVAN[79] IN PARALLEL-COUPLED DUCT ANALYSIS

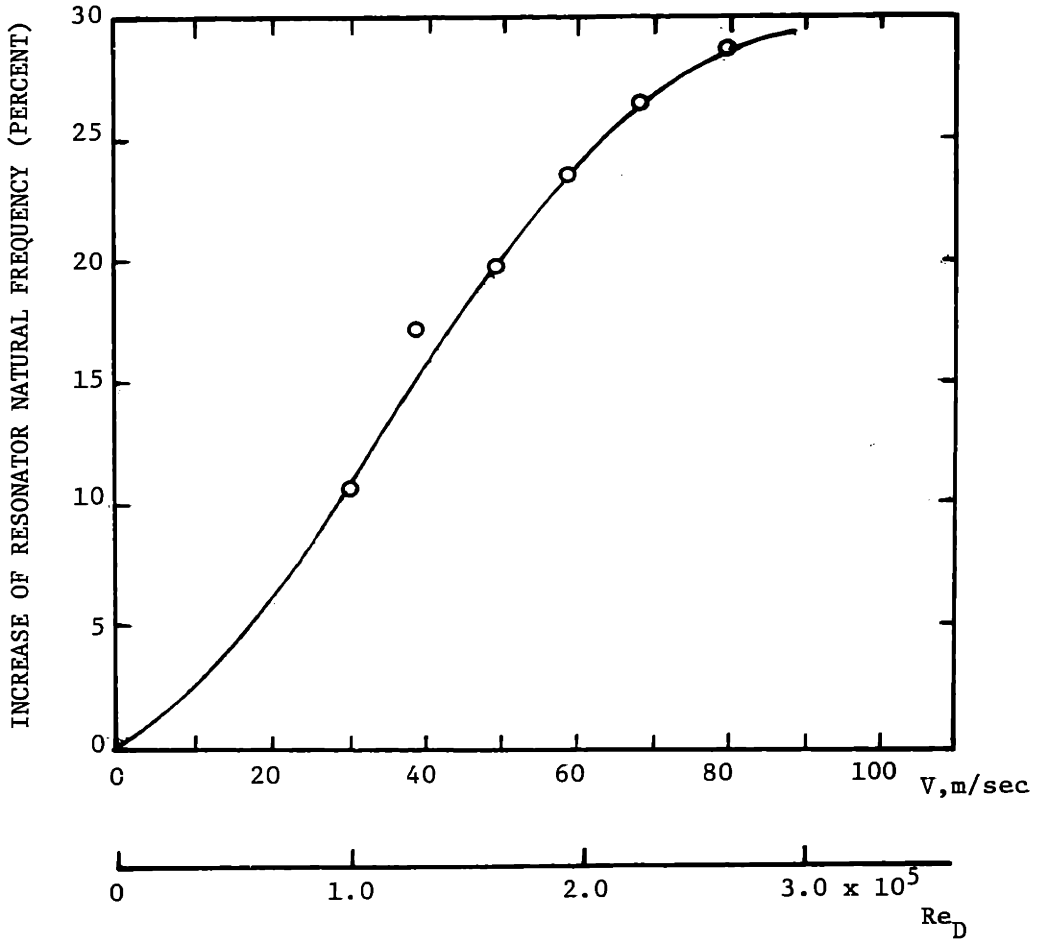

FIG. 65: EFFECT OF MEAN FLOW ON NATURAL FREQUENCY OF A HELMHOLTZ RESONATOR (ADAPTED FROM CHEN[59])

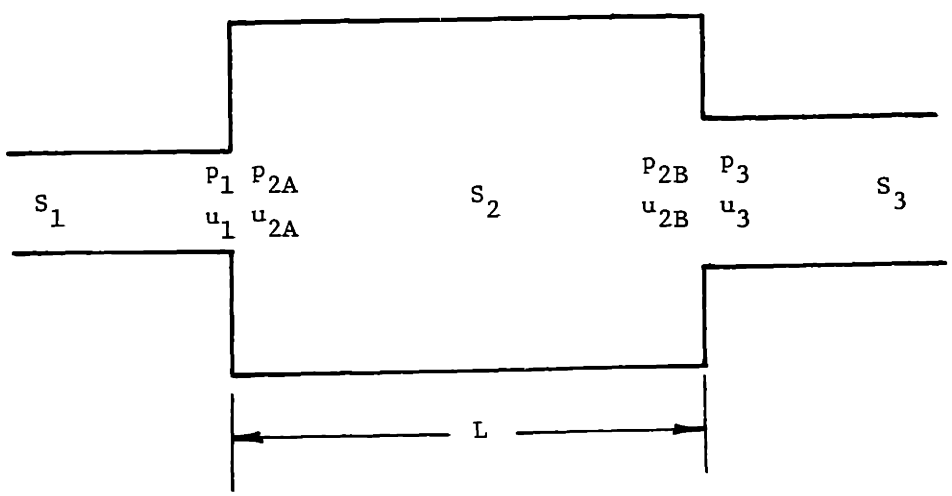

FIG. 66 : SIMPLE EXPANSION CHAMBER

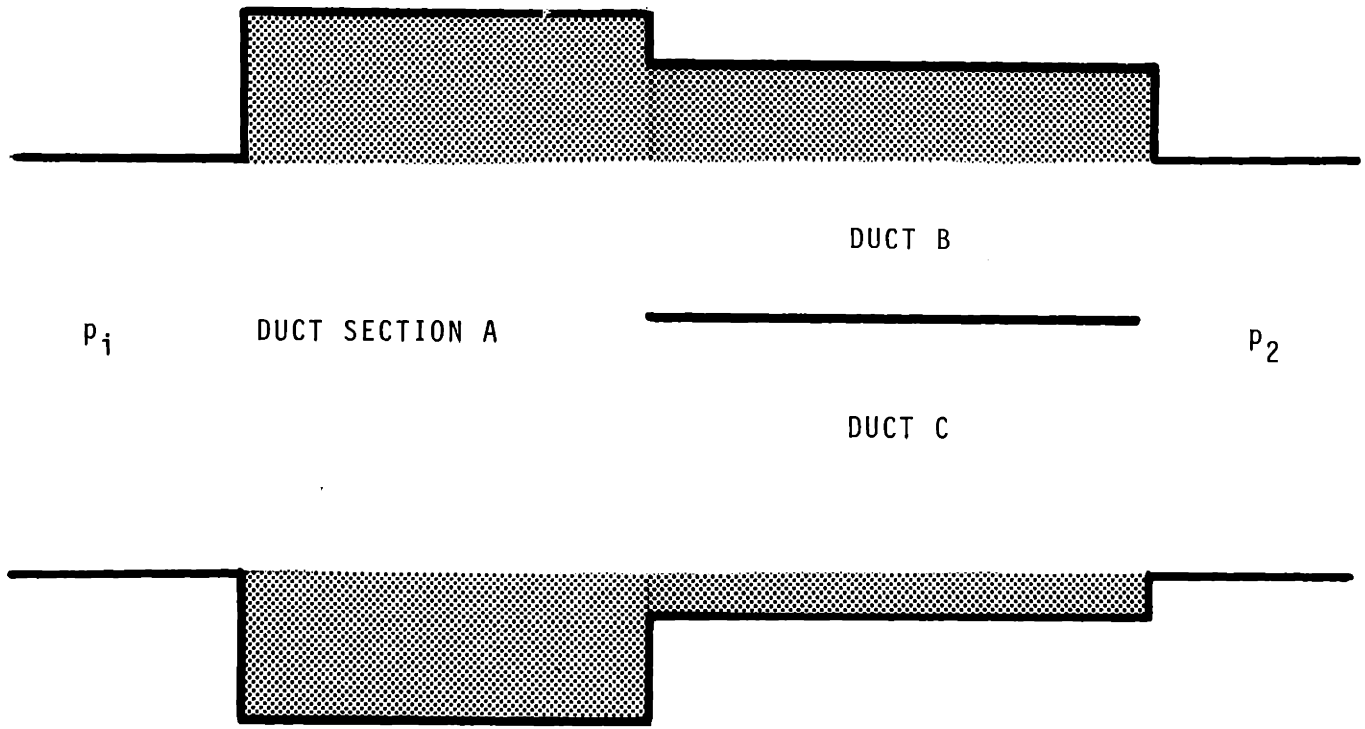

FIG. 67: SERIES-PARALLEL LINED DUCT COMBINATION

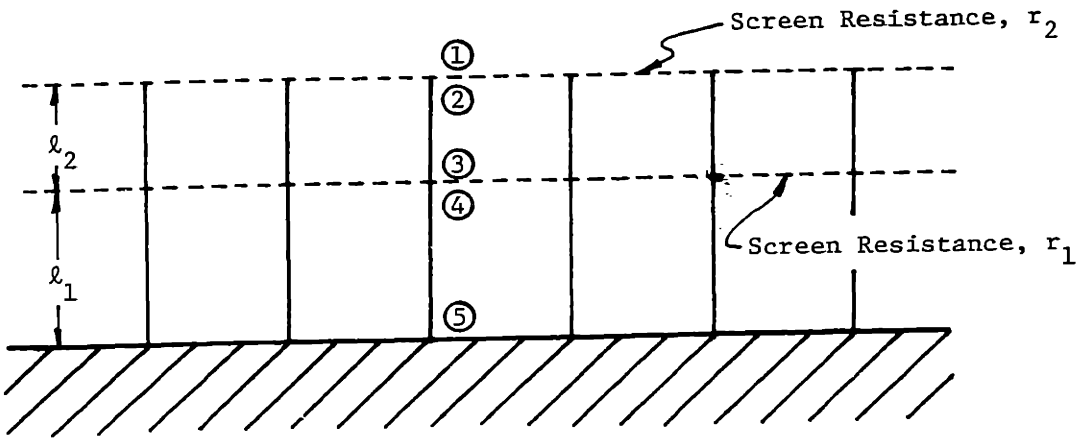

a) Point-Reacting Liner

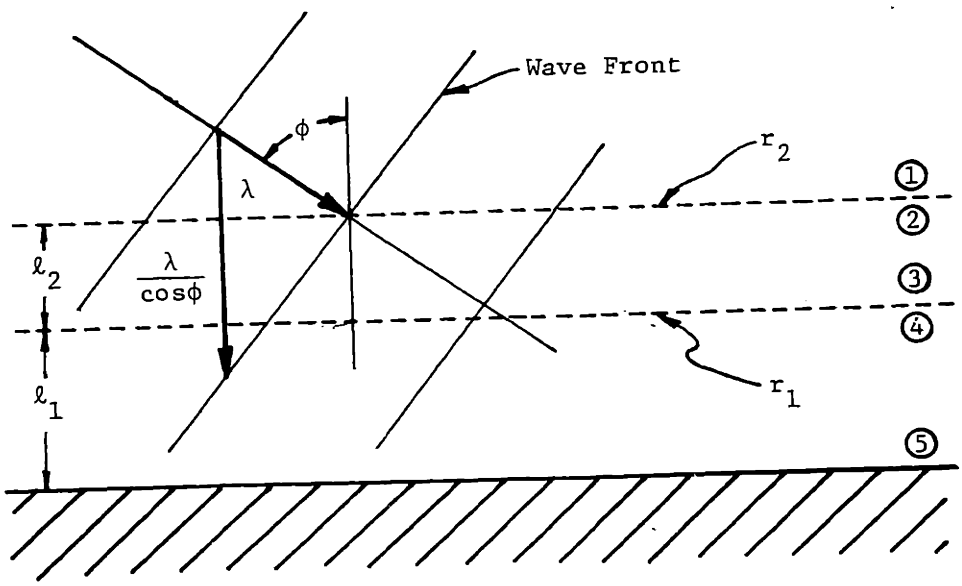

b) Liner with Distributed Reaction

FIG. 68: DOUBLE-SCREEN ACOUSTIC LINER CONFIGURATIONS

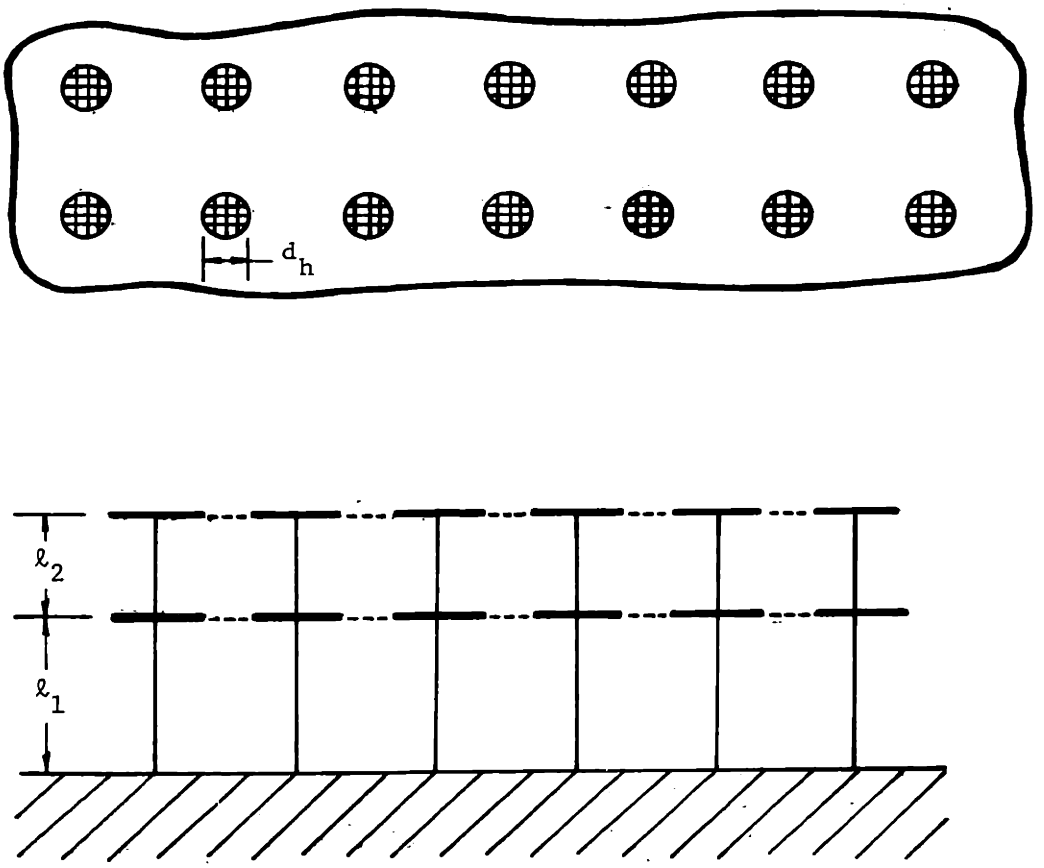

FIG. 69: COMPOSITE PERFORATED PLATE-RESISTIVE SCREEN DOUBLE LAYER ACOUSTICAL LINER

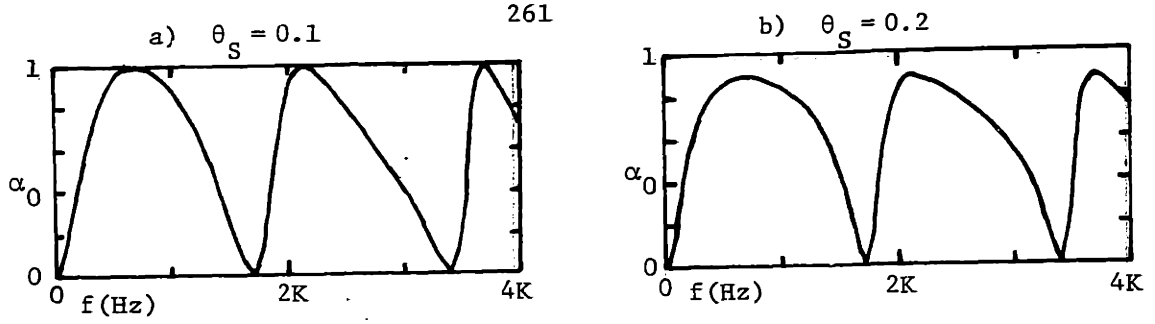

SINGLE SCREEN LINERS

(σ = 0.10)

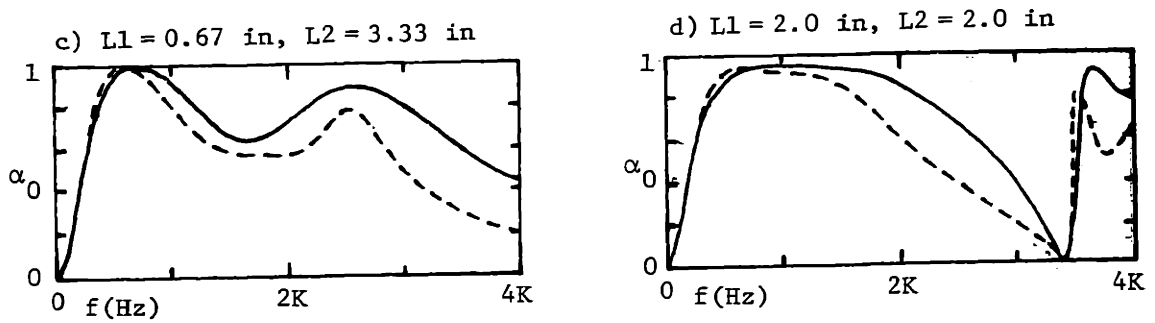

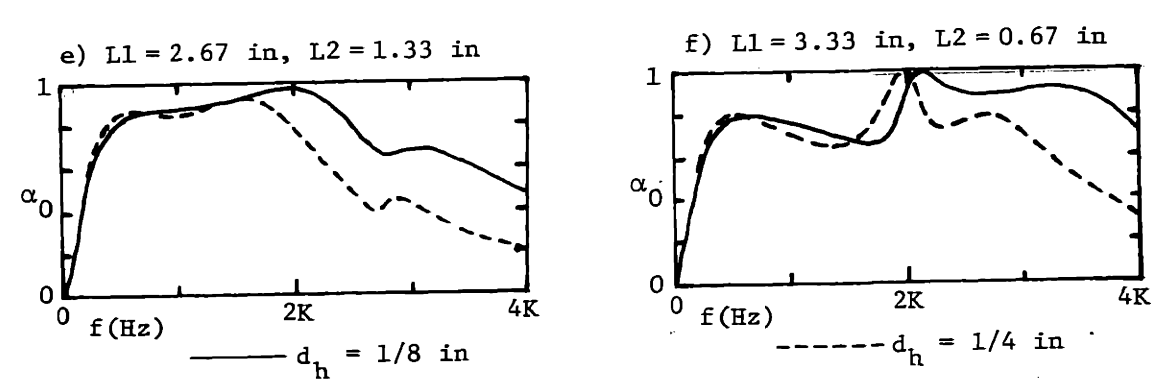

DOUBLE SCREEN LINERS

($\theta_1 = 0.2$, $\theta_2 = 0.1$, $\sigma_1 = \sigma_2 = 0.1$)

FIG. 70: ABSORPTION COEFFICIENT FOR 4 INCH THICK COMPOSITE PERFORATED PLATE-RESISTIVE SCREEN LINERS

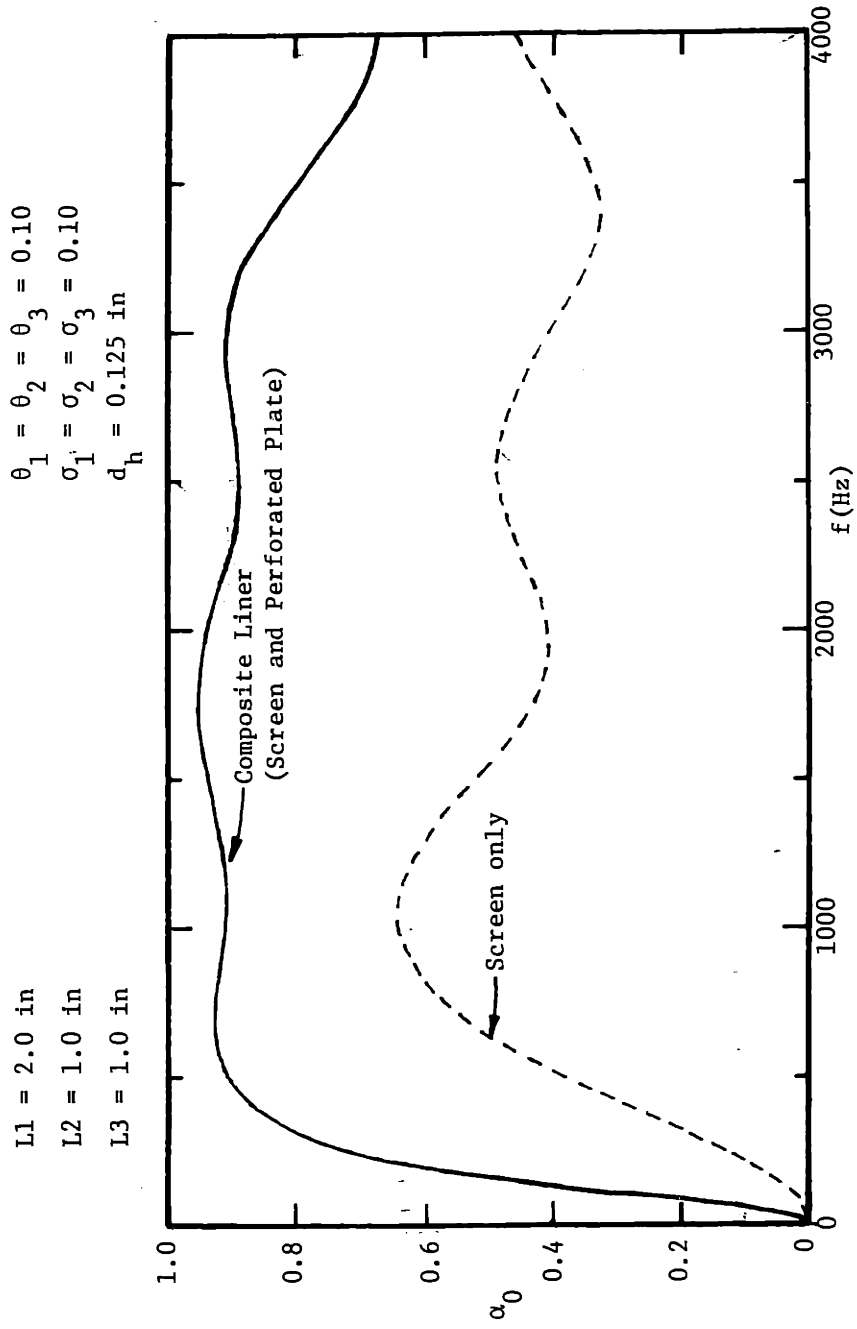

FIG. 71: ABSORPTION COEFFICIENT OF TRIPLE SCREEN LINER

CHAPTER V

CONCLUSIONS AND RECOMMENDATIONS FOR FURTHER WORK

5.1 Conclusions

A method to enhance the low frequency sound attenuation characteristics of a lined duct has been presented. A rigid, longitudinal splitter plate is used to separate the lined duct section into two parallel branch ducts. The phase speed of the fundamental mode in each branch duct is a function of the liner configuration and can differ substantially from the free space phase speed. By lining the parallel duct elements dissimilarly, destructive interference of the fundamental mode of the transmitted wave occurs downstream of the parallel absorbers. For frequencies below the duct cutoff frequency, higher order modes generated at the exit of the parallel absorbers do not propagate.

The sound field at the exit of either branch duct not only transmits a sound wave into the exit duct but also induces a negative-going wave to travel toward the entrance of the adjacent branch duct. At frequencies for which this round-trip path length approximates an integral number of wave lengths strong reflections occur at the entrance of the parallel duct assembly. These interference effects which result from placing the splitter plate into the lined duct can increase the low frequency transmission loss of the duct more than two fold over a broad frequency band and as much as 5 dB/unit duct width at selected frequencies.

The advantages of this new method of sound attenuation over previous methods are:

1. Thinner acoustic liners can be used to obtain a desired attenuation at low frequencies.

2. For ducts having mean flow the fluid dynamic pressure drop induced by the parallel duct will be less than a resonator system having equal acoustic attenuation.

3. The parallel duct configuration is tunable by either:

   a. Changing the length of the splitter plate.

   b. Moving the splitter plate laterally or axially in the duct.

4. Low frequency attenuation can be achieved in existing hard-wall ducts by inserting a lined splitter into the duct.

The unique features in this new method of low frequency sound attenuation are:

1. The use of a rigid splitter to divide the duct into adjacent parallel elements for purposes of increasing the sound attenuation.

2. The use of phase speed differences in the fundamental mode of dissimilarly lined ducts to cause reactive attenuation in a lined duct in addition to the attenuation due to the dissipative liner.

Commercial applications of parallel lined duct filters include the reduction of low frequency noise in:

1. Air delivery systems
2. Intake ducts
3. Ducts due to in-duct process equipment or machinery noise
4. Piston engine exhausts (gasoline or diesel)
5. Stationary gas turbine electric power plants
6. Inlet and exhaust silencers in aircraft engine test facilities.

5.2 Recommendations for Further Work

Although many aspects of sound transmission through lined ducts in parallel have been studied in this research effort, many more areas remain to be explored. First, a better understanding of the sound transmission characteristics of narrow lined ducts must be obtained both with and without mean flow. In particular, at a given sound frequency the effect of partition spacing, duct height and liner thickness on determining the degree of reaction of the liner surface (and hence the duct phase speed characteristics) needs to be determined. The "phase speed" (or more accurately, the speed of propagation of the surface of constant phase) in a lined duct having a length shorter than the wavelength should be investigated.

Work should be directed toward the design of acoustical liners to produce specified phase speed characteristics in ducts. Decoupling (if possible) the effects of the liner on the attenuation and the phase speed in a duct should be investigated. In particular, the development of liners producing comparable attenuation spectra but different phase speeds, which would be ideal for parallel lined ducts, should be attempted.

More tests of parallel duct configurations should be conducted. Of particular importance would be tests in which parallel ducts are arranged in series to provide broadband attenuation and tests involving three or more ducts in parallel. These tests should be conducted on models which are as large as practical to minimize the effects of visco-thermal attenuation encountered in model scale experiments. Also, continuous tone or broadband noise sources should be used so that the muffler performance can be measured in a "steady state" noise environment.

APPENDIX I

DETERMINATION OF COUPLING COEFFICIENTS FOR PARALLEL DUCTS

In Chapter 3 the equations relating acoustic pressure and particle velocity in the exit duct to the acoustic pressure and particle velocity in the branch ducts were derived as

$$u_2 = \frac{S_A}{S_2} u_{2A} + \frac{S_B}{S_2} u_{2B} \tag{A1.1}$$

$$p_{2A} = p_2 + \zeta_{AA} u_{2A} + \zeta_{AB} u_{2B} \tag{A1.2}$$

$$p_{2B} = p_2 + \zeta_{BA} u_{2A} + \zeta_{BB} u_{2B} \tag{A1.3}$$

where the coupling coefficients are defined as

$$\zeta_{AA} = \frac{1}{S_A} \sum_{m=1}^{\infty} (\int \psi_m dS_A)^2 (\frac{k}{k_{mx}}) \tag{A1.4a}$$

$$\zeta_{AB} = \frac{1}{S_A} \sum_{m=1}^{\infty} (\int \psi_m dS_A)(\int \psi_m dS_B)(\frac{k}{k_{mx}}) \tag{A1.4b}$$

$$\zeta_{BA} = \frac{1}{S_B} \sum_{m=1}^{\infty} (\int \psi_m dS_B)(\int \psi_m dS_A)(\frac{k}{k_{mx}}) \tag{A1.4c}$$

$$\zeta_{BB} = \frac{1}{S_B} \sum_{m=1}^{\infty} (\int \psi_m dS_B)^2 (\frac{k}{k_{mx}}) \tag{A1.4d}$$

In this Appendix coupling coefficients for rectangular and cylindrical ducts will be derived.

A1.1 Coupling Coefficients for Rectangular Ducts

In the exit duct of height d_2 the wave function can be expressed as

$$\psi_m = (\cos k_{my} y)/N \tag{A1.5}$$

when $k_{my} = m\pi/d_2$. To determine the normalization factor, N, set

$$\int_0^{S_2} \psi_m^2 \, dS_2 = 1$$

Evaluating the integral yields $N = \sqrt{S_2/2}$. Thus

$$\psi_m = \sqrt{\frac{2}{S_2}} \cos k_{my} y \tag{A1.6}$$

To determine the coupling coefficients first determine

$$\int \psi_m \, dS_A = \sqrt{\frac{2}{S_2}} \int_{d_B}^{d_2} \cos k_{my} y \, dy$$

$$= \frac{1}{k_{my}} \sqrt{\frac{2}{S_2}} (\sin k_{my} d_2 - \sin k_{my} d_B)$$

$$= - \sqrt{\frac{2}{S_2}} \frac{\sin k_{my} d_B}{k_{my}} \tag{A1.7a}$$

$$\int \psi_m \, dS_B = \sqrt{\frac{2}{S_2}} \int_0^{d_B} \cos k_{my} y \, dy$$

$$= \frac{1}{k_{my}} \sqrt{\frac{2}{S_2}} (\sin k_{my} d_B) \tag{A1.7b}$$

Note that

$$\sin k_{my} d_A = \sin\left[k_{my}(d_2 - d_B)\right]$$

$$= \sin k_{my} d_2 \cos k_{my} d_B - \cos k_{my} d_2 \sin k_{my} d_B$$

$$= (-1)^{m+1} \sin k_{my} \qquad \text{(A1.8)}$$

Also the axial wave number can be written as

$$k_{mx} = (k^2 - k_{my}^2)^{1/2}$$

which for low frequencies reduces to

$$k_{mx} \simeq i\, k_{my} \qquad \text{(A1.9)}$$

The coupling coefficients given in Eqs. (A1.4a-d) can be determined using Eqs. (A1.7a,b), (A1.8) and (A1.9)

$$\zeta_{AA} = -i \frac{2kd_A}{\pi} \sum_{m=1}^{\infty} \frac{1}{m} \left(\frac{\sin k_{my} d_A}{k_{my} d_A}\right)^2 \qquad \text{(A1.10a)}$$

$$\zeta_{AB} = i \frac{2kd_B}{\pi} \frac{d_B}{d_A} \sum_{m=1}^{\infty} \frac{1}{m} \left(\frac{\sin k_{my} d_B}{k_{my} d_B}\right)^2 \qquad \text{(A1.10b)}$$

$$\zeta_{BB} = -i \frac{2kd_B}{\pi} \sum_{m=1}^{\infty} \frac{1}{m} \left(\frac{\sin k_{my} d_B}{k_{my} d_B}\right)^2 \qquad \text{(A1.10c)}$$

From Eqs. (A1.4b) and (A1.4c) it can be seen that

$$\zeta_{BA} = \frac{d_A}{d_B} \zeta_{AB} \qquad \text{(A1.10d)}$$

A1.2 Coupling Coefficients for Cylindrical Ducts

In the exit duct of radius r_B the wave function can be expressed as

$$\psi_{emn} = \cos(m\phi)\ J_m\left(\frac{\pi\beta_{mn}r}{r_B}\right)/N \qquad \text{(A1.11a)}$$

$$\psi_{omn} = \sin(m\phi)\ J_m\left(\frac{\pi\beta_{mn}r}{r_B}\right)/N \qquad \text{(A1.11b)}$$

where N is the normalization factor. When spinning modes are absent, $m = 0$. Thus

$$\psi_{omn} = 0 \qquad \text{(A1.12a)}$$

$$\psi_{emn} = \psi_{e0n} = \psi_{0n} = J_0\left(\frac{\pi\beta_{0n}r}{r_B}\right)/N \qquad \text{(A1.12b)}$$

where

$$\beta_{0n} = \frac{2r_B}{c}\,\nu_{0n}$$

ν_{0n} = Characteristic frequency of the n^{th} radial mode in the exit duct

To determine the normalization factor, N, set

$$\int_0^{r_B}\int_0^{2\pi} \psi_{0n}^2\, r\, dr\, d\theta = 1 \qquad \text{(A1.13)}$$

Substituting Eq. (A1.12b) into Eq. (A1.13) and integrating from 0 to 2π yields

$$\frac{2\pi}{N^2}\int_0^{r_B} r\left[J_0\left(\frac{2\pi\nu_{0n}r}{c}\right)\right]^2 dr = 1 \qquad \text{(A1.14)}$$

Let

$$\gamma = \frac{2\pi\nu_{0n}}{c} r$$

Then Eq. (A1.14) can be written as

$$\frac{c^2}{2\pi N^2 \nu_{0n}^2} \int_0^{\frac{2\pi\nu_{0n}}{c} r_B} \gamma [J_0(\gamma)]^2 d\gamma = 1 \qquad \text{(A1.15)}$$

From Abramowitz and Stegun[112] [Eq. (11.3.34)]

$$\int_0^z t J_0^2(t) dt = \frac{z^2}{2} \left[J_0^2(z) + J_1^2(z) \right]$$

Thus, the normalization factor can be determined as

$$N = \sqrt{\pi}\, r_B \left[J_0^2(k_{0nr} r_B) + J_1^2(k_{0nr} r_B) \right]^{1/2} \qquad \text{(A1.16)}$$

where $k_{0nr} = \frac{2\pi\nu_{0n}}{c}$

Equation (A1.12b) can then be written as

$$\psi_{0n} = \frac{J_0(k_{0nr} r)}{\sqrt{\pi}\, r_B \left[J_0^2(k_{0nr} r_B) + J_1^2(k_{0nr} r_B) \right]^{1/2}} \qquad \text{(A1.17)}$$

To determine the coupling coefficients first determine

$$\int \psi_{0n} dS_A = \int_0^{2\pi} \int_0^{r_a} r\psi_{0n} dr d\theta$$

$$= \frac{2\sqrt{\pi}}{r_B \left[J_0^2(k_{0nr} r_B) + J_1^2(k_{0nr} r_B) \right]^{1/2}} \int_0^{r_a} r J_0(k_{0nr} r) dr \qquad \text{(A1.18)}$$

Letting $t = k_{0nr} r$

$$\int_0^{r_a} r J_0(k_{0nr}) dr = \frac{1}{k_{0nr}^2} \int_0^{k_{0nr} r_a} t J_0(t) dt \qquad \text{(A1.19)}$$

From Abramowitz and Stegun[112] [Eq. (11.3.20)]

$$\int_0^z t^2 J_{\nu-1}(t) dt = z^2 J_\nu(z) \qquad (\mathrm{Re}\, \nu > 0) \qquad \text{(A1.20)}$$

Evaluating Eq. (A1.19) using Eq. (A1.20) and substituting into Eq. (A1.18) yields

$$\int \psi_{0n} dS_A = \frac{2\sqrt{\pi}\, r_a J_1(k_{0nr} r_A)}{k_{0nr} r_B \left[J_0^2(k_{0nr} r_B) + J_1^2(k_{0nr} r_B) \right]^{1/2}} \qquad \text{(A1.21)}$$

$$\int \psi_{0n} dS_B = \int_0^{2\pi} \int_{r_A}^{r_B} r\psi_{0n} dr d\theta$$

$$= \frac{2\sqrt{\pi}}{r_B\left[J_0^2(k_{0nr}r_B) + J_1^2(k_{0nr}r_B)\right]^{1/2}} \int_{r_A}^{r_B} rJ_0(k_{0nr}r)dr \qquad \text{(A1.22)}$$

Evaluating the integral in the same manner used to evaluate Eq. (A1.19)

$$\int \psi_{0n} dS_B = \frac{2\sqrt{\pi}}{k_{0nr}r_B} \frac{r_B J_1(k_{0nr}r_B) - r_A J_1(k_{0nr}r_A)}{\left[J_0^2(k_{0nr}r_B) + J_1^2(k_{0nr}r_B)\right]^{1/2}} \qquad \text{(A1.23)}$$

The coupling coefficients given in Eqs. (A1.4a-d) can be determined using Eqs. (A1.21) and (A1.23).

$$\zeta_{AA} = \frac{4\pi}{S_A}\left(\frac{r_A}{r_B}\right)^2 k \sum_{n=1}^{\infty} \frac{1}{k_{0nr}^2 k_{nx}} \frac{J_1^2(k_{0nr}r_A)}{J_0^2(k_{0nr}r_B) + J_1^2(k_{0nr}r_B)} \qquad \text{(A1.24a)}$$

$$\zeta_{AB} = \frac{4\pi}{S_A} k \sum_{n=1}^{\infty} \frac{1}{k_{0nr}^2 k_{nx}} \frac{\left[\frac{r_A}{r_B} J_1(k_{0nr}r_A)\right]\left[J_1(k_{0nr}r_B) - \frac{r_A}{r_B} J_1(k_{0nr}r_A)\right]}{J_0^2(k_{0nr}r_B) + J_1^2(k_{0nr}r_B)} \qquad \text{(A1.24b)}$$

$$\zeta_{BB} = \frac{4\pi}{S_B} k \sum_{n=1}^{\infty} \frac{1}{k_{0nr} k_{nx}} \frac{\left[J_1(k_{0nr} r_B) - \frac{r_A}{r_B} J_1(k_{0nr} r_A) \right]^2}{J_0^2(k_{0nr} r_B) + J_1^2(k_{0nr} r_B)} \tag{A1.24c}$$

Finally, from Eqs. (A1.4b) and (A1.4c)

$$\zeta_{BA} = \frac{S_A}{S_B} \zeta_{AB} \tag{A1.24d}$$

APPENDIX II

LOW FREQUENCY APPROXIMATION TO THE NORMALIZED WALL REACTANCE FOR A RESONATOR LINER IN A CYLINDRICAL DUCT

Cho and Ingard[17] have shown that the normalized wall reactance for a resonator liner in a cylindrical duct (Fig. 6) can be expressed as

$$\chi_c = \frac{p}{\rho c u_r}\bigg|_{r=b} = -\frac{H_0^{(1)}(kb) + \alpha H_0^{(2)}(kb)}{H_1^{(1)}(kb) + \alpha H_1^{(2)}(kb)} \qquad \text{(A2.1)}$$

where

$$\alpha = -\frac{H_1^{(1)}[k(b+L)]}{H_1^{(2)}[k(b+L)]} \qquad \text{(A2.2)}$$

The Hankel functions can be expanded as Bessel functions of the first and second kind to yield

$$\alpha = -\frac{\{J_1[k(b+L)] + i\,Y_1[k(b+L)]\}^2}{J_1^2[k(b+L)] + Y_1^2[k(b+L)]} \qquad \text{(A2.3)}$$

For $kL \ll 1$ and $b \not\gg L$, $k(b+L)$ is small and the small argument approximations for the Bessel Functions can be used.[112]

$$J_1[k(b+L)] \simeq \frac{1}{2}\,k(b+L) \qquad Y_1[k(b+L)] \simeq -\frac{2}{\pi}\frac{1}{k(b+L)} \qquad \text{(A2.4a,b)}$$

Using Eqs. (A2.4a) and (A2.4b) in Eq. (A2.3) allows α to be written as

$$\alpha = 1 + i\,\frac{\pi}{2}\,[k(b+L)]^2 \qquad k(b+L) < 1 \qquad \text{(A2.5)}$$

Replacing the Hankel functions in Eq. (A2.1) with Bessel functions of the first and second kind yields

$$\chi_c = -\frac{J_0(kb)(1+\alpha) + iY_0(kb)(1-\alpha)}{J_1(kb)(1+\alpha) + iY_1(kb)(1-\alpha)} \tag{A2.6}$$

Using the following small angle approximations

$$J_0(kb) \simeq 1 - \frac{1}{4}(kb)^2 \qquad Y_0(kb) \simeq \frac{2}{\pi}\ln(kb) \tag{A2.7a,b}$$

$$J_1(kb) \simeq \frac{1}{2}kb \qquad Y_1(kb) \simeq \frac{1}{\pi}\frac{1}{kb} \tag{A2.7c,d}$$

in Eq. (A2.6) , the normalized mass reactance can be shown to be

$$\chi_c = [kL(1+\frac{L}{2b})]^{-1} \qquad k(b+L) < 1 \tag{A2.8}$$

If the inner radius, b, is denoted by r_i and the outer radius, b+L, is denoted by r_o, Eq. (A2.8) can be written as

$$\chi_c = \frac{2}{kr_i\left[(\frac{r_o}{r_i})^2 - 1\right]} \tag{A2.9}$$

APPENDIX III

COMPARISON OF THE PARALLEL LINED DUCT ACOUSTIC FILTER WITH PREVIOUSLY PATENTED PARALLEL DUCT FILTERS

In Section 1.2 three key features of the parallel lined duct acoustic filter (Ingard-Patrick device) studied in this thesis are presented. Briefly, these key features are:

(1) A rigid and continuous splitter plate is used to divide adjacent ducts.

(2) An acoustic liner is used in one or both of the adjacent ducts to cause the phase speed of the fundamental sound mode in the duct to differ substantially from the free space phase speed.

(3) The adjacent ducts are of equal physical length but of unequal acoustical length.

In the following paragraph each patent cited in Chap. 1 will be considered individually to emphasize specific differences from the device of Ingard and Patrick.

Allen and Kürtze (U.S. Patent 3,113,635)[7]

Allen and Kürtze state in Claim 1 of their patent[7] that the apparatus has "said means having a vibartional (sic) energy flow coupling between said conduits at predetermined positions on the adjacent conduit boundaries along a substantial portion of said distance ...". All other Claims reference Claim 1 either directly or indirectly through another Claim. This vibrational energy flow coupling, which is an essential feature of the device of Allen and Kürtze, violates a key feature of the device of Ingard

and Patrick of having a substantially rigid partition between the adjacent ducts. Indeed, the device of Allen and Kürtze would not work as indicated in the patent if the partition were rigid.

The device of Allen and Kürtze functions as a low-pass filter as indicated by the analytical curves presented in Fig. 13 of the patent. The amount of attenuation is essentially flat versus frequency above a given cutoff frequency. The device of Ingard and Patrick functions as neither a high-pass nor a low-pass filter but rather attenuates in selected low frequency bands quite effectively as shown in the experimental data plotted in Figs.

Bychinsky (U.S. Patent 3,948,346)[8]

In this device the phase speeds of the sound waves in the adjacent ducts are essentially identical. Different acoustical path lengths in the adjacent ducts are produced solely by different physical path lengths in the adjacent passages. This device lacks the second and third key features of the device of Ingard and Patrick.

Whitney (U.S. Patent 3,580,357)[9]

Whitney has patented a silencer incorporating adjacent ducts having different physical path lengths and, in addition, small phase speed differences caused by temperature and flow velocity differences in the adjacent ducts. Whitney's device did not use an acoustical liner to alter the phase speed within either or both ducts as specified in the Ingard and Patrick device.

Luxton (U.S. Patent 3,568,791)[10]

The device patented by Luxton clearly uses different physical path lengths as the sole means of producing a phase difference between sound waves at the exit end of the adjacent ducts. This device is essentially a version of a Herschel-Quincke tube discovered by Herschel[3] in 1833, applied by Quincke[4] in 1866 and discussed in the classical The Theory of Sound (Vol. II) by Lord Rayleigh[113] in 1877 and in many other texts on acoustics and introductory physics. The phase speed of the sound wave is not altered in either branch of Luxton's device.

Giordano (U.S. Patent 3,174,583)[11]

Giordano's device utilizes a perforated partition between the inner duct and outer annulus which permits vibrational energy flow coupling between the ducts along their common boundary. Such energy flow does not exist in the Ingard-Patrick device.

Zorumski (U.S. Patent 3,830,335)[12]

In the noise suppressor patented by Zorumski the partition between the inner duct and the outer annulus is nonrigid. The partition, which is comprised of porous material and rubber sealing compound, permits vibrational energy flow coupling between the adjacent ducts along their common boundary. Thus, Zorumski's device lacks the key feature of partition rigidity which is required in the device of Ingard and Patrick. The uniqueness of Zorumski's device, as presented in the claims, is the increased attenuation caused by mode reflections at the interfaces between duct elements in series. Sound reduction caused by interference between out-of-phase sound waves at the exit of the inner duct and outer annulus has not been claimed.

APPENDIX IV

CHOKED ORIFICE APPARATUS FOR MEASURING THE FLOW RESISTANCE OF ACOUSTIC MATERIALS

Sound propagation in a lined duct is governed by the complex acoustic impedance of the lined side walls. For dissipative liners at low frequencies the real part of the impedance, the acoustic resistance, is of primary importance to duct designers. Two methods, acoustical and aerodynamic, have been devised to measure the acoustic resistance of porous materials.

The acoustical method, first devised by Wente and Bedell,[114] uses an impedance tube which is terminated at one end by a sound source and at the other end by a porous sample with a rigid backing. By traversing a microphone probe to measure pressure maxima and minima along the axis of the tube the complex acoustic impedance of the sample can be determined. At low frequencies long tubes are required for which sound wave damping by the side walls becomes significant making accurate impedance measurements difficult.[115]

In the aerodynamic method,[116-118] a mean flow is used to simulate the acoustic particle velocity at low frequencies. The pressure drop induced across the sample by the mean flow is measured to determine the flow resistance, θ, of the sample

$$\theta = \frac{\Delta P}{\rho c U} \qquad \text{(A4.1)}$$

The flow resistance equals the acoustic resistance only when the mean flow, U, equals the rms particle velocity at the sound pressure level to which the liner is to be exposed.

For moderate sound pressure levels extremely low flow speeds are required. The rms particle velocity is 0.49 cm/sec (18 m/hr) at 100 dB and it increases (decreases) by an order of magnitude for each 20 dB increase (decrease) in the sound pressure level. Sometimes, because of the difficulty of producing such low speed flows accurately, flow resistance measurements are taken at higher flow speeds and the results are extrapolated to the low velocity range. This technique is acceptable for samples having laminar flow for which the pressure drop increases linearly with velocity. However, flow resistance measured in the turbulent range for which the pressure drop increases as the square of the velocity cannot be extrapolated with accuracy back to the linear range.[116] Perforated plates[119] and non-fully reticulated acoustical foams[120] are examples of liner materials having turbulent flow at low flow speeds.

In the ASTM standard flow resistance device[118] low speed flows are induced by the positive displacement of water drained from a holding tank through a metering valve. Although this device measures flow resistance quite accurately it is frequently not available in aerodynamic and acoustic test facilities. A much less complicated flow resistance device which uses any readily available low capacity vacuum source is shown in Fig. 72 The apparatus consists of two sections of a 2-in diameter plexiglas tube approximately 1 ft long through which airflow is induced by a miniscule choked orifice connected to a vacuum system at the downstream end of the tube. A porous specimen mounted within a 2-in diameter plexiglas mounting ring is clamped between the plexiglas tube sections as shown in Fig. 72 The static pressure drop across the specimen is measured on a slant

manometer board set at inclination angles between 1.5 and 90 degrees as required.

The magnitude of the flow induced for any interchangeable sonic orifice is set by the orifice-to-tube area ratio according to the compressible flow relation[121]

$$M_2\left[\frac{2}{\gamma+1}\left[1+\frac{\gamma-1}{2}M_2^2\right]\right]^{\frac{-(\gamma+1)}{2(\gamma-1)}} = \frac{A^*}{A_2} \qquad \text{(A4.2)}$$

where A_2 is the flow area of the tube and A^* is the effective choking area of the sonic orifice. A^* is related to A_H, the geometric area of the orifice, by the discharge coefficient C_D

$$A^* = A_H C_D$$

M_2 will differ from M_1, the Mach number at the face of the sample, because of the throttling effect of the resistive sample on the flow. Although the difference $M_2 - M_1$ was expected to be insignificant except for highly resistive liners at high simulated sound pressure levels, the following analysis was conducted to determine the limits of linear operation of the flow resistance device.

To find a relationship between M_1 and M_2 start with the continuity equation

$$\dot{m} = \rho_1 U_1 A_1 = \rho_2 U_2 A_2 \qquad \text{(A4.3)}$$

Using the following expressions

$$P = \rho RT \qquad P_1 = P_2 + \Delta P \qquad A_1 = A_2$$

$$T_t = T\left(1 + \frac{\gamma-1}{2}M^2\right) \qquad U = cM \qquad T_{t_1} = T_{t_2}$$

$$c = (\gamma RT)^{1/2}$$

where T_t is the stagnation temperature of the gas and R is the gas constant, Eq. (A4.3) can be written as

$$M_1\left(1 + \frac{\gamma-1}{2} M_1^2\right)^{1/2} = \left(1 - \frac{\Delta P}{P_1}\right) M_2 \left(1 + \frac{\gamma-1}{2} M_2^2\right)^{1/2}$$

However

$$\Delta P = \theta \rho c U_1$$
$$= \theta \rho c (\gamma R T_t)^{1/2} \left(1 + \frac{\gamma-1}{2} M_1^2\right)^{-1/2} M_1$$

and

$$P_1 = P_{t_1}\left(1 + \frac{\gamma-1}{2} M_1^2\right)^{-\left(\frac{\gamma}{\gamma-1}\right)}$$

Thus, the expression relating M_1 to M_2 can be written in final form as

$$\frac{M_1\left(1+\frac{\gamma-1}{2} M_1^2\right)^{1/2}}{1 - \frac{\theta \rho c c_t}{P_t} M_1 \left(1+\frac{\gamma-1}{2} M_1^2\right)^{\frac{\gamma+1}{2(\gamma-1)}}} = M_2\left(1+\frac{\gamma-1}{2} M_2^2\right)^{1/2} \qquad \text{(A4.4)}$$

where $c_t = (\gamma R T_t)^{1/2}$.

Using Eq. (A4.4) M_1 is plotted vs M_2 in Fig. 73 with θ as a parameter. For simulated pressure levels below 140 dB ($U_1 = 49$ cm/sec) there is no discernible difference between M_1 and M_2. At 150 dB ($U_1 = 156$ cm/sec), M_1 differs from M_2 by less than 4% for $\theta \leq 5$. Above 150 dB the throttling effect of the liner becomes increasingly important as M_2 diverges from M_1 with increasing flow speed.

Based upon these results a series of four orifice plates (Table A4.1) was made to permit operation of the flow resistance measuring device within

the linear range for samples having moderate flow resistance (i.e. $\theta < 5$). The four orifices induced velocities equivalent to 117, 125, 134 and 145 dB sound pressure level at the face of a $\theta = 1$ liner.

The flow resistance of eight samples of acoustical foam and one sample of fiberglass were measured at each simulated dB level (Fig. 74). For most of the samples tested the flow resistance was independent of the flow speed indicating laminar flow through the sample. These samples were acoustically linear within the dB range tested. The measured flow resistance of Scott Pyrell samples, however, increased rapidly with increasing mean flow indicating turbulent flow through the samples.[119] Upon inspection the Scott Pyrell foam was observed to have a non-fully reticulated pore structure which caused the turbulent flow.

TABLE A4.1

Orifice Dia (in)	Particle Velocity (cm/sec)	Sound Pressure Level (dB)
0.025	3.4	117
0.040	8.5	125
0.069	26.0	134
0.129	89.0	145

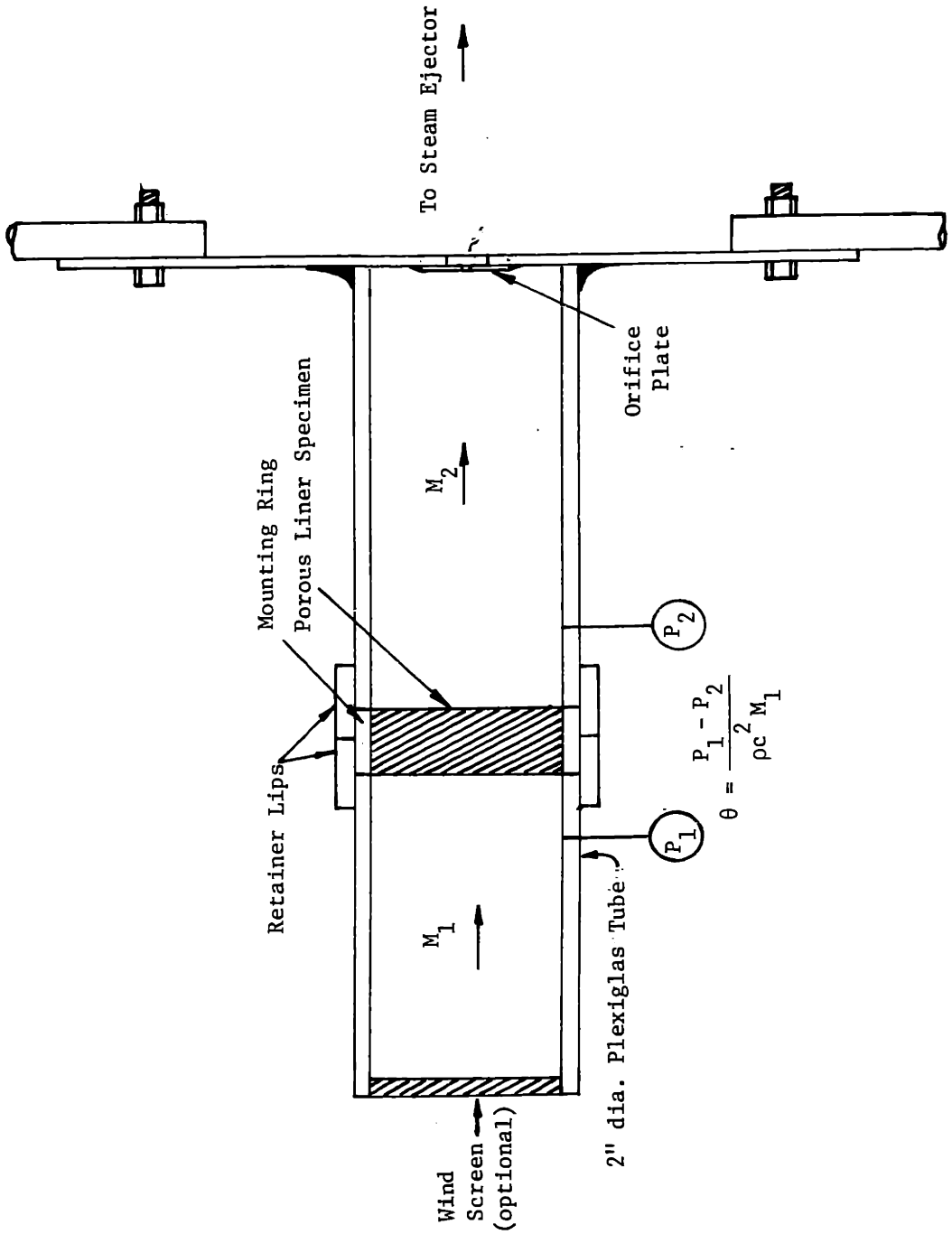

FIG. 72: CHOKED ORIFICE FLOW RESISTANCE DEVICE

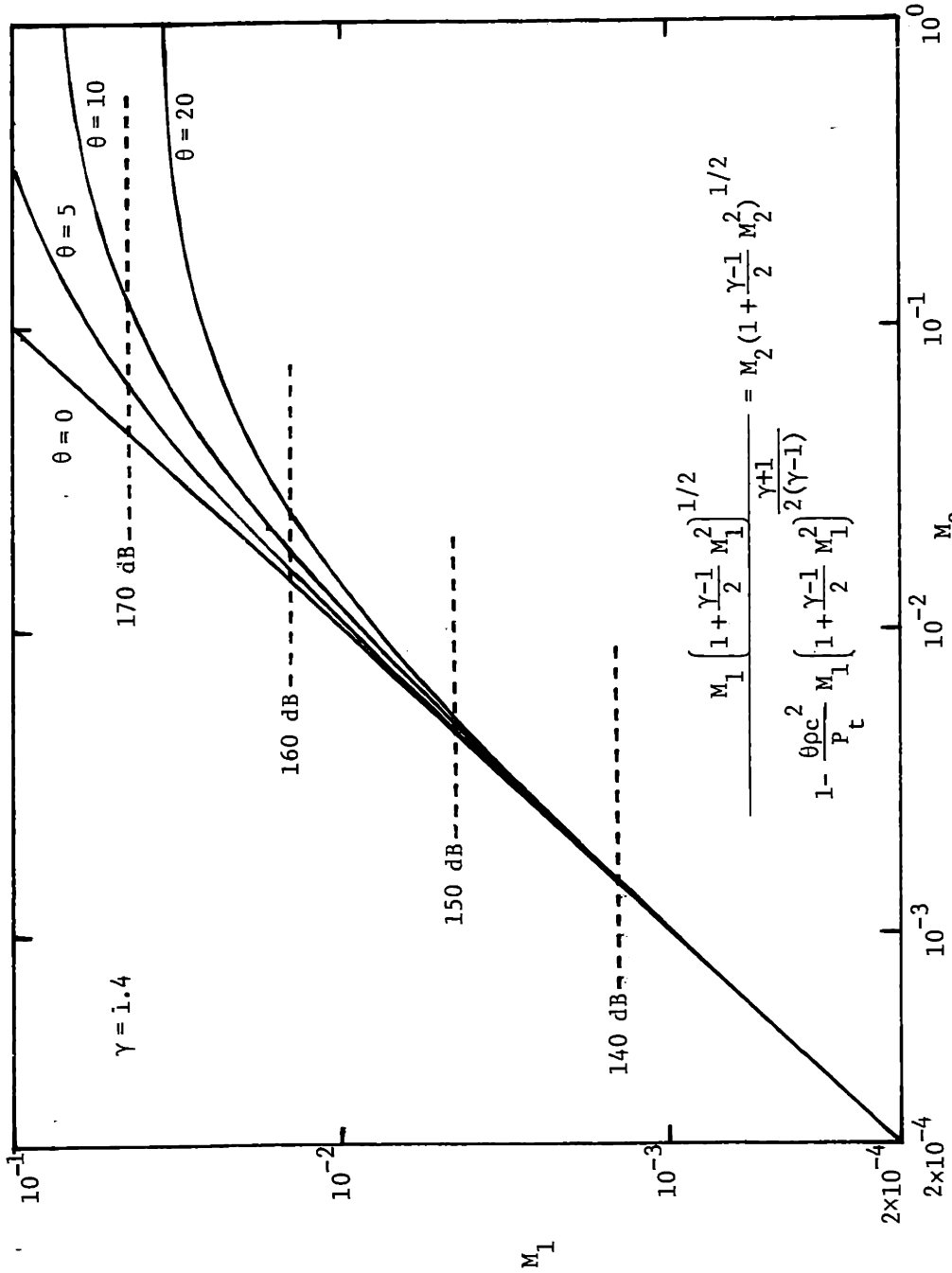

FIG. 73 : EFFECT OF THROTTLING ON FLOW THROUGH ACOUSTIC MATERIAL

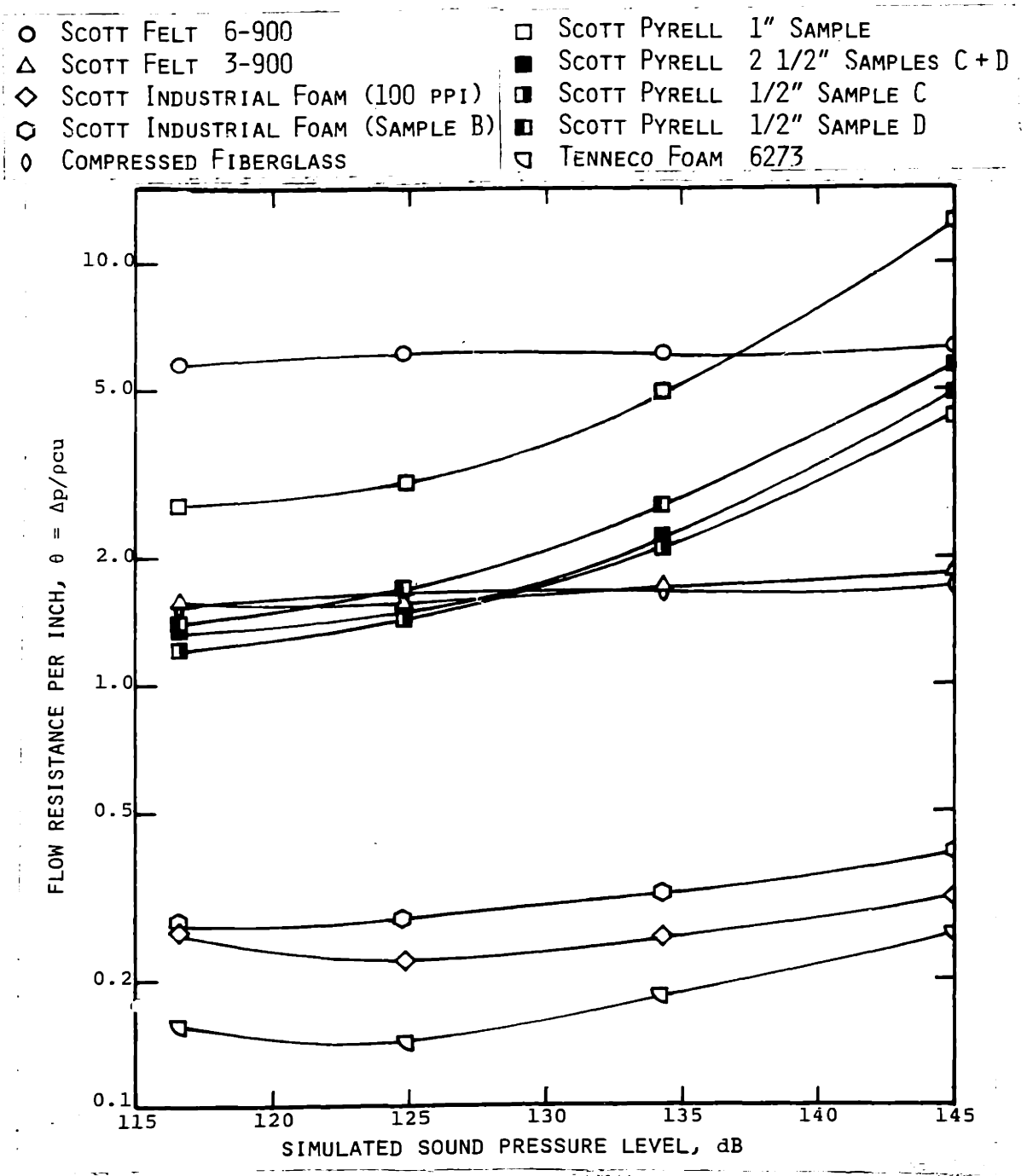

FIG. 74 : FLOW RESISTIVITY OF POROUS MATERIALS MEASURED IN CHOKED ORIFICE FLOW RESISTANCE APPARATUS

APPENDIX V

REDISTRIBUTION OF MEAN FLOW BETWEEN PARALLEL BRANCH DUCTS DUE TO FRICTION

For most parallel duct configurations the mean flow will encounter different frictional resistances in each of the branch ducts, especially if one branch duct is lined and the other(s) unlined. Since the mean flow strongly influences the phase speed in a lined duct, as shown in Sec. 2.1, the mean flow distribution between the branch ducts must be known before the performance of the parallel duct filter with mean flow can be predicted. To determine the effect of these differing frictional resistances on the redistribution of the mean flow between the branch ducts consider the two branch parallel duct configuration shown in Fig. 75a . Note that in this appendix upper case P and U are used to denote static pressure and mean flow velocity in the duct, respectively. In previous sections lower case p and u have been used to denote acoustic pressure and particle velocity, respectively.

Exit Conditions

First the boundary conditions must be established. Assume that at the exit of the parallel duct filter $P_{2A} = P_{2B}$. This assumption can be justified by considering the following paradox (refer to Fig. 75b). U_{2A} is not necessarily equal to U_{2B} causing a shear layer to develop at the exit of the parallel duct filter. The flow will mix viscously (with a resultant drop in pressure) to some "mixed-out" uniform condition downstream P_3 and U_3. Assume P_{2A} were larger than P_{2B}. Then the dividing streamline leaving the trailing edge of the plate would be sloped downward. Flow from

duct A would be confined by expanding streamlines and flow from duct B would encounter contracting streamlines. Since the flow is subsonic P_{2A} will tend to increase and P_{2B} will decrease in the downstream direction, thus accentuating the pressure differences between the two streams in the exit duct. Far downstream the flow should be uniform with constant pressure across the duct. Obviously a paradox exists indicating that the original assumption, that the static pressures in the exit streams differed, was invalid.

Entrance Conditions

The flow through duct B is expected to be less than the flow through duct A because of the increased frictional losses induced by the acoustic liner in duct B. Thus it can be assumed that the dividing streamline in the entrance duct will be curved as shown in Fig. 75c . Far upstream from the entrance of the parallel duct filter $P_0 = P_{0A} = P_{0B}$ and $U_0 = U_{0A} = U_{0B}$. The flow approaching branch duct A encounters converging streamlines causing $U_{1A} > U_{0A}$ and $P_{1A} < P_{0A}$. Similarly the flow approaching branch duct B is confined within diverging streamlines causing $U_{2A} < U_{0A}$ and $P_{2A} > P_{0A}$. Thus, at the entrance of the parallel duct filter

$$P_{1A} < P_{2A} \qquad U_{1A} > U_{2A}$$

Analysis

For low speed flows the total pressure, P_t, can be written as

$$P_t = P + \frac{1}{2} \rho U^2 \tag{A5.1}$$

Upstream of the parallel ducts the total pressure is assumed to be constant throughout the flow field. Thus, the static pressure changes

in the flows approaching the inlet of the A and B ducts are

$$\Delta P_{A_{0-1}} = P_{0A} - P_{1A} = \frac{1}{2}\rho(U_{1A}^2 - U_{0A}^2) \tag{A5.2a}$$

$$\Delta P_{B_{0-1}} = P_{0B} - P_{1B} = \frac{1}{2}\rho(U_{1B}^2 - U_{0B}^2) \tag{A5.2b}$$

The velocity within each branch duct is assumed to be constant between stations 1 and 2. The static pressure drop within each branch duct can be determined from the duct friction factors.

$$\Delta P_{A_{1-2}} = K_A \frac{\rho U_{1A}^2}{2} \qquad \Delta P_{B_{1-2}} = K_B \frac{\rho U_{1B}^2}{2} \tag{A5.3a,b}$$

$$K_A = c_{f_A} L/D_{h_A} \qquad K_B = c_{f_B} L/D_{h_B} \tag{A5.4a,b}$$

where c_{f_A} and c_{f_B} are skin friction coefficients and D_h is the hydraulic diameter of the branch duct.

The static pressure drop between stations 0 and 3 must be independent of the fluid path. Therefore

$$P_0 - P_3 = \Delta P_{A_{0-1}} + \Delta P_{A_{1-2}} + \Delta P_{A_{2-3}} = \Delta P_{B_{0-1}} + \Delta P_{B_{1-2}} + \Delta P_{B_{2-3}} \tag{A5.5}$$

Since $\Delta P_{A_{2-3}} = \Delta P_{B_{2-3}}$, substituting Eqs. (A5.2) and (A5.3) into (A5.5) yields

$$\frac{U_{1A}}{U_{1B}} = \left(\frac{1+K_B}{1+K_A}\right)^{1/2} \tag{A5.6}$$

Using the continuity equation at the entrance

$$U_{0A} S_{0A} = U_{1A} S_A \qquad U_{0B} S_{0B} = U_{1B} S_B \tag{A5.7a,b}$$

But

$$U_0 S_0 = U_{0A} S_{0A} + U_{0B} S_{0B} = U_{1A} S_A + U_{1B} S_B \tag{A5.8}$$

Substituting Eqs. (A5.7) and (A5.8) into (A5.6) yields

$$U_{1A} = \frac{U_0 \; S_0}{S_A \left[1 + \frac{S_B}{S_A} \left(\frac{1+K_A}{1+K_B} \right)^{1/2} \right]} \tag{A5.9}$$

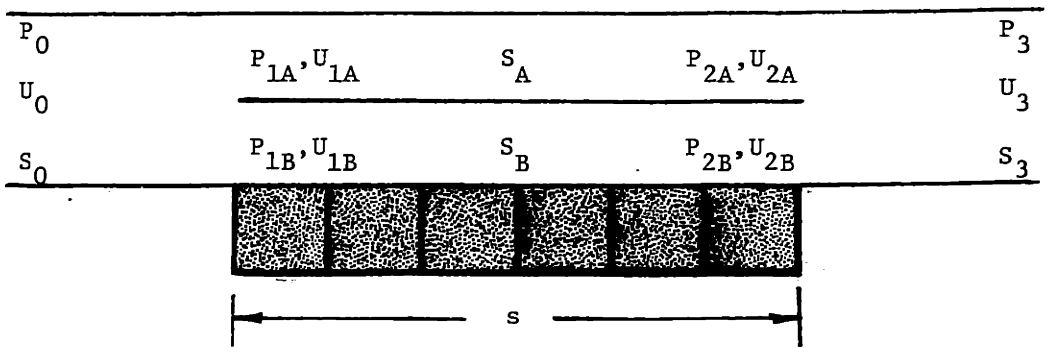

a) Dissimilarly Lined Parallel Ducts

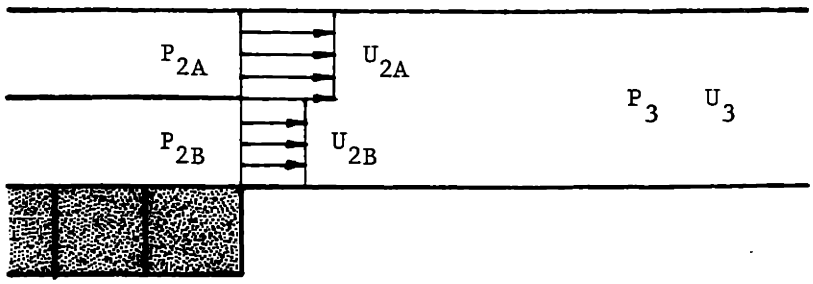

b) Exit Conditions

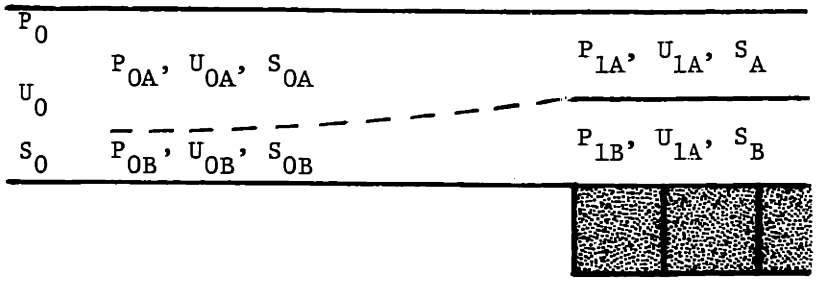

c) Entrance Conditions

FIG. 75 : MODEL FOR MEAN FLOW DISTRIBUTION BETWEEN BRANCHES OF PARALLEL DUCT FILTER

REFERENCES

1. Surowiec, M. W., "Silencing Experience with a Large Gas Turbine," SAE Paper No. 760908 (1976).

2. Cho, Y. C., and Ingard, K. U., "Attenuation of Sound in Lined Ducts," MIT Gas Turbine Lab. Rep. No. 119, Sept. (1974).

3. Herschel, Sir J.F.W., "On the Absorption of Light by Coloured Media, Viewed in Connexion with the Undulatory Theory," Phil. Mag. 3, 401 (1833).

4. Quincke, G., "Ueber Interferenzapparate für Schallwellen (About Interference Apparatuses for Sound Waves)," Pogg. Ann. 128, 6, 177-192 (1866).

5. Stewart, G. W., "The Theory of the Herschel-Quincke Tube," Phys. Review, 31, 696-698, April (1928).

6. Stewart, G. W., "The Theory of the Herschel-Quincke Tube," J. Acoust. Soc. Am. 17, 107-108 (1945).

7. Allen, C. H., and Kürtze, G., "Apparatus for Silencing Vibrational Energy," U.S. Patent No. 3,113,635, Dec. 10 (1963).

8. Bychinsky, W. A., "Wave Interference Silencer," U.S. Patent No. 3,948,349, Apr. 6 (1976).

9. Whitney, D. R., "Wave Interference Silencing System," U.S. Patent No. 3,580,357, May 25 (1971).

10. Luxton, R. E., "Air Ducting," U.S. Patent No. 3,568,791, March 9 (1971).

11. Giordano, M., "Muffler for Internal Combustion Engines," U.S. Patent No. 3,174,583, March 23 (1965).

12. Zorumski, W. E., "Noise Suppressor," U.S. Patent No. 3,830,335, Aug. 20, (1974).

13. Sivian, L. J.,"Sound Propagation in Ducts Lined with Absorbing Materials," J. Acoust. Soc. Am. 9, 77(A), 135-140 (1937).

14. Morse, P. M., "The Transmission of Sounds Inside Pipes," J. Acoust. Soc. Am. 11, 2, 205-210 (1939).

15. Vaidya, P. G., and Dean, P. D., "State of the Art in Duct Acoustics," AIAA Paper 77-1279, presented at AIAA 4th Aeroacoustics Conf., Atlanta, GA, Oct. 3-5 (1977).

References (cont'd)

16. Galaitsis, A. G., and Ingard, U., "Studies of Sound Absorption and Attenuation of Sound in Ducts," Final Report prepared under Grant Agreement DOT-OS-30011 for Dept. of Transportation, Washington, DC, Dec. (1973).

17. Cho, Y. C., and Ingard, K. U., "Attenuation of Sound in Lined Circular Ducts," MIT Gas Turbine Lab. Report No. 120 (Addendum to No. 119) April (1975).

18. Ingard, U., and Pridmore-Brown, D., " The Effect of Partitions in the Absorptive Lining of Sound-Attenuating Ducts," J. Acoust. Soc. of America 23, 5, 589-590, Sept. (1951).

19. Scott, R. A., "The Absorption of Sound in a Homogeneous Porous Medium," Proc. Phys. Soc. 58, 165-183 (1946).

20. Scott, R. A., "The Propagation of Sound Between Walls of Porous Material," Proc. Phys. Soc. 58, 358-368 (1946).

21. Kürze, U. J., and Ver, I. L., "Sound Attenuation in Ducts Lined with Non-Isotropic Material," J. Sound and Vibration 24 2, 177-187 (1972).

22. Tack, D. H., and Lambert, R. F., "Influence of Shear Flow on Sound Attenuation in a Lined Duct," J. Acoust. Soc. Amer. 38, 655-666 (1965).

23. Nayfeh, A. H., Sun, J. and Telionis, D. P., "Effect of Bulk-Reacting Liners on Wave Propagation in Ducts," AIAA Paper No. 73-227, Jan. (1973).

24. Anon., "Microprocessor-based Sound Deadener Cuts Low-Frequency Noise up to 20 dB in Tests," Electronics, 20-21, July (1978).

25. Ingard, U., and Patrick, W. P., "A New Approach to Acoustic Filtering with Lined Ducts," Proc. 3rd Interagency Symp. on University Research in Transportation Noise, University of Utah (G. Banerian and P. Dickinson, eds.) 522-532 (1975).

26. Morse, P. M., and Ingard, K. U., Theoretical Acoustics, McGraw-Hill Book Co., Inc., New York (1968).

27. Zwikker, C. and Kosten, C. W., Sound Absorbing Materials, Elsevier Publishing Co., Inc., New York (1949).

28. Rice, E. J., "Propagation of Waves in an Acoustically Lined Duct with a Mean Flow," NASA SP-207, 345-355 (1969).

References (cont'd)

29. Leskov, E. A., Osipov, G. L., and Yudin, E. J., "Experimental Investigation of Splitter Duct Silencers," Applied Acoustics 3, 47-56, (1970).

30. Kirchoff, G., Pogg. Ann., Bd. 134 (1868).

31. Ingard, U., and Singhal, V. K., "Sound Attenuation in Turbulent Pipe Flow," JASA (55)3, 535-538, March (1974).

32. Trimmer, J. D., "Resonant Frequencies of Certain Pipe Combinations," JASA 11, 129-133, July (1939).

33. Labaw, L. W., "Transmission of Sound Through Parallel Conduits," JASA 12, 232-240, Oct. (1940).

34. Labaw, L. W., "Acoustic Filtration in Parallel Conduit Structures," JASA 13, 345-352, Apr. (1942).

35. Hahn, D., "Über den sogenannten Interferenzvorgang im Quinckeschen Rohr (About the so-called Interference Effect in a Quincke Tube)," Annalen der Physik, 6th ed., 7, 81-87 (1950).

36. Fuller, C. R., and Bies, D. A., "A Reactive Acoustic Attenuator," presented at 93rd Meeting of Acoust. Soc. America, University Park, Pennsylvania, June 6-10 (1977).

37. Fuller, C. R., and Bies, D. A., "Propagation of Sound in a Curved Bend Containing a Curved Axial Partition," JASA 63(2), 681-686, March (1978).

38. Abdelhamid, A. N., "Augmenting Circular Silencer Performance Using Lined Radial Baffles," AIAA Paper No. 77-1357, presented at AIAA 4th Aero-Acoustics Conf., Atlanta, Oct. 3-5 (1977).

39. Purcell, W. E., "Systems for Noise and Vibration Control," Sound and Vibration (11)8, 4-30, Aug. (1977).

40. Dittmar, J. H., and Groeneweg, J. F., "An Experimental Study of the Effect of Treated Length of Fan Inlet Noise Suppressors," AIAA Paper 75-203, presented at AIAA 13th Aerospace Sci. Meeting, Pasadena, CA, Jan. 20-22 (1975).

41. Rice, E.J., et al.: "Acoustic and Aerodynamic Performance of a 6-Foot Diameter Fan for Turbofan Engines. III - Performance with Noise Suppressors," NASA TN D-6178 (1971).

References (cont'd)

42. Ko, S.-H., "Analysis for Sound Attenuation in the Acoustically Lined Annular Flow Duct Separated by an Elastic Circumferential Splitter," J. Sound and Vibration 36(1), 53-67 (1974).

43. Ko, S.-H., "Theoretical Analyses of Sound Attenuation in Acoustically Lined Flow Ducts Separated by Porous Splitters (Rectangular, Annular and Circular Ducts)," J. Sound and Vibration 39(4), 471-487 (1975).

44. Ingard, U., "Transmission Matrix for Parallel Lined Ducts," MIT Gas Turbine Lab. Techn. Memorandum 75-1, Jan. (1975).

45. Zwikker, C., et al., "Absorption of Sound by Porous Material, Part III," Physica 8(10), 1094-1101, Dec. (1941).

46. Galaitsis, A. G., "Nonlinear Effects in Sound Fields," Ph.D. Thesis, Dept. of Physics, Mass. Institute of Techn., Cambridge, MA (1972).

47. Ferris, C. D., Linear Network Theory, Chas. E. Merrill Books, Inc., Columbus, Ohio (1962).

48. Strecker, F., and Feldtkeller, R., "Grundlagen der Theorie des allgemeinen Vierpols," Elektrische Nachrichten-Technik 6(3), 93-112, March (1929).

49. Guillemin, E. A., Communication Networks, Vol. II: The Classical Theory of Long Lines, Filters and Related Networks, J. Wiley & Sons, New York (1935).

50. Huelsman, L. P., Circuits, Matrices and Linear Vector Spaces, McGraw-Hill Book Co., Inc. (1963).

51. Pipes, L. A., and Harvill, L. R., Applied Mathematics for Engineers and Physicists, 3rd ed., McGraw-Hill (1970).

52. Molloy, C. T., "Four-Pole Parameters in Vibration Analysis," Colloquium on Mechanical Impedance Methods for Mechanical Vibrations, Sect. 4 ASME, New York (1958).

53. Molloy, C. T., "Use of Four-Pole Parameters in Vibration Calculations," JASA 29(7), 842-853, July (1957).

54. Rubin, S., "Transmission Matrices for Vibration and their Relation to Admittance and Impedance," Trans. ASME, J. Eng. for Industry, B86(1), 9-21 (1964).

References (cont'd)

55. Rubin, S., "Mechanical Imittance- and Transmission-Matrix Concepts," J. Acoust. Soc. America 41(5), 1171-1179 (1967).

56. Lin, Y. K., and Donaldson, B. K., "A Brief Survey of Transfer Matrix Techniques with Special Reference to the Analysis of Aircraft Panels," J. Sound and Vibration 10(1), 103-143 (1969).

57. Leckie, F. A., "The Application of Transfer Matrices to Plate Vibrations," Ingenieur-Archiv 32(2), 100-111 (1963).

58. Snowdon, J. C., "Mechanical Four-Pole Parameters and their Application," J. Sound and Vibration 15(3), 307-323 (1971).

59. Stewart, G. W., "Acoustic Wave Filters," Physical Review 20(6), 528-551 (1922).

60. Webster, A. G., "Acoustic Impedance, and the Theory of Horns and of the Phonograph," Nat. Acad. of Sci. 5 (1919).

61. Mason, W. P., "A Study of the Regular Combination of Acoustic Elements, with Applications to Recurrent Acoustic Filters, Tapered Acoustic Filters and Horns," Bell System Tech. J. 6 (1927).

62. Stewart, G. W., and Lindsay, R. B., Acoustics - A Text on Theory and Applications, D. Van Nostrand Co., New York (1930).

63. Peterson, L. C., and Bogert, B. P., J. Acoust. Soc. Am. 22, 369 (1950).

64. Peterson, L. C., "Equivalent Circuits of Linear Active Four-Terminal Networks," Bell System Tech. J. 27, 593 (1948).

65. Brekhovskikh, L. M., Waves in Layered Media, Applied Mathematics and Mechanical Series VI, Academic Press, New York (1960).

66. Rybak, S. A., and Tartakovskii, B. D., "A Case of Total Acoustic Insulation in the Transmission of Sound through a Layer-Symmetric Wall," Soviet Physics-Acoustics 7, 404 (1961).

67. Igarashi, J., and Toyama, M., "Fundamentals of Acoustical Silencers. I - Theory and Experiment of Acoustic Low-Pass Filters," Aeronaut. Res. Institute Report No. 339, University of Tokyo, Dec. (1958).

68. Miwa, T., and Arai, M., "Fundamentals of Acoustical Silencers. II - Determination of Four Terminal Constants of Acoustical Elements," Aeronaut. Res. Inst. Report No. 344, Univ. of Tokyo, May (1959).

References (cont'd)

69. Igarashi, J., and Arai, M., Fundamentals of Acoustical Silencers. III - Attenuation Characteristics Studied by an Electric Simulator," Aeronaut. Res. Inst. Report No. 351, Univ. of Tokyo, Feb. (1960).

70. Wang, W. M., "Matrix Foundation in Acoustical Analysis of Mechanically Driven Fluid Systems," JASA 41(6), 1418-1423 (1967).

71. Wang, W. M., "Acoustical Analysis of a Multicylinder Air-Induction System," J. Acoust. Soc. Am. 42(6), 1244-1249 (1967).

72. Alfredson, R. J., "The Design and Optimization of Exhaust Silencers," Ph.D. Thesis, Institute of Sound and Vibration Research, University of Southampton, July (1970).

73. Alfredson, R. J., and Davies, P.O.A.L., "Performance of Exhaust Silencer Components," J. Sound and Vibration 15(2), 175-196, March (1971).

74. Ingard, K. U., "Acoustical Characteristics of One-Dimensional Barriers, I," MIT Gas Turbine Lab. Techn. Memorandum 73-1 (1973).

75. Ingard, K. U., Aeroacoustics and Noise Control, Lecture Notes in Acoustics, M.I.T. (1976).

76. Munjal, M. L., "Velocity Ratio-Cum-Transfer Matrix Method for the Evaluation of a Muffler with Mean Flow," J. Sound and Vibration 39(1), 105-119 (1975).

77. Munjal, M. L., et al., "A Rational Approach to the Synthesis of One-Dimensional Acoustic Filters," J. Sound and Vibration 29, 263-280 (1973).

78. Parrott, T. L., "An Improved Method for Design of Expansion-Chamber Mufflers with Application to an Operational Helicopter," NASA TN D-7309, Oct. (1973).

79. Sullivan, J. W., "Theory of a Discrete Element Method for Modeling Parallel-Coupled Muffler Components," presented at 94th Meeting Acoust. Soc. Am., Miami Beach, Dec. 12-16 (1977).

80. Zorumski, W. E., "Acoustic Theory of Axisymmetric Multisectioned Ducts," NASA TR R-419, May (1974).

81. Lansing, D. L., and Zorumski, W. E., "Effects of Wall Admittance Changes on Duct Transmission and Radiation of Sound," J. Sound and Vibration 27(1), 85-100, March (1973).

References (cont'd)

82. Lester, H. C., and Posey, J. W., "Duct Liner Optimization for Turbomachinery Noise Sources," NASA TM X-72789, Nov. (1975). Presented at 90th Meeting Acoust. Soc. Am., San Francisco, Nov. 4-7 (1975).

83. Munjal, M. L., and Sreenath, A. V., "Analysis and Design of Exhaust Mufflers - Recent Developments," Shock and Vibration Digest 5(11), 2-14 (1973).

84. Hogge, H. D., and Ritzi, E. W., "Theoretical Studies of Sound Emission from Aircraft Ducts," AIAA Paper No. 73-1012, presented at AIAA Aero-Acoustics Conf., Seattle, Oct. 15-17 (1973).

85. Arnold, W. R., "Sparse Matrix Techniques Applied to Modal Analysis of Multisection Duct Liners," AIAA Paper No. 75-514, presented at AIAA 2nd Aero-Acoustics Conf., Hampton, Virginia, March 24-26 (1975).

86. Rayleigh, J. W., "Some General Theorems Relating to Vibrations," Proc. London Math. Soc. 4, 357 (1873).

87. Shea, T. E., Transmission Networks and Wave Filters, D. Van Norstrand Co., New York (1929).

88. Janssen, J. H., "A Note on Reciprocity in Linear Passive Acoustical Systems," Acustica 8, 76-78 (1958).

89. Ten Wolde, T., "On the Validity and Application of Reciprocity in Acoustical, Mechano-Acoustical and other Dynamical Systems," Acustica 28, 23-32 (1973).

90. Belousov, Y. I., and Rimskii-Korsakov, A. V., "The Reciprocity Principle in Acoustics and its Application to the Calculation of Sound Fields of Bodies," Soviet Physics-Acoustics 21(2), 103-109 (1975).

91. Chernov, L. A., "Ray Curvature and the Reciprocity Principle in the Acoustics of a Moving Medium," Trudy Kom. Akust. 6, 63-65 (1951).

92. Galaitsis, A. G., "Measurement of the Acoustic Impedance of an Internal Combustion Engine," presented at 90th Meeting of Acoust. Soc. Am., San Francisco, Nov. 4-7 (1975).

93. Beckemeyer, R. J., "Transfer Matrix Method for Sound Transmission in Acoustically-Lined Horns," presented at 94th Meeting of Acoust. Soc. Am., Miami Beach, Dec. 12-16 (1977).

References (cont'd)

94. Ingard, U., "On the Theory and Design of Acoustic Resonators," J. Acoust. Soc. Am. 25(6), 1037-1061 (1953).

95. Cummings, A., "Sound Transmission at Sudden Area Expansions in Circular Ducts, with Superimposed Mean Flow," J. Sound and Vibr. 38(1), 149-155 (1975).

96. Ronneberger, D., "Experimentale Untersuchungen zum akustischen Reflexionsfaktor von unstetigen Querschnittsänderungen in einem luftdurchströmten Rohr," Acustica 19, 222-235 (1967/68).

97. Cummings, A., and Haddad, H., "Sudden Area Changes in Flow Ducts: Further Thoughts," J. Sound and Vibration 54(4), 611-612 (1977).

98. Lambert, R. F., "Side Branch Insertion Loss in Moving Medium," J. Acoust. Soc. Am. 28(6), 1059-1063 (1956).

99. Ingard, K. U., and Singhal, V. K., "Flow Excitation and Coupling of Acoustic Modes of a Side-Branch Cavity in a Duct," J. Acoust. Soc. Am. 60(5), 1213-1215 (1976).

100. Ingard, U., and Ising, H., "Acoustic Nonlinearity of an Orifice," J. Acoust. Soc. Am. 42(5), 6-17 (1967).

101. Groeneweg, J. F., "Current Understanding of Helmholtz Resonator Arrays on Duct Boundary Conditions," Basic Aerodynamic Noise Research, NASA SP-207, 357-368 (1969).

102. Chen, Y. N., "Lateral Helmholtz Resonator Silencer with Turbulence Absorption," Proc. Institution of Mech. Engineers 182, part 1(3), 60-72 (1967-68).

103. Meyer, E., et al., "Experiments on the Influence of Flow on Sound Attenuating in Absorbing Ducts," J. Acoust. Soc. Am. 30, 165-174 (1958).

104. Ingard, K. U., and Dean, L. W., "Excitation of Acoustic Resonators by Flow," Proc. 2nd Symp. on Naval Hydrodynamics, A CR-38, (R. D. Cooper, ed.) ONR, Dept of the Navy, Washington, DC, 137-150 (1958).

105. Bauer, A. B., and Chapkis, R. L., "Noise Generated by Boundary Layer Interaction with Perforated Acoustic Liners," AIAA Paper No. 76-41 presented at AIAA 14th Aerospace Sci. Meeting, Washington, DC, Jan. 26-28 (1976).

References (cont'd)

106. Hrubes, J. D., "Flow Generated Noise of Acoustical Duct Liners," M.S. Thesis, Dept. of Aero- and Astronautics, M.I.T. (1977).

107. Levine, H., and Schwinger, J., "On the Radiation of Sound from an Unflanged Circular Pipe," Physical Review 73(4), 383-406 (1948).

108. Carrier, G. F., "Sound Transmission from a Tube with Flow," Quarterly of Applied Mathematics XII, 457-461 (1956).

109. Mani, R., "Refraction of Acoustic Duct Waveguide Modes by Exhaust Jets," Quarterly Appl. Math. XXX, 501-520 (1973).

110. Savkar, S. D., "Radiation of Cylindrical Duct Acoustic Modes with Flow Mismatch," J. Sound and Vibr. 42(3), 363-386 (1975).

111. Embleton, T.W.F., "Mufflers," Noise and Vibration Control, (L. L. Beranek, ed.) McGraw-Hill, New York, 362-405 (1971).

112. Abramowitz, M., and Stegun, I. A., Handbook of Mathematical Functions, National Bureau of Standards, Washington, DC, 10th Printing, Dec. (1972).

113. Rayleigh, Lord J. W., Theory of Sound (London, 1877-78), Vol. II, Dover Press edition.

114. Wente, E. C., Bedell, E. H., Bell System Tech. J. 7, 1 (1928).

115. Beranek, L. L., "Precision Measurement of Acoustic Impedance," J. Acoust. Soc. Am. 12, 3-13, July (1940).

116. Brown, R. L., and Bolt, R. H., "The Measurement of Flow Resistance of Porous Acoustic Materials," J. Acoust. Soc. Am. 13(4), 337-344, April (1942).

117. Bies, D. A., "Acoustical Properties of Porous Materials," Noise and Vibration Control (L. L. Beranek, ed.) McGraw-Hill, New York, 245-269 (1971).

118. ASTM C522-69, "Standard Method of Test for Airflow Resistance of Acoustical Materials," American Soc. for Testing and Materials, 1916 Race Street, Philadelphia, PA 19103.

119. Mangiarotty, R. A., et al., "Duct-Lining Materials and Concepts," NASA SP-189, 29-50 (1968).

References (cont'd)

120. Bordone-Sacerdote, C., and Sacerdote, G. G., "A Method for Measuring the Acoustic Impedance of Porous Materials," Acustica 34, 77-80, (1975).

121. Shapiro, A. H., The Dynamics and Thermodynamics of Compressible Fluid Flow, I, Ronald Press, New York (1953).

122. Rostafinski, W., "Acoustic Systems Containing Curved Duct Sections," J. Acoust. Soc. Am. 60, 23-28 (1976).

BIOGRAPHY

William Paul Patrick was born in McKeesport, Pennsylvania on July 19, 1944. He attended public schools in Clairton, Pennsylvania before entering the Pennsylvania State University from which he graduated with a B.S. degree with honors in Aerospace Engineering in 1966. While at Penn State he obtained experience as a co-op student at Rocketdyne working on the design and development of the engines for the Saturn V rocket. He received his S.M. degree in Aeronautics and Astronautics from MIT in 1968. His S.M. thesis involved heat transfer measurements in highly cooled turbulent boundary layers. After receiving his S.M. degree he worked on the design, construction, and initial testing of the MIT Blowdown Compressor Facility as a research assistant until leaving in 1971 to accept a full-time job at the United Aircraft Research Laboratories (currently United Technologies Research Center) with which he had been affiliated since 1968 as a summer student and independent contractor. While at UTRC he has worked in many research areas including heat transfer in water-cooled turbine blades and vanes, visualization of particulate trajectories near the surface of film-cooled turbine blades and low Reynolds number mixing in chemical laser nozzle arrays. His current research project involves the development of a high frequency digital data acquisition system using hot-films and Kulite pressure transducers for compressor and turbine flow field mapping. Most of the work reported in this thesis was performed during a leave-of-absence from UTRC in 1974-76.